

Modelling of pile load tests in granular soils

Loading rate effects

Nguyen, Thanh

DOI

[10.4233/uuid:07dc4081-2436-4b6b-8f6d-b36d6a588047](https://doi.org/10.4233/uuid:07dc4081-2436-4b6b-8f6d-b36d6a588047)

Publication date

2017

Document Version

Final published version

Citation (APA)

Nguyen, T. (2017). *Modelling of pile load tests in granular soils: Loading rate effects*. [Dissertation (TU Delft), Delft University of Technology]. <https://doi.org/10.4233/uuid:07dc4081-2436-4b6b-8f6d-b36d6a588047>

Important note

To cite this publication, please use the final published version (if applicable).
Please check the document version above.

Copyright

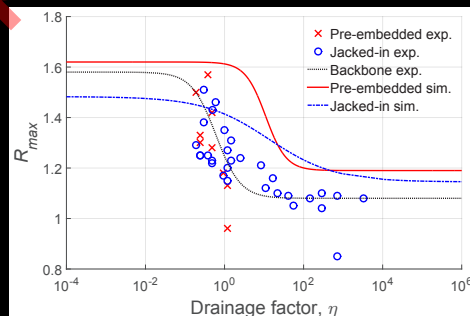
Other than for strictly personal use, it is not permitted to download, forward or distribute the text or part of it, without the consent of the author(s) and/or copyright holder(s), unless the work is under an open content license such as Creative Commons.

Takedown policy

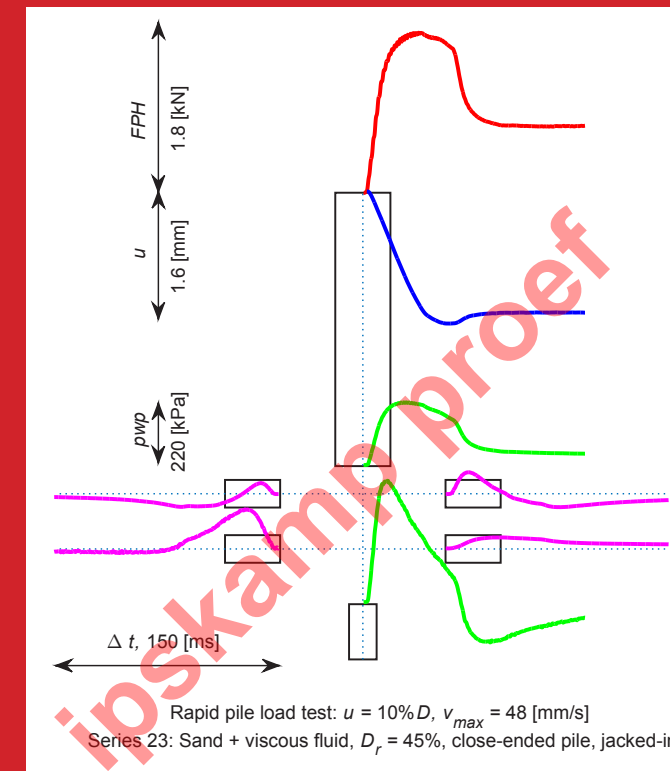
Please contact us and provide details if you believe this document breaches copyrights.
We will remove access to the work immediately and investigate your claim.

The interpretation of the rapid load test to an equivalent static capacity requires evaluating the load rate effect and the excess pore pressure effect since these two effects make the pile resistance of the rapid load test significantly higher than that of the static load test.

This thesis presents the experimental and numerical modelling of static and rapid pile load tests in granular soils in order to assess the rate effect and the excess pore pressure effect on the interpretation of a rapid pile load test.



MODELLING OF PILE LOAD TESTS IN GRANULAR SOILS LOADING RATE EFFECTS



CHI THANH NGUYEN

MODELLING OF PILE LOAD TESTS IN GRANULAR SOILS

LOADING RATE EFFECTS

Chi Thanh NGUYEN

MODELLING OF PILE LOAD TESTS IN GRANULAR SOILS

LOADING RATE EFFECTS

Proefschrift

ter verkrijging van de graad van doctor
aan de Technische Universiteit Delft,
op gezag van de Rector Magnificus prof. ir. K.Ch.A.M. Luyben,
voorzitter van het College voor Promoties,
in het openbaar te verdedigen op 17 oktober 2017 om 12:30 uur

door

Chi Thanh NGUYEN

Master of Science in Civil Engineering,
Technische Universiteit Delft, Nederland

geboren te Sofia, Bulgarije
Vietnamezen nationaliteit

Dit proefschrift is goedgekeurd door de

promotor	Prof. ir. A.F. van Tol
copromotor	Dr. ir. P. Hölscher

Samenstelling promotiecommissie:

Rector Magnificus, Prof. ir. A.F. van Tol, Dr. ir. P. Hölscher,	voorzitter Technische Universiteit Delft Technische Universiteit Delft
---	--

Onafhankelijke leden:

Prof. dr. A. Metrikine	Technische Universiteit Delft
Prof. dr. K.G. Gavin	Technische Universiteit Delft
Prof. dr. ir. A. Bezuijen,	University of Gent, Belgium
Dr. M. Brown,	University of Dundee, Scotland, UK
Dr. ir. P. Meijers,	Deltares, Delft, Netherlands



Keywords: rapid pile load test, granular soil, excess pore pressure, rate effect, excess pore pressure effect

Printed by: Ipskamp Drukkers

Front images: Modified version of Figure 4.9 in Chapter 4.

Back images: Figure 7.25 and 7.26 in Chapter 7.

Copyright © 2017 by C.T. Nguyen

ISBN 978-94-6186-858-9

An electronic version of this dissertation is available at
<http://repository.tudelft.nl/>.

CONTENTS

Summary	v
Samenvatting	ix
1 Introduction	1
1.1 Background	1
1.1.1 Pile load testings	1
1.1.2 Interpretation of the rapid pile load tests.	2
1.1.3 Influence of the installation methods	3
1.2 Objectives of the study	3
2 Literature review	5
2.1 Introduction	5
2.2 Pile load testing methods	5
2.2.1 Static pile load test.	6
2.2.2 Rapid pile load test.	7
2.3 Interpretation methods for pile loading tests	8
2.3.1 Interpretation of static pile load tests	8
2.3.2 Interpretation of rapid pile load tests	9
2.3.3 Interpretation with influence from installation methods.	12
2.4 Behaviour of dry sand during penetration	15
2.4.1 Literature	15
2.4.2 Summary	18
2.5 Behaviour of saturated sand during penetration	18
2.5.1 Literature	18
2.5.2 Summary	22
2.6 Loading rate effect in sand	23
2.6.1 Influence on sand strength.	23
2.6.2 Influence on pile/plate/foundation resistance.	27
2.6.3 Discussion	30
2.7 Excess pore pressure effect in sand	32
2.7.1 Direct effect	33
2.7.2 Indirect effect	33
2.7.3 Summary	35
2.8 Concluding remarks	36
3 Physical modelling	37
3.1 Introduction	37
3.2 Centrifuge modelling	38
3.2.1 Model scaling	38

3.2.2	Boundary condition	39
3.2.3	Summary	40
3.3	Model setup.	41
3.3.1	Mechanical setup	41
3.3.2	Sample setup	45
3.4	Experiment program	48
3.4.1	Loading scheme	48
3.4.2	Experiment procedure	49
3.4.3	Variations	50
3.5	Summary	51
4	Physical modelling - Results	53
4.1	Introduction	53
4.2	Derivation and notations	53
4.3	Static load tests	56
4.4	Rapid load tests	59
4.5	Pore fluid pressure in rapid load tests	62
4.5.1	General description	62
4.5.2	Response of PPTs with the same average loading rate	65
4.5.3	Symmetry of PPT's response	68
4.6	Reliability of tests	72
4.6.1	Repeatability of static and rapid force measurements	72
4.6.2	Repeatability of ratio of rapid force over static force	73
4.6.3	Repeatability of pore pressure measurement.	74
4.6.4	Conclusion.	75
4.7	Loading patterns and load-displacement responses	75
4.8	Conclusions.	77
5	Physical modelling - Interpretation	79
5.1	Introduction	79
5.2	Influence of penetration rate	79
5.2.1	Overview.	80
5.2.2	Constitutive rate effect.	83
5.2.3	Excess pore pressure effect.	84
5.2.4	Summary on the penetration rate effect	90
5.3	Influence of soil and pore fluid types	90
5.3.1	Static resistance	91
5.3.2	Ratio of rapid forces over static forces	93
5.3.3	Summary	98
5.4	Influence of initial relative density of soil	99
5.4.1	Static resistance	100
5.4.2	Ratio of rapid forces over static forces	101
5.4.3	Summary	106

5.5	Influence of pile installation methods.	107
5.5.1	Static resistance	107
5.5.2	Ratio of rapid forces over static forces	108
5.5.3	Summary	112
5.6	Influence of pile types.	114
5.6.1	Static resistance	114
5.6.2	Ratio of rapid forces over static forces	115
5.6.3	Summary	119
5.7	Conclusions.	120
6	Numerical modelling	123
6.1	Introduction	123
6.2	Brief review of mechanics of porous media	123
6.3	Governing equations and FE formulation	125
6.3.1	Governing equations.	125
6.3.2	Spatial discretisation.	126
6.3.3	Time discretization: Partition of Time Unity scheme.	127
6.4	Performance of PLAXIS-PTU	129
6.4.1	One-dimensional bar test	129
6.4.2	Saturated sandstone sample test of Grinten	130
6.4.3	Shallow foundation test of Hoang and Zienkewicz	132
6.4.4	Plaxis-PTU with interface elements	133
6.5	Conclusions.	135
7	Numerical modelling - Results	137
7.1	Introduction	137
7.2	Problem description	138
7.2.1	Modelling cases	138
7.2.2	Calculation geometry	138
7.2.3	Constitutive model.	138
7.2.4	Soil-pile interface	140
7.2.5	Initial conditions.	141
7.2.6	Simulation schemes and calculation phases	145
7.3	Simulation of static pile load tests.	147
7.3.1	Pile capacity at 10% D	147
7.3.2	Stress state	149
7.3.3	Summary	151
7.4	Simulation of rapid pile load tests.	151
7.4.1	Pile capacity at 10% D	152
7.4.2	Strain and pore pressure	153
7.4.3	Influence of pore pressure on rapid capacity.	156
7.4.4	Summary	158
7.5	Comparison with experiments	158
7.5.1	Evolution of the excess pore pressure	158
7.5.2	Influence of the drainage condition on the ratio of rapid over static pile forces	162

7.6	Conclusions.	164
8	Conclusions	167
8.1	Conclusions.	167
8.1.1	Responses of excess pore fluid pressure	167
8.1.2	Rate effect	168
8.1.3	Other effects	169
8.1.4	The unloading point method	170
8.2	Recommendations	170
A	Loading schemes	173
B	Preliminary simulations	177
B.1	Influence of interface	177
B.1.1	On static simulations	177
B.1.2	On dynamic simulations.	178
B.2	Influence of pre-stressing.	180
B.2.1	Prescribing volumetric expansion	180
B.2.2	Prescribing vertical displacements.	181
B.2.3	Prescribing horizontal displacements	182
C	Calculation phases in four simulation schemes	183
	List of notations	185
	References	193
	Acknowledgements	209
	Curriculum Vitae	211

SUMMARY

People have used pile foundations throughout history to support structures by transferring loads to deeper and stronger soil layers. One of the most important questions during the design of the pile foundation is the bearing capacity of the pile. The most reliable method for determining the bearing capacity is to use results from pile load tests. Traditionally, the static pile load tests have been used and more recent the dynamic tests. The rapid load test, at intermediate loading rates, was invented to overcome the disadvantages of the static tests (expensive and time-consuming) and the dynamic tests (the stress wave effects) and is conducted more and more in practice.

The interpretation of the rapid load test to an equivalent static capacity requires evaluating the load rate effect and the excess pore pressure effect since these two effects, in general, make the rapid resistance significantly higher than the static resistance. This thesis presents the experimental and numerical modelling of static and rapid pile load tests in granular soils in order to assess the rate effect and the excess pore pressure effect on the interpretation of a rapid pile load test.

In the experimental modelling, several series of rapid pile load tests and static pile load tests are performed in the geotechnical centrifuge at Deltares at the acceleration level of 40-g. Mixtures of sand/viscous fluid, silt/water and sand/water are used in order to create different drainage conditions for the rapid pile load tests. The rapid load tests are carried out with several loading rates and maximum pile loads. The displacement of the pile head, the forces in the pile head and pile tip and the excess pore pressure in the soil around the pile tip are measured. Both closed and open-ended piles are tested. The influence of installation method has been studied.

In the numerical modelling, static and rapid pile load tests are simulated by the Finite Element software Plaxis at the prototype scale. A research module, Plaxis-PTU, is applied. This model solves the dynamic two-phase Biot equation which couples the dynamic calculation and the consolidation analysis. The Plaxis-PTU module was verified. Several static and rapid pile load test calculations are carried out to evaluate the influence of permeability on the excess pore pressure response, and then assess the excess pore pressure effect on the increase of the rapid pile tip resistance over the static tip resistance.

The response of excess pore pressure depends strongly on the soil behaviour during the rapid load test.

Axisymmetric installation of the pore pressure transducers (PPT) around the penetrated pile in the experiments reveals an unexpected asymmetry of the responses of excess pore pressure. More precisely, it seems that the excess pore pressure response exhibits an initial elastic symmetric behaviour followed by asymmetric behaviour due to an asymmetric failure of the soil. The asymmetry of the excess pore pressure responses can be explained by these physical reasons (the asymmetry of failure and/or the heterogeneity of the soil bed) but an experimental reason (small differences in the distance of

each PPT from the pile centre line) cannot be excluded. The principal mechanism of the excess pore pressure effect is the presence of negative pore pressure due to the shear-induced dilatancy of the soil which increases the effective stress in the skeleton, hence, the soil strength and, therefore, the pile resistance. The excess pore pressure effect can be described with the drainage factor which can be determined from the soil properties, the pile radius and the loading duration of the test. This factor must be considered in the interpretation of the rapid pile load test results.

The constitutive rate effect can be determined from the fully drained tests since the excess pore pressure effect is negligible in such a test. The constitutive-rate effect results in an increase of 10% for the maximum pile tip resistance in the rapid test over the static value. The excess pore pressure effect plays a role in partially and undrained situations. It leads to an increase of up to 50% for the maximum tip resistance and the tip resistance at the unloading point (the equivalent static) in the rapid test over the static value. The relationship between the drainage factor and the normalised tip resistance (the ratio between the tip resistance in the rapid load test over the tip resistance in the static load test) are extended relative to earlier research for partially drained conditions by considering the silt/water mixture.

From the experiments, the conclusions for the ratio between the soil resistance at a displacement of 10% of pile diameter in a rapid test and a static test (the normalised tip resistance) read:

- The soil permeability has a strong influence on the normalised tip resistance. The normalised pile tip resistance increases with a decrease of the soil permeability due to an increase of the excess pore pressure effect.
- The relative density of the soil has a limited influence on the normalised tip resistance. The normalised pile tip resistance increases with a decrease of the initial relative density due to a decrease of the soil shear stiffness, and therefore, of the drainage factor.
- The installation method has a strong influence on the normalised tip resistance in which the normalised tip resistance of the pre-embedded pile is significantly higher than that of the jacked pile.
- The pile type and diameter have a limited influence on the normalised head resistance. The normalised head resistance of the close-ended pile is higher than that of the open-ended pile. The normalised head resistance of the small pile ($D = 11.2$ mm) is higher than that of the large pile ($D = 16$ mm).

In the numerical modelling, the influence of the installation process on the stress around the pile is simulated. The soil behaviour around the pre-embedded pile is modelled by adapting the soil properties in the vicinity of the pile; whereas the soil behaviour around the jacked pile is modelled by pre-stressing a soil block under the pile tip. The static capacity of the pile is reasonably achieved. The tip-dominant pile (the tip resistance is 70-80% of the total capacity) is reasonably described.

The simulations confirm the presence of excess pore pressure around the pile and its influence on the rapid tip resistance. A relationship between the drainage factor and the normalised tip resistance from the numerical modelling is found to have the same trend with that relationship from the experimental modelling.

The simulated pore pressure response has the same pattern with that from the experiment. The permeability has no influence on the general trend of the excess pore pressure response, but it has a significant effect on the magnitude of the maximum positive/negative excess pore pressure as well as the time that the peak values are reached.

SAMENVATTING

Al lange tijd worden paalfunderingen toegepast om de belasting van een constructie naar diepere en draagkrachtigere lagen af te voeren. Een van de belangrijkste vragen voor het ontwerp van een paalfundering is de draagkracht van de paal. De meest betrouwbare manier om de draagkracht te bepalen is een proefbelasting op een paal. Traditioneel worden hiervoor statische proefbelastingen uitgevoerd, meer recent ook dynamische. De snelle proefbelasting met een tussengelegen belastingssnelheid, is geschikt om de nadelen van de statische test (de hoge kosten en de lange uitvoeringsduur) op te lossen zonder de nadelen van de dynamische proefbelasting (het optreden van spanningsgolven in de paal). Snelle proefbelastingen worden steeds vaker uitgevoerd.

Bij de interpretatie van een snelle proefbelasting tot een equivalent statische draagkracht, moet gecorrigeerd worden voor de invloed van de belastingssnelheid en de optredende wateroverspanningen. Het verwaarlozen van deze twee invloeden leidt in het algemeen tot een overschatting van de equivalente draagkracht. Dit proefschrift presenteert de resultaten van experimenteel en numeriek onderzoek naar de statische en snelle proefbelastingen op palen in granulaire materialen met als doel de invloed van de belastingssnelheid en de optredende wateroverspanningen op de interpretatie te kwantificeren.

In de experimenten zijn verschillende series met statische en snelle proefbelastingen uitgevoerd in de geotechnische centrifuge van Deltares onder een versnellingsniveau van 40-g. De grond rondom de paal is gemodelleerd met zand waarin als porienvloeistof zowel water als een viskeuze vloeistof gebruikt is, en silt, waarin alleen water als porienvloeistof toegepast is. Hiermee zijn verschillende drainagevoorwaarden gecreëerd. De snelle proefbelastingen zijn uitgevoerd met verschillende belastingssnelheden en maximale belastingen. De verplaatsing van de paalkop, de krachten in de paalkop en de paalvoet en de wateroverspanningen in de grond rondom de paalpunt zijn gemeten. Zowel palen met een gesloten punt als met een open punt zijn beproefd. De invloed van verschillende installatiemethodes is onderzocht.

In de numerieke modellering zijn statische en snelle proefbelastingen gesimuleerd met het eindige elementen model Plaxis in prototype schaal. Het onderzoeksmodel Plaxis-PTU is hiervoor gebruikt. Dit model lost de dynamische Biot vergelijkingen op, waarin de dynamica en consolidatie theorie gekoppeld zijn. De Plaxis-PTU beschrijving is geverifieerd. Verschillende berekeningen voor statische en snelle proefbelastingen zijn uitgevoerd om de invloed van de doorlatendheid op de wateroverspanningen tijdens een snelle proefbelasting te onderzoeken. Daarna is het effect van de wateroverspanningen tijdens een snelle proefbelasting op de verhouding tussen de puntweerstand tijdens een snelle proefbelasting en een statische proefbelasting.

De gemeten wateroverspanningen worden sterk beïnvloed door het gedrag van de grond tijdens de snelle proefbelasting.

Bij een axiaal-symmetrische installatie van de waterspanningopnemers rondom de

paal worden onverwacht sterke asymmetrische waarden van de waterspanningen in de opnemers gevonden. Dit treedt vooral op als de grond plastisch vervormt. Deze asymmetrie kan een fysische achtergrond hebben (asymmetrisch bezwijkpatroon, heterogeniteit in de grond), of een experimentele achtergrond (kleine afwijkingen in de afstand tussen de paal en de afzonderlijke opnemers).

Het principe van het wateroverspanningseffect is het optreden van dilatantie door schuifspanningen. Dit leidt tot negatieve wateroverspanningen in de grond en een toename van de effectieve spanningen in het skelet. De daarbij behorende grotere sterkte van de grond resulteert in een grotere paal draagkracht. Het wateroverspanningseffect kan beschreven worden met de drainage factor, die wordt bepaald door de grondeigenschappen, de paaldiameter en de duur van de belasting. Deze factor moet beschouwd worden tijdens de interpretatie van een snelle proefbelasting.

Het constitutieve snelheidseffect kan bepaald worden uit een volledig gedraineerde test, omdat in dat geval het wateroverspanningseffect afwezig is. Het constitutieve snelheidseffect geeft bij een snelle proefbelasting een 10% hogere draagkracht bij de paalpunt dan de statische draagkracht. Het wateroverspanningseffect speelt een rol tijdens gedeeltelijk gedraineerde of ongedraineerde situaties. Dit effect leidt tot een toename tot 50% voor de maximale kracht en de equivalente statische kracht in het unloading point (ontlastingspunt) ten opzichte van de werkelijke statische draagkracht. De relatie tussen de drainage factor en de genormaliseerde punt weerstand is voor partieel gedraineerde proeven uitgebreid ten opzichte van eerder onderzoek en onderbouwd door het silt/water mengsel te beproeven.

Op basis van de experimenten kunnen voor de genormaliseerde puntweerstand (de verhouding tussen de puntweerstand in een snelle proefbelasting en de punt weerstand in een statistisch test) bij een verplaatsing van 10% van de paaldiameter, de volgende conclusies worden getrokken:

- De doorlatendheid van de grond heeft een grote invloed op deze verhouding. De genormaliseerde puntweerstand neemt toe met de afname van de doorlatendheid ten gevolge van het toenemende belang van het wateroverspanningseffect.
- De dichtheid van de grond heeft een beperkte invloed op deze verhouding. De genormaliseerde puntweerstand neemt toe met initiële dichtheid ten gevolge van de afname van de schuifsterkte van de grond en daarmee de drainage
- De methode van installatie heeft een grote invloed op deze verhouding, waarbij de genormaliseerde puntweerstand van de in de grond gevormde paal significant hoger is dan van de weggedrukte paal.
- Het type paal heeft een beperkte invloed op de genormaliseerde weerstand aan de paalkop. De genormaliseerde weerstand aan de paalkop is bij een paal met een gesloten voet hoger dan bij een paal met een open voet. De genormaliseerde weerstand aan de paalkop is voor een kleine paal ($D = 11.2$ mm) hoger dan voor een grote paal ($D = 16$ mm).

In de numerieke berekeningen is de invloed van de installatie methode op de spanningssituatie rondom de paalpunt gesimuleerd. De spanningssituatie bij de in de grond gevormde paal wordt aangepast door de eigenschappen in de omgeving van de paal aan te passen. De spanningssituatie in de grond rondom een ingedrukte paal wordt aangepast door de grond onder de paalpunt op te spannen. Hierdoor wordt het statisch gedrag

van de paal redelijk benaderd. De dominantie van de paalpunt voor de draagkracht (de puntweerstand is 70-80% van de totale weerstand) wordt redelijk beschreven.

De berekeningen bevestigen het optreden van wateroverspanningen rond om de paal en de invloed hiervan op de paalpunt weerstand tijdens een snelle proefbelasting. Op basis van de berekeningen is een relatie tussen de drainagefactor en de genormaliseerde puntweerstand afgeleid. Deze heeft dezelfde trend als de relatie die in de centrifuge proeven gevonden is.

De berekende wateroverspanningen hebben dezelfde trend als in de experimenten. De doorlatendheid van de grond heeft geen invloed op de algemene trend van de wateroverspanningen, maar heeft wel een grote invloed op de grootte van de maximale en minimale wateroverspanningen en ook op het tijdstip waarop de maximale waarden worden bereikt.

1

INTRODUCTION

1.1. BACKGROUND

1.1.1. PILE LOAD TESTINGS

People have used pile foundations throughout history to support structures by transferring loads to deeper and stronger soil layers [82]. Two of the most important and general questions related to the design of the pile foundation are the bearing capacity and the load-displacement relationship of the pile itself. The parameters that affect pile performance are, for convenience, divided into four categories as proposed by Leland [154]:

- soil characteristics (i.e. soil types such as sand/clay/gravels/... and soil properties such as stiffness/friction angle/cohesion/...),
- pile characteristics (i.e. pile types such as solid/hollow/H-section... and pile properties such as diameter/length/compressibility/...),
- methods of pile installation (i.e. bored, jacked, driven), and
- types of loading (i.e. based on loading duration such as static/dynamic/rapid and based on loading direction such as axial/lateral).

It is apparent that each category includes numerous parameters. The parameters within a category and especially between categories are not fully independent from each other; many of them are interrelated. Because of these interactions, it is generally difficult to describe and interpret the effects that parameters have on pile behaviour.

The most reliable method for determining the pile behaviour and, in particular, the ultimate bearing capacity is to use results from pile load tests [219]. Traditional static load tests provide the most precise method of evaluating the load-displacement response [229] because of the similarity in their loading condition with the loading condition in service of the pile. In practice, however, the static testing methods are not that attractive because they are expensive to set up and time-consuming to undertake. A typical static pile load test requires a massive construction frame, a reaction mass of 2-3 times of the designed load and a duration of days depending on soil conditions and types.

The dynamic testing methods provide an economic alternative for static load testing. A typical dynamic pile load test requires a reaction mass of about 2% of the designed load and a duration in the order of hours. However since the dynamic test relies on the impact

of a rigid mass at the pile head, damage of the pile head is not rare. Moreover, because the dynamic test is characterised by a short blow, of the order of a few milliseconds, the stress-wave effect in a pile is significant which sometimes causes damage to the pile due to tension waves [191]. On top of that, the translation of the dynamic resistance to an equivalent static capacity is not always unambiguous due to the stress wave effect.

An alternative method of pile load testing at intermediate loading rates, called rapid load testing, has been developed to overcome the above-mentioned drawbacks of both the static and dynamic testing methods [25] and is employed more and more in practice [40, 157, 188]. The reaction mass in a typical rapid loading test is about 5-10% of the ultimate capacity, the duration of a blow is about 50-400 ms and the time to perform of the test is in order of hours [125]. With the relatively long loading duration, the pile is continuously under compression, and it reacts as a rigid body with minimum influence from the stress wave effect [192].

1.1.2. INTERPRETATION OF THE RAPID PILE LOAD TESTS

In deriving the equivalent static results, the pile load test results of both the dynamic and rapid testing methods need to be interpreted to eliminate the dynamic and rate effects. In general, dynamic effects consists of, the energy radiation effect, the inertial effect, the damping effect, the load rate effect and the excess pore pressure effect. In the rapid load tests, the most important reasons for complicated interpretation come from the load rate effect and the excess pore pressure in the soil under and close to the pile toe [206].

The load rate effect, as defined by Whitman [281], is related to the constitutive behaviour of the soil and depends strongly on the loading rate of the pile load test. For fine-grained soils, i.e. clay, the load rate effect is associated with the viscous behaviour of the soil; while for granular soils, i.e. sand, the load rate effect is connected with the interlocking between particles [281]. The load rate effect on the soil strength and the pile resistance have been studied by many researchers for both clay [41, 53, 108] and sand [71, 92, 206, 271].

Several researchers [71, 120, 206] show that the generation of excess pore pressure during rapid load testing is a complex process with initially positive excess pore pressures due to compression followed in a second stage by negative excess pore pressure due to shearing and dilatancy. This last stage is supposed to be decisive for the bearing capacity [199, 206, 267]. The excess pore pressure effect on the pile resistance has been investigated by a limited number of researchers [123, 206, 258] and is proven to depend on not only the drainage condition (represented by the drainage factor η [118]) but also on the loading rate of the pile load test.

From many results of static and rapid pile load tests, McVay et al. [178] proposed to use a resistance factor ϕ to obtain the static bearing capacity of a pile from the rapid bearing capacity. The value of ϕ for sand and clay is 0.92 and 0.53, respectively [121, 178]. The database, developed by McVay et al. [178], was extended further by Hölscher and van Tol [121] with more case studies reported by Holeyman et al. [124, 126] and Opstal et al. [211]. The empirical reduction factor is called R by Hölscher and van Tol [121] and is recommended to have the values of 0.90 and 0.50 for sand and clay, respectively. It should be noted that these two values are from case studies with a real failure during the rapid load test (displacement of at least 5% of pile diameter).

1.1.3. INFLUENCE OF THE INSTALLATION METHODS

Based on the method of installation, piles are classified as either non-displacement or displacement piles. For the non-displacement pile, the strength and the stiffness of the soil are generally not altered during the installation process or the impact is limited. The installation of the displacement pile, on the other hands, significantly changes the soil stresses and properties such as density, strength, stiffness...

The influence of the installation method on the soil state leads to a different behaviour of displacement and non-displacement piles in an identical soil for both static, rapid and dynamic loading. This phenomenon is reported by Fonseca and Santos [85] and McVay et al. [178] when they measured the capacity of bored and driven piles during static and rapid or dynamic loadings and also by Hölscher and van Tol [121] when they investigated results of numerous static and rapid pile load tests. For pile load tests in the same soil, both McVay et al. [178] and Hölscher and van Tol [121] recommended different values of the empirical factor for the non-displacement pile and the displacement pile.

1.2. OBJECTIVES OF THE STUDY

The general objective of this study is to quantify the load rate effects for a proper interpretation of a rapid pile load test. That objective can be achieved through the following sub-objectives:

- to quantify the constitutive rate effect on the relation between the rapid capacity and the static capacity;
- to observe the evolution and distribution of excess pore pressure during the rapid pile load tests conducted in the geotechnical centrifuge and therefore to quantify the excess pore pressure effect on the relation between the rapid capacity and the static capacity.

In short, the relationships between the empirical factor R and the loading rate and between R and the drainage factor η will be investigated.

Besides the load rates effects, the influences of three other parameters on the interpretation of a rapid pile load test are also investigated in order to quantify their influence on the static and rapid capacities and hence determine the factor R representative for their influence. Those parameters are:

- the soil properties (sand versus silt, dense versus medium dense);
- the installation method (non-displacement versus displacement);
- the pile properties (11.3 mm-diameter versus 16 mm-diameter, open-ended versus close-ended).

The study follows two main approaches: experimental modelling in a centrifuge and numerical modelling in the research module Plaxis-PTU of the commercial Finite Element software Plaxis. By choosing a centrifuge configuration, detailed information on the soil deformation and pore fluid pressure is justified by the proper scaling of the stress state which is of crucial importance for a high confinement problem such as a pile loading [129, 255]. In Plaxis-PTU, the dynamic calculation and the consolidation analysis are coupled, the relative movement of the fluid with the solid is considered. Consequently,

an evolution of excess pore pressure during the rapid pile load test can be simulated more realistically for partially drained loading condition.

In order to complete the objectives of the study, the following work has been done:

- The literature related to the topic of the thesis is reviewed in chapter 2. The topic of interests includes the static and rapid pile load testing methods and their interpretation methods, behaviour of dry and saturated sand during penetration tests and pile load tests, the loading rate effect on the sand strength and the pile resistance, and the effect of excess pore pressure.
- The theoretical principles and the mechanical realisations of the experimental program in a centrifuge configuration are investigated and are presented in chapter 3. In the experimental program, the soil type, the soil density, the pile type, the installation method, the magnitude of prescribed displacement, the configuration of the pore-pressure transducers and the loading duration of the rapid pile load tests are varied.
- The results of the experimental program are presented and discussed in chapter 4. Interpretation and implications of the experimental results are given in chapter 5.
- The governing equations of the porous media and their numerical implementation in Plaxis-PTU are summarised and given in chapter 6. The applicability of Plaxis-PTU for the simulation of the rapid pile load test is shown.
- The input of the simulation for the rapid pile load test and the simulation results are presented in chapter 7. The numerical model does not simulate the installation process itself, but the effects of different installation processes are taking into account by several techniques. Comparisons of the numerical bearing capacity versus the experimental capacity and the numerical versus the experimental R are given.
- The results of this study and the recommendations for further research are given in chapter 8.

2

LITERATURE REVIEW

2.1. INTRODUCTION

Granular soils consist of separate particles. Its behaviour is governed by the grain properties, the arrangement of the grains and the contact forces between the grains. The strength and stiffness of granular soils have a non-linear dependence on stress and strain level as well as loading history. In a process including pile installation and several stages of pile loading, the soil experiences many complex conditions and their properties will alter dramatically [277]. During the installation process, gross deformations occur which changes significantly the soil state as well as properties, especially the density and thus the related properties. In static pile loading, the soil at different locations exhibits different loading conditions such as compression, shearing with contraction and/or dilation. During dynamic or rapid pile loading, a soil element at one location even follows different paths of loading, unloading and reloading and may exhibit all three above mentioned loading conditions at different moments. Saturated soil behaves with even more complexity due to the interaction between the soil and the pore fluid.

This chapter briefly describes the static and rapid pile load testing methods and their interpretation methods. Then, in order to have insight into the physics of the pile-soil-fluid interaction, the behaviour of dry and saturated sand during penetration and/or loading tests are summarised based on published research. The effects of loading rate and excess pore pressure on the strength and stiffness of sand and pile resistance are also reviewed and discussed.

2.2. PILE LOAD TESTING METHODS

The various pile testing methods are best characterised by the duration of the applied force and the induced strain in and/or displacement of the pile. The tests involving large forces applied for a long period, such as static load tests, are used to assess pile bearing capacity; while small energy and low strain tests are used to assess pile integrity. The high strain dynamic and rapid load tests are used to assess pile bearing capacity by using dynamic effects (i.e. generating a force or stress through the intervention of mass and acceleration) [125]. In the high strain dynamic load tests, the force is applied over a typical period of 5-20 ms while in the rapid load tests, a typical period of loading is about

50-400 ms [125].

The wave number is defined as the ratio between the length of the applied pulse load and the length of the pile [192] as follows:

$$N_w = \frac{T \times c}{L} \quad (2.1)$$

in which T is the duration of the applied load (sec), L is the length of the tested pile (m), and c is the velocity of stress wave propagation in a pile (m/s). According to the Research Committee on Rapid Load Test Methods in Japan, the load testing method can be classified based on the wave number N_w [157] as:

- $N_w < 10$: a dynamic load test
- $10 \leq N_w \leq 1000$: a rapid load test
- $N_w > 1000$: a static load test

2.2.1. STATIC PILE LOAD TEST

A conventional static pile load test includes the building of a reaction system around the test pile and loading the pile incrementally, usually with a hydraulic jack. The reaction system can be a system which is anchored by a number of reaction piles or a system of reaction mass. The test load is measured with a load cell, and the pile head displacement is measured with a levelling system (LVDT or dial gauges). For load deformation tests, strain gauges embedded within the pile are used to determine the load distribution along the pile length.

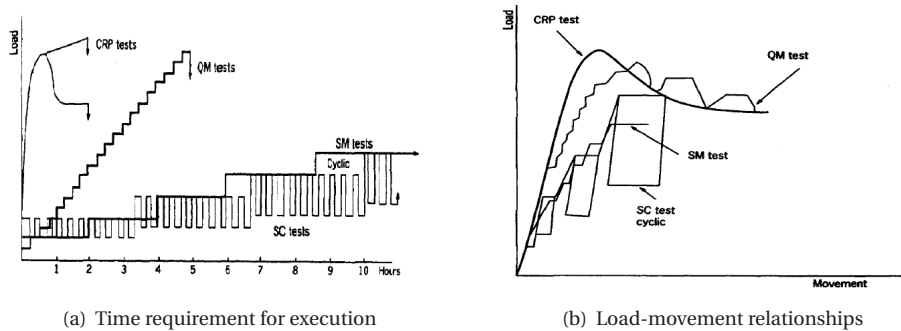


Figure 2.1: Comparison of four static load test methods, Fellenius [74]

A properly performed static load test generally provides the most accurate bearing capacity data because the loading method compares to service loading with respect to the loading time. Although the results of the static test are the most reliable, the tests are generally only used under specific requirements due to the relatively high cost and time required for performing the test compared to dynamic load tests.

In the practice of the static pile load testing, many pile load test methods have been reported in detail [15, 46, 61, 197, 275, 276], in which four methods can be identified as the basic load test methods [144]: the slow maintained load test method (SM test),

the quick maintained load test method (QM test), the constant rate of penetration test method (CRP test) and the Swedish cyclic test method (SC test). The comparison of those four methods is given by Fellenius [74] for a required-time in Figure 2.1(a). Fellenius suggested that, from the time duration point of view, the more time consuming tests such as the Slow ML and the Swedish cyclic should be clearly justified instead of the quick tests such as the CRP and the Quick ML. Another comparison for a typical load-movement curves on a friction pile in clay is given also by Fellenius [74] as in Figure 2.1(b). It can be seen that the curve procedured by the CRP is well defined and illustrates clearly the pile behaviour; the Quick ML only provides indication of the pile behaviour but it can not capture the peak value [74]. The remaining two methods, the Slow ML and the Swedish cyclic, provide very little information and can not show the failure of the pile [74].

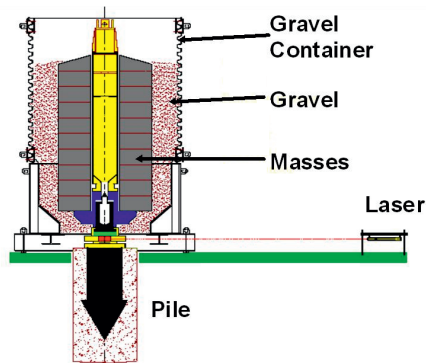
2.2.2. RAPID PILE LOAD TEST

A rapid pile load test, similar to a dynamic pile load test, relies on the impact loading of a pile. However, in a rapid pile load test, the transmitted energy is spread over 10-20 times longer period than the typical loading duration of a conventional dynamic pile load test [125] in order to reduce the wave propagation effects.

In practice, there are two types of load testing methods regarded as a rapid pile load test namely the dynatest [98] or the pile load tester [241] and the statnamic test [25, 191].



(a) Rapid pile load test 8MN [188]



(b) Schematic of Rapid pile load test [93]

Figure 2.2: Rapid pile load test

In the dynatest or the pile load tester, a large mass is dropped onto the pile head with a spring placed in between. The spring is attached to the pile head in the dynatest or to the bottom of the falling mass in the pile load tester. The spring stiffness, the mass weight and the drop height are varied to control the magnitude and loading duration of the applied force. The applied load on the pile head, the displacement and acceleration of the pile head are measured during the test.

In the statnamic test, a reaction mass is accelerated in the direction opposite to the test load direction by igniting the fuel. On completion of the upward stroke, the reaction

mass is caught in its highest position by a gravel catching system for the larger testing devices or a hydraulic and a mechanical catching mechanism for the smaller testing devices. Since the reaction mass is accelerated at about 20 times higher than the earth gravitational level, the weight of the reaction mass required is only 5-10% of the required force [206]. The applied load on the pile head is measured by a load cell, the displacement of the pile head is monitored using an optical device (i.e. a laser beam), and the acceleration of the pile head is measured using an accelerometer mounted on the pile head as shown in Figure 2.2.

The most common statnamic rigs typically have testing capacities of 3 to 4 MN and, in practice, devices have been produced with applied loads ranging from 0.1 to 60 MN. Moreover, because the statnamic load test depends not on the gravity but the inertia force, it can be performed in any direction of vertical, horizontal, inclined and even a tension test [188].

2.3. INTERPRETATION METHODS FOR PILE LOADING TESTS

For the safety and the serviceability of a foundation, the determination of the bearing capacity and the load-displacement characteristic is crucial. In the static pile loading tests, because of the similarity in their loading condition with the loading condition in service of the foundation, the load-displacement relationship is immediately available by plotting the load and displacement data. Therefore the main task of interpretation is defining the bearing capacity. In the dynamic or rapid pile load tests, however, both the bearing capacity as well as the load-displacement characteristic is far from those of the foundation in service. Interpretation of results from the dynamic or rapid pile loading tests, therefore, is deriving results of the equivalent static loading tests.

In this section, interpretation methods of the static pile load test and the rapid pile load test from the literature are briefly described. Then the influence of installation methods on interpretation methods of rapid pile load tests is presented.

2.3.1. INTERPRETATION OF STATIC PILE LOAD TESTS

Generally, load and settlement data are plotted together to create a load-settlement curve which is used to determine the failure load so that an allowable pile capacity can be calculated.

The ultimate failure load for a pile is defined as the load at which the pile has fully mobilised the soil resistance, which means the settlement increases drastically under sustained load. However, full mobilisation of the pile may require large settlements that may exceed the acceptable range of the soil-pile system. Other failure definitions consider arbitrary settlement limits derived from certain requirements or procedures. Terzaghi [256] proposed a definition of the bearing capacity of piles in load tests as the load corresponding to a pile head deformation of 10% of the pile diameter. This method, later, is used by many other practice engineers and researchers [20, 266, 274]. In the literature, many other interpretation methods have been used to determine the bearing capacity for different pile and soil types or testing procedures [75] such as: De Beer and Wallays' method [21], Butler and Hoy's method (or the shape of curve method) [46], Chin's method [54], Davisson's method (or the slope tangent method) [63], Brinch Hansen's criterion [109], Mansur and Kaufman's method (or the tangent intersection)

[174], Mazurkiewicz's method [177], and Veen's method [262]. Details on those methods are described in the corresponding references.

2.3.2. INTERPRETATION OF RAPID PILE LOAD TESTS

As mentioned above, interpretation of rapid pile loading tests is to derive the corresponding results of the equivalent static loading tests such as the load-displacement curve and the pile capacity. Since the rapid load test is also a dynamic event, the rate effects (including the stress-wave effect, the inertial effect, the constitutive rate effect, the excess pore pressure effect, the radiation of energy effect) may have a certain effect on the results and need to be taken into account during interpretation [191]. In practice, many interpretation methods based directly on the rapid pile load results are proposed which can be classified into two groups, one based on the concentrated mass model [191] and the other on the one-dimensional stress wave model [202]. Details of the interpretation methods can be found in the mentioned references, the evaluation of the performance as well as the experience with the use of technical parameters of these methods can be found in [178, 206, 212, 248]. Besides direct interpretation methods based on the experimental rapid pile load test, numerical methods (i.e. Finite Element method) [17, 127, 178] can also be used to analyse the rapid load test. This section briefly describes the most important methods.

The concentrated mass model is based on the assumption that the stress-wave effect in the pile is negligible due to the long wavelength of the test which is reasonable when the wave number N_w is larger than 12 [192]. With this assumption, Middendorp et al. [192] assumed that the pile behaves as a rigid body during the rapid test and its behaviour can be modelled as a single-degree-of-freedom system.

The equilibrium equation for the pile mass is [191]:

$$F_{rap} = F_{soil} + F_{inertia} \quad (2.2)$$

in which:

- F_{rap} is the applied rapid load;
- F_{soil} is the soil resistance of the pile;
- $F_{inertia}$ is the inertial force of the pile mass, $F_{inertia} = M \times a_t$ with M is the pile mass and a_t is the acceleration of the pile head.

The soil resistance consists of the static resistance F_u and the damping resistance F_v , $F_{soil} = F_u + F_v$ in which:

- $F_u = K \times u_t$ with K is a spring stiffness represented the full static behaviour of the pile reaction,
- $F_v = C \times v_t$ with C is a damping coefficient and v_t is the velocity of the pile head.

It should be noted that, originally, Middendorp et al. did not consider the pore pressure effect in [191] or assumed that it has negligible influence or it is a part of the damping term [187] in order to simplify the analysis. Equation 2.2 can be written as:

$$\begin{aligned} F_{rap} &= F_u + F_v + F_a \\ &= K \times u_t + C \times v_t + M \times a_t \end{aligned} \quad (2.3)$$

Consequently, the static resistance of the pile during the rapid test can be computed as:

$$F_u = F_{rap} - C \times v_t - M \times a_t \quad (2.4)$$

In order to back calculate the static resistance from the rapid results, only the damping coefficient C needs to be determined as the pile mass M , velocity v_t and acceleration a_t are known.

Among many methods based on the concentrated mass model, the unloading point (UP) method [191] was the first published and also the most widely used method for the rapid load testing. In the UP method, the load-displacement curve of the rapid loading test is divided into several parts and the damping coefficient C is determined in each part. Bielefeld and Middendorp [27] indicated that the UP method might over predict the static capacity by as much as 20% if stress wave phenomena are present. They found that for $N_w > 12$ the UP method is valid and for $N_w < 12$ the stress wave phenomena needs to be accounted for. Brown [42] provided a detailed procedure for an interpretation following the UP method.

Based on the UP method, the modified unloading point (MUP) method [166] is proposed for testing a short pile when $N_w > 12$. However, if a strong bearing layer supports the pile tip, then the rigid body assumption is still violated [166]. Another method based on the UP method is the segmental unloading point (SUP) method [145] which is used for testing a long pile with $N_w < 12$. A drawback of the MUP and SUP method is a requirement of additional instrumentation, the MUP requires other instrumentation at the bottom of the pile shaft whereas the SUP requires several levels of instrumentation along the pile shaft in addition with the other two at the pile top and bottom. Matsumoto et al. [175] proposed an analytical method, based on the UP method, in which both the damping value C and the spring stiffness K are considered as non-linear. This method predicts a more-accurate pile head stiffness [175].

For the rapid load testing in clay, Hyde et al. [138] noted that the rate effect is highly non-linear, therefore, in order to have an accurate estimation the relationship between the dynamic soil resistance and the penetration rate and the damping coefficients have to be predetermined using laboratory tests [41]. Based on a series of model pile tests in clay at different loading rates, Brown et al. [41, 43, 44] proposed a model (known as the Sheffield Model) to interpret the rapid pile load test in clay as following:

$$\begin{aligned} \frac{\tau_d}{\tau_s} &= 1 + \alpha \times v_t^\beta - \alpha \times v_s^\beta \\ F_u &= \frac{F_{rap} - M \times a_t}{1 + \alpha \times v_t^\beta - \alpha \times v_s^\beta} \end{aligned} \quad (2.5)$$

in which

- τ_d and τ_s are the limiting values of the rapid and static pile shaft friction,
- v_s is the lowest pile velocity used to determine the ultimate static shaft friction,
- α and β are the damping coefficient determined from the model pile tests.

This model gives a good estimation of the ultimate pile resistance [43] but under-predicts the initial elastic stiffness [108]. Anderson et al. [12] improved the model of

Brown by taking into account a proportional exponent of the velocity term, Equation 2.6, or a proportional multiplier of the velocity term, Equation 2.7.

$$F_u = \frac{F_{rap} - M \times a_t}{1 + \alpha \left(\frac{v_t}{v_s} \right)^\beta \left(\frac{F_{rap}}{F_{rap}^{ult}} \right)} \quad (2.6)$$

$$F_u = \frac{F_{rap} - M \times a_t}{1 + \alpha \left(\frac{F_{rap}}{F_{rap}^{ult}} \right) \left(\frac{v_t}{v_s} \right)^\beta} \quad (2.7)$$

with F_{rap}^{ult} is the ultimate rapid load. Anderson et al. [12] proved that their model generates a good prediction of the static load-settlement curve. Examples of the interpretation of the rapid pile load test by the unloading point method to obtain the load-displacement curve of the static load test made by Brown and Powell [44] in the ground of brown London clay and unweathered blue clay, and Anderson et al. [12] in the ground of sandy clay, gravely clay and clay with gravel are given in Figure 2.3.

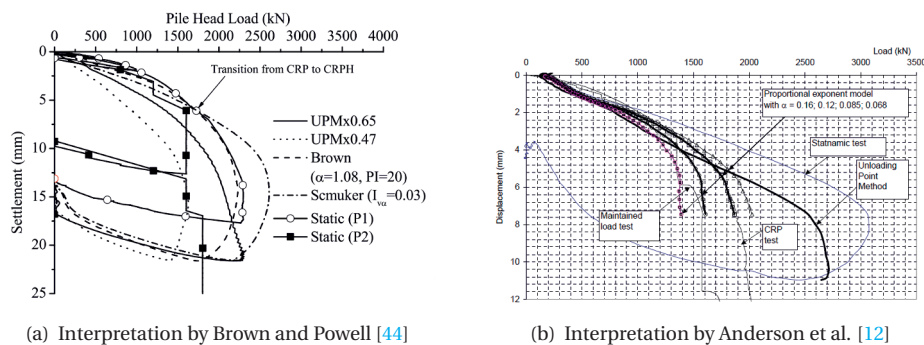


Figure 2.3: Interpretation of the rapid pile load test

The one-dimensional stress-wave model is based on the Smith stress wave equation used widely in the analysis of the dynamic pile load testing. The first attempt to analyse the pile response during a rapid test and to predict the pile capacity is credited to El Nagar and Novak [202]. In their approach, a one-dimensional model is used to represent the pile-soil system, and a signal matching analysis is used to achieve a satisfactory match between the computed and measured responses during the rapid test. The main soil parameters considered in the analysis are the shear modulus, the shear strength of the soil, the soil bearing at the tip and the damping factor.

Since the soil reactions to pile movement under transient loads are rather complex, the soil properties are adjusted iteratively during a signal matching analysis. The manual matching process is cumbersome even for an experienced engineer, therefore, an automatic matching technique is proposed by several authors [27, 84, 193, 200, 201, 230]. The combination of the one-dimensional stress-wave model and the automatic matching techniques represents an efficient tool to analyse the response of both rigid and flexible

piles during the static testing and calculate the pile capacity [84, 176] but critical review of the final solution by an experienced engineer is still recommended [201].

Finite element method is also used to analyse the rapid pile load test.

Horikoshi et al. [127] modelled a rapid pile load test in a soil deposit consisting of loam, clay and fine sand layers. The soil behaviour was assumed to be linear elastic, and soil parameters were taken from standard soil investigation. The shear modulus of soil was varied to find the best fit between the simulation and the rapid field test result of the pile head response; later this derived shear modulus was used in the static simulation to calculate the static capacity. Following this simple matching procedure, a reasonable estimation of the initial pile stiffness was achieved, but the ultimate pile resistance was not simulated due to the linear elastic model [127].

McVay et al. [178] simulated the static pile load test and the rapid pile load tests with variations of the load magnitude and duration. McVay et al. indicated that dynamic forces (i.e. damping, inertia) increase with an increase of the load magnitude or a decrease of the load duration due to higher particle velocities. For a load duration higher than 240 milliseconds, there is negligible difference between the dynamic and the static response.

Bakker et al. [17] performed a drained and undrained dynamic analysis of a rapid pile load test and indicated that rate effects can be partially explained by undrained behaviour of the soils and partially by soil mass moving with the pile. Those two phenomena need to be taken into account to get better agreement between numerical results and physical/field test.

It should be noted that simulations of the rapid pile load test, mentioned above, do not consider the rate dependency viscous behaviour of the soil. Moreover, the pore water fluid is not explicitly taken into account as a separate material but only implicitly through the undrained analysis.

2.3.3. INTERPRETATION WITH INFLUENCE FROM INSTALLATION METHODS

In practice, a difference in the bearing capacity and stiffness between displacement piles and non-displacement piles is found which actually comes from the pile installation process. In general, non-displacement piles have a lower bearing capacity as well as side friction compared to displacement piles because the installation of non-displacement piles weakens whereas the installation of displacement piles strengthens the surrounding soils [135]. Kulhawy [155] showed that the ratio of the coefficient of earth pressure over the coefficient of earth pressure at rest is about 0.75-2 for displacement piles and is about 0.7-1 for non-displacement piles. Fleming et al. [82] suggested that ratio for 'conventional' bored piles is about 0.7, for continuous flight auger piles is 0.6-0.9 and for cast-in-situ driven piles is 1.2. Numerous researches are investigating the influence of the installation process on the performance of the pile and the underlying mechanism of the installation process [2, 37, 67, 184, 245, 277-280, 296].

This section, however, is interested in the influence of the installation process on the comparison between the static pile load tests and the rapid pile load tests on granular soils. McVay et al. [178] proposed use of a resistance reduction factor ϕ_M to obtain the static bearing capacity of a pile from the rapid bearing capacity and recommended dif-

ferent values of ϕ_M for different soil types. Later, Hölischer and van Tol [121] realised the important influence of the installation methods and further suggested to use different values of R (similar to ϕ_M) for non-displacement and displacement piles. The static capacity is the multiplication of R with the rapid capacity. Reports on such data in the literature are summarised.

Fonseca and Santos [85] described an international prediction event on the behaviour of bored, CFA and driven piles field tests in the University of Porto. Soil properties at the site consist of fine to medium sand up to the depth of 20.3 m. The bored and CFA piles have a diameter of 60 cm, and the driven piles have a square section of 35×35 cm. All piles have an embedded length of 6 m. The static pile load test and the high strain dynamic pile load test are performed on three piles, one pile of a type. The bearing capacity is determined as the capacity at the displacement of 10% diameter. Results from load tests show that the reduction factor R for the bored and CFA piles is about 0.80-0.84 and for the driven pile is about 0.86.

McVay et al. [178] presented a database of rapid and static pile load testings on three types of piles namely drilled shafts (13-18 m length, 71-99 cm diameter), prestressed concrete piles (7-53 m length, 40-91 cm diameter) and steel pipe piles (11-38 m length, 33-78 cm diameter). The static capacity of piles is determined by the Davisson's method or the projected failure envelope estimation. The piles from McVay et al. data are founded in sand, silt, soft rock and clay; however, in this thesis only piles in sand and silt are of interest. McVay et al. summarised the R factor for drilled shafts in silt as 0.59-0.81 and in sand as 1.12, for driven piles in silt as 0.62-1.05 and in sand as 0.68-1.27. Examples of the interpretation of the rapid pile load test by the unloading point method with and without the reduction factor R taking into account the installation method to obtain the load-displacement curve of the static load test made by McVay et al. [178] in the ground of peat overlying silt sand with silt and clayey pockets, and Anderson et al. [12] in the ground of sandy clay, gravely clay and clay with gravel are given in Figure 2.3.

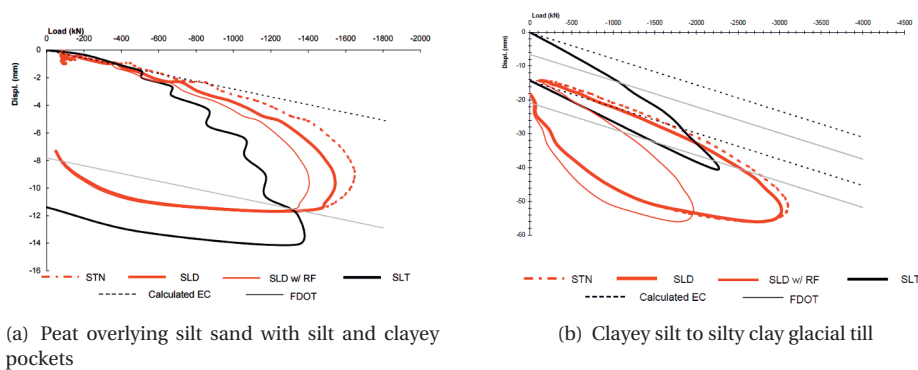


Figure 2.4: Interpretation of the rapid pile load test by McVay et al. [178] with and without the reduction factor R

Rahman et al. [228] studied the load and resistance factors from the data from pile driving analysers and static load tests of North Carolina Department of Transportation,

US. Three types of piles are considered: opened-end concrete piles with diameters of 1.4 and 1.7 m and wall thickness of 0.12 and 0.15 m, closed-end concrete square piles with the size from 0.3 to 0.5 m and steel HP piles with the size of 12×53 cm and 14×73 cm. All piles are driven piles and founded on cohesionless soil. All of the tests are non-failure tests, and the bearing capacity is determined by the Davission method. Data provided by Rahman et al. indicates the value of R for concrete cylinder piles is 0.72-1.55, for concrete square piles is 0.69-1.40 and for steel HP pile is 1.31-2.06.

Long [168] presented a database of pairs of rapid and static tests on bored piles around Ireland. The database focuses on medium-to-large diameter piles with a diameter varied between 300 mm and 900 mm. Most of the piles are constructed of concrete using the continuous flight auger (CFA) technique and are reinforced over their full length. The ground conditions comprise mostly medium dense to dense glacial and fluvioglacial gravels. The pile load of 0.5, 1.0 and 1.5 specified working load of typical 600-3000 kN are applied, the settlements of all tests are smaller than 10 mm. The average ratio of the settlement in the static test over that of the rapid test ranges from 1.14-1.25.

Hölscher and van Tol [121] extended the McVay database [178] with data from the field tests in sand reported by Holeyman and Charue [126], Middendorp [189], Opstal and van Dalen [211]. Hölscher and van Tol indicated the R factor is 0.77-1.06 for displacement piles in sand, 0.69-1.29 for drilled piles in sand.

Justin [146] reported the result of the pile load test obtained at a construction site at Ara Damansara (Selangor, Malaysia). The site condition is formed by two types of soil: sand in the top layer and very stiff or hard sandy silt in the next layer. The piles are concrete drill shaft piles with a diameter of 0.6 m and precast driven reinforced concrete square piles with a size of 0.4×0.4 m. All piles were not tested until failure, and the ultimate pile load capacity is interpreted by the Davission's criteria. For bored pile, 2 MLT results and 14 PDA results are obtained, the value of R varies from 1.0 to 1.1. For driven pile, 2 MLT results and 6 PDA results are obtained, the value of R ranges from 0.68 to 0.73.

Table 2.1: Ratio of the static capacity over the rapid/dynamic capacity

Author	Loading type	Bored/CFA/Drilled		Driven	
		Sand	Silt	Sand	Silt
Fonseca and Santos [85]	High strain dynamic		0.80-0.84	0.86	
McVay et al. [178]	Statnamic	1.12	0.59-0.81	0.68-1.27	0.62-1.05
Rahman et al. [228]	Pile driving analyzer			0.72-1.55 ¹	
				0.69-1.40 ²	
				1.31-2.06 ³	
Long [168]	Hammering	1.14-1.25 ⁴			
Holeyman and Charue [126], Hölscher and van Tol [121], Middendorp [189], Opstal and van Dalen [211]	Statnamic/Dynamic	0.69-1.29		0.77-1.06	

¹ opened-end, ² closed-end, ³ HP = H-section bearing piles, ⁴ R for displacement

Table 2.1 summarises ranges of the R factor for displacement and non-displacement piles in the literature. However, data from the literature is highly scattered due to a high

variety of loading types, soil conditions.

2.4. BEHAVIOUR OF DRY SAND DURING PENETRATION

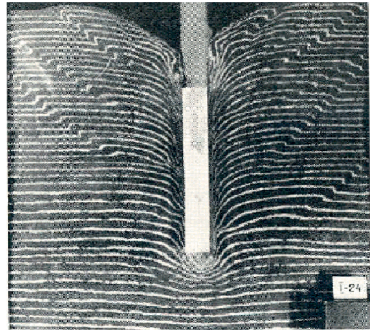
In the literature, numerous studies on the behaviour of granular soils during static penetration of an object such as a pile or a CPT has been conducted. These studies indicate that sand particles move differently depending on their relative location to the penetrometer. From the deformation pattern, zones of different behaviour (shearing, compression, dilation) around the penetrometer are located, the strain field can be identified, and the stress level can be estimated qualitatively. This section reviews some of the studies.

2.4.1. LITERATURE

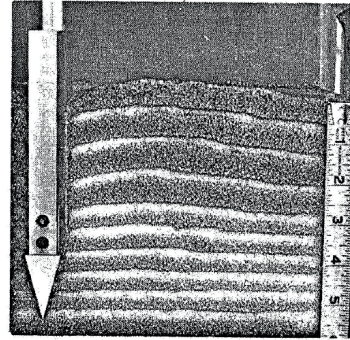
A series of model piles were installed by Berezantzev et al. [24] into layered sand without surcharging the soil. Berezantzev et al. indicate that the pattern of soil movement is a series of slip surfaces along the pile, see Figure 2.5(a). Similar experiments were conducted by Mikasa and Takada [194] in the 1-g test set-up and a centrifuge. At the 1-g state, the observation is similar to that of Berezantzev et al.; however, in the centrifuge, a confined penetration mechanism is revealed with compression around the pile tip. The confinement is pointed out due to the influence of the dilatancy behaviour which is significant under the high-stress level [129, 194].

Durgunoglu and Mitchell [70] conducted a static penetration test of a pile in dry sand in a plain strain configuration to investigate different failure mechanism. Based on photographs taken during the penetration, Durgunoglu and Mitchell suggested that there are many shear surfaces developed during penetration, Figure 2.5(b). The discontinuous, step-wise development of the shear surfaces is due to the fact that during the gradual increase of load on a soil, the shear strength is not immediately mobilised at all points on the potential slip surface, but initially only at the points where the shear stresses are the largest. From these points, the rupture gradually extends to other points along the slip surface, and further penetration is required in order to develop the full shear resistance of the soil along another shear surface.

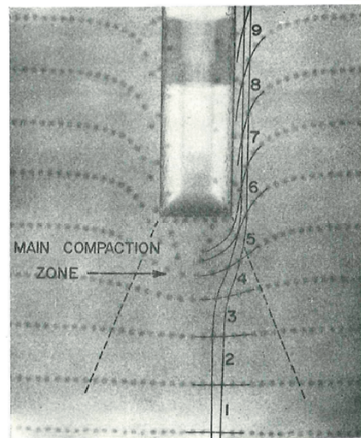
Robinsky et al. [234, 235] performed a jacked installation of a pile ($L/D = 16-17$) in dry silica sand with a relative density of 37% to 57% and used the X-ray method to track the movement of the lead shot markers embedded in the soil model. From the displacement vectors of the lead shot, contours of volumetric strain are deduced which indicate compressive volumetric strain of up to 11% under the pile tip and expansive volumetric strain along the pile shaft. A zone approximating the shape of a cone is found beneath the pile extending downwards and outwards from the edge of the pile, Figure 2.5(c). At the cone boundaries, vertical compression ceases, and vertical expansion begins to take place. The process of sand displacement and compaction below a pile is followed by sand movements adjacent to the pile shaft that decreases the sand density in the immediate vicinity of the pile shaft. The sand movements along the pile shaft reduce the angle of internal friction of a thin layer of soil in contact with the pile.



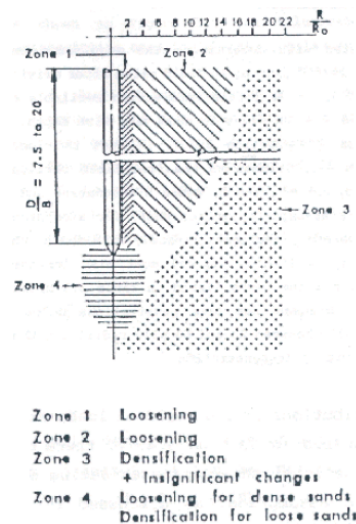
(a) Failure mechanisms at low stress, Berezzantzev [24]



(b) Failure surfaces, Durgunoglu and Mitchell [70]



(c) Slip lines and compaction zone, Robinsky et al. [234, 235]



(d) Changes in density, Chong [55]

Figure 2.5: Behaviour of dry soil during penetration

Chong [55] used a penetrometer ($L/D = 20$) equipped with thermal probes to measure density variations around a model pile penetrated into silica sand with a relative density of 40% to 80%. Four general zones of behaviour are identified by Chong as shown in Figure 2.5(d), however, this indication is not supported by quantitative measurements.

Allersma [9] penetrated an embedded model pile into crushed glass under a plane strain condition and employed a photoelastic method to observe the principal stress directions and calculate the strain field. The crushed glass flows around the pile tip at constant volume, with failure occurring by a wedge-type Prandtl mechanism. From the

observed results, the author proposed that the base capacity is governed by the peak friction angle, Figure 2.6(a).

The displacement around a pile in a plane strain model was investigated by Yasafuku and Hyde [297] using different coloured layers of sand. They found that the deformation zone under the pile tip resembles a spherical expansion in an infinite medium, Figure 2.6(b). Based on this observation, Yasafuku and Hyde propose that the cavity expansion theory is a suitable analytical method to predict the end-bearing capacities of piles in sand.

White et al. [277–280] used a novel deformation measurement system based on particle image velocimetry (PIV) and close-range photogrammetry to investigate the soil behaviour around the penetrating pile ($L/D = 20$) in a dry sand bed with a relative density of 34% to 55% in a plain-strain configuration. By comparing a series of adjacent images, the following measurements can be obtained:

1. soil displacement and strain paths,
2. streamlines of soil flow,
3. soil movement adjacent to the pile shaft.

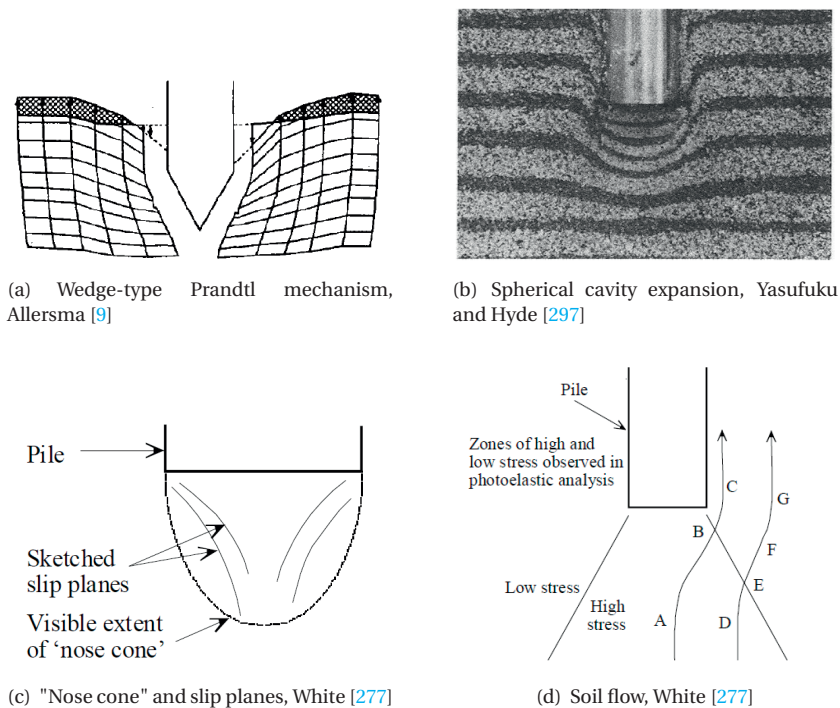


Figure 2.6: Behaviour of dry soil during penetration

White et al. [277, 278] reported that the deformation consists primarily of downward movement under the pile and of horizontal displacements in the far field. The displace-

ment vectors radiate from the pile tip downwards and to the side which suggests the penetration mechanism is more comparable to cavity expansion. The zone of downward displacement is concentrated closely around the pile shaft, whereas the horizontal displacement decays slowly with offset distance. A region of highly crushed soil (the "nose cone" similar to one of Robinsky et al. [235]) below the pile tip is observed in both sands of low and high crushing strength. Discrete slips of soil slides out from the nose cone and flow around the shaft of the pile, Figure 2.6c.

White [277] indicates that the soil that flows through the nose cone forms the interface layer adjacent to the pile shaft and follows streamline ABC and the soil in the near field follows streamline DEF, Figure 2.6(d). Along streamline AB, very high stress and very high shear strain are encountered, leading to volumetric compression and possible particle breakage. Along the streamline BC, significant volume compression continues, creating a net increase in density. High stress and high shear strains are encountered along streamline DE, resulting in compaction and some particle breakage. On leaving the zone of high stress, the soil is heavily over-consolidated and will dilate when it shears along streamline EF.

2.4.2. SUMMARY

During the penetration of a penetrometer at a low-stress level, the sand behaviour is governed by frictional strength, in which the arrangement of shear planes is influenced by the relative density and the angle of friction.

At the in-situ stress level, however, the sand behaves much more complicated since the influence of the dilatancy behaviour is much more significant. Under the pile tip, the existence of the main compaction zone (a nose cone) is clear, and inside that zone, the sand is mainly in compression. Sand particles flow around the nose cone and along the shaft to create zones of loosening soil. Further under the pile tip, about $2-5 D$, the sand is also mainly in compaction to create a high-stress zone. On leaving this zone, the soil will dilate.

2.5. BEHAVIOUR OF SATURATED SAND DURING PENETRATION

The behaviour of saturated sand during static penetration is expected to resemble the behaviour of dry sand since the loading rate is so small that the pore water has enough time to dissipate and causes no influence on the stress state or deformation of saturated sand. However during dynamic penetration, especially when the loading duration is faster than the consolidation duration of the soil, the interaction between sand particles and the pore water is significant, and the excess pore pressure builds up. This section presents some observations from the literature during dynamic penetration of an object in saturated sand.

2.5.1. LITERATURE

Clayton and Dikran [59] performed dynamic penetration tests with a penetrometer into saturated sands. The tests involved the driving over a distance of 100 mm of a 25 mm diameter, 200 mm length, 60° cone-ended penetrometer by repeated blows of a 10 kg weight falling 430 mm. Leighton Buzzard sand (fine sand with $d_{50} = 0.11$ mm) and Woolwich Green sand (well-graded gravelly sand $d_{50} = 1.0$ mm) are used. Figure 2.7(a)

presents a measurement of the excess pore pressure at position 1 on the penetrometer, during one blow loading, as a function of time. In the case of fine sand (Leighton Buzzard), the sand is initially sheared, and the excess pore pressure dissipates from overpressure (positive excess pore pressure). In the case of well-graded gravelly sand (Woolwich Green), the sand is initially compressed then sheared, and a decay of the negative excess pore pressure occurs at the end. Clayton and Dikran indicated that in both sands, the dilative behaviour occurs at the end of penetrometer motion. Figure 2.7(a) also shows that the maximum negative excess pore pressure measured during penetration also depends on the position of the transducer.

Yagi et al. [290] conducted dynamic and static penetration tests of a 60° , 2.66 cm diameter cone in loose and dense Toyoura sand ($d_{10} = 0.12$ mm). The cone is driven by dropping a weight of 3.88 kg from 24 cm height. Figure 2.7(b) shows typical changes of pore pressure measured at the cone base during a blow of the hammer. In the loose sand, just after the blow, an occurrence of a positive peak suggests compressive soil behaviour under the pile base. In contrast, in the dense sand a negative peak appears which indicates the dilative behaviour of the soil under the pile base. In the loose soil, a remarkable residual pore pressure occurs which, as Yagi et al. suggested, may be caused by repeated compression and shear of the soil around the tip due to repeated blows and by insufficient drainage in the duration of tenths of a second.

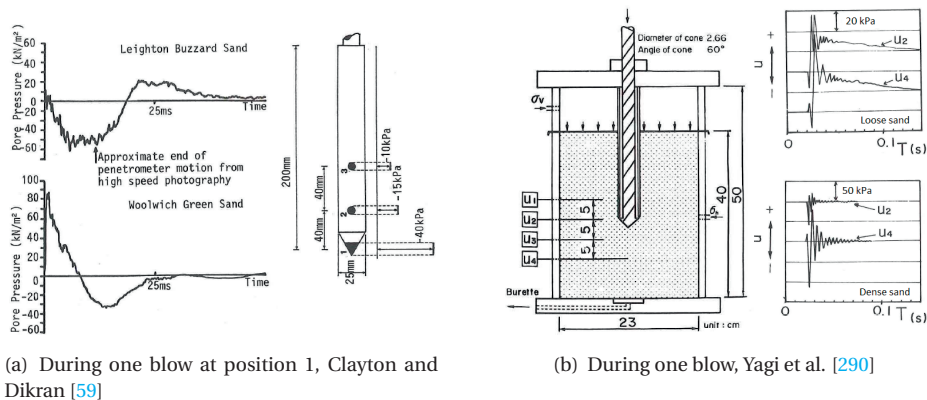


Figure 2.7: Behaviour of excess pore pressure during dynamic pile load tests

Hölscher and Barends [118] measured the excess pore pressure during pile driving and pile testing of a pre-fabricated reinforced concrete pile at the testing event of the stress wave conference 1992 in Delft, the Netherlands. The pile tip is located in a dense sand layer at the depth of 18.2 m. The pore pressure transducer is placed 0.5 m away and 0.2 m below the pile tip. Figure 2.8(a) shows the excess pore pressure as a function of time of the last driving blow. It is clear that the dynamic test and the statnamic test have a similar trend of the excess pore pressure response. As the pile is loaded, the soil is compressed which results in positive excess pore pressure; then dilation occurs resulting in extension of the soil which leads to negative excess pore pressure. In the statnamic

pile load test, the time for the excess pore pressure to dissipate is about 200 ms equal to the loading duration which indicates that the soil behaviour is partially undrained. The maximum negative pore pressure is about 170 kPa in the dynamic test and about 90 in the static test.

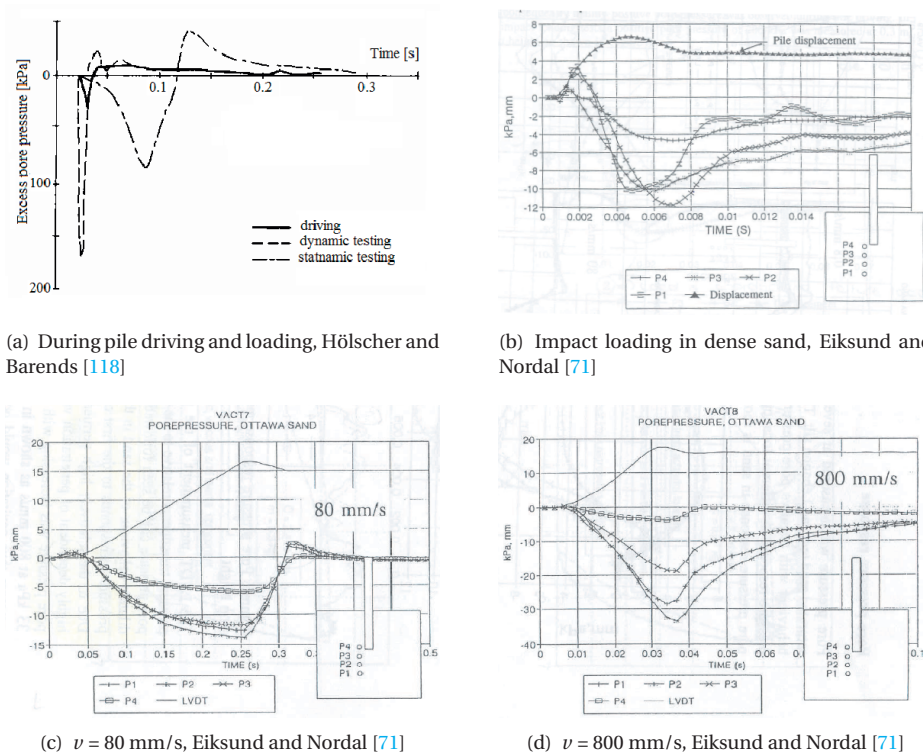


Figure 2.8: Behaviour of excess pore pressure during pile load tests

Eiksund and Nordal [71] performed a series of model pile tests at 1-g state with a measurement of the excess pore pressure close to the pile tip. The model pile is a closed end steel tube of 107 cm length, 63.5 mm diameter. The pile is driven with penetration velocities ranging from 0.8 to 1100 mm/s in a chamber which filled with Ottawa sand. Through measurements at different loading velocities, Eiksund and Nordal summarized the general tendency of the excess pore pressure as follows: initially the excess pore pressure increases to a peak positive value corresponding to the first compression wave from the pile tip, then large negative pore pressure follows caused by dilating behaviour of sand and this excess pore pressure increases back to a stationary situation from the under-pressure one, Figure 2.8(b-d). In some cases, when penetration stops, the pile may rebound which leads to contractive behaviour in the sand and some positive pore pressure occurs. The largest negative excess pore pressure measured at the highest loading velocity of 1100 mm/s is 30 kPa.

Nguyen [206] conducted a series of centrifuge model pile load test to investigate the

effects of the loading rate and the excess pore pressure by varying the loading velocity and the soil permeability on the rapid resistance of a pile, and deriving the static capacity from the rapid resistance at the unloading point. The model pile represents a prototype of 12 m length and 0.45 m diameter pile. The pile is jacked to a depth of $20 D$ into saturated Baskarp sand and is loaded statically and rapidly. Figure 2.9 presents the sketch up of Nguyen's experiment together with the measurement of the pile head displacement and the excess pore pressure during rapid loading. The excess pore pressure measurement is drawn at locations of the pore pressure transducers. A general trend is observed at the location of the pile tip and of transducer number 2 (wsm2) with positive excess pore pressure due to compression followed by negative excess pore pressure due to shearing and subsequently dissipation. At the location of the transducer number 1 (wsm1) however, a totally opposite reaction is observed due to the occurrence of a shear plane in front of the fixed transducer when soil particles slide around during the downward movement of the pile. At the location of the transducer number 3, it seems that the compression behaviour is dominant; the excess pore pressure reaches the maximum positive value and then dissipates. The maximum negative excess pore pressure is about 50 kPa in a dense sand test and about 100 kPa in a medium dense sand test at the highest loading velocity. Nguyen also found that the magnitude of the maximum/minimum excess pore pressure depends not only on the loading rate but also on the soil permeability. For the higher loading rate or the lower soil permeability, the magnitude is higher.

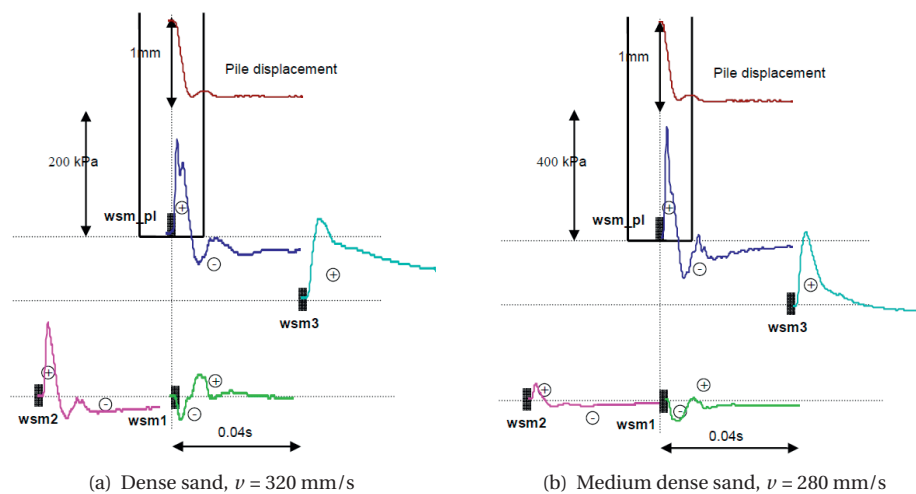


Figure 2.9: Behaviour of excess pore pressure during rapid pile load tests, Nguyen [206]

Hölscher et al. [122] reported two pile load field tests of a pre-fabricated reinforced concrete pile at Waddinxveen, the Netherlands. The pile length is 10.50 m with a cross section of $35 \times 35 \text{ cm}^2$ and the pile tip is located in a sand layer at a depth of around 10 m. The pore pressure transducers are placed one in the middle of the pile tip and one at around 0.3 m away and 0.05 m above the pile tip. Figure 2.10 shows the measurements of the excess pore pressure at the pile tip (with a legend of "toe") and in the soil (with a

legend of "soil"). The measurements at the pile tip are judged not reliable by Hölscher et al. because of two unexpected and unexplainable behaviours which are their lower peak values in comparison with the values of the measurements in the soil and their slow development in comparison with the loading time of the test. The measurements of the excess pore pressure in the soil are characterised by an initial increase up to 137 kPa due to the compression of the fluid, then an under-pressure of 80 kPa is observed apparently due to the shearing of the sand and dissipation.

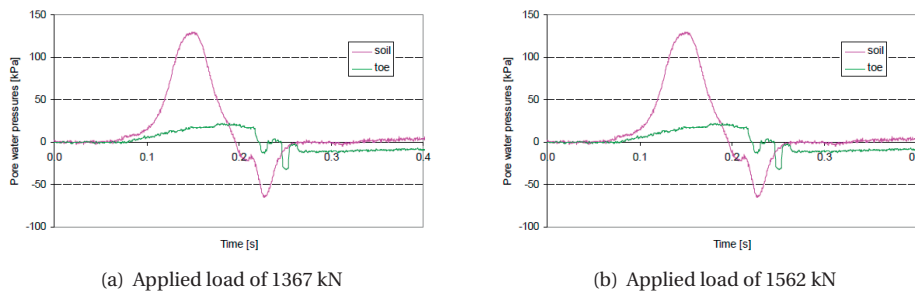


Figure 2.10: Behaviour of excess pore pressure during rapid pile load tests, Hölscher et al. [122]

2.5.2. SUMMARY

An axial force on the pile head results in a downward displacement of the pile, which will mobilise resistance of the soil to resist pile penetration. Consequently, the soil will be compressed and sheared. Depending on soil density, granular soils can respond with contractive or dilative shearing behaviour. Depending on the loading time and soil properties, excess pore pressure can build up and effect soil strength.

Based on the observations in the literature, the general behaviour of the saturated granular soil and the reaction of the excess pore pressure associated during dynamic penetration or pile loading can be summarised. For the soil at the tip of the penetrometer and/or the pile [122, 206]:

- As the pile goes down, the soil is initially compressed regardless of the soil density. Due to compression of the soil, initially pore pressure increases up to a maximum positive excess pore pressure. This positive excess pore pressure produces decreased effective stresses and hence a lower strength of the soil and the lower resistance of the penetrometer/pile.
- If the pile displacement is small enough that the pile motion stops or reverses before the shearing occurs then soil particles slowly rearrange themselves; consequently, the excess pore pressure dissipates to the static equilibrium from the positive excess pore pressure. The similar phenomenon happens when the loading duration is long enough that an arrangement of soil particles happens slower than the fluid flow.
- If the pile displacement is large enough that the shearing and dilatancy of the soil occurs and if the loading duration is short enough that an arrangement of soil particles happens faster than the fluid flow then the soil dilation leads to a reduction in

pore pressure. The excess pore pressure reduces dramatically to a maximum negative excess pore pressure which leads to decreased effective stresses and hence a higher strength of the soil and the higher resistance of the penetrometer/pile. Finally, the negative excess pore pressure dissipates to the static equilibrium.

For the soil at the pile shaft [71], when the pile is loaded, the soil is slightly compressed and then mainly sheared due to the dominance of the shearing and dilatancy behaviour. Consequently, the excess pore pressure, first, increases to a low-magnitude positive excess pore pressure, then, reduces dramatically to a high-magnitude negative excess pore pressure, and finally, dissipates to the static equilibrium from under-pressure.

The behaviour of the soil under the pile tip depends strongly on the loading mode at that location. If the soil is mainly in shearing, as in the location of P1-P3 in the experiment of Eiksund and Nordal [71], then the behaviour of the soil and the behaviour of the excess pore pressure associated are similar to those of the soil at the pile shaft. If the soil is mainly in compression, as in the location of wsm-3 in the experiment of Nguyen [206], then only the positive excess pore pressure is recorded and after the pile pulse, the excess pore pressure dissipates to the static equilibrium from over-pressure. If the soil is initially compressed and subsequently sheared, as in location of wsm-2 in the experiment of Nguyen [206], then the behaviour of the soil and the behaviour of the excess pore pressure associated are similar to those of the soil at the pile tip.

2.6. LOADING RATE EFFECT IN SAND

It is well known that when the rate of loading is increased the maximum bearing capacity can alter [267]. Therefore, it is important to investigate the possible influence of loading rate on bearing capacity. The loading rate here is defined by Whitman [281] as the relationship between the rapidity of loading and the shearing strength of a soil. By this definition, the loading rate effect is related to the constitutive behaviour of the soil.

In the literature, roughly two types of loading rate tests can be identified. The first one is the standard soil tests when the dependency of the soil strength on the loading rate is investigated by carrying out soil tests with higher loading rates. The second type is the soil-steel interface tests and the pile-soil interaction tests which are used to study the effect of the loading rate on the side friction and the tip resistance of a pile. This section summaries studies in the literature on the loading rate effect in sand.

2.6.1. INFLUENCE ON SAND STRENGTH

Casagrande and Shannon [49] were among the first to study the effect of strain rate on the shear strength of soil by performing triaxial compression tests on dry Manchester sand at confining pressures from 30 to 90 kPa with strain rates up to 115%/s. They concluded that the internal friction angle increases by 10% and the shear strength increases by 15% while the initial modulus of deformation remains constant.

Seed and Lundgren [247] performed drained and undrained triaxial tests on dense saturated sands at a confining pressure of 200 kPa with strain rates up to 1000%/s. Seed and Lundgren found that during transient drained testing, the pore water did not have sufficient time to drain fully, and consequently testing approached undrained conditions. This resulted in compressive strength increases of 35 to 40% in which 15-20% is

due to rate effect, and 20% may be related to the generation of negative pore pressures resulting from a tendency of the sand to dilate.

Whitman and Healy [283] performed drained (vacuum triaxial) and undrained tests on dense and loose sands at low confining pressures (70 kPa) and loading strain rates up to 500%/s. Whitman and Healy indicated that the drained shear strength increased by approximately 10% and the undrained shear strength increased 40-100% from the static value. They also suggested that the undrained shear strength varies with strain rate only when the excess pore pressures are time dependent. Healy [112, 113] conducted triaxial tests on saturated silty sand to study the dependence of dilation on shear strain rate and showed that sands expand more during rapid shear than during slow shear. This idea is confirmed by Whitman [282], and Whitman explained the increase of friction angle at very rapid strain rates on the basis that interlocking between particles becomes more effective when the particles are not given sufficient time to find the easiest path to pass one another. Whitman [282] conducted a triaxial test in loose saturated sand and reported an increase in strength of up to 200% for the strain rate of 1100%/s which is induced by the negative pore pressure as a consequence of dilatancy.

Schimming et al. [242] studied the loading rate effects on the shear strength of sand in a direct shear device. Dry loose samples, dry dense samples, and dense saturated samples were tested under three loading rates. Schimming et al. indicated that no rate effect was found on maximum shear resistance and friction angle of the tested sand, but the maximum shear resistance in the dynamic test on dense saturated sand was slightly higher than that of dense dry sand. Hungr and Morgenstern [137] also used the ring shear device to examine the behaviour of dry and wet Ottawa sand at high loading rate (0.1 cm/s and 98 cm/s) and different normal stresses (20 kPa and 200 kPa). In the range of test conditions, Hungr and Morgenstern also concluded that rate effects do not influence the shear strength and friction angle.

Gibson and Coyle [96] performed drained and undrained triaxial tests on fine and coarse saturated sands at the confining pressure of 100 kPa. Dynamic loading is presented by the falling of a dropping mass from varying heights generating different impact velocities from 0.2 to 3.5 m/s. Three types of sands are used in the tests which are Ottawa sand, Arkansas sand, and Victoria sand; they vary in grain size and angularity. Depending on the sand type, the shear strength at the loading velocity of 0.6 m/s is 40-100% higher than the static strength. As the loading velocity increases up to 3.5 m/s, the shear strength increases 20-50% more.

Lee et al. [164] performed drained dry and undrained triaxial tests on sand samples of different densities at low to moderate confining pressures (1.0 to 15 kPa) with strain rates up to 250%/s. Lee et al. found a nearly 100% increase in initial tangent modulus and a 7% increase in strength of loose sand at all confining pressures and of dense sand at low confining pressure. Dense sand at high confining pressure showed a 20% increase in strength. Lee et al. suggested that the difference in shear strength of tests in different densities and confining pressures is indicative of a change in the mechanism of shear strength mobilisation. The larger shear strength increases may be caused by the energy required for particle crushing.

Jackson et al. [140] presented an uniaxial response of three dry sands subjected to intense transient pressure loadings (10 MPa to 80 MPa) with various rise times (a few

tenths of a millisecond to a few minutes). Jackson et al. confirmed that loading rate had a relatively minor effect on the stress-strain response for loading times greater than 1 msec; however within the 0.1-1 msec rise time, secant modulus values at 10 MPa increase by an order of magnitude. They also noticed that the overall response changes in character as the loading rate is increased above 10 MPa/msec, the stress-strain curve rapidly shifted from "stiffening" (concave to the stress axis) to "yielding" (concave to the strain axis).

Akers [4] conducted uniaxial compression tests on partially saturated, poorly graded calcite sand to study the strain rate effects on the confined modulus. Akers showed that at the early stage of loading the static and dynamic tests have a similar stiffness; however, from approximately 1% strain, the dynamic tests begin to exhibit a higher stiffness. At the maximum strain rate of 50%/s, an increment of 60% is found for the dynamic modulus.

Farr [73] performed uniaxial tests on carbonate and quartz sand to investigate one-dimensional loading rate effects. The testing device is capable of producing a loading with a rise time from 0.0004 s up to 155 s. The soil sample cavity is 1.27 cm high and 9.65 cm in diameter. Farr showed an increase of 20 to 100% in elastic modulus with shortening loading time. Farr also observed that about 10-15% axial strain, the influence of rate effect on the modulus is insignificant.

Fukuoka [88] performed a high-speed high-stress ring shear tests on two types of saturated sand to investigate the variation of the friction angle during shearing. The soil sample has a diameter of 6 cm and a height of 6-8 cm. Available shear speed ranges between 0.001 cm/s and 150 cm/s. Fukuoka indicated that the friction angle during shear increases 2.5° for Toyoura sand ($d_{50} = 0.2$ mm) and 1.4° for Shirakawa river sand ($d_{50} = 1.4$ mm) when the shear speed was changed from 0.01 to 100 cm/s.

Yamamuro and Lade [294] conducted drained and undrained triaxial compression tests on dense sands at a confining pressure of 34.0 MPa with rates up to 0.74%/s. Yamamuro and Lade indicated a 2% increase in shear strength under compressive loading conditions during the drained tests and an increase of 7% during the undrained tests. In addition, an increase in strain rate leads to increasing dilatant tendencies. Moreover, grain size analysis indicated that reduced particle crushing is the mechanism for increased shear strength at greater strain rates. Yamamuro et al. [1, 292, 293] conducted a series of drained triaxial compression tests in loose and medium dense sand (relative densities of 36 and 58%) at two confining pressures of 100 and 350 kPa and strain rates up to 1760%/sec. Yamamuro et al. found the rate effects in the sand of 30% in shear strength, and of 100% in secant modulus. Moreover, with the increasing strain rates, the elastoplastic stiffness increases significantly of up to 115% more than static values), the maximum principal stress ratios increased moderately of up to 30%, and the volumetric strains become more dilatant.

Al-Mhaidib [7] performed a direct shear tests on dry sand ($d_{50} = 0.07$ mm, a relative density of 64%) to study the influence of shear rate on the friction angle. The shear apparatus has dimensions of 100×100 mm, the sand sample is sheared at different speeds from 0.0048 to 0.9 mm/min. The test results showed an increase of 6° for the internal friction angle of sand (from 38.7 - 46.5°) when the shear rate increases from the minimum to the maximum speed. Mhaidib also indicated an increase of about 7° for the friction angle between sand and smooth and rough steel surfaces with the same increase of the

shear rate.

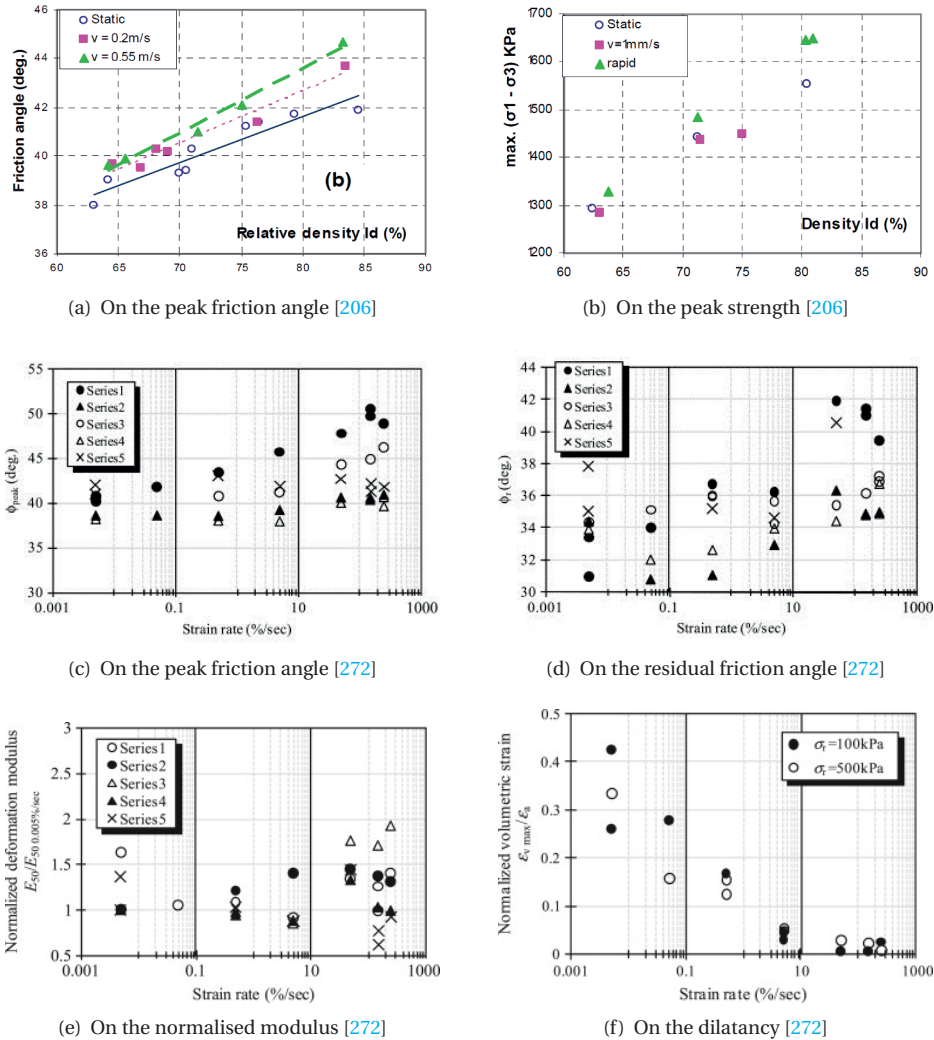


Figure 2.11: Loading rate effect in sand

Saito et al. [238] conducted an undrained ring shear test to study the relationship between the shear strength and the shear rate in saturated silica sand ($d_{50} = 0.04$ mm). The soil sample is set in a doughnut-like shape with the outer and inner diameter are 175 and 125 mm respectively. The sample is sheared at different rates from 0.1 mm/s up to 10 mm/s. During the test, the pore water pressure is measured. Saito et al. indicated that in slow shearing stages up to 0.1 mm/s, the pore water pressure increases with the shear displacement; however, in fast shearing stages larger than 1 mm/s, the pore water

pressure suddenly dropped to a negative value. Saito et al. indicated that at all shear rate stages, the friction angle of the soil sample is around 34° and thus the friction angle is independent of the shear rate.

Nguyen [206] conducted an extensive series of triaxial tests on dry and saturated Itterbeck sand to study the rate effect on the shear strength. The maximum loading velocity is about 0.6 m/s. Three different sand densities are tested, namely: medium dense (relative density of 60%), dense (70%) and very dense (80%). In the dry sand, Nguyen showed that the loading rate influences the peak friction angle (up to 3°) and the shear strength (up to 20%) and the influence is stronger with the higher relative density of the sample. In saturated sand, the peak strength derived from the rapid test is only 6% higher than the static value, however, Nguyen suggested that the true increment is higher because cavitation of the pore water might have occurred in the test which may interfere the true rate effect.

Omidvar et al. [210] performed a series of uniaxial compression and triaxial tests on dry sand at different loading rate to investigate the behaviour of sand under high strain rate loading. Omidvar et al. reported that when strain rate exceeds 10/s, significant increases of up to 30% in shear strength and more than 100% in dynamic modulus are found.

Watanabe and Kusakabe [272] performed a series of monotonically increasing triaxial compression tests on dry and saturated Toyoura sand to study the effects of loading rate on sand behaviour. The strain rate is varied in the range of 0.005%/s to 250%/s. Watanabe and Kusakabe indicated that the internal friction angle only increases about 7% for dry sand when the loading rate increases from the minimum to maximum value, but it can increase about 25% for saturated sand. The deformation modulus increases with increasing loading rate, for saturated sand the maximum increment is about 100%, and for dry sand the maximum increment is about 30%.

2.6.2. INFLUENCE ON PILE/PLATE/FOUNDATION RESISTANCE

Flemming [83] conducted a series of model pile tests in saturated sand to investigate the influence of loading rate on the skin friction of the pile. The loading velocity is varied from 0.003 mm/min to 100 mm/min. Flemming showed that the skin friction increases with increasing penetration rates, the maximum increment is found 20% for the tests of 100 mm/min, and the increment of 3-7% is found for the tests of 0.003 mm/min.

Vesic et al. [267] performed dynamic bearing capacity tests of a shallow foundation on dry and saturated sands with the loading velocity varies from 25.4×10^{-5} to 25.4 cm/s. The shallow foundation is a circular, rigid, rough plate having a diameter of 101.6 mm and resting on the sand surface. It is shown that first a decrease in bearing capacity of 30% (in comparison with the static bearing capacity) as the loading velocity increases up to 5.0×10^{-3} cm/s. However, when the loading velocity further increases up to 25 cm/s the dynamic bearing capacity slightly increases. In tests with dry sand, the bearing capacity in the fastest test is comparable with the static bearing capacity. In tests with saturated sand, however, the increment of the bearing capacity in the test with loading velocity of 1 cm/s is more than 30% higher than the static bearing capacity and is about several times higher in the fastest test. Similar results are reported by Whitman and Lascher [284].

Jezequel [143] performed an electrical cone penetrometer field test in medium dense silty sand with different loading velocities from 0.2 to 2 m/s. Jezequel showed an increase in total cone resistance of 7% for sand above the water table, and a decrease of 20% for submerged sand. Jezequel suggested that this is the influence of the "negative dilatancy" of the sand.

Dayal and Allen [64] studied the penetration rate effect on the strength of sand by constant velocity penetration tests performed with different velocities of 0.13, 1.18, 13.9 and 81.14 cm/s. The cone penetrometer has a diameter of 35.6 mm and an area of 10 cm² for the base and 150 cm² for the sleeve. During penetration, the cone resistance, sleeve friction, and penetration velocity were recorded. From the experimental results, Dayal and Allen indicated that for sands the effects of penetration velocity on the cone resistance and the sleeve friction are insignificant.

Heerema [114] performed a shearing test of a steel plate under constant normal stress at different velocities to study the influence of the horizontal stress and the pile velocity on the sleeve friction of a steel pile. This test can be classified in a middle position between a classical simple shearing test and a model pile test [53]. The velocities vary from 7×10^{-4} m/s to 0.6 m/s, and the horizontal stresses vary from 50 to 240 kPa. The tests performed on sands suggested that the sleeve friction is linearly dependent on the normal stress and independent of the loading velocity.

Kamp [147] presented results from a series of cone penetration tests with different penetration rates by Fugro in 1976 in Leidschendam, the Netherlands. The tests are taken to a maximum depth of 8.5m below ground level; the soil consists of medium dense to dense fine sand to that depth. A Fugro cone with electric friction side is used. The penetration rates applied are 0.2, 1, 10, 20 and 100 mm/s. Kamp showed that both the cone resistance and the local side friction increase with increasing penetration rate. In comparison between the test of 0.2 mm/s and the test of 100 mm/s, the increments are found 15% and 38% for the cone resistance and the side friction respectively. Kamp also reported results from other cone penetration tests by Fugro in the North Sea. A Fugro cone is penetrated into the very dense fine sand at the water depth of around 165 m. Different rates of penetration of 0.033, 2, 16, 17 and 20 mm/s are applied. The cone resistance of the test with 20 mm/s is about 15% higher than that of the test with 2 mm/s. Similarly, the cone resistances of the tests with 16 and 17 mm/s are about 10.5 and 12.5% higher than that of the test with 0.033 m/s.

Eiksund and Nordal [71] conducted dynamic pile load tests with loading velocities ranging from 0.8 to 1100 mm/s on Ottawa sand in a calibration chamber. The model pile of 107 cm length and 63.5 mm diameter is driven with different rate till the displacement of more than 20% pile diameter. The curve of pile resistance-displacement for different loading velocities shows no distinction for the tests with the loading velocity of 0.8 to 80 mm/s and an increase of less than 10% with a velocity of 1100 m/s.

Al-Mhaidib [6] performed static and dynamic pile load tests on a model pile in sand in a cylindrical tank at the 1-g condition. The model pile is made of steel, having a diameter of 30 mm and a length of 600 mm. The cylindrical tank has a diameter of 500 mm and a height of 700 mm. The soil is a poorly graded sand which is prepared at three densities as loose of 30%, medium of 55% and dense of 80% relative density. Al-Mhaidib indicated that the bearing capacity of the model pile increases with increasing the rate of loading

and the sand density has a strong influence on the relationship between the bearing capacity and the loading rate. The load-displacement curves for all tests indicated that as the applied loading velocities increase from 0.01 mm/min to 1 mm/min, the total pile resistance increases 80% for tests carried out in loose sand and 30% in medium and dense sand.

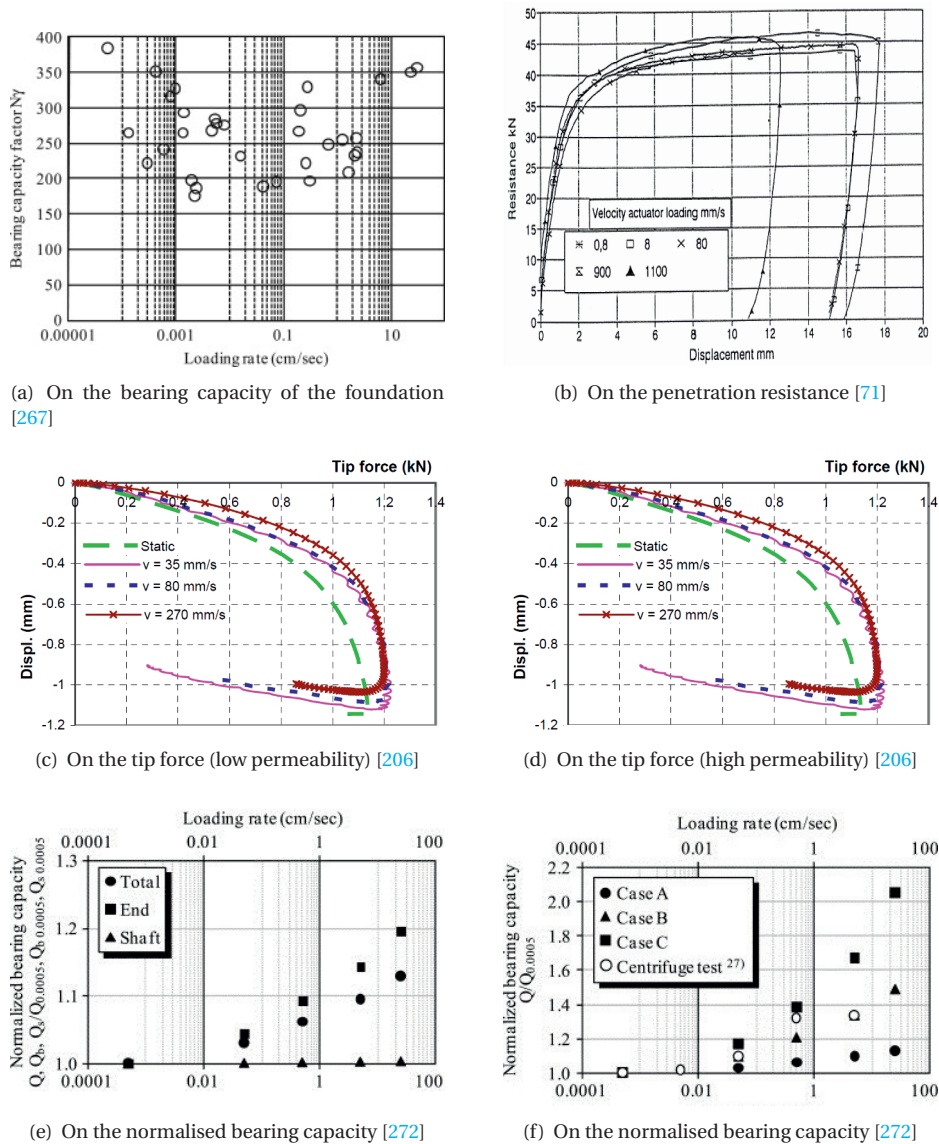


Figure 2.12: Loading rate effect pile/plate/foundation resistance

Bolton et al. [36] presented results from the cone penetration tests in dense Fontainebleau sand ($d_{50} = 0.22$ mm, relative density from 81-86%) in the centrifuge from five European centrifuge centres. The cone diameter is from 10 to 12 mm. They confirmed that small, and generally negligible, effects are observed in dry sand when increasing the penetration rate from 2.5 mm/s to 20 mm/s. Takemura and Kouda [254] studied results from the cone testings in dry sand in the centrifuge with the penetration rate from 0.17 to 2.7 mm/s and concluded that no apparent difference is observed.

Gennaro et al. [92] conducted a series of model pile tests in a calibration chamber to study the effects of the loading rate on pile resistance. A moderately-loose Fontainebleau sand is used. The instrumented pile features a diameter B of 20 mm and a height of 830 mm. The chamber is designed for the simultaneous and independent application of a vertical and horizontal pressure at the soil sample. Isotropic consolidation stresses of 100 and 200 kPa are applied. Loading velocities of 0.0017 to 1 mm/s are applied. Two ratios of embedded length L over pile diameter of 17.25 and 25 are tested. The tests results showed that there is an increase of the tip resistance with increasing loading velocity, the maximum increment is found to be 20-30% for a pile test with $L/B = 17.25$. The shaft friction, however, decreases with increasing loading velocity, the maximum decrement is found to be 30-40% for a pile test with $L/B = 25$.

Nguyen [206] presented two series of a model pile load test in a calibration chamber by Dijkstra [66] in unsaturated sand and by Archeewa [13] in saturated sand. The calibration chamber has a diameter of 1.9 m and a height of 3.2 m. The model pile is a Dutch standard penetration cone with a diameter of 36 mm, the point surface of 10 cm² and the sleeve area of 150 cm². The penetration rate is varied from 1 to 20 mm/s. The test results showed that the sleeve friction is independent of the penetration rate, the tip resistance is also independent of the penetration rate for the tests in saturated sand. In unsaturated sand, the tip resistance increases with increasing penetration rate; an increment of 20% is found between the tests of 1 mm/s and of 20 mm/s.

Nguyen [206] performed a series of static and rapid pile load tests in a centrifuge in drained and partially drained sand to study the effects of loading rate and excess pore pressure. The pile diameter is 11.3 mm, the loading velocity is varied from 23.5 to 320 mm/s with a loading duration from 50 to 10 ms. The test results showed that the pile resistance is higher during a rapid load test than during a static load test. Nguyen indicated that the increment of the rapid resistance over the static resistance is due to both rate effect and excess pore pressure effect. In general, for the tip resistance, the rate effect is about 10%, but there is no rate effect for the shaft friction.

Watanabe and Kusakabe [271] carried out a series of model pile load tests at a centrifuge acceleration field, with varying loading rate from 0.005 to 50 mm/s applied at the pile head. The test results showed an increase of the total bearing capacity as well as the stiffness at the pile head with increasing loading rate and the maximum increments of 50% and 80% are found for the bearing capacity and for the stiffness respectively.

2.6.3. DISCUSSION

The observations in the literature of the loading rate effect on sand strength from shear, uniaxial and triaxial tests can be summarised as in Table 2.2. The maximum rate is calculated in term of strain rate per seconds when possible for a better comparison. It seems

that the rate effect is more pronounced during the triaxial tests than during the shear tests since most of the results of the shear tests show no rate effect.

It is clear from Table 2.2 that the loading rate influences the sand strength and stiffness not only for saturated conditions when the interaction between sand and pore fluid exists but also for dry condition. For dry sand and for loading rates from 4% to 250% per seconds, the shear strength increases about 7-20%, the friction angle increases about 7-10% and the deformation modulus increases about 30-100%. For saturated sand and a loading rate from 0.12% to 1760% per seconds, the shear strength increases about 10-150%, the friction angle increases about 5-25%, the compressive strength increases about 35-40% and the deformation modulus increases about 20-100%.

Table 2.2: Loading rate effect on sand strength

Author(s)	Test	Sand sample	Max rate	Effect
Casagrande and Shannon [49]	triaxial	dry	115%/s	$\phi +10\%$, $\tau +15\%$
Seed and Lundgren [247]	triaxial	saturated	1000%/s	$E_c +35-40\%$
Whitman and Healy [283]	triaxial	saturated	500%/s	$\tau +10-100\%$
Schimming et al. [242]	shear	dry	n/a	no rate effect
Hungr and Morgenstern [137]	shear	dry, saturated	0.98 m/s	no rate effect
Gibson and Coyle [96]	triaxial	saturated	3.5 m/s	$\tau +40-150\%$
Lee et al. [164]	triaxial	dry	250%/s	$E_e +100\%$, $\tau +7-20\%$
Farr [73]	uniaxial	saturated	(155 s)	$E_e +20-100\%$
Fukuoka [88]	shear	saturated	2500%/s	$\phi +1.4-2.5^\circ$
Yamamuro and Lade [294]	triaxial	saturated	0.12%/s	$\tau +2-7\%$
Yamamuro et al. [1, 292, 293]	triaxial	saturated	1760%/s	$E_{50} +100\%$, $\tau +30\%$
Al-Mhaidib [7]	shear	dry	0.015%/s	$\phi +6^\circ$
Saito et al. [238]	shear	saturated	0.01 m/s	no rate effect
Nguyen [206]	triaxial	dry	4%/s	$\phi +3^\circ$, $\tau +20\%$
		saturated		$\tau +6\%$
Watanabe and Kusakabe [272]	triaxial	dry	250%/s	$\phi +7\%$, $E_{50} +30\%$
		saturated	250%/s	$\phi +25\%$, $E_{50} +100\%$

ϕ = friction angle, τ = shear strength

E_c = compressive strength, E_e = elastic modulus, E_{50} = deformation modulus

The loading rate effect on the pile resistance from five test types in the literature is summarised in Table 2.3. The maximum rate is normalised by the diameter of the pile for a better generalisation.

Although the loading rate has a strong influence on the sand strength, it seems that it has a small or negligible influence on the pile resistance in dry sand. The model pile test in dry sand of Al-Mhaidib indicating the loading rate effect is questionable because of the large deviation from the other authors as well as the very small rate of 55.7×10^{-5} D/s. The field penetration test in dry sand of Jezequel indicating the loading rate is also questionable because it is hard to have a dry layer of sand above a saturated layer, the dry layer might actually be in unsaturated condition.

The loading rate has a significant influence on the deep and shallow foundation resistance in saturated sand. In general, an increment of 10-80% is found for the total capacity of a model pile in a calibration chamber or in a centrifuge while an increment of several times is found for the capacity of the shallow foundation rested on the sand surface. The rate effect on the shaft friction has no general tendency due to missing of the literature or contradiction of the results from the literature, observations of an incre-

ment up to 38% as well as of a decrement up to 40% are found. The rate effect on the tip resistance is quite universal with an increment of 10% up to 30%. However, as all of the literature is for saturated sand, it is not clear if the excess pore pressure effect is totally excluded or not.

Table 2.3: Loading rate effect on pile resistance

Author(s)	Test	Sand sample	Max rate (D/s)	Effect Effect
Fleming [83]	A	saturated	0.042	friction +3-20%
Vesic et al. [267]	D	dry	2.54	no rate effect
Jezequel [143]	C	saturated	0.556	capacity +40%-several times
		dry		tip +7%
Dayal and Allen [64]	C	saturated	22.5	tip -20%
		n/a		no rate effect
Heerema [114]	E	n/a	n/a	no rate effect
Kamp [147]	C	saturated	2.85	tip +10-15%, side +38%
Eiksund and Nordal [71]	A	saturated	17.3	total +10%
Al-Mhaidib [6]	A	dry	55.7×10^{-5}	total +30-80%
Bolton et al. [36]	A	dry	2.08	negligible
Takemura and Kouda [254]	A	dry	2.7	negligible
Gennaro et al. [92]	A	saturated	0.05	tip +20-30%, shaft -30-40%
Al-Mhaidib [6]	E	dry	n/a	friction angle +7°
Dijkstra [66], Nguyen [206]	A	unsaturated	0.55	tip +20%
Archeewa [13], Nguyen [206]	A	saturated	0.55	no rate effect
Nguyen [206]	B	saturated	28.31	tip +10%
Watanabe and Kusakabe [271]	B	saturated	n/a	capacity +50%, stiffness + 80%

A = a model pile test in a calibration chamber, B = a model pile test in a centrifuge
C = field penetration test, D = shallow foundation, E = sand-steel friction

2.7. EXCESS PORE PRESSURE EFFECT IN SAND

From the literature, it is evident that excess pore pressure is generated during a dynamic and rapid pile load test in sand. Generally, due to the dilatancy of the sand, negative excess pore pressure is generated, that reaches the maximum magnitude depending on the loading rate and sand properties, and finally, dissipates in the consolidation time of the sand. In specific cases when the compression behaviour is dominant or when the soil still behaves elastically, only positive excess pore pressure occurs and which later dissipates.

The effect of excess pore pressure in the dynamic resistance of a pile in sand is reported widely in the literature. In general, there are two different mechanisms for the influence of the excess pore pressure on the dynamic resistance of pile in sand. The first mechanism is a direct one, in which the excess pore pressure under the pile tip contributes directly to the tip resistance of a pile. The second mechanism is an indirect one, in which the excess pore pressure alters the effective stress and hence the soil stiffness and strength of the soil surrounding the pile [59, 60, 195]; consequently, the pile resistance changes. Another possibility is that the change of the effective stress along the failure surface created around the pile during pile loading also affects the pile resistance [206]. This section describes these mechanisms.

2.7.1. DIRECT EFFECT

During rapid pile loading in the saturated soil bed, the water under the pile tip may contribute extra bearing capacity, especially in the undrained condition, since the water is incompressible. This might be true because the pore pressure under the pile tip is not negligible in comparison with the initial stress level at the pile tip. However, direct comparison of the magnitude of the excess pore pressure with the total stress under the pile tip during rapid loading in Nguyen [206] shows that the excess pore pressure has negligible influence because the magnitude of the excess pore pressure is less than 1% of the total stress.

2.7.2. INDIRECT EFFECT

During a study that focused on factors which influence the blow count of the standard penetration test (SPT), Mitchell et al. [195] concluded that the generation and dissipation of excess pore pressure during the SPT might have a major influence on the resulting blow count on two opposite ways. During driving, fine and loose sands generate significant positive excess pore pressures. This positive excess pore pressure results in a decrease of the effective stresses and hence the recorded blow count gives decreased values. But dilatant soils generate negative pore pressures which results in higher effective stress levels, therefore, the blow count yield increased values. Clayton et al. [59, 60] and Yagi et al. [290, 291] indicated the same conclusions based on their experiments of dynamic and static penetration tests of a cone in loose and dense sand. The conclusion that the effect of excess pore pressure on the dynamic resistance during SPT is due to changes in the effective stress levels directly under the tip which seems to be reasonable because their measured peak excess pore pressure is about 10-25% of the initial effective stress levels.

The same explanation was employed by Mes and McDermott [181] to explain the prevention of the large diameter open-ended pipe pile from further penetration into very dense silty sand although no measurement of the excess pore pressure is available. Morgano [199] also used that explanation for the increase of penetration resistance observed through a dynamic loading test on a closed-end steel pipe piles driven in medium loose to medium compact silty sand although no information on the excess pore pressure measurement is given.

In the practice of dynamic and rapid pile load testing, there are also reports on the influence of pore pressure changes on the resistance during loading. From the results of Eiksund and Nordal [71], Hölscher et al. [118, 120, 121], and Nguyen [206], it is clear that with the presence of the negative excess pore pressure, directly under or close to the pile tip, the dynamic resistance is higher than the static resistance. The explanation is as presented above.

Back in 1965, Vesic et al. [267] performed experiments to investigate the dynamic bearing capacity of footings in both dry and submerged sand. Vesic et al. found that for a footing in dry sand, there is not much difference in the bearing capacity at different loading velocities; however, for a footing in submerged sand, the bearing capacity increases quite significantly when the loading velocity increases from 2.54×10^{-4} to 25.4 cm/s. Vesic et al. claimed an increase of the bearing capacity in submerged sand due to the negative excess pore pressure which increases the shear strength of the sand.

Kutter [159] observed that negative pore pressures generated during shear make the undrained resistance greater than the drained resistance during dynamic pile load tests and plough pulling tests. As Kutter [159] stated that the observed phenomena of the stiffening/softening behaviour during dynamic loading are pervasive, but not well understood or explained. Based on large data sets of element tests (simple shear, cyclic triaxial, and torsional hollow cylinder tests), dynamic pile load tests, plough pulling tests, Kutter indicated that:

- shear-induced dilatancy of a saturated granular soil media tends to cause an increase of the mean effective stress which results in increased tangent shear modulus and hence increased shear resistance;
- contractive tendency results in a decrease of the mean effective stress which leads to a decrease of the tangent shear modulus and hence a decrease of the shear resistance.

SOIL STIFFNESS

In the literature, the influence of the effective stress level on the shear modulus of sands has been investigated extensively. Janbu [142], Duncan and Chang [69], Wroth et al. [289], Bellotti et al. [22] and Houlsby and Schnaid [130] studied the dependence of the elastic shear modulus on the mean effective stress and the density and concluded that the shear moduli increase with increasing mean effective stress and increasing density.

Hardin and Black [110], Lee et al. [162], Molenkamp [198] and Salgado et al. [239] performed the triaxial tests and bender element tests on Ottawa sand and crushed quartz sand to formulate a relationship between the shear modulus and the void ratio, the grain shape, the fraction of fine and the isotropic effective stress level. They observed a strong dependence of the shear modulus on the mean effective stress and the fine content.

Presti [221], Presti et al. [222] and Yamashita et al. [295] presented the results of drained triaxial compression tests, resonant column tests and torsional shear tests on three sands and connected the shear modulus and the secant Young's modulus with the relative density or the void ratio, the axial strain level, the stress ratio K_0 and the effective stress level. They indicated that the secant Young's modulus is significantly dependent on the effective stress levels and K_0 and the shear modulus is significantly dependent on the effective stress levels and the relative density or the void ratio.

Bødker [19] performed the bender element test for Baskarp and Lund sand and indicated that the maximum shear modulus G_{max} is primarily influenced by changes in the mean effective stress p' and slightly influenced by applying shear stress.

It can be concluded from the literature that the shear modulus and the secant Young's modulus are strongly influenced by the effective stress level. Presence of negative excess pore pressure increases the effective stress levels and hence apparently increases the modulus.

PILE RESISTANCE

The bearing capacity theory is based on the plasticity approach developed by Prandtl [220] and is developed further by many authors [182, 183, 257]. It is formulated that the bearing capacity of a foundation is a product of the overburden pressure at the base level,

the effects of the skin friction along the foundation shaft and the normal and tangential components of the stress along the failure surfaces created by the passive earth area.

The theory successfully predicts the bearing capacity of shallow foundations and is extended to deep foundation and cone penetration problems. That extension of the theory requires an assumption of a failure surface. There are several proposed failure mechanisms for the deep penetrometer which can be briefly described as following [70, 301]:

- the failure surface ends at the base level, Terzaghi [257];
- the slip surface develops widely and back to the shaft, Meyerhof [183];
- the slip surface ends under the base level, Berezantzev et al. [24] and Vesic [264];
- the failure surface develops vertically, Hu [133]

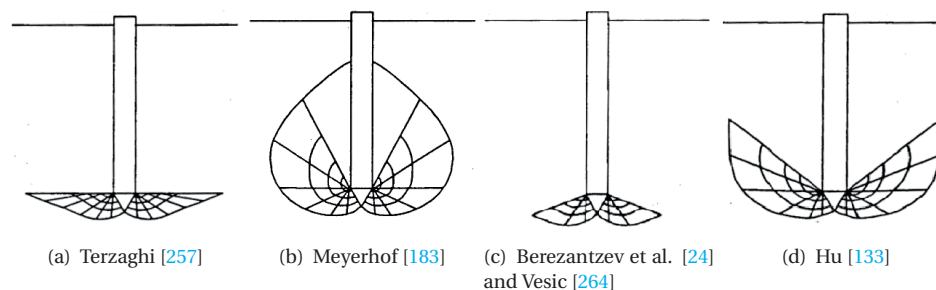


Figure 2.13: Proposed failure surface for deep foundations

The influence of excess pore pressure is then not limited to the stress level at the pile tip and shaft but also to the stress components along the failure surfaces or, more general, in the shearing zones. As Nguyen [206] pointed out, because of the ambiguity of the failure surfaces, it is generally impossible to provide a quantitative comparison of the magnitude of the stress level and the magnitude of excess pore pressure along the failure surfaces. Nguyen suggested that magnitudes of the initial stresses and the excess pore pressure would be in the same order, therefore, any difference in the excess pore pressure may cause the change in the stresses at the shearing zone and then the pile tip resistance.

2.7.3. SUMMARY

From the literature, it is clear that excess pore pressure has an influence on the dynamic and/or rapid resistance of a penetrometer by affecting on the effective stress right under the base level of the tip or on the stiffness and the shear strength of the soil around a penetrometer.

For the dynamic penetration problem of the SPT, the influence of the excess pore pressure is straightforward. An increase of the dynamic resistance over the static resistance can be explained directly by an increase of the effective stress right under the tip since the excess pore pressure is about 10-25% of the initial effective stresses.

For the rapid loading of a pile, the influence of the excess pore pressure is complicated. Since the excess pore pressure is less than 1% of the effective stress at the pile tip

level during the rapid pile loading, direct comparison of the excess pore pressure and the effective stress suggests no influence of the excess pore pressure [206]. However, there is numerous evidence in the literature on the effect of the excess pore pressure in increasing the rapid resistance over the static resistance [71, 120, 121, 206]. Explanations for this phenomenon can either be an increase of the effective stress inducing an increase of soil stiffness and strength [19, 59, 60, 290, 291] or an increase of the effective stress along the failure surface around the pile contributing to the pile resistance [206].

2.8. CONCLUDING REMARKS

The static pile load test is still the most reliable method to predict the bearing capacity as well as the load-displacement characteristic of the pile. In a case when the pile is not fully mobilised to show a clear ultimate bearing capacity, the bearing capacity at 10% of the pile diameter is used. The rapid pile load test is capable of predicting the static bearing capacity when the loading rate effect and the excess pore pressure effect are considered in a correct way.

The loading rate clearly influences the sand strength and stiffness in both dry and saturated conditions. The effect of the loading rate on the pile resistance founded in dry sand is negligible. For the piles founded in saturated sand, however, the effect of the loading rate is widely agreed to be significant on both the total bearing capacity and the tip resistance. The loading rate effect on the shaft friction, however, is not clear.

Excess pore pressure occurs during dynamic and rapid penetrations. In the dynamic CPT or SPT, the positive excess pore pressure directly under the penetrometer tip contributes to an increase of the dynamic resistance over the static resistance. In the rapid pile load test, although the excess pore pressure is significant compared to the initial effect stress at the pile tip level, it is insignificant in direct comparison with the effective stress during the rapid loading. However, accumulation of excess pore pressure along the failure surfaces around the pile may be the main reason for an increase of the rapid resistance over the static resistance. In order to gain more insight of the excess pore pressure effect on the pile resistance, experimental and numerical investigations on the evolution of the excess pore pressure inside the soil body and the influence of soil properties on the generation and dissipation of the excess pore pressure during the rapid pile load test are conducted. Chapter 3, 4 and 5 presents an experimental investigation in a centrifuge; chapter 6 and 7 present a numerical investigation using the finite element method.

The installation method may also influence the ratio of the static capacity over the rapid/dynamic capacity of a pile. The influence of the installation process is incorporated into the experimental and numerical studies of this thesis. Different approaches to simulate the effect of the installation process are discussed and presented in chapter 6 and 7.

3

PHYSICAL MODELLING

3.1. INTRODUCTION

This chapter discusses the physical modelling of the pile load tests in this study and then presents details of the setup. The small-scale model pile load tests are normally conducted using either the conventional 1- g configuration (g is the gravitational acceleration) or the centrifuge one, the N - g configuration. The main differences between those two configurations are the absolute stress level at the pile tip and the stress gradient along the pile shaft. The stress level at the pile tip can be easily replicated by a surcharge loading in the 1- g configuration; however, the surrounding stress level along the pile shaft, varying from zero at the ground surface to a few hundred kPa close to the pile base, can only be reproduced in the centrifuge configuration. These gravity effects are significant because the confining pressure, which is highly dependent on the stress level [69], governs the soil behaviour [253]. Because of the advantage on the stress scaling, the centrifuge configuration is employed in physical modelling of the pile load tests in this study.

As mentioned and proven in the literature, the loading rate effects have a substantial influence on the mobilised resistance of the pile during the rapid load test. Due to those effects, the pile resistance in the rapid load test is significantly higher than the pile resistance in the static load test. The increase of the pile resistance in the rapid load test depends strongly on the loading rate and on the drainage condition of the soil. In order to comprehend the influence of the loading rate and the behaviour and the effect of the excess pore pressure on the pile resistance during the rapid load test, experimental modelling of pile load tests was conducted in the geotechnical centrifuge at Deltares. In the experimental program, series of axial rapid pile load tests and, consecutively, axial static pile load test were performed in a saturated granular soil. Moreover, not only the loading rate was varied to investigate the loading rate effect but also the drainage condition was diversified by using different soil types and different fluid's viscosity to study the behaviour and the influence of the excess pore pressure.

In the experimental modelling, the first three series were conducted in 2007 and analysed in detail by Nguyen [206]. Afterward, six series are conducted in 2009 [169] and eight more series are performed in 2011 [205]; this thesis will present in detail the results

and interpretation of these fourteen series of pile load tests together with results from three series in 2007 of Nguyen [206]. This chapter will present the setup of the above mentioned seventeen series of pile load test. First, scaling laws and boundary conditions special for a pile-soil-fluid interaction problem are considered. Then the model setup with mechanical and material properties is described. Finally, the experimental program is given. The results of the physical modelling are presented in chapter 4 and analysed in chapter 5.

3.2. CENTRIFUGE MODELLING

3.2.1. MODEL SCALING

By using a centrifuge with a certain acceleration level, soil models placed in a container at the end of the centrifuge arm can be accelerated so that they are subjected to an inertial radial acceleration field stronger than earth's gravity. Soil held in a model container has a free upper surface, and within the soil body, the stress increases with depth at a rate related to the soil density and the magnitude of the acceleration field. For a centrifuge model subjected to an inertial acceleration field of N times earth's gravity the vertical stress at depth h_m will be identical to that in the corresponding prototype at depth h_p where $h_p = N \times h_m$ [255]; N is called the scale of an experiment. This basic scaling law of centrifuge modelling implies that the increment in vertical stress per scaled length in the model equals the increment of stress per length in the prototype and that the stress and the soil behaviour in a scaled model are expected to be identical to that in a prototype [244].

The scaling rules for basic quantities in physical modelling are well derived in the literature [91, 246, 255]; they are summarised in Table 3.1.

Table 3.1: Scaling rules for centrifuge modelling [90, 246, 255]

Parameter	Model	Prototype
Length/Displacement	N^{-1}	1
Velocity	1	1
Acceleration	N	1
Force	N^{-2}	1
Stress	1	1
Strain	1	1
Area	N^{-2}	1
Volume	N^{-3}	1
Density	1	1
Mass	N^{-3}	1
Stiffness	N^{-1}	1
Elastic moduli	1	1
Material damping	N^{-2}	1
Permeability	N	1
Time for dynamic events	N^{-1}	1
Time for consolidation events	N^{-2}	1

It can be seen from Table 3.1 that there is a difference in the time scale factors of the dynamic event N^{-1} (i.e. generation of excess pore pressure) and the consolidation process N^{-2} (i.e. dissipation of excess pore pressure). This inconsistency on the time

scale means that using the same soil and pore fluid in model and prototype is not suitable for simultaneous similitude of dynamic and consolidation events. In order to unify time scaling factors for dynamic and consolidation events, the consolidation process is slowed by reducing the permeability of the model soil N times [158]. This can be achieved by either increasing the viscosity of the fluid or by decreasing the particle size of the soil; however only the first option is suitable for modelling the pile load test since the second option raises issues associated with particle size effects [91, 158].

3.2.2. BOUNDARY CONDITION

This section summaries the scale effects arising from the relationship between the particle size of the soil, the diameter of the pile, the diameter of the container and the properties of the pore fluid.

RELATION OF SOIL, PILE AND CONTAINER

A further complication in geotechnical modelling is that a representative failure mechanism, which is represented by the width and the extent of shear and rupture bands in cohesionless soils, depends significantly on the grain size of the soil. The grain sizes used in the model correspond to much larger soil grains in the prototype; therefore, scaling of sand-size particles would require usage of clay-size particles, but these have significantly different constitutive characteristics [216]. In many cases, the same soils are used in the model as in the prototype.

By using the same soil with the prototype and a pore fluid with high viscosity, the requirement of scaling is satisfied. However, two other questions may arise. The first one is the influence of the model pore fluid on the mechanical properties of the soil; this question will be discussed in the next section. The second question is the dependency of the failure mechanism on the grain size of the soil or, in short, the grain size effect. In literature, many researchers examined the grain size effect on the problems of cone penetration testing, shaft friction mobilisation of piles and pile load testing in sand in both 1- g and centrifuge configurations.

Bolton et al. [35, 36, 103] investigated the grain size effect on the resistance of the CPT in granular soils with different mean grain size ($d_{50} = 220, 440$ and $900 \mu\text{m}$) in a centrifuge. They concluded that no effect of the grain size was found for the ratio of the pile/cone diameter (D) over the mean grain size of sand of larger than 30-50. Moreover, a requirement for the ratio of the container diameter (D_C) over D is necessary in order to avoid the wave reflection from the boundary of a container [206]. This ratio, however, depends on the velocity of the penetration, the loading duration of interest and the relative density of the soil bed [206]. For the CPT of Bolton et al. [35, 36] with the maximum velocity of 20 mm/s , a value of D_C/D_p larger than 20 is suggested.

Garnier and König [91], Foray et al. [86] and Fioravante [80] studied the shaft friction modelling of a model pile in dry sand in a centrifuge and concluded that a ratio of $D_p/d_{50} > 80-100$ allows the grain size effects to be minimized on a frictional interface between the pile and the sand.

De Nicola and Randolph [208] investigated the capacity and the plugging behaviour of a model pipe pile in silica flour ($d_{50} = 50 \mu\text{m}$) in a centrifuge. The model pile has the inner diameter D_i of 16 mm and the wall thickness t of 1 mm . In order to minimize the

scale effects, they concluded that the ratios $t/d_{50} > 9-10$ and $D_i/d_{50} > 200$.

RELATION OF SOIL AND FLUID

As mentioned before, if the same soil is used in a model and a prototype, the model pore fluid must have a higher viscosity than that of the prototype pore fluid. This approach is frequently applied in some different ways such as: using silicone oil [132, 151, 172, 302] or using water solutions with various chemical components [8, 65, 252]. Based on an extensive study, Allard and Schenkeveld [8] recommended the following requirements for an ideal substitute pore fluid:

- the model pore fluid should cover a wide range of viscosity and offer a density very close to the one of water, and the fluid must be chemically polar so it can be used with silts and clays;
- the constitutive behaviour of the soil with the model pore fluid in the centrifuge environment must be the same as the soil with water in the prototype, the soil-fluid interaction and the stress-strain properties of the soil must be preserved;
- the fluid must be non-toxic and soluble in water, the fluid must be stable, and the components should be readily available.

Although silicone oil is often used as a viscous pore fluid, there are a number of apparent drawbacks: (1) silicone oil is classified as hazardous; (2) its unit weight is significantly different from that of water depending on the grade of silicone oil used, therefore, necessitating corrections are required; (3) at a small hydraulic gradient, clogging of dense sand was observed with silicone oil [65, 132, 302]. On the other hand, a water solution with hydroxypropyl methylcellulose (HPMC) powder is also used frequently as a viscous fluid because HPMC solutions are available in a wide range of viscosity from 0-500 cSt (water has a viscosity of 1 cSt = 10^{-6} m²/s). However the saturation procedure of a sand sample with HPMC is much more time-consuming than silicone oil [132]; moreover, HPMC solutions exhibit non-Newtonian behaviour which makes the soil-fluid interaction is altered [8, 252]. Because of their disadvantages, both silicon oil and HPMC are not chosen for the pore fluid in this thesis. The viscous fluid used in this thesis was developed by Allard and Schenkeveld [8] and will be described in details in Section 3.3.2.

3.2.3. SUMMARY

A centrifuge configuration offers a good approach for scaling the stress field from a prototype to a model. There are several requirements for a proper centrifuge modelling of a dynamic pile-soil-fluid interaction problem.

In modelling a problem of pile-soil interaction, the scale effect and the grain size effect are proven to be important in reproducing the pile resistance and the shaft friction, a ratio of D_p/d_{50} be larger than 80-100 is required [36, 80, 86, 91]. For a problem with a pipe pile, the following requirements $t/d_{50} > 9-10$ and $D_i/d_{50} > 200$ are recommended [208].

In modelling a problem of coupled dynamic and consolidation events, there is a conflict in the time scale factors of the dynamic calculation (N^{-1}) and the consolidation analysis (N^{-2}). In order to unify the time scale factor, the most frequent used approach is increasing the viscosity of the pore fluid. Allard and Schenkeveld [8] recommended

several requirements for an ideal substitute pore fluid in which preservation of soil behaviour and soil-fluid interaction is of crucial.

3.3. MODEL SETUP

Details of the model piles and the model container are presented in this section. Information about the properties of the soils and the pore fluid are given. The sample preparation procedure is described.

The centrifuge modelling is conducted in the centrifuge of Deltares (formerly known as Geo-Delft). This is a 7-m beam centrifuge with a swinging platform mounted at the end of a horizontal beam. During the spinning up of the centrifuge, the platform moves from the horizontal position to the vertical in-flight position. An artificial gravitational level of maximum 300-g can be achieved at the maximum spinning speed; however, at this high acceleration level, a vacuum should be applied in the whole chamber test to reduce the frictional effect.

Due to the availability of the equipment, the acceleration level of 40-g is chosen for the experimental program.

3.3.1. MECHANICAL SETUP

The mechanical setup of the centrifuge modelling consists of a model pile, an assembly place to hoist the whole setup, a soil fill container, a loading system and other instrumentation and is the same as used in research in Nguyen [206]. Overview of the model setup is given in Figure 3.1.

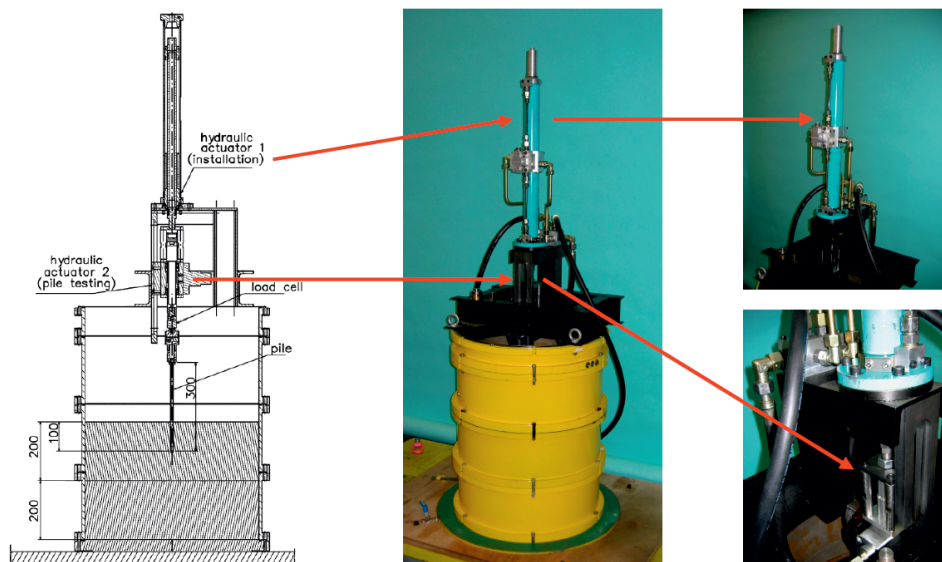


Figure 3.1: Mechanical setup of model tests [169]

ASSEMBLY PLATE

The assembly plate is the steel foundation plate for the model setup with a size of 1.92 m length, 0.92 m width and 5 cm thickness. This plate provides a firm foundation for the model setup and makes it possible to hoist the whole model setup in the centrifuge from the ground floor in the assembly hall.

MODEL CONTAINER

The model container is circular steel with the inner and outer diameters of 589 and 600 mm respectively and the height of 793 mm. The container consists of five steel cylindrical rings (one ring of 100 mm height and three rings of 231 mm height) assembled on one another by watertight connections using O-seals. Three model piles were used, see below. This container filled with soil is used in tests with pile A and C; in tests with pile B, an extra ring of 50 mm height is used to make the height of the container 843 mm. In the lowest of the three containers, watertight feeds are made for transducer cables inside the containers.

MODEL PILES

Three model piles, made of steel, are used in the experimental program. Characteristics of these three model piles are given in Table 3.2.

Table 3.2: Model piles used in the experiment

Parameter	Units	Pile A	Pile B	Pile C
Length	mm	300	300	320
Diameter	mm	11.3	16	11
Open-ended or Close-ended		Close	Close	Open
Wall thickness (for open-ended)	mm			0.5
Length in prototype	m	12	12	12.8
Diameter in prototype	m	0.45	0.64	0.44
Wall thickness (for open-ended)	m			0.02

The container-to-pile diameter ratios are 52 for pile A/C and 37 for pile B; and the ratios of the distance from the pile tip to the base boundary is 26 for pile A/C and 18 for pile B. These two ratios are satisfied to be free from the boundary effect on the penetration performance [36, 216].

All three piles are equipped with a load cell on the pile head to measure the applied load. The two close-end piles have a load cell on the pile tip to measure the tip resistance and a pore pressure transducer on the pile tip to measure the pore pressure directly below the pile tip. Details of the instrumentation are given later in this section.

LOADING SYSTEM

A loading frame is constructed to control the applied forces on the pile and is connected to the top of the soil fill container. The pile loading system and measurement devices are attached to the loading frame.

The loading system consists of two hydraulic actuators mounted in the loading frame. The first-large actuator is fixed on the loading frame and is used to install the pile to the

starting point before loading. The second-smallest actuator is fixed to the actuator rod of the first one and is used to perform pile load tests. The model pile and the small actuator are firmly connected before the spinning up of the centrifuge; they move together during loading. This type of connection contributes to the loosening of the soil along the pile shaft during the spinning up of the centrifuge. The fastest loading of the small actuator, which can be achieved, has a duration of 7.5 ms and a displacement of 5 mm.

MEASUREMENT SETUP

In order to investigate the load rate effect and the excess pore pressure effect, several quantities are monitored during pile load testing.

The loading process is displacement-controlled. During the tests, the displacement of the actuators is controlled through the servo-control system. The displacement of the large actuator is measured during the installation process of the pile. The displacement of the small actuator is measured during static and rapid pile load tests. Measurement of the displacement employs a transducer which is an integrated part of the servo-control system.

It should be mentioned that there are three different servo-control systems used in the rapid pile load tests in the year of 2007, 2009 and 2011; the different systems lead to some differences in the pile response during loading which will be pointed out later.

The applied force on the pile head and the reaction force on the pile tip are measured by two load cells, which are mounted at the pile head and are integrated into the pile tip, respectively. The load cells are a miniature force transducer U9B made by HBM Inc. with a calibrated working range of 0-10 kN and an accuracy of ± 0.007 kN.

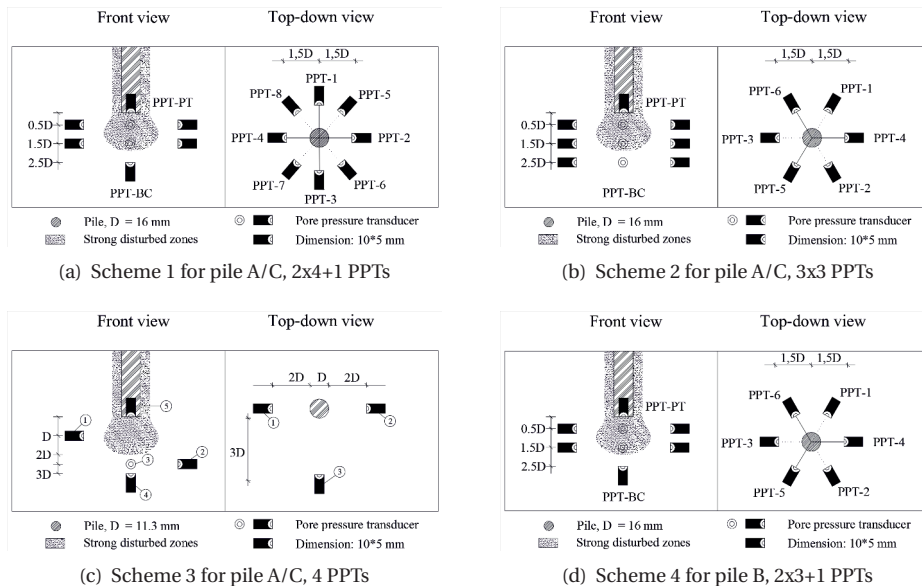


Figure 3.2: Locations of pore pressure transducers

The pore pressure at the pile tip is measured by an integrated pore pressure transducer (PPT) in the pile tip. Two types of PPT are used; the transducer PDCR 82 Druck type 1000 ± 0.26 kPa is used for Pile A (the close-ended pile with a diameter of 11.3 mm) and the transducer EBP-C1 AP.vd.Berg 1000 ± 0.25 kPa is used for Pile B (the close-ended pile with a diameter of 16 mm).

The pore pressure in the soil model is measured by four to seven pore pressure transducers of PDCR 82 Druck type. The PPTs are placed beneath and at the flank of the pile following four different schemes. The first scheme is used for two series in 2009, nine PPTs are installed in two layers of four PPTs and one more at the container bed, Figure 3.2(a). The second scheme is used for one series in 2009, nine PPTs are installed in three layers of three PPTs, Figure 3.2(b). The third scheme is used for three series in 2009, four PPTs are installed at different locations, Figure 3.2(c). The fourth scheme is used for eight series in 2011, seven PPTs are installed in two layers of three PPTs and one more under the pile, Figure 3.2(d).

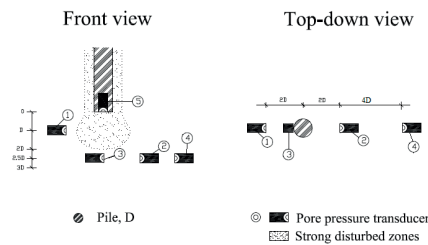


Figure 3.3: Locations of pore pressure transducers in Nguyen's tests - Scheme 5, 4 PPTs

The transducers are fixed to the bottom of the container by L-shape steel frames as shown in Figure 3.4.

In the interpretation of the experiments, the model tests of Nguyen [206] are also taken into consideration. In those tests, Nguyen used pile A, the same load cells and the pore pressure transducers of PDCR 82 Druck type. The installation of the PPTs in Nguyen's tests (scheme 5) consists of four PPTs installed at different locations, Figure 3.3. The transducers in Nguyen's tests are fixed by vertical steel rods to the container's bottom.

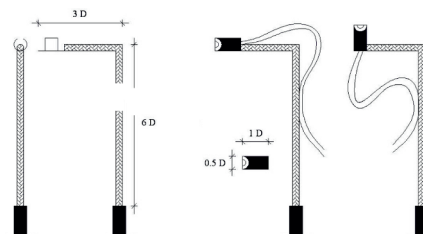


Figure 3.4: Steel stands of PPTs in 2009 and 2011 experiments

All of the pore pressure transducers have a filter at the head; the filter is a porous

stone disk for the PDCR 82 Druck, whereas the filter is a porous copper disk for the EBP-C1. The pore pressure transducers in the soil bed are always kept saturated with still water at the atmospheric pressure before and after the test. The pore pressure transducers at the pile tip is submerged in still water and subjected to a small amount of negative pressure (about -0.01 Pa) to maintain saturation before and after the test.

3.3.2. SAMPLE SETUP

SOIL

In the centrifuge pile loading tests, two types of soil are used, namely: Baskarp sand and silt. The grain size distribution and the classification parameters of Baskarp sand and silt, determined in Deltares laboratory [8], are shown in Figure 3.5 and Table 3.3.

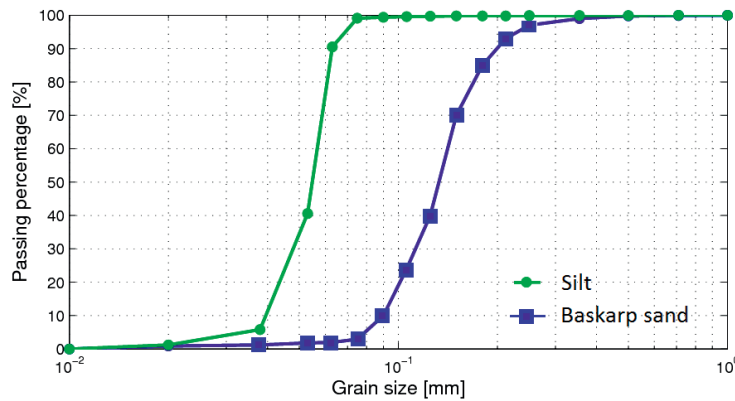


Figure 3.5: The grain size distribution of soils

Table 3.3: Parameters of soils

Parameters	Dimension	Baskarp sand	Silt
Density grains	kg/m^3	2.647	2.650
d_{10}	μm	90	
d_{50}	μm	130	58
d_{90}	μm	200	
Min. porosity	%	34	42.2
Max. porosity	%	46.9	53.9
Permeability at $n = 34\%$	m/s	6.5×10^{-5}	1.5×10^{-5}
Friction angle at $n = 40\%$	degree	41	38
Pile A: D_p/d_{50}		86	193
Pile B: D_p/d_{50}		123	276
Pile C: t_p/d_{50}		3.85	8.62

The pile diameter-to-mean grain size ratios are 86 in the sand sample and 193 in the silt sample for pile A and 123 in sand and 276 in silt for pile B. These two ratios are beyond the requirements to avoid the scale effects in modelling of the penetrometer resistance and the shaft friction [80, 86, 91].

In consideration of the requirement of De Nicola et al. [208] for the ratios of the inner diameter D_i and the wall thickness of the pipe pile t over the mean grain size of the soil d_{50} , the silt sample just satisfies with values of 178 and 8.6, respectively; while in the sand sample, values of those ratios are 79 and 3.9, respectively. Regarding the prototype, the test of the pipe pile with the silt sample is a normal application of an open-ended pile in a sea-bed sand, whereas the test with the sand sample is an extreme case in a fine gravel layer which sometimes happens in reality.

In order to check the wave reflection problem, Nguyen [206] conducted rapid pile load tests with pile A ($D = 11.3$ mm) and Baskarp sand in the same container and measured the pore pressure reaction. Nguyen reported that with a penetration rate up to 80 mm/s there is no evidence of wave reflection. There occurs wave reflection for a penetration rate up to 300 mm/s, but the tendencies of pile resistance development and pore pressure variation are the same. Therefore, Nguyen concluded that the reflected waves are small and can be neglected [206]. The wave reflection phenomenon will be checked later in this thesis.

PORE FLUID

Allard and Schenkeveld [8] developed a non-toxic water-based chemical solution (a mixture of water and sodium carboxymethyl cellulose). They conducted series of validation tests on this model pore fluid in both 1-g and centrifuge environment to extensively investigate its physical properties, permeability in soil, and responses in monotonic and cyclic triaxial loading conditions. Allard and Schenkeveld [8] concluded that:

- high accuracy, repeatability and stability are obtained in preparing the pore fluid and saturating soil samples;
- the intrinsic permeability κ of sand sample ($d_{50} = 130 \mu\text{m}$) is not altered by the model pore fluid, and there is no alteration of the sand behaviour due to the model pore fluid;
- for temperatures range from 10°C to 30°C (the minimum and maximum expected temperatures for a test run in the Deltares centrifuge under normal conditions), the density of the fluid can be considered as the one of water and the kinematic viscosity can vary from 1 to 300 cSt depending on weight percentage of water/chemical components in pore fluid.

The viscous fluid developed by Allard and Schenkeveld [8] is therefore suitable for the centrifuge pile loading tests and was used in this study.

During a rapid pile loading test in a saturated soil sample, the drainage condition has a significant influence on the mobilised pile resistance [118, 206]. The pile resistance increases when the drainage condition changes from drained to partially drained to undrained due to the existence of the negative excess pore pressure that increases the effective stress of the soil at the pile, tip [206]. The drainage condition is represented by a dimensionless parameter η , known as the drainage factor, which relates to a certain degree of consolidation during the loading period of the test [118]. The drainage factor is defined by Hölscher and Barends [118] as the ratio between the permeability over the critical permeability, the value which leads to 30% drainage during one hammer blow, as

following:

$$\eta = \frac{G \times T}{\gamma \times r^2} \times k = \frac{G \times T}{\gamma \times r^2} \times \frac{K \times g}{\nu} = \frac{G \times T}{\rho \times r^2} \times \frac{K}{\nu} \quad (3.1)$$

in which:

- G is the sand shear modulus [N/m²];
- T is the loading duration [s];
- γ is the volumetric weight of the pore fluid [N/m³];
- r is the pile radius [m];
- k is the hydraulic conductivity of the soil [m/s];
- K is the intrinsic permeability of the soil [m²];
- g is the gravitational acceleration, $g = 9.81$ [m/s²];
- ν is the kinematic viscosity of the fluid [m²/s];
- ρ is the mass density of the pore fluid [kg/m³].

Based on a series of centrifuge rapid pile loading tests, Nguyen [206] recommended that a value of 5 is considered as the boundary value between the partially drained and drained conditions; whereas the value of 0.01 is the boundary between the partially drained and undrained conditions.

Taking a loading duration of a rapid loading test, 100 ms, as the representative loading duration for the prototype rapid loading test, the loading duration of the model test should be 2.5 ms (with the chosen scaling factor of 40). However, the shortest duration that the actuator can achieve is 7.5 ms, which may have a significant effect on the drainage condition and consequently on the excess pore pressure effect during a model rapid pile test. In order to still stimulate the same drainage condition in the model, the viscosity of the pore fluid has to be increased three times which means the model pore fluid needs to be $3 \times 40 = 120$ times more viscous than water (or 120 cSt). Nguyen [206] argued that with the pore fluid viscosity of 120 cSt, the influence of the excess pore pressure is not significant; consequently, in order to study the excess pore pressure effect, he suggested to create a more-partially drained situation by increasing the pore fluid viscosity to 300 cSt. This recommendation is applied in Nguyen's experiment [206] and also in the experiment of this study.

SAMPLE PREPARATION

The granular soil sample is prepared by raining the soil with the drizzle method in a water container and compacting the soil with the shockwave compaction method; Rietdijk et al. [233] describe these two techniques in details. The combination of these two methods allows preparation of a high homogeneity soil bed with a relative density of $30\text{-}70\% \pm 0.5\%$ depending on the type of soil. After compaction of the soil sample, the water can be replaced by a viscous fluid with a viscosity of as high as 300 cSt. The main steps of the preparation procedure are:

- fill the container with de-aired water;
- shower the wet sand/silt under the water surface by a pumping system;
- wait till soil particles settle down, a very loose soil sample with a relative density of nearly 0% is created at the end of this step;

- lower down the water level until a height of several centimetres above the soil surface by gently sucking out the water from the top of the container;
- compact the whole soil package by impact - dropping the whole container from a height of several centimetres - until the required density is reached, let the water drain out both from the top and the bottom of the container;
- remove the top soil layer (about 10 - 15 cm) where the soil in this layer is less compacted and homogeneous than the soil in deeper depths;
- (optional) pump a viscous fluid in from the top and drain the water out from the bottom of the container, so the pore water is gradually replaced by the viscous fluid.

3.4. EXPERIMENT PROGRAM

3.4.1. LOADING SCHEME

The pile load tests in the experiments are displacement-controlled following the pattern shown in Figure 3.6. It should be noted that the loading pattern here is for the rapid load test with two branches of loading and unloading; the imposed displacement u can take different magnitude of up to 25% D ; the loading duration T of up to 50 [ms]. For the static load test, only the loading branch is applied with the imposed displacement $u = 10\%D$ and the loading duration $T = 676.6[s]$; therefore the static load test can be considered as the constant rate penetration (CRP) test.

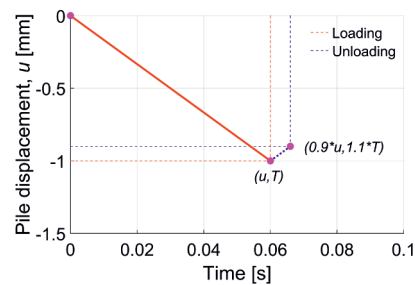


Figure 3.6: Displacement-controlled loading pattern in the pile load test

In all pile load test series, almost the same loading program is carried out. This loading program consists of seven stages:

- (1) the installation of the pile (for the pre-embedded pile, this stage is omitted),
- (2) the first four rapid pile load tests with the same loading duration T_1 [ms],
- (3) the first static pile load test,
- (4) the second four rapid pile load tests with the same loading duration T_2 [ms],
- (5) the second static pile load test,
- (6) the last four rapid pile load tests with the same loading duration T_3 [ms],
- (7) the last static pile load test.

The loading durations T_1 , T_2 and T_3 can be 10 ms, 20 ms or 50 ms.

In Nguyen's experimental program [206], the above loading program is used. Four different magnitudes of displacement are used in the rapid load tests as 1%, 2%, 5%

and 10% D . In the experimental program in 2009, with the intention of minimum disturbance for the first two rapid load tests, in the series of fast rapid load tests (loading duration of 10 ms), only two rapid load tests with displacements of 1% and 10% D are conducted. The average loading rates of rapid load tests v_{ave} in Nguyen [206] and in the 2009 [169] experimental program are presented in Table 3.4.

Table 3.4: Average loading rates of rapid load tests [% D /s] in Nguyen [206] and in the 2009 [169] experimental program

	Displacement [% D] Duration [ms]	1	2	5	10
Slow-rate, v_{ave}	50	20	40	100	200
Average-rate, v_{ave}	20	50	100	250	500
Fast-rate, v_{ave}	10	100	200	500	1000

After the experimental program in 2009, consideration of the average load rate in the rapid load test realises the similarity in the average load rate of the experimental program of Nguyen [206] and the one in 2009 [169] as shown in Table 3.4. In that table, cells with the same colour have comparable average load rates. In order to compare the effect of the same load rate at different displacements, especially at the large displacement when plastic deformation is expected, and the negative excess pore pressure is significant, the displacement magnitudes of the experimental program in 2011 are adapted. In the slow rapid loading series, the test of 2% D displacement is replaced by the test of 2.5% D displacement, the test of 25% D displacement is added; and in the average loading series, the test of 5% D displacement is replaced by the test of 4% D displacement. The loading rates of the experimental program in 2011 are given in Table 3.5.

Table 3.5: Average loading rates of rapid load tests [% D /s] in the 2011 [205] experimental program

	Displacement [% D] Duration [ms]	1	2	2.5	4	5	10	25
Slow-rate, v_{ave}	50	20		50		100	200	500
Average-rate, v_{ave}	20	50	100		200		500	
Fast-rate, v_{ave}	10	100	200			500	1000	

Details of the applied velocity and loading duration of all rapid and static tests following the loading scheme of Nguyen's experimental program [206], the experimental program in 2009 [169] and the experimental program in 2011 [205] are given in Appendix A.

3.4.2. EXPERIMENT PROCEDURE

The procedure of each centrifuge load test consists of five phases as following:

Phase 1: preparation

- assemble the soil container and pore pressure transducers,

- assemble the soil container and pore pressure transducers,
- mount the pile and the pile-frame,
- prepare the soil sample following the drizzle method and the impact compaction method,
- replace the water with the viscous fluid if required (tests in Baskarp sand).

Phase 2: before starting

- hoist the soil container into the centrifuge container,
- connect the electrical and hydraulic system,
- connect the plungers to the pile,
- unmount the pile-frame,
- start registration,
- record "zero-value" of all transducer.

Phase 3: spinning up

- spin up the centrifuge,
- gradually rotate the centrifuge container to the horizontal position and fix the centrifuge container,
- keep the spinning velocity of 79.43 rpm (which is equivalent to the gravitational level of 40-g),
- check for the steady state of all transducers.

Phase 4: performing test

- install the pile to the final depth if required (with the jacked-in installation),
- unload the pile by reducing a displacement of the pile until the pile head force is approximately 0 ± 0.01 kN,
- perform the loading scheme **Appendix A**.

Phase 5: spinning down

- spin down the centrifuge to 45 rpm,
- release the container fixation,
- spin down the centrifuge to halt,
- stop data acquisition,
- disconnect the electrical and hydraulic systems,
- unhoist the soil container.

3.4.3. VARIATIONS

There are several variations of the boundary condition of the experiment of Nguyen [206], the experiment in 2009 [169] and the experiment in 2011 [205]. They are as following:

- two types of the pile installation method, namely jacked-in and pre-embedded;
- three types of the material combinations, namely sand and viscous fluid, silt and water and sand and water;
- four relative densities of the soil, namely: loose 36%, medium dense 45%, medium dense 54% and dense 65%.

3.5. SUMMARY

This chapter presents the detail information on the setup of seventeen pile loading test series conducted in the geotechnical centrifuge at Deltares.

Table 3.6: Properties of performed centrifuge testes

Series	Year	Soil type	D_r [%]	Fluid type	Installation	Pile type	D [mm]	PPTs installation
2	2007 ¹	Sand	54	Viscous	Jacked-in	Close-ended	11.3	Scheme 5
3	2007 ¹	Sand	36	Viscous	Jacked-in	Close-ended	11.3	Scheme 5
4	2007 ¹	Sand	65	Water	Jacked-in	Close-ended	11.3	Scheme 5
11b	2009 ²	Sand	65	Viscous	Pre-embedded	Close-ended	11.3	Scheme 1
11j	2009 ²	Sand	65	Viscous	Jacked-in	Close-ended	11.3	Scheme 1
12	2009 ²	Silt	65	Water	Jacked-in	Open-ended	11.0	Scheme 3
14	2009 ²	Silt	65	Water	Jacked-in	Close-ended	11.3	Scheme 3
15	2009 ²	Sand	65	Viscous	Pre-embedded	Close-ended	11.3	Scheme 2
16	2009 ²	Sand	65	Water	Jacked-in	Open-ended	11.3	Scheme 3
21	2011 ³	Sand	65	Viscous	Jacked-in	Close-ended	16.0	Scheme 4
22	2011 ³	Sand	65	Viscous	Pre-embedded	Close-ended	16.0	Scheme 4
23	2011 ³	Sand	45	Viscous	Jacked-in	Close-ended	16.0	Scheme 4
24	2011 ³	Sand	45	Viscous	Pre-embedded	Close-ended	16.0	Scheme 4
25	2011 ³	Sand	65	Viscous	Jacked-in	Close-ended	16.0	Scheme 4
26	2011 ³	Sand	65	Viscous	Pre-embedded	Close-ended	16.0	Scheme 4
27	2011 ³	Silt	65	Water	Jacked-in	Close-ended	16.0	Scheme 4
28	2011 ³	Silt	45	Water	Jacked-in	Close-ended	16.0	Scheme 4

¹ Nguyen [206], ² [169], ³ [205]

Among the seventeen series of pile load tests, the first three series, namely series 2, 3 and 4, were performed in Nguyen's research [206]. The remaining series were conducted in this study, the first six series were performed in 2009 [169] and the last eight series were performed in 2011 [205]. All of the pile load series were executed under the gravitational level of 40-g. The Baskarp sand and silt are used as a soil material. De-aired water and the viscous fluid with the viscosity of 300 cSt are used as a fluid material. Table 3.6 summarises properties of the entire pile load series performed. The measurement data and the details on the performance of each centrifuge test series can be found in the corresponding factual report [169, 205]. In the series 11 to 16, the tip reaction force measurement is missing. In the series 21 and 22, because of missing information of PPT-PT and FPT during the slow loading series, the series was halted and the instrumentation is fixed. After that the series continued with the average and fast loading series, and the slow loading series was performed again at the end of the test.

4

PHYSICAL MODELLING - RESULTS

4.1. INTRODUCTION

In this chapter, the experimental results from the physical modelling are presented. First, the load-displacement relationship from the static load tests and the rapid load tests are given in section 4.3 and 4.4. Due to the large numbers of the rapid load tests, only typical results are presented. The full report of the static and rapid load tests can be found in the following documents [169, 205, 206]. Then, the behaviour of the excess pore fluid pressure corresponding to each loading velocity and each magnitude of imposed displacements is investigated in details in section 4.5. The repeatability of the tests is analysed in section 4.6 based on several pairs of identical tests which were conducted. The loading patterns applied and their corresponding load-displacement responses are discussed in section 4.7. Finally, concluding remarks on the experimental results are given in section 4.8.

It should be mentioned here that the presented results of force, pressure, displacement and time in this chapter and Chapter 5 are in the model scale which are directly measured or derived from measured values at the acceleration level of 40 times the gravitational level. The values in the prototype scale can be found by scaling up with appropriate scaling factors from Table 3.1.

4.2. DERIVATION AND NOTATIONS

During the rapid load test, the pile can be considered as a rigid body as argued by Middendorp [191], so the applied (measured) force or the rapid pile force (F_{rap}) is equal to the sum of the soil force and the inertia force of the pile. Therefore, the soil force can be calculated as:

$$F_{soil} = F_{rap} - F_{inertia} = F_{rap} - M \times a \quad (4.1)$$

where M is the pile mass and a is the pile acceleration. The soil force is composed of the static force, the damping force and the pore pressure force [191] as follows:

$$F_{soil} = F_{static} + F_{rate} \quad (4.2)$$

The static force F_{static} is actually the sum of the pile shaft friction and the pile tip resistance. The force F_{rate} considers the penetration rate effect, which actually consists of

the pore pressure effect F_{pwp} , the constitutive rate effect F_{const} , and the damping effect F_{damp} . The pore pressure effect concerns the presence of the negative and/or positive excess pore pressure which affects the effective stress [282]; whereas the constitutive rate effect relates to the interlocking of the soil grains, which increase the soil strength during rapid loading [281]. The damping effect takes into account the influence of the velocity of the pile and can be computed $F_{damping} = C \times v$ in which C is a damping ratio and v is the pile velocity. These two effects, the constitutive rate effect and the damping effect are hardly distinguished, therefore they will be considered as one otherwise it will be stated.

In chapter 4 and 5, two values of the rapid pile force are considered which are the maximum value, F_{max} , and the value at maximum displacement or the so-called unloading point, F_{up} . The two factors R_{max} and R_{up} are then defined [206] as the normalisation of the maximum force and the unloading point force, respectively, by the static force F_{static} at the same displacement:

$$R_{max} = \frac{F_{max}}{F_{static}} \quad R_{up} = \frac{F_{up}}{F_{static}} \quad (4.3)$$

The velocity and acceleration of the pile are calculated numerically as the first and second derivative of the measured pile displacement as follows:

$$v_i = \frac{u_{i+1} - u_i}{\Delta t} \quad a_i = \frac{u_{i-1} - 2 \times u_i + u_{i+1}}{\Delta t^2} \quad (4.4)$$

with u_i is the displacement at the time step i and Δt is the time increment between two consecutive recorded data.

In chapter 4 and 5, there are some other notations which are used in tables or figures as:

- PLT : the pile load test series
- SLT : the static load test
- RLT : the rapid load test
- PPT : the pore pressure transducer
- FPH : the pile head applied-force which is a measured quantity minus the pile inertial force
- FPT : the measured pile tip reaction-force
- FPS : the derived pile shaft force, $FPS = FPH - FPT$
- Displ, Velo, Acce : the measured displacement and derived velocity and acceleration of the pile head

As mentioned in Section 3.4, in each pile load test series, there are seven stage of loading with maximum fifteen pile load tests. The notation of those tests are given here to assist the reader. Let's consider the series number 2 of the close-ended pile, $D = 11.3$ [mm], installed by the jacked-in method in the sand and viscous fluid soil bed with the relative density $D_r = 54\%$, the loading stages in this series are notated as in Table 4.1/. Table 4.2 summarises properties of all centrifuge pile load tests performed in Deltares geo-centrifuge. All pile load tests are grouped in the order of the installation method

(column 1), the pile type and diameter (column 2 and 3), the soil type and relative density (column 4 and 5), the pore fluid type (column 6), the number of PPTs (column 7). Two last columns give the number of tests and the year of performing. Of 17 tests, tests 2 to 4 were conducted by Nguyen [206] and used here as a reference and for comparison.

Table 4.1: Loading stages for the series 2: Sa 54 Vi J C 11.3

Stages	Tests	Remarks
1	Installation	No notations
2	Rapid loading 1 R-2-1-1% D R-2-1-2% D R-2-1-5% D R-2-1-10% D	Slow-rate loading Maximum displacement of 1% D Maximum displacement of 2% D Maximum displacement of 5% D Maximum displacement of 10% D
3	S-2-1	Static loading 1, displacement of 10% D
4	Rapid loading 2 R-2-2-1% D R-2-2-2% D R-2-2-5% D R-2-2-10% D	Average-rate loading Maximum displacement of 1% D Maximum displacement of 2% D Maximum displacement of 5% D Maximum displacement of 10% D
5	S-2-2	Static loading 2, displacement of 10% D
6	Rapid loading 3 R-2-3-1% D R-2-3-2% D R-2-3-5% D R-2-3-10% D	Fast-loading rate Maximum displacement of 1% D Maximum displacement of 2% D Maximum displacement of 5% D Maximum displacement of 10% D
7	S-2-3	Static loading 3, displacement of 10% D

Table 4.2: Properties of performed centrifuge testes

Installation	Pile	D [mm]	Soil	D_r [%]	Fluid	PPTs	Test	Year	Notation	
Jacked-in	Close-ended	16	Sand	65	Viscous	2 x 3 + 1	21	2011	Sa 65 Vi J C 16	
		16	Sand	65	Viscous	2 x 3 + 1	25	2011	Sa 65 Vi J C 16	
		16	Sand	45	Viscous	2 x 3 + 1	23	2011	Sa 45 Vi J C 16	
		11.3	Sand	65	Viscous	2 x 4 + 1	11j	2009	Sa 65 Vi J C 11.3	
		11.3	Sand	54	Viscous	4	2	2007	Sa 54 Vi J C 11.3	
		11.3	Sand	36	Viscous	4	3	2007	Sa 36 Vi J C 11.3	
		11.3	Sand	65	Water	4	4	2007	Sa 65 Wa J C 11.3	
		16	Silt	65	Water	2 x 3 + 1	27	2011	Si 65 Wa J C 16	
		16	Silt	45	Water	2 x 3 + 1	28	2011	Si 45 Wa J C 16	
	11.3	Silt	65	Water	4	14	2009	Si 65 Wa J C 11.3		
	Open-ended	11.3	Sand	65	Water	4	16	2009	Sa 65 Wa J O 11.3	
		11.3	Silt	65	Water	4	12	2009	Si 65 Wa J O 11.3	
	Pre-embedded	Close-ended	16	Sand	65	Viscous	2 x 3 + 1	22	2011	Sa 65 Vi E C 16
			16	Sand	65	Viscous	2 x 3 + 1	26	2011	Sa 65 Vi E C 16
16			Sand	45	Viscous	2 x 3 + 1	24	2011	Sa 65 Vi E C 16	
11.3			Sand	65	Viscous	2 x 4 + 1	11b	2009	Sa 65 Vi E C 11.3	
11.3			Sand	65	Viscous	3 x 3	15	2009	Sa 65 Vi E C 11.3	

4.3. STATIC LOAD TESTS

In this section, first, typical measurements of the pile forces and the displacement of a SLT are given, then the measured axial forces on the pile head and the pile tip are plotted together with the calculated shaft friction as a function of the pile head displacement.

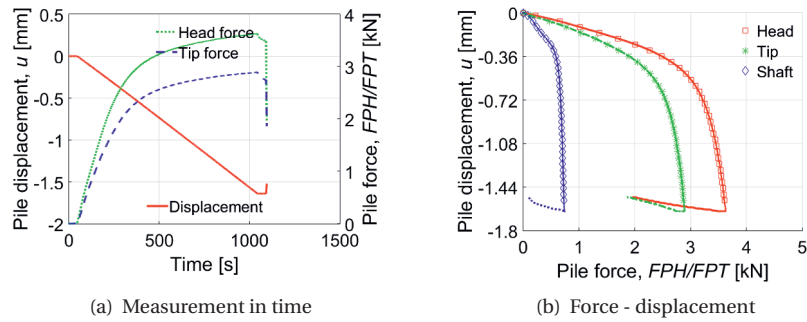


Figure 4.1: Typical results of SLT, test S-25-1

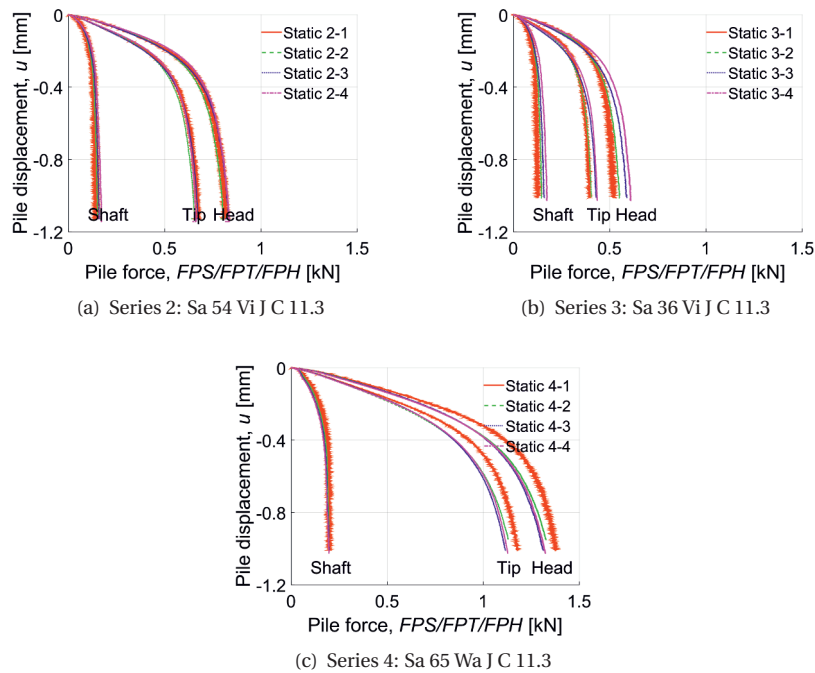


Figure 4.2: Pile displacement versus forces in SLTs of series 2, 3 and 4 in 2007 [206]

The measured head force and tip force in time from test S-25-1 (sand sample of D_r

= 65% with viscous fluid) are given in Figure 4.1(a), and the force-displacement curves of test S-25-1 are given in Figure 4.1(b). It can be seen that the tip force contributes approximately 80% of the total force, the shaft friction reaches an ultimate value at a displacement of approximately 5% D , whereas the tip force seems to continue increasing.

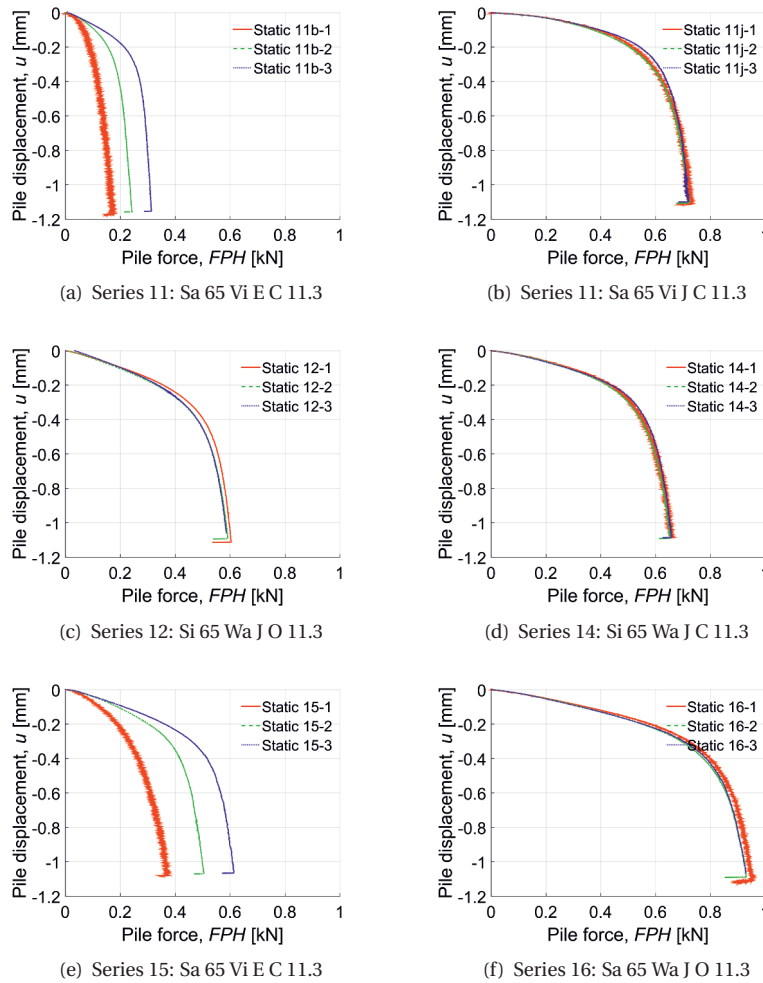


Figure 4.3: Pile head forces versus displacement in SLTs of tests in 2009 [169]

The force-displacement curves of all static loading tests in 2007, 2009 and 2011 are given in Figures 4.2, 4.3 and 4.4. In each pile load testing series, there were three or four static loading tests, as mentioned at the end of chapter 3. The SLTs were performed before or after the rapid load testing series. In Figures 4.2 to 4.4, the force-displacement curves of those SLTs in the same PLTs are differentiated with the number 1, 2, 3 and 4 which represents the order of the corresponding SLTs.

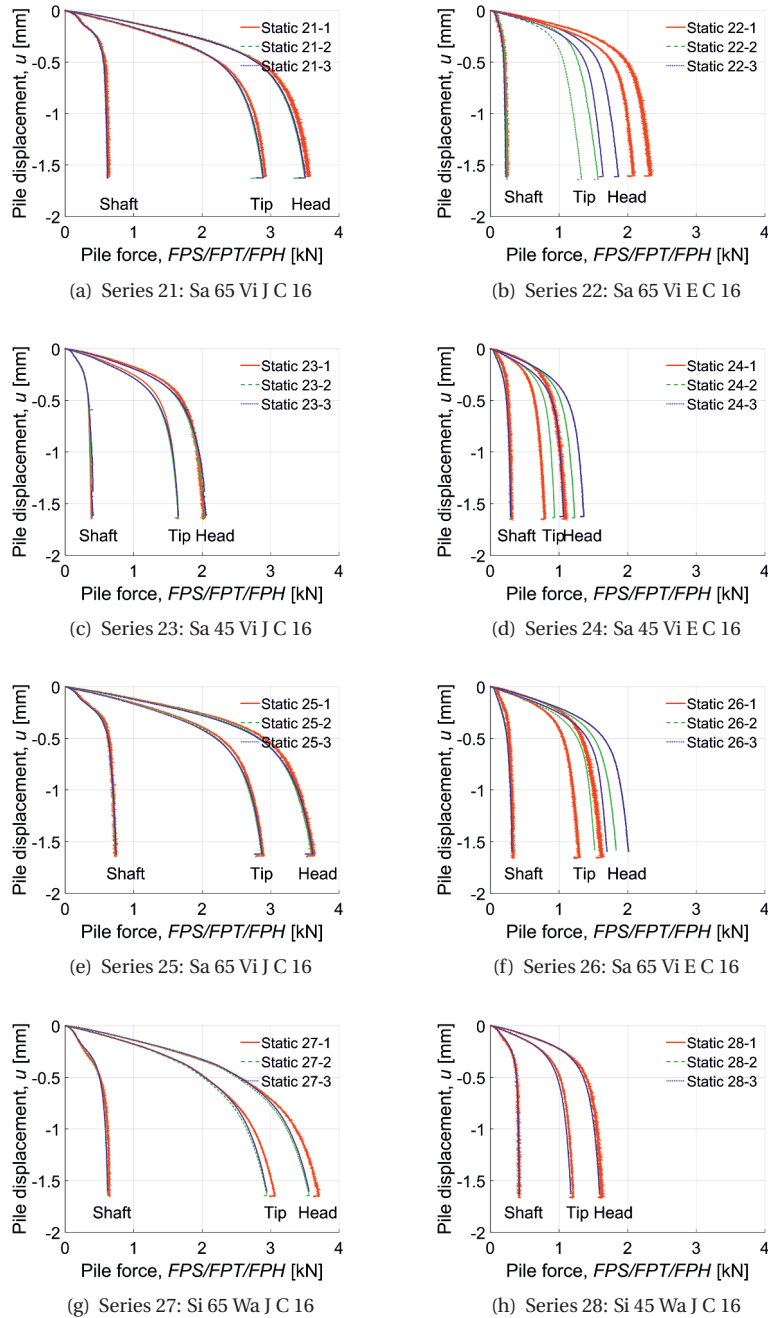


Figure 4.4: Pile displacement versus forces in SLTs of tests in 2011 [205]

Note: The tip reaction force measurement is missing in PLTs 11 to 16 therefore only the head force is available. In series 11, there were actually two PLTs; one is with the pile pre-embedded at $10 D$ (named as 11b) and the other is with the pile jacked-in until $20 D$ (named as 11j).

It can be seen from Figures 4.2-4.4 that there is a certain scattering of the force-displacement curves of static loading tests in each series. Generally, curves of the later SLTs show a higher maximum force than that of the previous ones, especially for the series with the pre-embedded pile. In particular, the difference between the maximum static force of the first SLT and the last SLT for the jacked pile is about 14% (Figure 4.2(b)), whereas that difference for the pre-embedded pile is up to 47% (Figure 4.3(d)). The increase of the pile force can be explained from the densification of the soil around the pile during the pile penetration process. As mentioned before, there are several RLTs between two consecutive SLTs with a total displacement of about $18\% D$. As the pile penetrated further into the soil body, the soil along the pile shaft and under the pile tip is densified which leads to an increase in the soil strength and hence in the pile resistance [67]. Similar observations on the increase of the pile force and actual evidence (from the void ratio measurement) for the soil densification are reported by Dijkstra [67].

The tip force in all SLTs is about 70 to 90% of the total force and, in general, is fully mobilised with a displacement of $10\% D$. On the other hand, the shaft friction is fully mobilised from a displacement of about $5\% D$.

4.4. RAPID LOAD TESTS

In this section, typical measurements of the rapid loading tests with different imposed displacements are given. For those RLTs, the following information is given: (1) the measured tip force and the calculated head and shaft forces with time, (2) the imposed displacement with time, (3) the derived velocity with time, and (4) the pile forces as a function of the pile displacement. Due to the large number of the RLTs in each series, this section only presents some typical results during RLTs with imposed pile displacements of 1%, 2%, 5% and 10% D in series 21, 22 and 25 in Figures 4.5 - 4.8. The full detail of all RLTs can be found in the following documents [169, 205, 206]. In Figures 4.5(a,c,e,g), the forces and displacement are plotted as a function of time, whereas the force-displacement curves are plotted in Figures 4.5(b,d,f,h). The captions of the sub-figures are the name of the corresponding RLTs.

It can be seen from Figure 4.5 that due to the small prescribed displacement of 1% and 2% D , both the tip force and the shaft friction in tests R-21-1-1% and R-22-1-2% do not reach the ultimate value, Figure 4.5(b,d). In tests R-22-2-5% and R-25-2-10%, as the prescribed displacement is large enough, the shaft friction is fully mobilised with a clear failure pattern, Figure 4.5(f,h). However, even with the prescribed displacement of 10% D , the tip force does not achieve its ultimate value, Figure 4.5(h).

It should be mentioned that in those rapid load tests, the inertia force is less than 3% when compared with the maximum pile head force, therefore, it can be considered as negligible. Nevertheless, the inertia force is still calculated and subtracted from the head force in the interpretation of the rapid load tests.

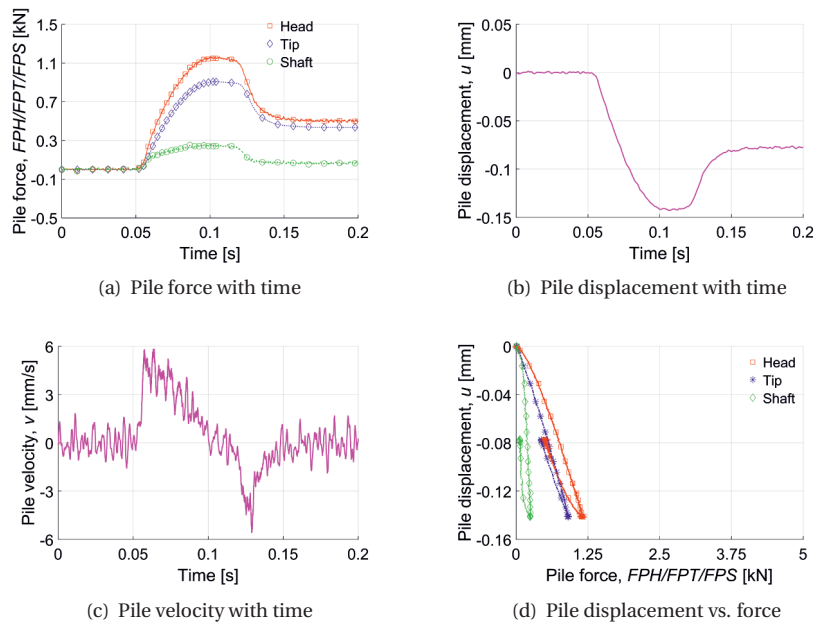


Figure 4.5: Results from test R-21-1-1%: series 21, $v_{ave} = 3.33$ mm/s, $u_{max} = 1\%D$

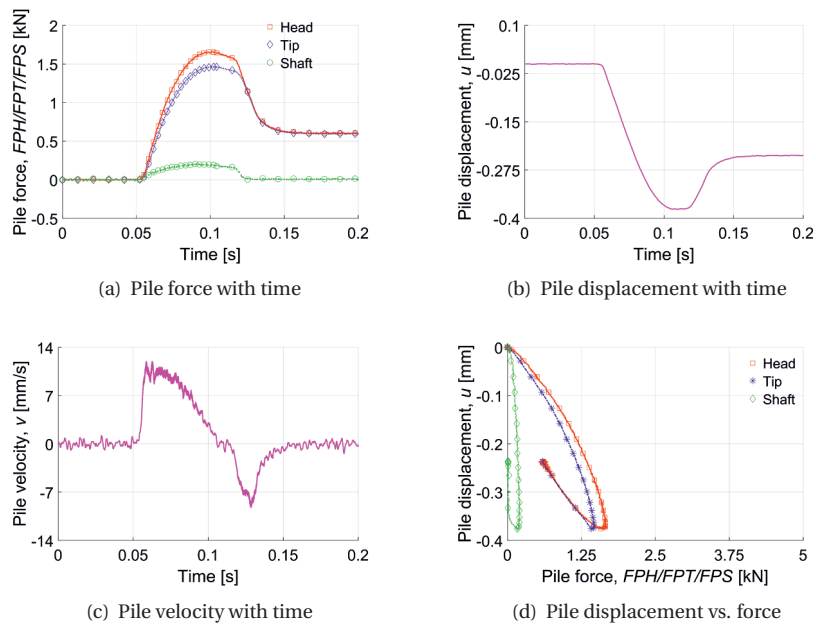


Figure 4.6: Results from test R-22-1-2%: series 22, $v_{ave} = 8.44$ mm/s, $u_{max} = 2\%D$

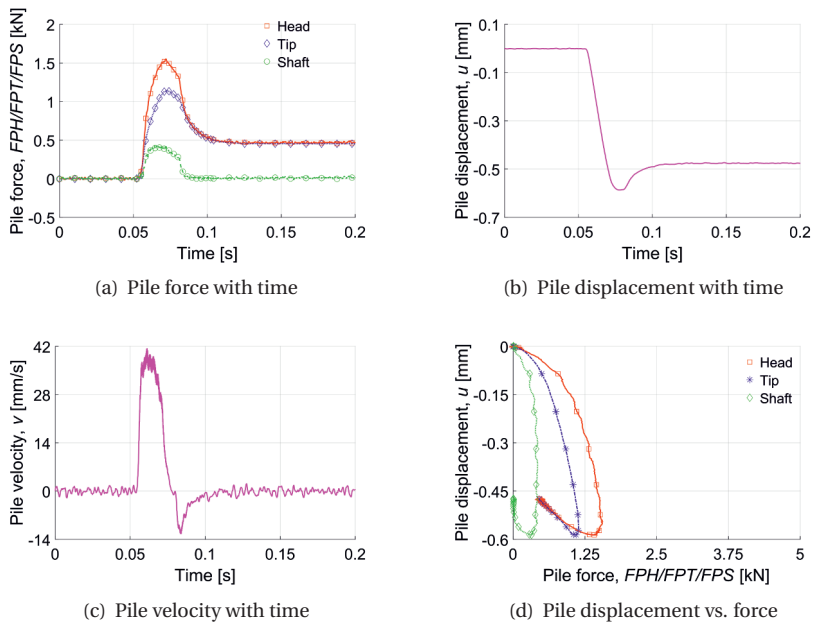


Figure 4.7: Results from test R-22-2-5%: series 22, $v_{ave} = 43.24$ mm/s, $u_{max} = 5\%D$

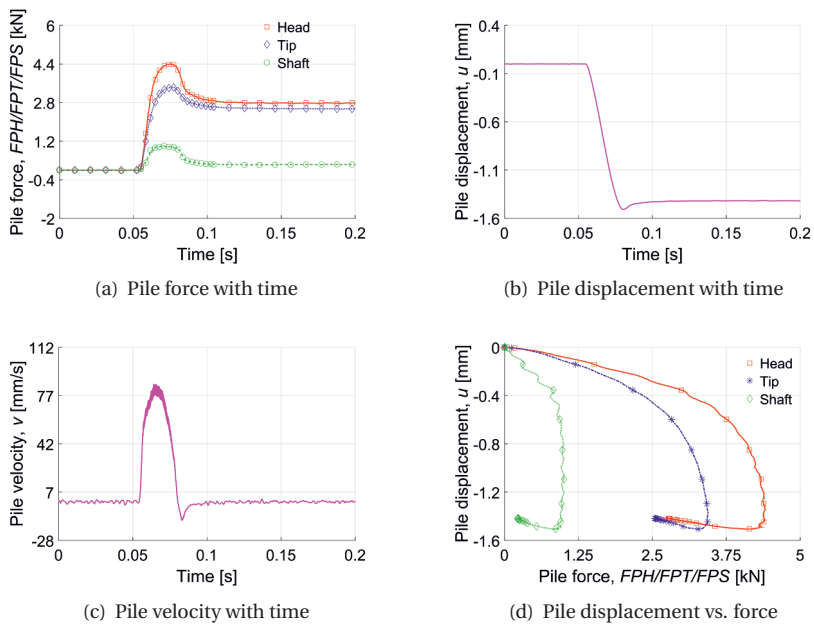


Figure 4.8: Results from test R-25-2-10%: series 25, $v_{ave} = 86.49$ mm/s, $u_{max} = 10\%D$

4.5. PORE FLUID PRESSURE IN RAPID LOAD TESTS

4.5.1. GENERAL DESCRIPTION

In this section, the general behaviour of the excess pore pressure is described. During the rapid loading tests, different responses of the excess pore pressure, measured by the pore pressure transducers, occur depending on the location of the PPTs.

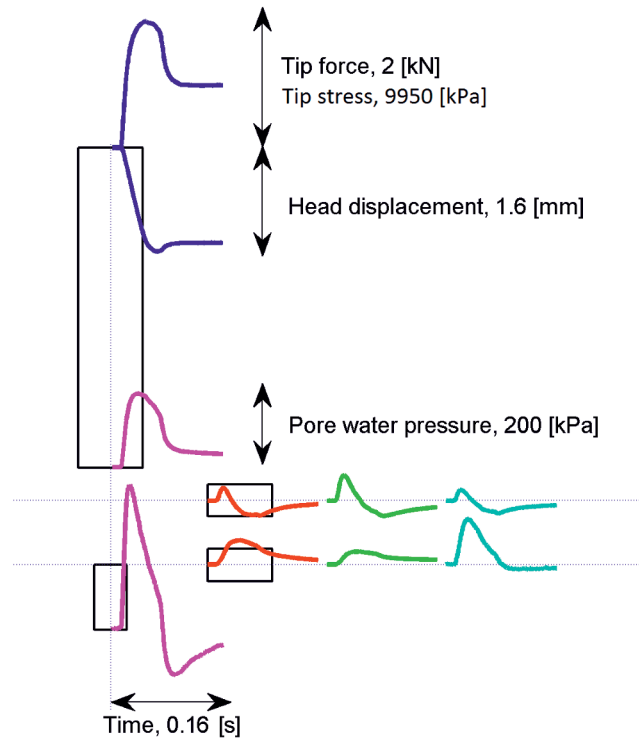


Figure 4.9: Response of PPTs following the second setup from test R-22-2-10%, sand $D_r = 45\%$ - viscous fluid, $v_{ave} = 86.49$ mm/s

As mentioned in chapter 3, there are five schemes of PPT setup. These five schemes can generally be classified into two types. In the first setup type, there are four PPTs placed at different locations around the pile tip and one mounted on the pile tip; in the second setup, there are six, eight or nine PPTs axis-symmetrically placed on two or three layers at different depth under the pile tip and also one mounted on the pile tip. Responses of PPTs installed as the first setup type are summarised by Nguyen [206], so they are not repeated here. Responses of PPTs installed as the second setup type are described in this section.

Figure 4.9 introduces an overview of pore pressure measurements together with measurements of the pile tip force and the pile head displacement from the rapid load test

R-22-2-10% in the soil sample of 45% relative density and viscous fluid. Pore pressures measured in the soil bed of six PPTs (Figure 3.2) are presented in two lines but it should be noted that three PPTs in each line are actually at the same distance from the pile centre but in different directions.

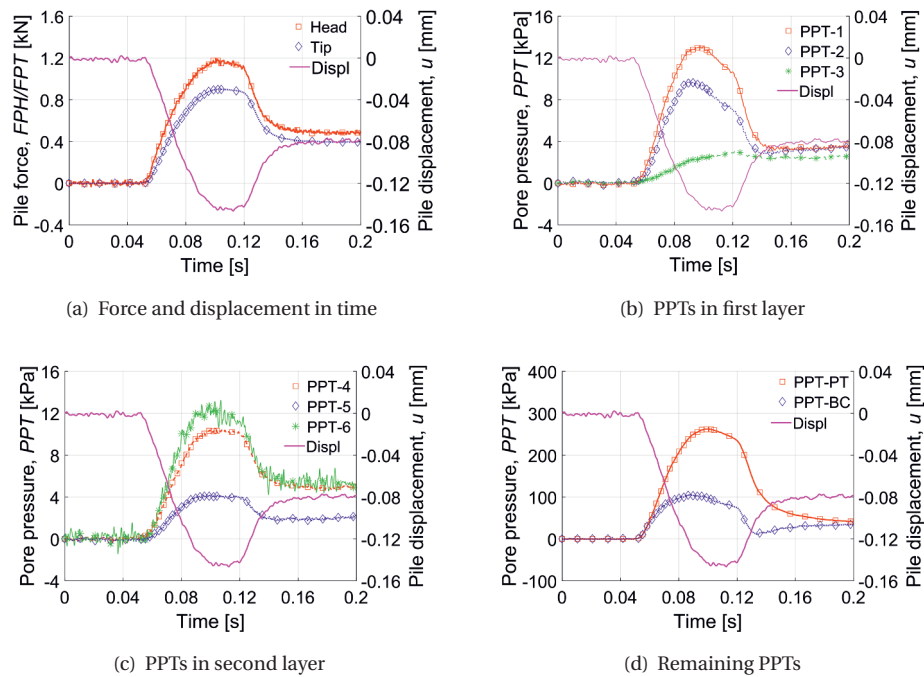


Figure 4.10: Results from test R-25-1-1%, sand $D_r = 65\%$ - viscous fluid, $v_{ave} = 3.33$ mm/s

The general overview of the measured signals can be described as following: (1) as the pile goes down, the tip force increases to the maximum value corresponding to the fact that the pile resistance increases, and when the pile bounds the tip force reduces to the final value; (2) the PPT transducers at the pile tip (PPT-PT) and on the second layer (PPT-4,5,6) exhibit mostly positive excess pore pressure, whereas the PPTs transducers at the bed (PPT-BC) and on the first layer (PPT-1,2,3) experience both the positive and negative excess pore pressure. The connection between the evolution of the excess pore pressure and the pile/soil movement will be explained in next sections.

Figure 4.10 presents measurements of the pore pressure of PPTs in the first layer (b), in the second layer (c) and in the pile tip and in the soil bed (d) of the rapid test R-25-1-1% in the soil sample of 45% relative density and viscous fluid. This is an RLT with the smallest load rate together with the smallest displacement. Figure 4.10 shows a similar trend of all PPTs' responses. Excess pore pressure of all PPTs gradually increases to a maximum positive value as the pile penetrates into soil and gradually dissipates to a static value as the pile rebounds. It seems that with such a small displacement of 1% D , the soil under and around the pile behaves elastically and experiences compression,

therefore, the induced excess pore pressure is only positive. The maximum value of excess pore pressure is about 250 kPa under the pile tip, about 95 kPa at a depth of $2.5 D$ under the pile tip and only about 14 kPa at locations of other PPTs.

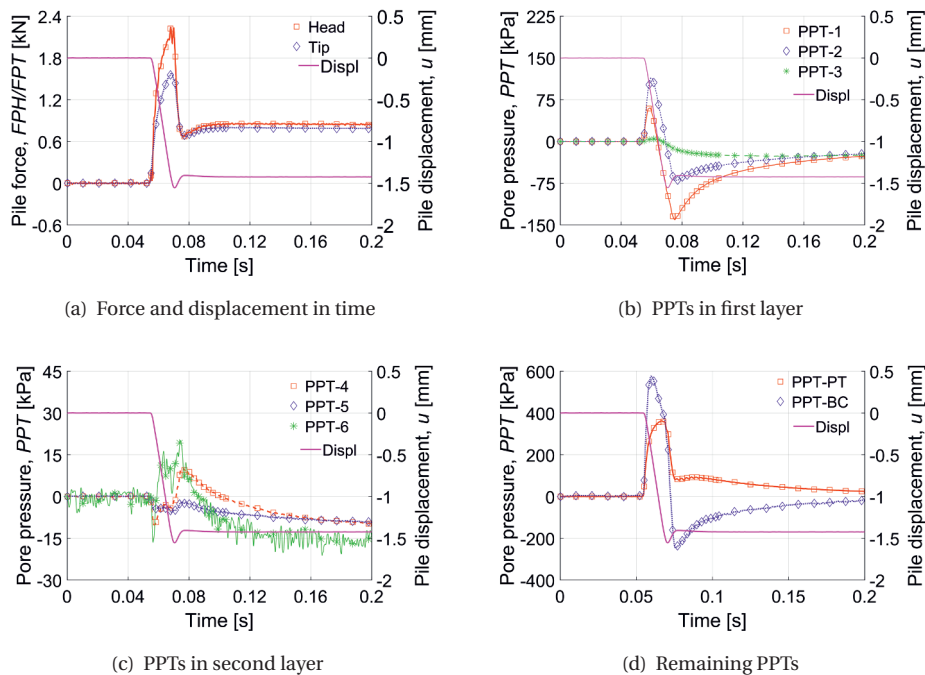


Figure 4.11: Results from test R-24-3-10%, sand $D_r = 45\%$ - viscous fluid, $v_{ave} = 177.77$ mm/s

Figure 4.11 presents results of the rapid test R-24-3-10% in the soil sample of 45% relative density and viscous fluid. This is an RLT with the largest load rate together with the largest displacement. In Figure 4.11, there are two opposite tendencies of excess pore pressure evolution which can be described as following. Figure 4.11(b,d) shows the similar tendency for pore pressure responses of the PPTs at the pile tip (PPT-PT), in the first layer (PPT-1, 2 and 3) and at the container base (PPT-BC) as: a rapid increase to a maximum positive value, rapid decrease to a maximum negative value and then gradual dissipation to the static value. This trend is also observed at the location of PPT-PT and PPT-2 in the rapid load tests with 10% D-displacement of Nguyen's experiment program [206] as mentioned in chapter 2. On the other hand, Figure 4.11(c) shows an opposite tendency for a response of the PPTs in the second layer (PPT-4, 5 and 6) as: a rapid decrease to a maximum negative value, a rapid increase to a maximum positive value and then gradual dissipation to the static value.

The evolutions of the excess pore pressure in Figure 4.11 can then be explained as following [71, 206]:

- At the initial stage when the pile starts moving downward, the soil right under the

pile tip is compressed therefore the pore fluid is squeezed and hence the excess pore pressure is positive as shown at the location of PPT-PT in Figures 4.11(d). For the soil under the pile tip, if the soil skeleton is compressed then the excess pore pressure is positive. This phenomenon is recorded by PPT-1, PPT-2, PPT-3 and PPT-BC as shown in Figures 4.11(b,d). However, if the soil is sheared along the pre-existed weak surfaces then the pore volume increases, the fluid is sucked in therefore the excess pore pressure is negative. This phenomenon is logged by PPT-4, PPT-5, PPT-6 as shown in Figure 4.11(c).

- As the pile continues moving downward, there are three possibilities for the response of the excess pore pressure. The soil right under the pile tip rigidly moves with the pile therefore the excess pore pressure reaches its maximum positive value and dissipates to a stationary value from over-pressure as the pile come to rest. This phenomenon is recorded by PPT-PT in Figures 4.11(d). If the soil is sheared after the initial compression then the excess pore pressure reaches its maximum positive value before the pile bounces back, subsequently decreases to the maximum negative and finally dissipates from under-pressure, PPT-1, PPT-2, PPT-3 and PPT-BC in Figures 4.11(b,d). On the other hand, if the soil is compressed after the initial shearing then the excess pore pressure reaches its maximum negative value, subsequently increases to the maximum positive value and finally dissipates from over-pressure, PPT-4, PPT-5, PPT-6 in Figure 4.11(c).

In general, the pore pressure responses of all PPTs are consistent. The behaviour of these PPTs can be categorised as follows:

1. gradually increase to a maximum positive value and gradually dissipate to the static value as all PPTs in Figure 4.10 or PPT-PT in Figure 4.11;
2. rapid increase to a maximum positive value, rapid decrease to a maximum negative value and gradually dissipate to the static value as PPT-1, PPT-2, PPT-3 and PPT-BC in Figures 4.11(b,d);
3. rapid decrease to a maximum negative value, rapid increase to a maximum positive value and gradually dissipate to the static value as PPT-4, PPT-5, PPT-6 in Figure 4.11(c).

The first behaviour is representative for a PPT in the rapid loading tests with a slow-rate loading and a small imposed displacement, soil behaviour around a PPT is still in an elastic regime. The second and third behaviour is representative for a PPT in the rapid loading tests with the average- to fast-rate loading and the medium to large prescribed displacement, the soil behaviour is in a plastic regime and exhibits both the compression and shearing. If the PPTs are located in the soil zone where the contractive behaviour is dominating then the second behaviour is expected; conversely, if the soil zone has the dilative behaviour dominating then the third behaviour is expected for the response of the PPTs.

4.5.2. RESPONSE OF PPTs WITH THE SAME AVERAGE LOADING RATE

The pore fluid pressure at the pile tip and the pile head displacement from different RLTs in series 23 are plotted as a function of time in Figure 4.12. The pore fluid pressure measured by PPT-1 in the soil body together with the pile head displacement from different

RLTs in series 23 are plotted as a function of time in Figure 4.13. In each sub-figures of Figures 4.12 and 4.13, three RLTs of the same series with comparable average loading rates but different imposed displacements are considered.

It can be seen from Figure 4.12 and 4.13 that the response of PPTs has an almost identical start but later has a significantly different response. The same average loading velocity can explain the identical start; while the different response is caused by a different behaviour of the soil due to different magnitudes of the prescribed displacement magnitudes [123].

At loading, the pore space is initially tightened by elastic deformation leading to the positive pore pressure measurement in the PPTs. It is clear that when the displacement of the pile increases from 1% to 5% D, the maximum positive excess pore pressure also increases, Figures 4.12(a) and 4.13(a). However when the pile displacement is large enough, i.e. larger than 5% D, the maximum positive excess pore pressure does not increase any further, Figures 4.12(b) and 4.13(b) show a comparable maximum positive excess pore pressure for three RLTs with different maximum imposed displacements.

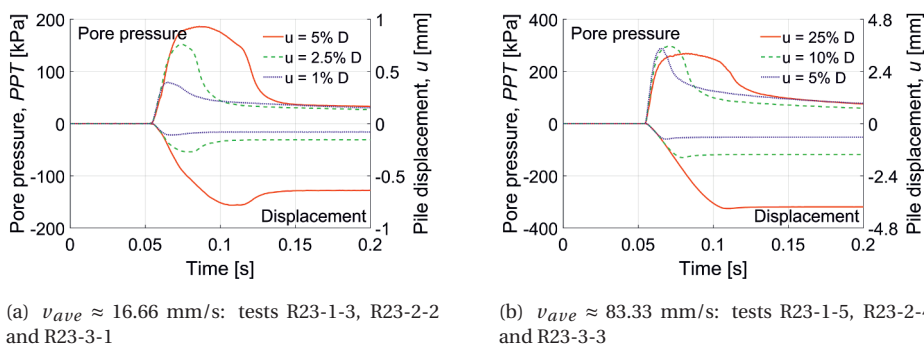


Figure 4.12: PPT-PT from RLTs with the same average loading speed

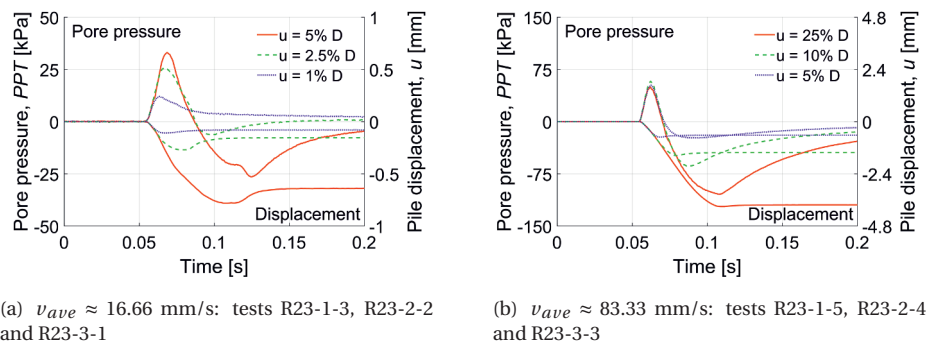


Figure 4.13: PPT-1 from RLTs with the same average loading speed

Figure 4.12 shows that there is only positive pore pressure at the pile tip (PPT-PT). Further examination of PPT-PT data of all RLTs with the 16 mm-diameter pile confirms that the PPT-PT only shows positive pore pressure. The results from Figure 4.12 are different from the results of test series R-2 and R-3 as analysed by Hoelscher et al. [123]. In those tests, there are both positive and negative excess pore pressures at the pile tip (PPT-PT). Further examination of PPT-PT data of all RLTs with the 11.3 mm-diameter pile confirms that the PPT-PT shows both positive and negative pore pressure. The difference on the general response of the PPT-PT of RLTs with the 16 mm-diameter pile and the 11.3 mm-diameter pile can be explained by the size of the core of the nose-cone under the pile tip as illustrated in Figure ???. That nose-cone core normally has a width of 1/2-2/3 of the pile diameter, and inside the nose-cone core there is only compression while outside and around the nose cone, soil particles are sheared and create a shear band [207, 277]. With the 16 mm-diameter pile, the size of the nose-cone core is about 8-12 mm that totally covers the pore pressure transducer of 5 mm-diameter hence there is only positive pore pressure in front of the transducer. On the other hand, the nose-cone core under the 11.3 mm-diameter pile does not totally cover the pore pressure transducer, therefore, the soil in front of the transducer admits both compression and shearing hence there are both positive and negative pore pressure in front of the transducer.

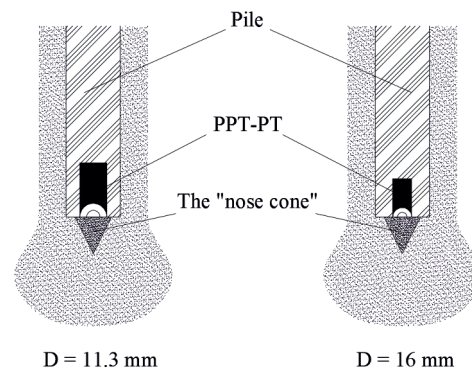


Figure 4.14: Relation between the width of the "nose cone" and the dimension of the PPT-PT

On the other hand, Figure 4.13 shows that an existence of the positive and negative excess pore pressure measured by PPT-1 depends on the magnitude of the imposed displacement. On test R23-3-1, Figure 4.13(a), with the imposed displacement of 1% D, there is only positive excess pore pressure which can be explained as the pile stops and bounces back when the soil still behave elastically, therefore, excess pore pressure dissipates after reaching the maximum positive value. On other tests in Figure 4.13, there are both the positive and negative excess pore pressure, and the test of a larger imposed displacement has a larger maximum negative excess pore pressure. When the pile continues penetrating, the pore volume deforms plastically, contracts, squeezes out water and leads to the rearrangement of soil particles, the soil particle dilates. Depending on the duration and hence the magnitude of the force, the number of soil particles involving in the dilation process differs. The larger imposed displacement and the longer the

loading duration, the more soil particles are sheared which leads to a bigger shear zone and a higher magnitude of the negative pore pressure.

4.5.3. SYMMETRY OF PPT'S RESPONSE

Figures 4.15 and 4.16 present the response of PPTs of the first layer in test 21, at the slow loading rate (R-21-1) and the fast loading rate (R-21-3), with different imposed displacement from 1% to 10% D . These two figures give details on the behaviour of PPTs at the same distance from the pile centre line.

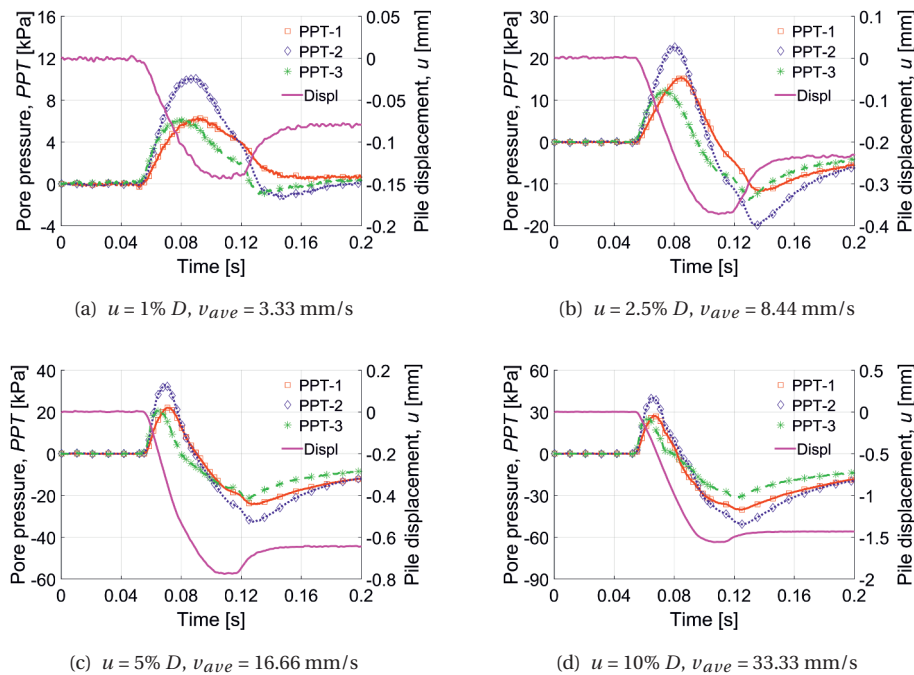


Figure 4.15: Pore fluid pressure for slow-rate loading tests in series 21 (sand 65%, viscous fluid)

At 1% D displacement - Figure 4.15(a), PPT-2 and PPT-3 have almost an identical start with PPT-1. After several milliseconds, first PPT-3 then PPT-2 and finally PPT-1 reach the maximum values and start to dissipate back to the static values. Since there is no negative excess pore pressure development, it is expected that the applied pile force corresponding to 1% D displacement causes only the elastic compression of soil pore volume at the locations of all three PPTs.

At 2.5% D displacement - Figure 4.15(b), at 5% D displacement - Figure 4.15(c) and at 10% D displacement - Figure 4.15(d), PPT-2 and PPT-3 still have an almost identical start. Again, first PPT-3, then PPT-2 and finally PPT-1 reach their maximum values. After reaching the maximum positive values, they decrease to the maximum negative values and then dissipate. Apparently, even at the small displacement of 2-5% D , which is gen-

erally considered as in the elastic working range of a pile in practice, the shear failure still occurs in accordance with the presence of the negative excess pore pressure.

In Figure 4.16, all three PPTs have an almost identical start and somewhat similar behaviour. However, the PPTs have different maximum values and reaching the maximum value at a different time. In all tests, first PPT-3 reaches the maximum value then PPT-1 does and finally PPT-2; the magnitude of the maximum values of the positive pore pressure of PPT-3 is the smallest one and of PPT-2 is the biggest one.

At displacements of 1 and 2.5% D - Figure 4.16(a,b), the negative excess pore pressure does not occur; in these cases, it seems that when a small load is applied in a short period, soil particles are only elastically compressed. At displacements of 5 and 10% D - Figure 4.12(c,d), negative pore pressure occurs at all PPTs as the pile force is larger and is maintained for longer time duration.

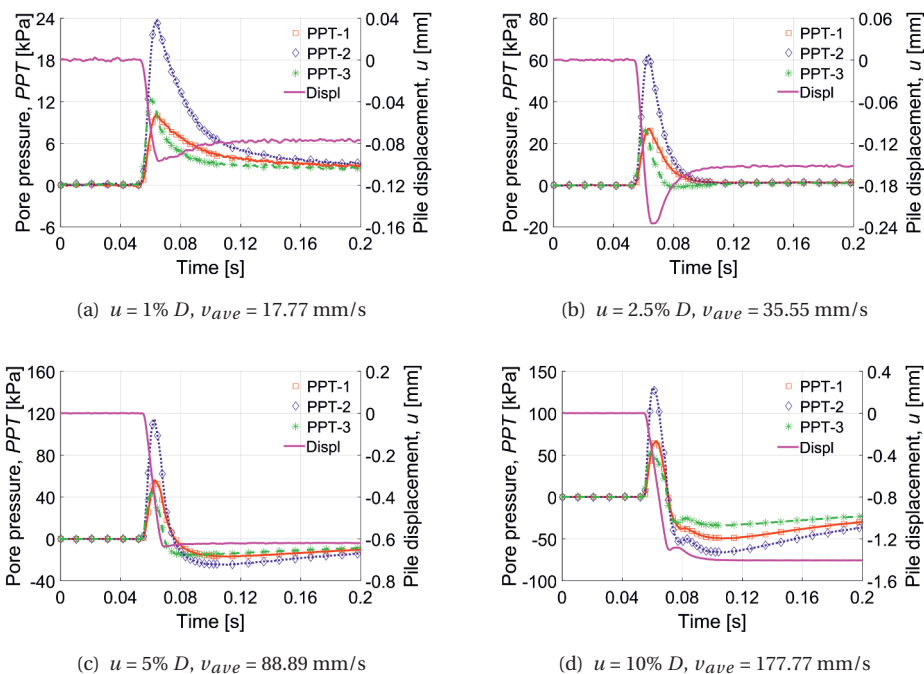


Figure 4.16: Pore fluid pressure for fast-rate loading tests in series 21 (sand 65%, viscous fluid)

It can be seen from Figure 4.15 and 4.16 that the PPT-2 has the largest value of the maximum positive and/or negative pore pressure in all rapid loading tests of series 21. In other series, there is always a certain PPT that has the largest value of the maximum positive and/or negative pore pressure in all rapid loading tests. It seems that the soil body will continue to be sheared at the location where previously a shear failure occurred.

Further examination of all RLTs in the test series 11, 15 and 21 to 28 confirms that responses of PPTs installed axis-symmetrically are asymmetrical in both elastic and plastic working ranges. The axis-symmetrically installed PPTs start to respond almost at the

same time and have the same tendency, but they have a delay in reaching the maximum value (0.5 to 10 ms) and show a difference in the magnitude of the maximum values (several to 60 kPa or up to $\pm 30\%$ of the average value). It should be noted that, as these PPTs are positioned axis-symmetrically around the pile centre line with an angle of 90° or 120° , if the pile penetrates perfectly vertically into the soil bed the reaction of PPTs are expected to be identical.

However, there are three reasons that may make the response of PPTs asymmetrical. The first reason is the exact location of PPTs; a measurement of PPTs' position before and after loading tests normally reveals 1-2 mm movement out of position, which may be caused by the sample preparation process. The second reason is the eccentricity of the loading plunger that has the maximum variation of 0.5 mm. The third reason is the heterogeneity of the soil bed; according to Allard and Schenkeveld [8], the porosity measured in different locations has a maximum variation of $\pm 0.5\%$ at the same depth within the soil sample. In the next paragraphs, discussions and explanations on the asymmetrical measurements of PPTs are given in relation to those above-mentioned technical reasons.

Within a rapid pile load test, the maximum value of excess pore pressure at different PPTs' location depends on the magnitude of the applied load, the distance from the pile and the pore volume compressibility at that location. When a force is applied into a pile, pore pressure occurs under the pile tip and its magnitude depends on the magnitude of the applied force. By using the cavity expansion theory, excess pore pressure around a penetrating cone is found to decrease logarithmically in the horizontal direction and linearly in the vertical direction in accordance with the distance from the cone body in undrained and partially drained situations [50, 265]. As mentioned in Chapter 3, the rapid loading tests in this thesis with sand and viscous fluid or with silt and water as pore fluid can be considered as partially drained, therefore following a cylindrical cavity expansion induced by the pile penetration, the distribution of pore pressure can reasonably be assumed as [50, 106, 186]:

$$p(r^*) = A \times \left(\frac{r}{r^*}\right)^2 \quad (4.5)$$

in which $p(r^*)$ the excess pore pressure at the distance r^* from the pile center ($r^* = 1.5D$ for the location of PPT-1 to PPT-3), A the parameter takes into account the strength of the soil and the excess pore pressure at the pile tip, r the pile radius. By using this type of equation with $r = 8$ mm and $r^* = 24$ mm, ± 2.5 mm difference in r^* may lead to about 15% different in $p(r^*)$.

A difference in the soil porosity (the third reason) will have a certain effect on the value of soil properties such as the shear modulus and the friction angle [19, 110, 221, 222, 295] and consequently on the soil compressibility factor which can be calculated as [162, 221, 298]:

$$\zeta = \exp\left(\frac{3.07 \sin \phi \times \log(2I_r)}{1 + \sin \phi}\right) - 3.8 \tan \phi \quad (4.6)$$

in which, I_r the rigidity index of the soil which is given by [239]:

$$I_r = \frac{G_{50}}{\sigma'_v \tan \phi} \quad (4.7)$$

with G_{50} the secant shear modulus at 50% the ultimate shear stress, ϕ the friction angle and σ'_v the effective vertical stress. The difference of $\pm 0.5\%$ porosity can lead to 2% difference in the friction angle [34, 243] and 5% difference in the shear modulus [222] hence about 7% difference in the soil compressibility following Equation 4.6 and 4.7. If the relationship between the soil compressibility and the magnitude of pore pressure generation is assumed to be linear, then the difference of $\pm 0.5\%$ porosity can lead to the difference of 7% excess pore pressure.

The relative density of the soil can also be linked to the cone penetration resistance in an exponent relationship [18] as:

$$q_c = C_0 \times \exp(D_r \times C_2) \times \sqrt{\frac{p_a}{\sigma'_v}} \quad (4.8)$$

where C_0 and C_2 are soil constants and p_a is the atmospheric pressure; or in a simpler formulation [156] as:

$$q_c = 305 \times Q \times D_r^2 \times \sqrt{\frac{p_a}{\sigma'_v}} \quad (4.9)$$

with Q is a factor considering the strength, the compressibility and the over-consolidation of the soil. Following either Equation 4.8 or 4.9, the difference of $\pm 0.5\%$ porosity can lead to the difference of 5% or 10% of the cone penetration resistance, respectively. Again, if the relationship between the soil compressibility and the magnitude of pore pressure generation is assumed to be linear, then the difference of 15% excess pore pressure can be found.

From the above arguments, certain discrepancies on the value of the maximum excess pore pressure are expected. Although, it is not an easy task to find a concrete quantitative explanation, a sum of 30% difference in the excess pore pressure can be explained by the difference in the location of the PPTs and the difference in the local porosity. Moreover, a difference in the soil compressibility factor may lead to the difference of the compression and/or dilation zone created during pile loading; therefore, it can explain the time for pore pressure generation.

CONCLUSION

Three general behaviours of the pore pressure response are measured by the PPTs in this study. They can be briefly described as following: (1) gradually increase to a maximum positive value and gradually dissipate to the static value as all PPTs; (2) rapid increase to a maximum positive value, rapid decrease to a maximum negative value and gradually dissipate to the static value; and (3) rapid decrease to a maximum negative value, rapid increase to a maximum positive value and then gradual dissipate to the static value.

Although having the same tendency of evolution, the pore pressure responses of PPTs in the same layer in the soil and at the same distance from the pile centre show a difference in the magnitude of the maximum value and a delay in reaching the maximum value. There are several causes for this asymmetric response of those PPTs; they can be the heterogeneity of the soil bed, the difference in distance of each PPTs from the pile centre line and the alignment of the pile during loading. These reasons are capable of explaining the difference of up 30% on the value of the maximum excess pore pressure

measured by symmetrically located PPTs. It is a high possibility that the failure surface under the pile tip is not symmetric; however this assumption is not supported in this thesis because there is not enough detailed view of soil deformation under the pile during the test. Only advanced experimental technique such as X-ray tomography can provide such an observation. On the other hand, a three-dimensional DEM simulation with the radius of the soil particles following the grain distribution curve may provide a feasible alternative to provide more insight into the asymmetric response of the PPTs.

4.6. RELIABILITY OF TESTS

Reliability of the tests performed is of great importance. The performance, range and accuracy of measurement devices are given in Section 3.3.1. This section will compare the force, the displacement and pore pressure measurements for pairs identical tests to examine the repeatability of tests. The following two tests are selected: series 21 and 25 of the jacked-in pile in sand of 65% relative density with viscous fluid, and series 22 and 26 of the pre-embedded pile in sand of 65% relative density with viscous fluid.

4.6.1. REPEATABILITY OF STATIC AND RAPID FORCE MEASUREMENTS

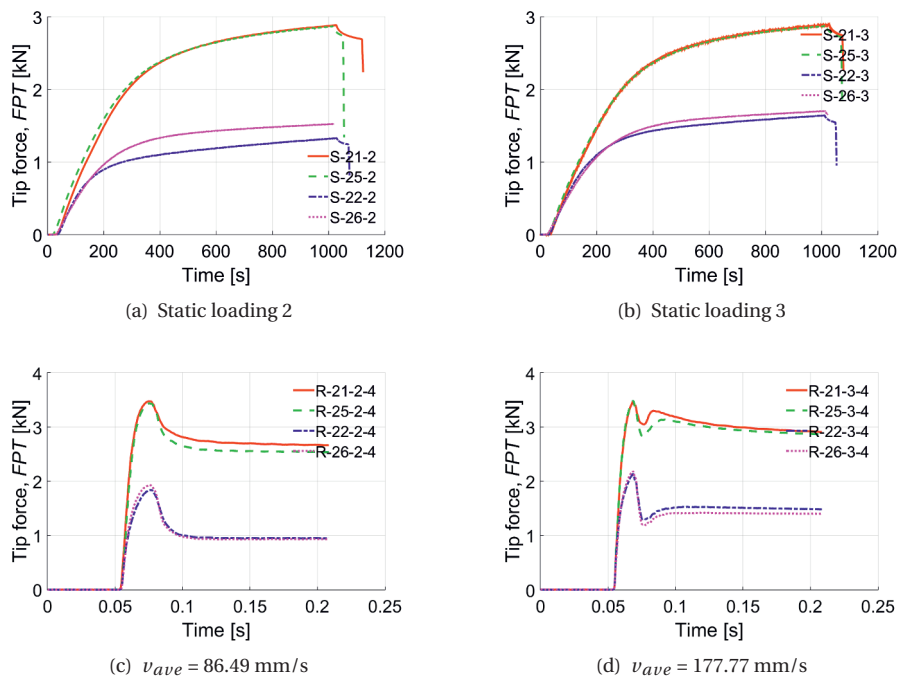


Figure 4.17: Repeatability of tip force with time, series 21 & 25: jacked-in, series 22 & 26: pre-embedded

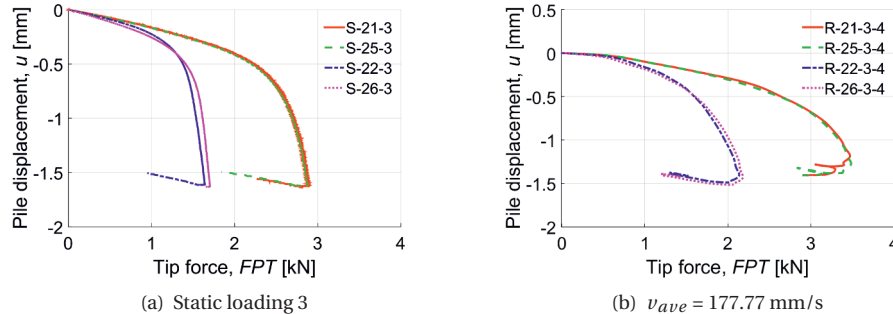


Figure 4.18: Repeatability of tip force-displacement, series 21 & 25: jacked-in, series 22 & 26: pre-embedded

The tip force measurements with time of the second and the third static loading tests are given in Figure 4.17(a,b) and of the average- and fast-rapid loading tests with the pile displacement of 10% D are presented in Figure 4.17(c,d). The pile displacement as a function of the tip force is plotted in Figure 4.18(a) for the static loading tests and in Figure 4.18(b) for the rapid loading tests.

In the static loading, the series of the jacked-in pile show a high repeatability with an identical evolution of the pile tip force and an identical force-displacement relationship, Figures 4.17(a,b) and 4.18(a). The series of the pre-embedded pile, on the other hand, show a lower repeatability, Figures 4.17(a,b) and 4.18(a). A scattering of up to 30% can be found in the first static loading; however, the scattering reduces to 15% in the second loading and less than 5% in the third loading.

The repeatability of the rapid load tests is high with a scattering in force of less than 5% at any comparable moment for both the jacked-in pile and the pre-embedded piles, Figure 4.17(c,d). The force-displacement relationship also shows a high repeatability with small differences at the end, Figure 4.18(b).

4.6.2. REPEATABILITY OF RATIO OF RAPID FORCE OVER STATIC FORCE

For the interpretation purpose, the absolute values of the rapid force are important, but the ratio of the rapid force over the static force is of greater concern. Although there is a difference in each of the static force of every PLT, the analysis of the rapid force is not affected because the comparisons are made between every rapid load tests with their closest static load tests in the same sequence of loading as pointed out by Nguyen [206]. Table 4.3 and 4.4 presents the ratio of the rapid force over the static force at the maximum load and at the unloading point load to illustrate the repeatability of the experiment program.

Table 4.3 and 4.4 show that, for series 21 and 25 of the jacked piles, the maximum difference of the ratio of the maximum force over the static force between two comparable loadings is 10% for the tip force at the slow-rapid loading and for the shaft force at the average-rapid loading. For the other comparable loadings, the difference is less than 5%. The difference of the ratio of the unloading point force over the static force follows the same trend. This is a reasonable percentage of difference since the repeatability of the

static force and the rapid force of the jacked-pile tests shows less than 5% difference.

Table 4.3: Repeatability of R_{max} , series 21 & 25: jacked-in, series 22 & 26: pre-embedded

Series	Head Loading rate			Tip Loading rate			Shaft Loading rate		
	Slow	Average	Fast	Slow	Average	Fast	Slow	Average	Fast
21	1.21	1.22	1.27	1.27	1.23	1.25	1.15	1.30	1.55
	1.18			1.20			1.17		
25	1.15	1.25	1.29	1.15	1.22	1.25	1.21	1.44	1.65
22	1.15	1.53	1.46	1.13	1.42	1.33	1.59	2.36	2.82
26	1.09	1.35	1.42	0.96	1.28	1.3	1.83	2.14	2.33

For series 22 and 26 of the pre-embedded piles, the maximum difference of the ratio of the maximum force over the static force between two comparable loadings is 15% for the tip force at the slow loading and 17% for the shaft force at the fast loading. For the other comparable loadings, the difference is about 5-10%. The difference of the ratio of the unloading point force over the static force for the tip force and the head force is lower than 10%; but for the shaft force, it can be up to 30% at the slow loading and 15% for the average and fast loading. This is also a reasonable percentage of difference because the repeatability of the static forces of the pre-embedded pile reveals the difference of up to 15-30%.

Table 4.4: Repeatability of R_{up} , series 21 & 25: jacked-in, series 22 & 26: pre-embedded

Series	Head Loading rate			Tip Loading rate			Shaft Loading rate		
	Slow	Average	Fast	Slow	Average	Fast	Slow	Average	Fast
21	1.10	1.14	1.16	1.18	1.16	1.15	0.86	1.05	1.19
	1.09			1.12			0.95		
25	1.05	1.16	1.18	1.08	1.15	1.16	0.96	1.19	1.24
22	1.04	1.36	1.31	1.06	1.32	1.23	0.88	1.54	1.84
26	0.98	1.22	1.26	0.91	1.20	1.21	1.24	1.31	1.55

4.6.3. REPEATABILITY OF PORE PRESSURE MEASUREMENT

The pore pressure measurement of PPT-1 and PPT-2 are presented in Figure 4.19. In Figure 4.19(a), the response of PPT-1 during the slow loading tests is given; in Figure 4.19(b), the response of PPT-2 during the average loading tests is given. There is no pore pressure measurement of the pile tip in those four tests to be compared. It can be seen that, with the same loading condition, the pore pressure measurements at the same location have the same general behaviour but the magnitude of peak values can vary by a factor of 2 or more and the moment of the peak value can be shifted up to 50 ms.

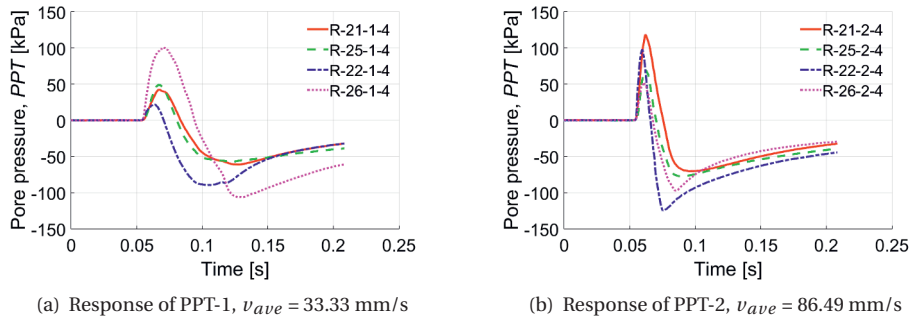


Figure 4.19: Repeatability on pore pressure, series 21 & 25: jacked-in, series 22 & 26: pre-embedded

4.6.4. CONCLUSION

From the repeatability examination, it can be concluded that the pile force measurements are reliable and that the pore pressure measurements in the soil body only give a qualitative indication on the phenomenon but not a quantitative.

The static and rapid forces of the jacked piles show a high repeatability with a scattering of less than 5%. The ratio between the rapid force and the static force shows repeatability with a scattering of less than 10%.

The rapid force of the pre-embedded piles shows a high repeatability with a difference of less than 5%. However, the static force shows a low repeatability with a scattering of up to 30%. The ratio between the rapid force and the static force therefore shows a low repeatability with a scattering that can be up to 10% for the head and tip forces and 15% for the shaft force (in an extreme case of the slow loading, a difference of 30% for the shaft force is recorded).

4.7. LOADING PATTERNS AND LOAD-DISPLACEMENT RESPONSES

In this section, the loading patterns and the load-displacement responses produced by three servo-control systems mentioned in chapter 3 are evaluated. Figure 4.20 presents the typical measurements and calculated data from three fast-rate rapid load tests of three series 2, 11 and 21 (the loading duration of 10 [ms], the maximum displacement of 10% D) to represent the typical results obtained from the three servo-control systems used in this study. The loading pattern and the load-displacement response from the rapid pile load test from the first test in Waddinxveen [122] are also presented to have a rough comparison on the modelling of the centrifuge tests. It should be noted that the rapid loading in the field test is the force-controlled whereas in the experiment the rapid loading is displacement-controlled.

It can be seen from Figure 4.20(a) that the imposition of the displacement pattern of 10% D downward then 1% D upward was imposed well in series 21-28, reasonably well in series 02-04 although that imposition is fairly steep in comparison with that of the series 21-28 or with that of the field test. The imposed pattern was poor in series 11-16 with considerable rebounds. Consequently, the head force was unstable for a significant duration (about two times of the intended loading duration), Figure 4.20(b). Moreover,

the loading rate in series 11-16 was an increase to the maximum value then an immediate decrease and a rebound, Figure 4.20(c,d). This is opposite to the loading rate in series 02-04 and 21-28, which had a duration of maintaining the high loading rate that helped the pile was in a pushing-down state for a certain period, Figure 4.20(c,d). This is a typical feature of the rapid pile load test [190].

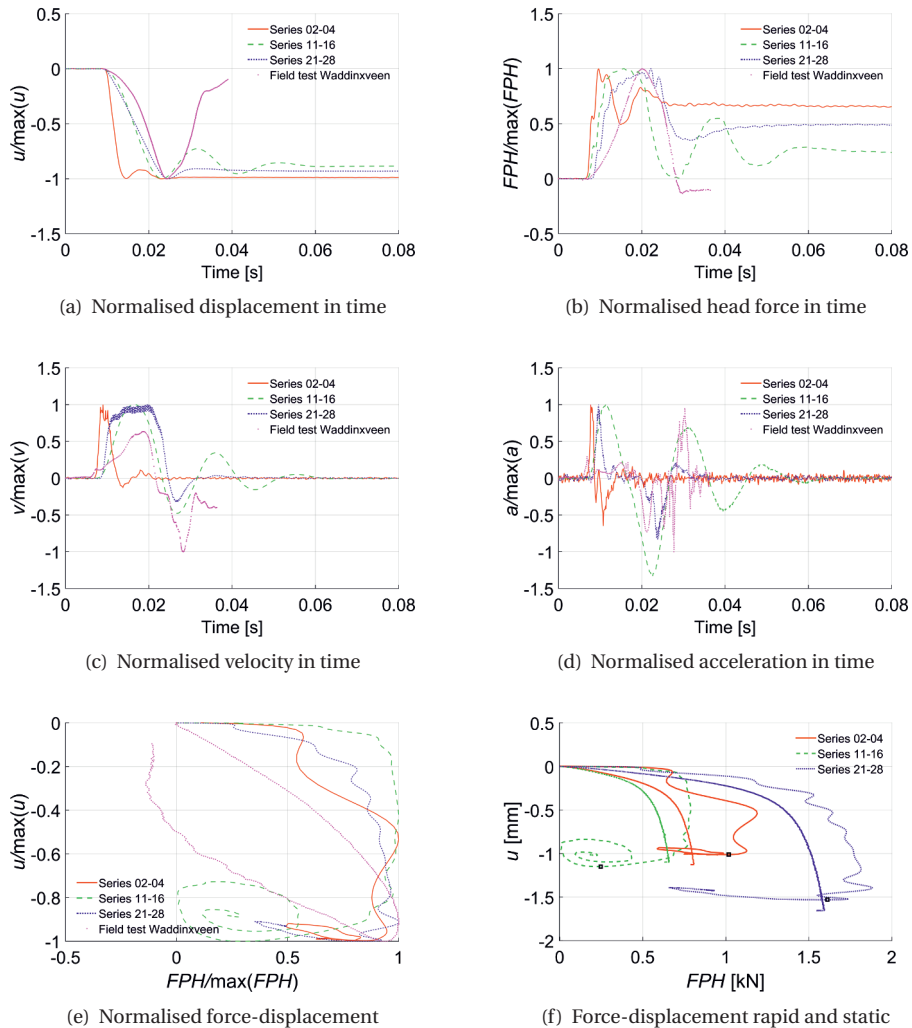


Figure 4.20: Loading patterns from three servo-control systems

The poorly imposed loading pattern of series 11-16 led to a very stiff response in the load-displacement curve, Figure 4.20(e); moreover, it made the pile head force at the unloading point significantly lower than the static pile head force. These two shortcomings

did not occur with the imposed loading pattern in series 02-04 and 21-28. As reminded by McVay et al. [178] and Paikowsky [212], the response of series 11-16 may result in a poor prediction of the unloading point method during the interpretation of the rapid pile load test. From this point of view, the analysis on the ratio of the rapid pile force at the unloading point over the static pile force will have a limited practical meaning, therefore, it will not be carried out.

In comparison with the field test in Waddinxveen [122], the imposition of the displacement pattern in series 21-28 has a good agreement with the displacement pattern in the field test, in Figure 4.20(a); the displacement patterns in other series are either too steep (in series 2-4) or too much rebounded. The force patterns and the velocity patterns in the experiment are much steeper than those of the field test, in Figure 4.20(b-d) which results in the much stiffer force-displacement curve as in Figure 4.20(e).

4.8. CONCLUSIONS

In this chapter, presentation and discussion on the results of the centrifuge pile load testing series are given. The centrifuge tests analysed in this study were conducted in the manner that the stress wave numbers in the pile, the loading patterns and the pile behaviour are similar with those of the prototype tests. Consequently, the remarks derived from the centrifuge scale are applicable to the prototype scale.

For a series of static load tests, there is an increase of the pile force from the first static test to the last one due to the densification of soil around the pile associated with pile penetration. The increase of the pile force is more significant for tests with the pre-embedded pile than for tests with the jacked pile. In the static load test, the tip force is about 70-90% of the total force which is a typical tip-dominant case. In general, the tip resistance is not fully mobilised within a displacement of 10% D . On the other hand, the shaft friction shows a clear failure from a displacement of 5% D . The repeatability of the static load tests with the pre-embedded pile increases from the first to the last one as the scattering reduces from 30% to 5%. The static load tests with the jacked pile have a high repeatability with the scattering of 5% only.

For the rapid load test, the tip resistance is about 60-80% of the total force and is not fully mobilised for a displacement of smaller or equal to 10% D . The shaft friction, however, is fully mobilised from the displacement of 5% D . The repeatability of the rapid load tests is high with the scattering of less than 5%. The values of R_{max} and R_{up} have a good repeatability with the scattering of 5-15%.

The typical behaviour of the pore pressure response is closely related to the magnitude and duration of the loading force. It is characterised by two or three phases: (1) an increase to a maximum positive excess pore pressure due to elastic compression of soil; (2) a decrease to a maximum negative excess pore pressure thanks to delative behaviour of soil particles (in case the loading force is sufficient to cause plastic shearing deformations in soil); and (3) a dissipation to the static value due to consolidation of soil. An occurrence of the positive and negative excess pore pressure in the rapid load test, in general, depends on the magnitude of the imposed displacement and the loading duration. The repeatability of the pore pressure measurements is not high; the responses have the same general behaviour, but the magnitude of the peak values can vary by a factor of 2.

In an attempt to examine the symmetry of the pore pressure response during the pile loading process, it is found that the responses of PPTs placed at the same depth and the same distance from the pile centre are not symmetrical. They have the same tendency of evolution but different maximum positive and/or negative values (difference of up to 30%) and a delay in reaching the maxima. Several causes can result in this asymmetric response which are the homogeneity of the soil bed (the material cause) and the difference in distance from the pile to the PPTs (the geometrical cause).

The loading patterns and the load-displacement responses of the three servo-control systems employed in this study are evaluated. It is seen that the system used in series 11-16 gave a poorly imposed loading pattern, a very stiff response in the load-displacement curve and a very low unloading point force in comparison to the static pile force. The last shortcoming may result in the poor interpretation of the unloading point method for the rapid load tests of series 11-16, therefore, the analysis of the ratio of the unloading-point rapid force over the static force will not be carried out for series 11-16.

5

PHYSICAL MODELLING - INTERPRETATION

5.1. INTRODUCTION

The experimental results presented in Chapter 4 are further investigated in this chapter to answer the research questions of this study which are assessments of the load rate effect and the excess pore pressure effect on the relationship between the rapid capacity and the static capacity. On top of that, the influence of the soil properties, the installation method and the pile type on the rapid and static capacities are also evaluated. As mentioned in Chapter 4, the values of all measurements in this chapter are in the model scale.

The influence of the penetration rate including the constitutive rate effect and the excess pore pressure effect on the increase of the rapid capacity over the static capacity are investigated in section 5.2 based on two basic parameters namely the loading rate and the drainage factor. The observations and explanations of these effects are given in detail. Furthermore, the relationship between the drainage condition η , proposed by Hölscher and Barends [118], and the normalised pile resistance R , initiated by Nguyen [206], is further extended.

Besides the two generic parameters (the loading rate and the drainage factor), other parameters such as soil and pore fluid types, soil density, pile type, pile installation method also have a certain influence on the penetration rate effect. Moreover, these latter parameters are also practically important to give an on-site indication of the penetration rate effect. Therefore in section 5.3 to 5.6, the influence of the differences in soil and pore fluid types, initial soil density, pile installation method and pile type are examined, first on the static resistance of the pile and, second on the penetration rate effect (in particular on R_{max} and R_{up}). Each parameter is investigated through four groups of test series (from now on, only "series" are referred to as a test series for short), in which each series is different from the other by the studied parameter.

5.2. INFLUENCE OF PENETRATION RATE

Based on the relationship between the ratios of the rapid forces over the static forces and the loading rate/the drainage factor, this section examines the effect of penetration rates on the increment of the rapid forces over the static force. As mentioned at the beginning

of Chapter 4, the rapid force comprises of the static force, the inertia force and the forces related to the loading rate and the pore pressure. By excluding the inertia force, the difference of the rapid force over the static force is the forces related to the loading rate and the pore pressure and are often referred to together as the penetration rate effect. The force related to the pore pressure can be considered as the excess pore pressure effect; it depends not only on the drainage condition of the pile test but also on the loading rate of the test. The forces related to the loading rate, excluding the pore pressure force, can be considered as the rate effect, which relates strongly to the intrinsic behaviour of soil material. Those forces can be the constitutive term and the viscous term, their contributions depend strongly on a soil type, a magnitude of imposed displacements and they are hard to clearly distinguish.

In this section, first, an overview of the influence of the drainage factor and the loading rate on the increase of the rapid forces over the static one is given. Then this influence is analysed in more detail, and finally, the quantitative suggestions of those influences are given.

5.2.1. OVERVIEW

For the overview of the effect of loading rate from the results of the physical modelling, Figure 5.2 shows the relationship between the ratios of the maximum and the unloading-point rapid tip force over the static tip force against the penetration rate. The similar figure is first built by Nguyen [206], and data from that source are presented by diamond-symbol points, the results from the centrifuge experiments in 2009-2011 are presented by points with square-symbol. As suggested by Nguyen [206], the relationship between the penetration rate and the ratio of the rapid over the static force can be roughly estimated by the power-law relationship. In Figure 5.1, the upper bound and lower bound estimation of the relationship between the penetration rate and the ratio of the rapid over the static pile force with a power-law form are also presented. These upper and lower bounds are produced by making the least-square fitting of the highest and lowest data points corresponding to each value of the drainage factor, respectively.

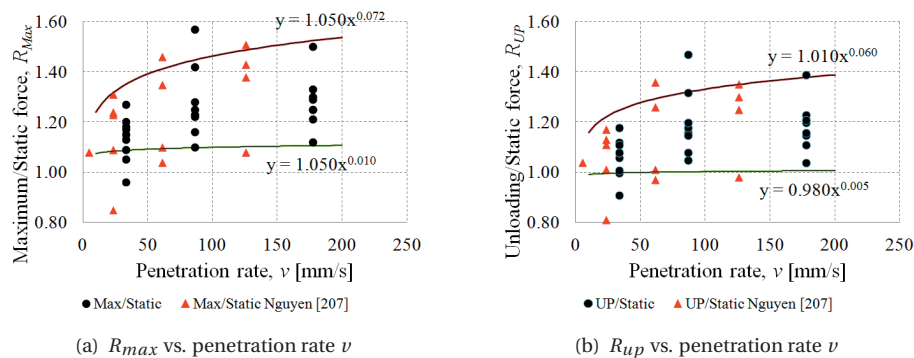


Figure 5.1: Influence on the ratio of maximum and unloading-point tip force over static tip force

Besides the effect of the loading rate, the excess pore pressure also has a significant

influence on the mobilised pile resistance. The significance of the excess pore pressure is not only controlled by the loading rate but also by the drainage condition of the pile loading test. Hölscher et al. [118, 119] pointed out that during dynamic loading on a pile, the drainage condition has a significant influence on a mobilised pile resistance and proposed to use the drainage factor η , Equation 3.1, to represent the drainage condition. Nguyen [206] later proved the importance of the drainage condition by plotting the relationship between the drainage factor and the ratio between the rapid over the static pile force and clearly showed that the ratio increases when η decreases. Figure 5.2 is an upgraded version of Nguyen's figure [206] in which Nguyen's data (cross-symbol points) shows the relationship for the range of the drainage factor smaller than 2.48 and larger than 142 and data from the centrifuge experiments in 2009-2011 (square-symbol points) add more information for the range of the drainage factor smaller than 110.

Representative backbone curves for the relationship between the ratio of the rapid force over the static force R and the drainage factor η of all data points in Figure 5.1 can be formulated by the following equation:

$$R = \hat{a} + \frac{\hat{b}}{1 + \hat{c} \times \eta^{\hat{d}}} \quad (5.1)$$

This equation is employed by numerous authors, such as Finnie and Randolph [79], House et al. [131], Chung et al [57] and Oliveira et al. [209], when they constructed the relationship between Normalised resistance of T-bar or cone against the non-dimensional velocity V , which can roughly be considered as the inverse of η , with \hat{a} , \hat{b} , \hat{c} and \hat{d} are constants used to fit the curve with the available data points. Table 5.1 represents six sets of $(\hat{a}, \hat{b}, \hat{c}, \hat{d})$ to create six curves on Figure 5.2 in which there are two main backbone curves and corresponding to each main curve, there are two upper bound and lower bound curves. As mentioned previously, the main backbone curve is produced by making the least-square fitting of all data points; whereas the upper and lower bounds are elaborated by making the least-square fitting of the highest and lowest data points corresponding to each value of the drainage factor, respectively.

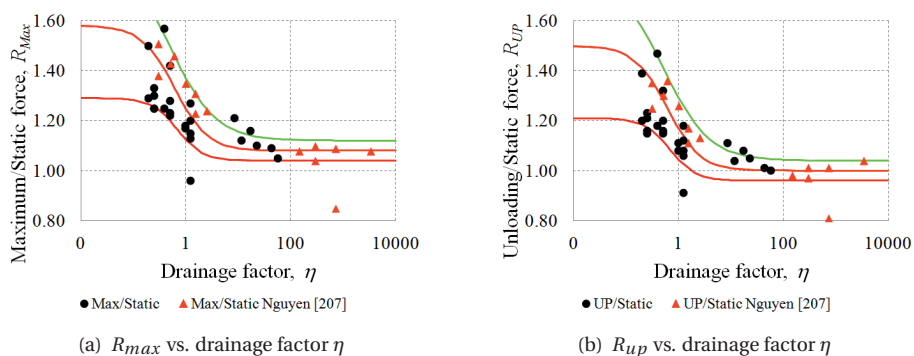


Figure 5.2: Influence of the loading rate on the ratio of maximum and unloading-point tip force over static tip force

It is worth to mention that the data points in Figure 5.2 and 5.1 are rather scattered. The data points with the same penetration rate or the same drainage factor are not similar because other governing parameters of the pile load tests are different; those parameters can be the soil type (sand or silt), the fluid type (water or viscous fluid), the pile installation method (pre-embedded or jacked), the pile type (open- or close-ended). Figure 5.2 and 5.1, therefore, serve as the general description of the influence of the penetration rate and the drainage factor on the normalized pile resistance. Later, other figures in Section 5.3 to 5.6 will isolate each parameters for a better presentation and indication.

Since both the constitutive rate effect and the excess pore pressure effect dependent on the loading rate of the test, it is not easy to distinguish these two components. Fortunately, there are two phenomena that assist one to separate the two effects. The first phenomenon is the existence of the unloading point [191] on the load-displacement curve of a rapid pile loading test at which the downward movement of the pile ceases, and the pile starts bouncing back. As the velocity of the pile is zero at the unloading point, the loading rate effect vanishes [191] and therefore only the excess pore pressure effect exists at that moment [206]. Based on the existence of the unloading point, the well-known unloading point method was proposed [27, 191] to extract the static pile load-displacement curve from the rapid pile load-displacement curve. The second phenomenon is the strong influence of the drainage condition of the pile loading test on the excess pore pressure effect as mentioned by Hölscher et al. [120]. Nguyen [206] noticed that if the drainage factor is larger than a certain value (142) then, even in a test of high loading rates (up to 125 mm/s), there is a negligible excess pore pressure effect. Based on this realisation, Nguyen classified his tests according to the drainage condition to distinguish the constitutive rate effect and the excess pore pressure effect. In particular, the series of sand and water (series 4, $\eta = 142 - 714$) was considered having a fully drained condition and used to investigate the constitutive rate effect solely. On the other hand, the series of sand and viscous fluid (series 2 and 3, $\eta = 0.30 - 2.48$) was considered as "partially drained" series. These series were employed to analyse the excess pore pressure effect.

Table 5.1: Summary of the rate effect and the pore pressure effect

	Backbone for Maximum/Static			Backbone for UP/Static		
	Lower	Main	Upper	Lower	Main	Upper
\hat{a}	1.04	1.08	1.12	0.96	1.00	1.04
\hat{b}	0.25	0.50	0.75	0.25	0.50	0.75
\hat{c}	2.00	2.00	2.00	2.00	2.00	2.00
\hat{d}	1.80	1.40	1.00	1.80	1.40	1.00

Following the unloading point method [191] and Nguyen's classification [206], the influence of the constitutive rate effect and the excess pore pressure effect are investigated in this section by considering three groups of different drainage conditions: fully drained (series of sand and water, $\eta = 142 - 714$), partially drained (series of silt and water, $\eta = 8 - 55$) and nearly undrained (series of sand and viscous fluid, $\eta = 0.19 - 2.48$). It is worth to mention that "fully drained", "partially drained" and "nearly undrained" are relative terms which imply that tests with sand and viscous fluid have a lower permeability (de-

terminated from material properties) than tests with silt and water, and these tests have lower permeability than tests with sand and water. It will be pointed out later that in the "partially drained" and "nearly undrained" series, the excess pore pressure effect is different whilst the constitutive rate effect is similar. The findings of Nguyen [206] on those effects are revisited and supplemented; besides, more detail and possible explanations for those finding are given.

5.2.2. CONSTITUTIVE RATE EFFECT

As mentioned previously, the series in sand and water are chosen to investigate the constitutive rate effect. There are two pile loading test series in sand and water, which are series 4 and series 16. Since there is no information on the tip force and hence the shaft force in series 16, series 4 is the only available series to investigate the rate effect.

EXPERIMENTAL EVIDENCE

Series 4 was performed and analysed in detail by Nguyen [206], Nguyen concluded that there is no pore pressure effect on the loading series in sand and water due to that fact that the ratio of the rapid force at the unloading point, at which the influence of the loading rate vanished, over the static force is about unity. Moreover, Nguyen [206] also pointed out that the influence of the rate effect on the increase of the maximum rapid force over the static force is reasonably constant in the conducted loading rates, see Figure 5.3(a). Therefore, Nguyen [206] suggested that there is no damping effect. Consequently, the increase of the maximum force over the static force in this series is solely due to the constitutive rate effect. For the maximum tip force, this increment is found to be 10% [206], Figure 5.3.

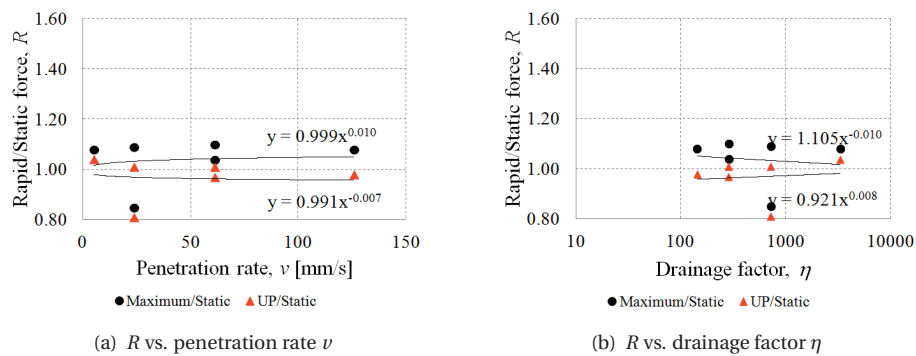


Figure 5.3: Normalised rapid tip forces in drained tests

POSSIBLE EXPLANATION

As Whitman [281] pointed out, the strain rate effect can lead to an increase of about 10 to 15% of the friction angle of sandy soil and even only 10% increase in the friction angle can lead to a large increase in bearing capacity of a pile. The mechanism of the increase of the friction angle with increasing strain rate can be explained by the fact that the interlocking between particles becomes more significant when the particles are not

given sufficient time to find the easiest path to past one another during loading [242, 281, 283].

5.2.3. EXCESS PORE PRESSURE EFFECT

In the previous section, the analysis of the fully drained pile load testing series [206] suggested that the constitutive rate effect is a cause of about 10% increase of the rapid pile force over the static pile force and there is no pore pressure effect on those fully drained pile load tests. In this section, the partially drained pile load testing series (with silt and water) and the nearly undrained pile load testing series (with sand and viscous fluid) will be analysed to quantitatively determine the excess pore pressure effect and re-examine the constitutive rate effect. It should be mentioned that Nguyen [206] investigated the nearly undrained pile load tests and concluded that the rapid pile load force is about 40% higher than the static pile load force thanks to the excess pore pressure effect only. Nguyen's finding will be examined later in this section.

EXPERIMENTAL EVIDENCE

The dependency of the ratios of the rapid forces over the static force on the loading rate and on the drainage factor are presented in Figure 5.4 for the partially drained tests (tests with silt + water) and in Figure 5.5 for the nearly undrained tests (tests with sand + viscous fluid).

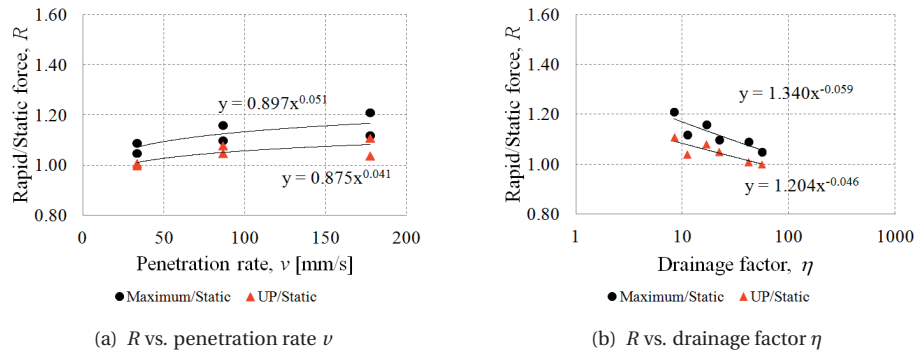


Figure 5.4: Normalised rapid tip forces in partially drained (silt + water) tests

There is a clear increase of the rapid forces over the static force, Figure 5.4. Without the constitutive rate effect, the excess pore pressure effect creates an increase about 0 to 10% of the unloading force over the static force. The excess pore pressure effect and the constitutive rate effect together makes an increase of about 10 to 20% of the maximum force over the static force which means the constitutive rate effect causes an increase of 0-10% of the maximum force. It then can be concluded that for the pile load testing series in a partially drained condition, the constitutive rate effect makes an increase of about 0-10% of the maximum tip force that is similar to the constitutive rate effect for the fully drained pile load testing series. And, the excess pore pressure effect causes an increase of about 0-10% of both the maximum tip force and the unloading point force. The increase

of the pile force rises nonlinearly with the increase of the loading rate between 23-177 mm/s and with the decrease of the drainage factor from 55 to 8.

Similar to Figure 5.4, Figure 5.5 also shows a clear nonlinear increase of the rapid forces over the static force with the increase of the loading rate between 23-177 mm/s and with the decrease of the drainage factor from 2.48 to 0.19. In particular, the excess pore pressure effect increases about 6 to 47% of the unloading force over the static force. The excess pore pressure effect and the constitutive rate effect together increase about 13 to 57% of the maximum force over the static force. Consequently, the constitutive rate effect again causes an increase of 7-10% of the maximum force. It can be concluded that, for the pile load testing series in a nearly undrained condition, the constitutive rate effect increases about 7-10% of the maximum tip force and the excess pore pressure effect increases about 6-47% of both the maximum tip force and the unloading point force.

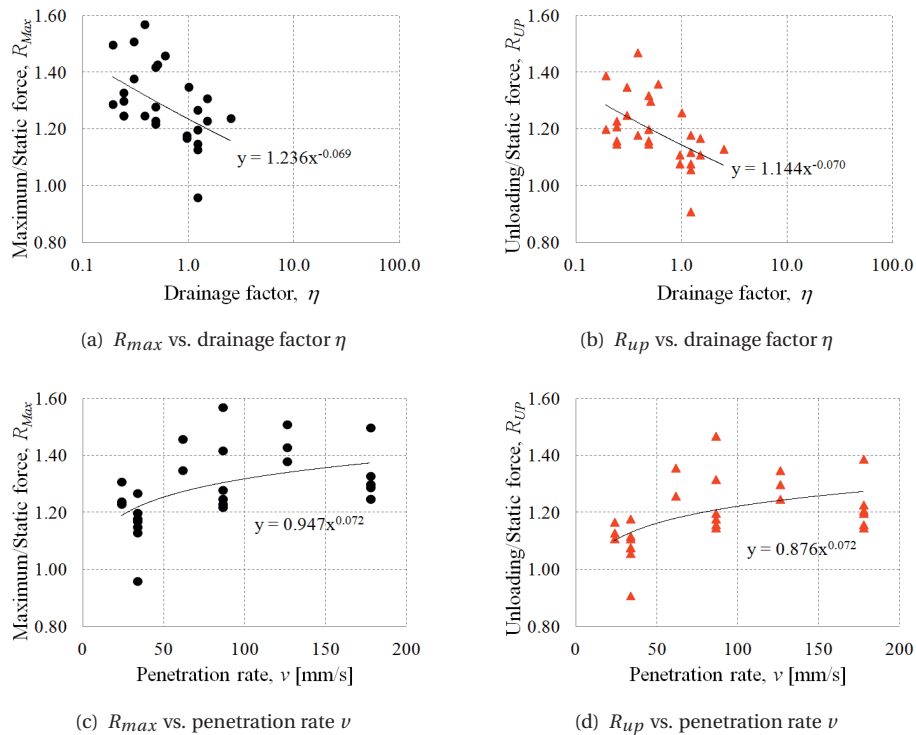


Figure 5.5: Normalised rapid tip forces in nearly undrained (sand + viscous fluid) tests

POSSIBLE EXPLANATION

In order to further investigate the mechanism of the excess pore pressure effect, one can use several different theories such as the bearing capacity formula API [139], the classical bearing capacity theory [182, 220, 256, 257] or the cavity expansion theory [96, 104, 266, 297, 300].

Following the bearing capacity formula suggested by API [139], the ultimate bearing

capacity of the pile can be determined as:

$$Q = Q_c + Q_p = f \times A_f + q \times A_p \quad (5.2a)$$

$$f = K_0 \times \sigma'_v \times \tan \delta \quad (5.2b)$$

$$q = N_q \times \sigma'_v \quad (5.2c)$$

$$\sigma'_v = \sigma_v - p \quad (5.2d)$$

in which Q_f and Q_p are skin friction resistance and total end bearing, A_f and A_p are side surface area and gross end area of a pile, f is the unit skin friction capacity, q is the unit end bearing capacity, K_0 is the coefficient of lateral earth pressure (ratio of horizontal to vertical normal effective stress), δ is the friction angle between the soil and pile wall, N_q is the dimensionless bearing capacity factor, σ'_v is the effective overburden pressure, p is the hydrostatic pore pressure and σ_v is the overburden pressure at the point of interest.

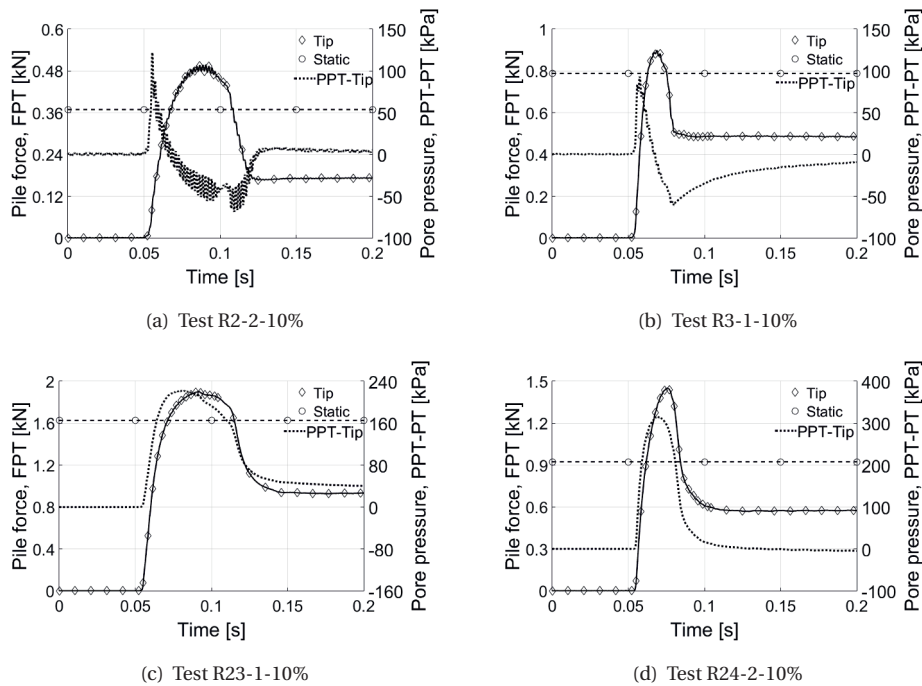


Figure 5.6: Tip forces and pore pressure with time

Since the unit end bearing capacity relates directly to the effective stress level at pile tip, a negative pore pressure will increase the effective stress and thus will increase the unit end bearing capacity of a higher rapid force than a static force. This argument seems to be reasonable in some tests, such as R-3-1-10% as shown by Nguyen [206] in Figure 5.6(b). At the pile tip, p is 128 kPa for the 16-mm pile and 89.6 kPa for the 11.3-mm pile; and σ_v is 333.67 kPa for the 16-mm pile and 233.58 kPa for the 11.3-mm pile. Figure

5.6(a) implies that when the negative pore pressure occurs, the increase of the rapid force over the static force occurs also and this increase disappears when there is no more negative excess pore pressure. The maximum negative excess pore pressure (about 50 kPa), following Equation 5.2, will then have a significant contribution to the bearing capacity of the pile as the value of N_q is about 82 corresponding to the value of the peak friction angle ϕ of about 41° .

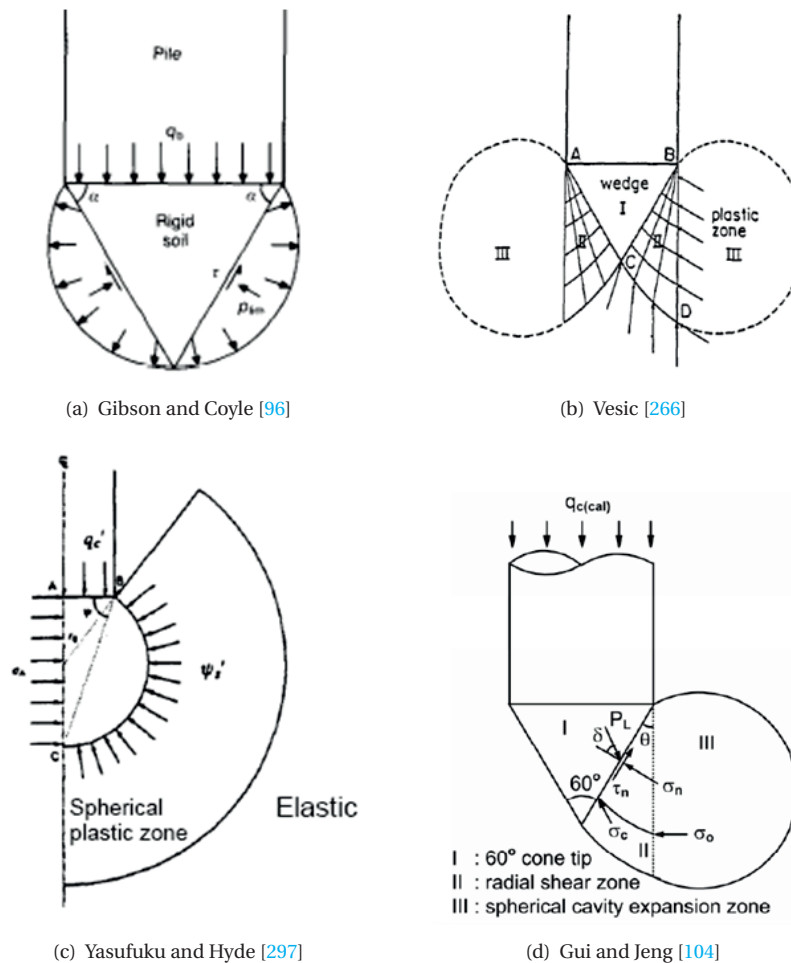


Figure 5.7: Cone resistance and cavity limit pressure [105]

The above argument, however, is not applicable for many other tests because there is not a qualitative relationship between the excess pore pressure and the increment of the rapid force over the static force. The negative pore pressure occurs after the rapid force reaches the maximum value (Figure 5.6(b), test R-2-2-10%) or there is no negative pore pressure at all (Figure 5.6(c) and 5.6(d) of tests R-23-1-10% and R-24-2-10%, respec-

tively). On the other hand, the gradients of the excess pore pressure close to the pile tip are very large, and the increase of the tip capacity will be correlated with an average effective stress; which is difficult to assess on only a few measured values. It then comes to the same conclusion of Nguyen [206] that although there is a pore pressure effect, there is no direct relationship, both qualitative and quantitative, between the value of excess pore pressure at the pile tip and the increment of the rapid force over the static force.

Another explanation for the pore pressure effect can be based on the cavity expansion theory, and the existence of shear failure surfaces around the pile tip as suggested by Nguyen [206]. The cavity expansion theory was proposed by Gibson and Coyle [96] and then was developed further by many researchers as Vesic [266], Ladanyi and Johnson [160], Lee et al. [163], Carter et al. [48], Gui and Jeng [104] and Yasufuku and Hyde [297]. Figure 5.7 presents the assumed relationships between cone resistance and cavity limit pressure proposed by several researchers. Following the cavity expansion theory, the end bearing pressure, q_b or q_c , is related to the cavity limit pressure, and the cavity limit pressure is related to the effective vertical and horizontal stress along the plastic expansion zone. Apparently, during the shearing failure of the soil, the negative pore pressure that occurs in the plastic expansion zone, increases the effective stress along the plastic expansion zone, and consequently increases the end bearing pressure of the pile.

Although there is no quantitative information about the exact location as well as the area of the shear failure surface, based on Figure 5.8, the area of the shear failure surface is expected to be much larger than the tip area and can be up to 5 to 10 times of the pile diameter. Since the PPT-1 to PPT-3 are placed closely to the zone of high shear strain generalized by Robinsky and Morrison [234], White and Bolton [277, 279] and Nguyen [207], the negative pore pressure on the shear failure surface may be in the same order as the negative pore pressure measured at those locations. The maximum negative pore pressure at the shear failure surface is, therefore, about 2 to 4 times smaller than the maximum negative pore pressure at the pile tip.

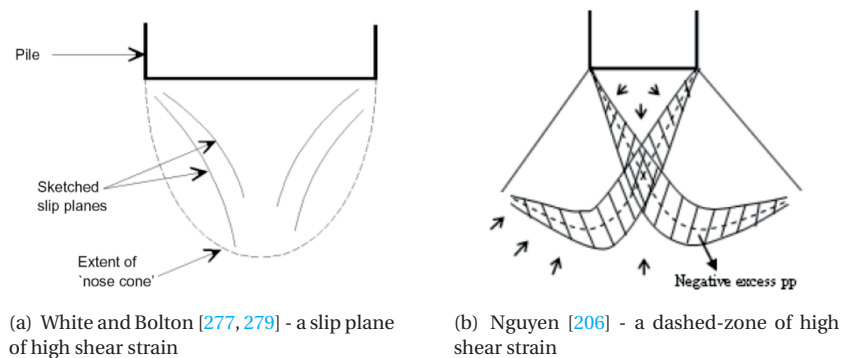


Figure 5.8: Expected zone of high shear strain under the pile tip

Summing up the increase of the effective stress due to the negative pore pressure all along the failure surface around the pile tip can make a reasonable contribution to the

increase of the rapid force due to the pore press over the static force [206]. Figure 5.9, based on the concept of the failure surfaces from the pile tip [182, 183, 220, 257], the concept of the "nose cone" under the pile tip [207, 277, 279] and the concept of negative excess pore pressure contribution in the high shear zone [206], illustrates the high shear strain zone around the pile and the direction of the fluid flow. Along the nose cone and the pile shaft, as the soil is mainly sheared, the soil volume tends to increase and hence the negative excess pore pressure occurs so that the fluid can flow in. Similar phenomenon also occurs along the failure surfaces which start from the "nose cone" tip and develops through the locations of the head of the pore pressure transducers in the first layer. This assumption seems to be reasonable since the negative excess pore pressure was recorded at the locations of the pore pressure transducers in the first layer (PPT-1 to PPT-3) as shown in Figures 4.11 and 4.13 to 4.16 during the rapid load tests.

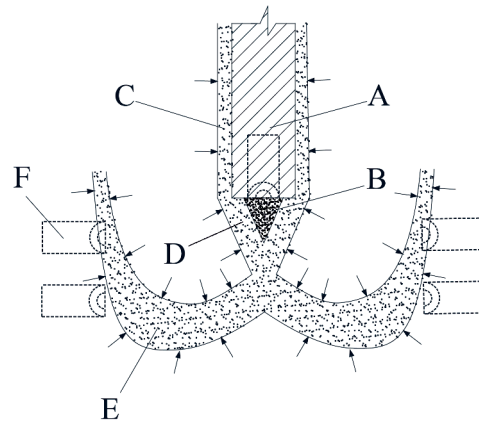


Figure 5.9: Expected zone of high shear strain and negative excess pore pressure, adapted from Nguyen [206, 207]. Notation: (A) the pile; (B) the "nose cone" under the pile tip where the soil is mainly compressed - this assumption was observed in [279] and will be confirmed numerically in Figure 7.12; (C) the soil zone along the pile shaft with high shear strain & dilatancy and negative excess pore pressure - this assumption was observed in [71, 279] and will be confirmed numerically in Figure 7.11; (D) the soil zone along the "nose cone" which has high shear strain and negative excess pore pressure - this assumption was observed in [279] and in [206] regarding the shear strain and the negative excess pore pressure, respectively; this assumption will be confirmed numerically in Figure 7.17; (E) the soil zone which starts from the nose cone and passes through the PPTs inside the soil body, this soil zone has high shear strain and negative excess pore pressure - this assumption (regarding the negative excess pore pressure) was proposed by Nguyen [206] and observed at the locations of PPT-1 to PPT-6 in this study; (F) the PPTs, in this figure, there are four PPTs in the soil body corresponding to PPTs in the first layers (PPT-1 to PPT-3) and PPTs in the second layers (PPT-4-PPT-6) and one in the pile tip (PPT-PT).

In an attempt to explain the excess pore pressure effect, test R-23-2-10% is analysed with several assumptions and facts such as (1) the failure surface area following Yasufuku's assumption [297] is about 5 times larger than the tip area - about 1000 mm²; (2) the increase of the rapid resistance over the static resistance 0.397 kN divided along the failure surface is about 397 kPa; (3) the maximum negative excess pore pressure at PPT-1 is about 50 kPa and is considered equal to the negative pore pressure on the failure surface. Then the increase in the effective stress is 50 kPa or 13% of the increment of the

rapid resistance over the static resistance. It should be noted that the above arguments on the pore pressure effect are qualitatively only with a "weak" numerical example. They are not a full explanation for the pore pressure effect. It is more reasonable to check the pore pressure effect and the above explanations with a numerical tool. This work is performed in Chapter 7.

5.2.4. SUMMARY ON THE PENETRATION RATE EFFECT

It can be concluded from this section that both the constitutive rate effect and the excess pore pressure effect increase the maximum tip force and the unloading tip force of the rapid pile load tests. Whilst the constitutive rate effect depends strongly on the loading rate, the excess pore pressure effect depends both on the drainage factor of the tests and on the loading rate. In general, a lower drainage factor or a higher loading rate leads to a higher ratio of the maximum or unloading point force over the static force (R_{max} and R_{up}) [121, 206]. This generality leads to two general trends which will be shown in more detail in the next section:

- for rapid pile load tests of the same set of materials, the loading tests with a higher loading rate (a lower drainage factor) will have a higher value of R_{max} and R_{up} ;
- for rapid pile load tests of the same loading rate, the loading tests with a higher drainage factor (determined directly from material properties) will have a lower value of R_{max} and R_{up} .

Table 5.2: Summary of the rate effect and the pore pressure effect

Test types	Drainage factor	Constitutive rate effect maximum % of increase	Pore pressure effect maximum % of increase
Fully drained	142 - 714	10	0
Partially drained	8 - 55	0-10	0-10
Nearly undrained	0.19 - 2.48	7-10	6-47

Through numerous centrifuge rapid pile loading test series conducted by Nguyen [206] and performed in this thesis, it is recommended that the value of the drainage factor of approximately between 55 and 142 can be used as an indicator to take into account the excess pore pressure effect. In particular, the excess pore pressure is negligible in the pile load test with the value of η larger than 142, and it is significant in the test with η smaller than 55. Although there is no experimental evidence in the range between 55 and 142 of η , the trend-lines curves in Figure 5.2 suggest the existence of the pore pressure effect. Table 5.2 summarises the influence factors of the true rate effect and the pore pressure effect representing by the maximum increment of the rapid force over the static force regarding percentage.

5.3. INFLUENCE OF SOIL AND PORE FLUID TYPES

In this section and the next three sections, the influence of differences in the soil and pore fluid types, the initial soil density, the pile installation and the pile type will be examined within the context of not only a general behavior but also the static resistance

and the ratio of the rapid over the static resistances. Each parameter is investigated through four groups of tests, in which each test is different from the other by the studied parameters. Among four parameters, the soil and fluid types and the initial soil densities have the most influence on the drainage condition since they directly control the permeability, therefore, they will be considered first in section 5.3 and 5.4, respectively; then pile installation methods and pile types follow in section 5.5 and 5.6, respectively.

It should be mentioned here that the power-law in the form of $R = \hat{a} \times v^{\hat{b}}$ is employed to generalise the relationship between the factor R and the loading velocity of the pile in Figure 5.2, this power-law form will also be used in Sections 5.3 to 5.6 to illustrate the influence of the soil and pore fluid types, the initial soil density, the pile installation and the pile type. On the other hand, although the form $R = \hat{a} + \frac{\hat{b}}{1 + \hat{c} \times \eta^{\hat{d}}}$ is appointed to generalise the relationship between the factor R and the drainage factor η in Figure 5.1, it will not be used in Sections 5.3 to 5.6 to illustrate the influence of the soil and pore fluid types, the initial soil density, the pile installation and the pile type since the range of the drainage factor in each group of series considered in Sections 5.3 to 5.6 is relatively rather and the number of data points is relatively low (less than 5 for each relation) to generate a non-trivial fitting law. Instead, for the illustration purpose, the form of $R = \hat{a} \times v^{\hat{b}}$ is again employed for the relationship between R and η .

The influence of material types is studied, in this section, by three types of combined materials, which are sand and viscous fluid, silt and water, and sand and water. Of the three types, the mixture of sand and viscous fluid has the lowest permeability, as silt with viscous fluid was not tested due to the complex preparation procedure, therefore the lowest value of the drainage factor whereas sand and water has the highest permeability hence the highest value of drainage factor. The drainage factor is not important in the static load test because the loading time is long enough for pore fluid to flow out of pore space before it can build up any excess pore pressure and alters the static force. However, during the rapid load test, the loading time is far shorter than the dissipation time of the excess pore pressure, and then the drainage factor becomes an important factor to assess the influence of penetration rate and excess pore pressure on pile resistance [119, 121, 206].

5.3.1. STATIC RESISTANCE

Soil and pore fluid type have a big influence on the static force, but there is not a general trend for all groups and/or all tests. Table 5.3 summarises the maximum and scatter of the static head force and a contributing percentage of the tip resistance to the head force in each test series in each group (recall that each series has three static pile load tests).

Within group 1 of OEP, the test series of sand and water have a much higher head force (0.96 kN) than that of the silt and water series (0.61 kN). Without the influence of loading rate and excess pore pressure, this significant difference can only come from the difference in either the grain size or the friction angle of the soil or both. If the OEP is plugging and behaves as the CEP, then Equation 5.2 can be used to determine the unit end bearing and the shaft friction of a pile in cohesionless soils. As the friction angle of Baskarp sand is 2° higher than the friction angle of silt (40° compares to 38°), the value of N_q of series 16 is significantly larger than that of series 12 [184, 203] and the value of

the friction angle between the pile shaft and the soil of series 16 is slightly higher than that of series 12. Consequently, series 16 has 30-50% higher tip bearing and 10% higher shaft friction at the same level of effective stress than series 12. On the other hand, if the OEP is not plugging then the difference in grain sizes can explain the difference in the head force. The mean grain size d_{50} of the sand is 2.5 times larger than that of the silt that makes the ratio of the pile wall thickness over the grain size, t/d_{50} , is 3.9 for the sand and 8.6 for the silt. In prototype terms, the OEP series with silt is closer to the normal use of open-end piles in coarse grain sand; while the OEP series with sand is an extreme case in gravels or pebbles. As suggested by Burland and Burbidge [45] and Kara and Gunduz [148], the CPT resistances in gravel can be 30-50% higher than that in coarse grain sand.

Table 5.3: Influence of soil and pore fluid types on static force

Group	Series	Properties	Max. head [kN]	Scatter [%]	Tip [%]
Group 1	12	Si 65 Wa, J 0 11.3	0.61	6	
	16	Sa 65 Wa, J 0 11.3	0.96	3	
Group 2	4	Sa 65 Wa, J C 11.3	1.40	6	85-86
	11j	Sa 65 Vi, J C 11.3	0.73	1-3	
	14	Si 65 Wa, J C 11.3	0.66	1	
Group 3	21	Sa 65 Vi, J C 16	3.56	1-3	78-80
	25	Sa 65 Vi, J C 16	3.63	1-3	80-82
	27	Si 65 Wa, J C 16	3.70	4	80-82
Group 4	23	Sa 45 Vi, J C 16	2.07	2	80-81
	28	Si 45 Wa, J C 16	1.62	3	73-74

Within group 2 of CEP with the 11.3 mm diameter pile, the head force of the series 4 with sand and water (1.40 kN) is almost twice that of the series 11j with sand and viscous fluid (0.73 kN). And the head force of series 11j is 11% higher than that of series 14 with silt and water (0.66 kN). The small difference of the head force of the series 11j and the series 14 can again be explained by the difference in the grain size and the friction angle of silt and sand. However, the significant difference between the series 4 and the other series is not yet clear. Among these three series, differences can be pointed out as the soil types, the fluid types and the loading and servo control system (the system used for the series 11j and 14 is different from the system used for the series 4 as mentioned in section 4.7). As discussed above, the difference in soil types can only lead to 50% increase of the force. The difference in fluid types does not play an important role as limited literature [34, 36] observe only a negligible change in shaft friction as the viscous fluid acts as a lubricant for sand sliding against steel interface. Moreover, without the influence of excess pore pressure, the big difference of the static resistance should probably come from the difference in the loading and servo control system, and it is hard to quantitatively explain for this.

Within group 3 of the CEP series with the 16 mm diameter pile in the soil bed with the relative density of 65%, the pile head force in sand and viscous fluid is comparable with that in silt and water; the difference is less than 5%. However, within group 4 of the CEP series with the 16 mm diameter pile in the soil bed with the relative density of

45%, the head force of the series in sand and viscous fluid are higher 28% than that of the series in silt and water. The big difference between group 2 and 3 is still not clear. It may be possible that with a lower degree of densification (a lower relative density), the difference in the friction angle between sand and silt are larger which leads to a larger difference in the maximum static force.

5.3.2. RATIO OF RAPID FORCES OVER STATIC FORCES

In this section, the relationship of the soil and fluid types with the ratio of the rapid force over the static force is given. In consideration of the drainage condition, the series of sand and water (series 4 and 16) have the highest values of the drainage factor with η ranging from 142.85 to 714.24. The series of silt and water (series 12, 14, 27 and 28) have the second highest values of η ranging from 8.27 to 110.30; and the series of sand and viscous fluid (series 11j, 21, 23 and 25) have the lowest values of η ranging from 0.19 to 2.38.

The two general trends mentioned in section 5.2.4¹ hold for head force, tip resistance and shaft friction in almost all loadings, some exceptional cases will be pointed out. Within a series of the same loading rate, the general trends are more pronounced for the shaft, then for the head and the tip in the sense that the ranges of R_{max} and R_{up} are largest for the shaft and smallest for the tip. Brown [41] showed similar trend of rate effects in the tip resistance and the shaft resistance in which both of them were directly measured. However, it should be noted that in this thesis the tip resistance is directly measured, and thus more reliable than the values of the shaft resistance. The head force is derived from the measured head force and the calculated inertia force, which is again derived from the measured displacement. The shaft friction is derived from the head force and the tip resistance, and it is about 8 to 10 times smaller than the other forces. In other words, the tip resistance is the least susceptible to any possible inaccuracy of the measurement system, compared to the head force and the shaft friction. Besides, the tip resistance is widely used in the practical situation of a pile foundation, Nguyen [206], therefore only R_{max} and R_{up} of the tip resistance will be considered whenever they are available otherwise R_{max} and R_{up} of the head force will be taken into consideration.

Tables 5.4 summarizes the ratios of the maximum of the head, tip and shaft rapid forces over the corresponding static forces at the same displacement of 10% D (R_{max}); and Table 5.5 summarizes the ratios of the unloading point head, tip and shaft forces over the static forces at the same displacement of 10% D (R_{up}). In addition, the drainage factors for each series are given.

¹A lower drainage factor or a higher loading rate leads to a higher value of R_{max} and R_{up} and vice versa.

Table 5.4: Influence of material on R_{max}

Group	Series	Properties	Drainage factor			Head			Tip			Shaft		
			Slow	Average	Fast	Slow	Average	Fast	Slow	Average	Fast	Slow	Average	Fast
Group 1	12	Si 65 Wa, J O 11.3	110.30	44.12	22.06	1.10	1.2	1.14						
	16	Sa 65 Wa, J O 11.3	714.24	285.70	142.85	0.97	1.02	1.00						
Group 2	4	Sa 65 Wa, J C 11.3	714.24	285.70	142.85	0.97	1.10	1.41	0.85	1.04	1.08	1.61	1.68	3.11
	11j 14	Sa 65 Vi, J C 11.3 Si 65 Wa, J C 11.3	714.24 110.30	285.70 44.12	0.45 22.06	1.15 1.10	1.14 1.22	1.61 1.26	1.09	1.10		1.69	1.56	
Group 3	21	Sa 65 Vi, J C 16	1.19	0.45	0.24	1.21	1.22	1.27	1.27	1.23	1.25	1.15	1.30	1.55
	25	Sa 65 Vi, J C 16	1.19	0.45	0.24	1.15	1.25	1.29	1.15	1.22	1.25	1.21	1.44	1.65
Group 4	23	Sa 45 Vi, J C 16	0.94	0.38	0.19	1.16	1.33	1.40	1.17	1.25	1.29	1.28	1.94	2.10
	28	Si 45 Wa, J C 16	41.34	16.53	8.27	1.05	1.16	1.26	1.09	1.16	1.21	1.05	1.28	1.67

Table 5.5: Influence of material on R_{up}

Group	Series	Properties	Drainage factor			Head			Tip			Shaft		
			Slow	Average	Fast	Slow	Average	Fast	Slow	Average	Fast	Slow	Average	Fast
Group 1	12	Si 65 Wa, J O 11.3	110.30	44.12	22.06	1.02	0.87	0.63						
	16	Sa 65 Wa, J O 11.3	714.24	285.70	142.85	0.95	0.77	0.56						
Group 2	4	Sa 65 Wa, J C 11.3	714.24	285.70	142.85	0.83	0.98	1.02	0.81	0.97	0.98	0.97	1.04	1.24
	11j 14	Sa 65 Vi, J C 11.3 Si 65 Wa, J C 11.3	714.24 110.30	285.70 44.12	0.45 22.06	1.01 1.04	0.99 0.69	0.45 0.52	1.01	1.01		1.02	1.88	
Group 3	21	Sa 65 Vi, J C 16	1.19	0.45	0.24	1.10	1.14	1.16	1.18	1.16	1.15	0.86	1.05	1.19
	25	Sa 65 Vi, J C 16	1.19	0.45	0.24	1.05	1.16	1.18	1.08	1.15	1.16	0.96	1.19	1.24
Group 4	23	Sa 45 Vi, J C 16	0.94	0.38	0.19	1.04	1.18	1.24	1.08	1.18	1.20	0.86	1.21	1.42
	28	Si 45 Wa, J C 16	41.34	16.53	8.27	0.97	1.02	1.13	1.01	1.08	1.11	0.86	0.88	1.21

GROUP 1 OF JACKED 11.3 MM DIAMETER OEP IN SOIL BED OF 65% RELATIVE DENSITY

Figure 5.10 presents the dependence of R_{max} of the head force on the penetration rate and the drainage factor, respectively, in the series in silt and water (series 12) and the series in sand and water (series 16). The trend-lines, representing those relationships with the power law as suggested by Nguyen [206], are also plotted in Figure 5.10.

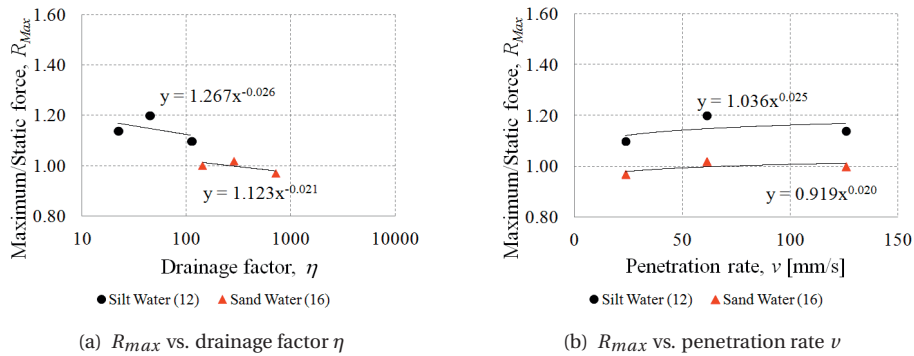


Figure 5.10: Influence of material type in group 1

The series of silt and water has a higher value of R_{max} of the head force than the series of sand and water at any conducted pile loading rate, Figure 5.10(a). This agrees well with the general trend since the drainage factor of the series of silt and water are lower than that of the series of sand and water, Figure 5.10(b). The maximum force increase for the series of silt and water is 20%; and for the series of sand and water, the increase is insignificant. The negligible increase of the maximum rapid force over the static force in the series of sand and water implies the absence of both the rate effect and the excess pore pressure effect in this series. The triviality of the excess pore pressure effect and possible missing of the damping effect in the series of sand and water is already found by Nguyen [206]. However, the absence of the constitutive rate effect is strange because Nguyen [206] reported the constitutive rate effect in both his triaxial tests and centrifuge pile loading series 3 and 4.

In the series 12 and 16 of group 1 of OEP and the series 11j and 14 of group 4 of CEP, the values of R_{up} decrease with a decrease of the drainage factor, Table 5.5, which is unexpected. The reason for this strange behaviour was discussed in Section 4.7; and as stated, the analysis on the R_{up} values of the test series 11 to 16 is not carried out anymore.

GROUP 2 OF JACKED 11.3 MM DIAMETER CEP IN SOIL BED OF 65% RELATIVE DENSITY

Figure 5.11 shows the dependency of the ratios of the rapid tip resistance over the static tip resistance on the drainage factor and the loading rate for the series 4 in sand and water. It can be seen that the maximum resistance has a constant increase of 5-10% over the static resistance, Figure 5.11(a,b), and the unloading point resistance has the same value as the static resistance, Figure 5.11(c,d). As Nguyen [206] pointed out, since the changes of the drainage factor and the loading rate do not affect the increase of the rapid resistance over the static resistance (at the unloading point), it is apparent that the excess

pore pressure does not influence this increase and the increase of 10% of the maximum resistance is purely due to the constitutive rate effect.

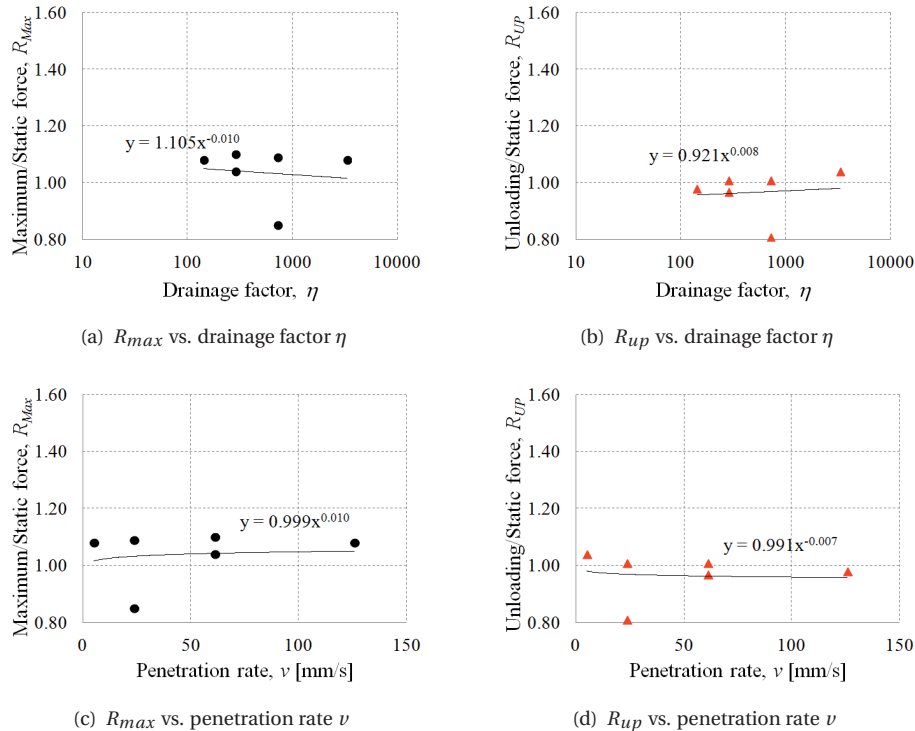


Figure 5.11: Influence of material type in group 2

GROUP 3 OF JACKED 16 MM DIAMETER CEP IN SOIL BED OF 65% RELATIVE DENSITY

Figure 5.12 shows the relationship between R_{max} - subfigures (a,b) and R_{up} - subfigures (c,d) with the loading rate and the drainage factor for the series in sand and viscous fluid (series 21 and 25) and the series in silt and water (series 27). The best-fit trend lines following the power relationship between R_{max} and R_{up} with the loading rate and the drainage factor are included.

The values of R_{max} and R_{up} of the tip force in the series of sand and viscous fluid are higher than those of the series of silt and water at all conducted pile loading rates, Figure 5.12(a,c). This corresponds well with the fact that the drainage condition of the series of silt and water is much better than that of the series of sand and viscous fluid, Figure 5.12(b,d). Moreover, it can be seen that the distance between two trend lines in Figure 5.12(a) is quite similar to that in Figure 5.12(c) which suggests that the rate effect of series in sand and viscous fluid is similar to that of series in silt and water. Consequently, the higher increase of R_{max} and R_{up} of series in sand and viscous fluid in comparison with those of series in silt and water comes mainly from the excess pore pressure effect.

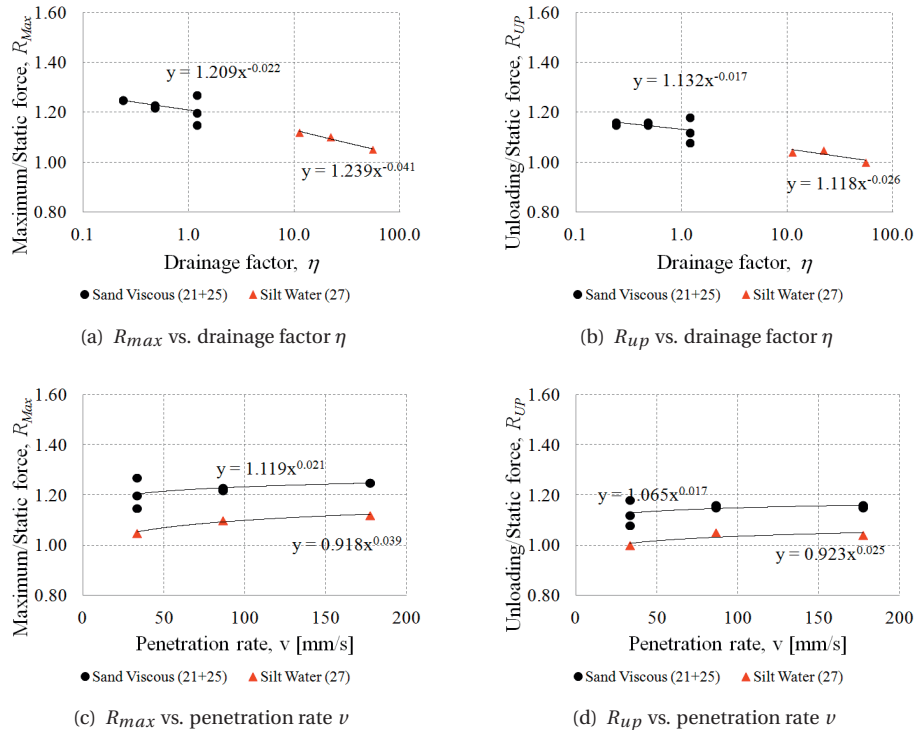


Figure 5.12: Influence of material type in group 3

In the series in sand and viscous fluid, the increase of the rapid resistance over the static resistance is about 15% to 27% at the maximum value and about 8% to 18% at the unloading value. In the series in silt and water, R_{max} has a range from 5% to 12% and R_{up} has a range from 0% to 5%.

GROUP 4 OF JACKED 16 MM DIAMETER CEP IN SOIL BED OF 45% RELATIVE DENSITY

Figure 5.13 illustrates the relationship between the ratio of the rapid forces over the static force with the drainage factor for the series in sand and viscous fluid (series 23) and the series in silt and water (series 28). This figure with the added trend lines clearly confirms the general trends of R_{max} and R_{up} : a higher increase of the rapid force over the static force is found for a test with a lower value of the drainage factor at any performed loading rates. Besides, the estimated power-law suggests a similar dependence of R_{max} and R_{up} on the penetration rate and the drainage factor of series 23 and 28. Similarly to group 3: (1) the rate effects in two series of group 4 are similar; (2) the higher increase of R_{max} and R_{up} of series 23 in comparison with those of series 28 comes mainly from the excess pore pressure effect.

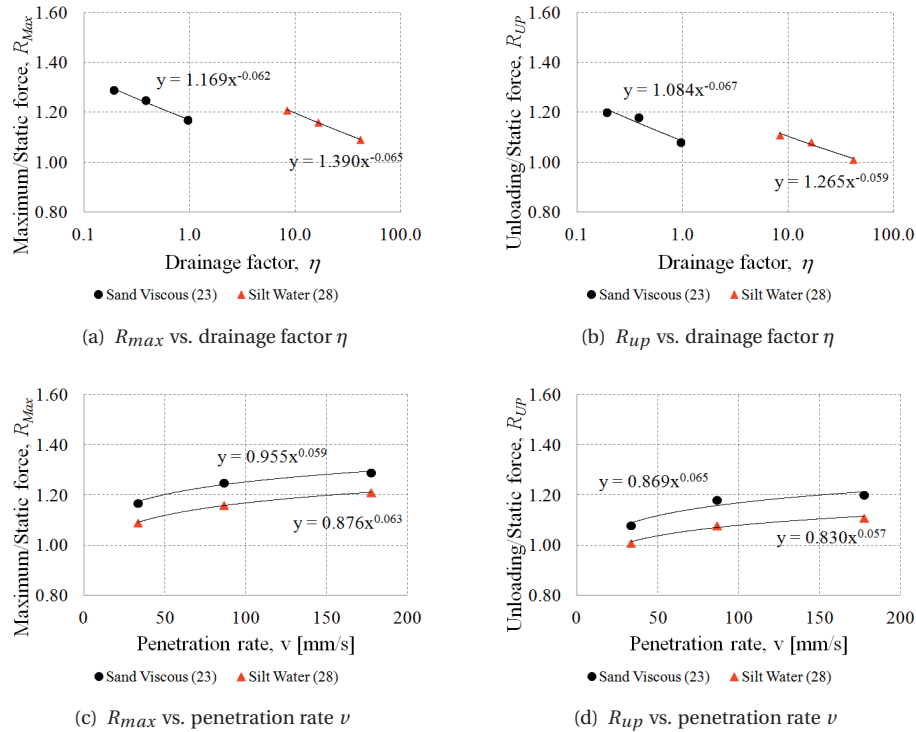


Figure 5.13: Influence of material type in group 4

The increase of the maximum rapid force over the static force for the series of sand and viscous fluid is 17%-29% and for the series of silt and water is 9% to 21%. At the unloading point, the increase of the rapid force over the static force for the series of sand and viscous fluid is 8%-20% and for the series of silt and water is 1% to 11%.

5.3.3. SUMMARY

Table 5.6 summarises the influence of the soil and fluid types on the static force and the ratios of the rapid force over the static force; as mentioned at the beginning of this section, only the tip force is considered. The construction of Table 5.6 follows:

- In the second column, the static tip forces of the pile load test series in sand and viscous fluid are considered as a reference (100%); hence the static forces of the series in silt and water and sand and water are compared with the static force of the series in sand and viscous fluid in term of percentage.
- In the third and fourth columns, the influence of the soil and fluid types are illustrated by the increase of the maximum force and the unloading point force over the static force (at the same displacement) in term of a percentage of increase. Since the influence of the material types also depends on the loading rate, the values in Table 5.6 are presented with the upper and lower bounds corresponding to

the highest and lowest conducted loading rates respectively.

Table 5.6: Influence of soil and pore fluid types

Soil and fluid types	F_static %	F_max/F_static % of increase	F_up/F_static % of increase
Sand and viscous fluid	100	17 - 29	8 - 20
Silt and water	53 - 102	5 - 21	1 - 11
Sand and water	n/a	10	0

The soil and fluid types have a certain influence on the static force in which the tip resistance in the series with sand and viscous fluid can range from similar to double that of the series in silt and water. The difference of the tip resistances is found to be insignificant when the soil is initially dense; whereas with the loose initial density, that difference can be up to two times. Considering the suggestion of Meyerhof [184] and NAVFAC [203] on the relationship between the increase of the soil friction angle and the increase of the unit bearing capacity, the static tip resistance of the series in silt and water should be in the range of 66 - 77% of that of the series in sand and viscous fluid. The wider range observed in Table 5.6 implies a further influence from the material properties.

The soil and fluid types have a significant influence on the ratios of the rapid forces over the static force through the rate effect and the excess pore pressure effect which contributes to the increase of the rapid force over the static force. As the rate effect comes mainly from the soil properties, the excess pore pressure effect is determined by the properties of both soil and fluid.

From the Table 5.6, it can be seen that the material types, the main determinants for the drainage condition of a rapid pile load test [119, 121, 206], strongly affect the excess pore pressure effect and hence the increase of the rapid force over the static force. Of the three material combinations (10 test series) considered in this section, the test series in sand and water have the smallest increase of the rapid force over the static force corresponding to the fact that their drainage factor is the highest one. And, the test series in sand and viscous fluid have the highest increase corresponding to the lowest drainage factor. In particular, the excess pore pressure effect is negligible in series of sand and water, up to 11% in series of silt and water and up to 20% in series of sand and viscous fluid. On the other hand, the constitutive rate effect is found to cause 10% increase of the rapid force over the static force in series of sand and water in which the damping effect is missing. In other series, it is hard to state whether the damping effect is missing or not. Nevertheless, the constitutive rate effect and the damping effect causes an increase of 4 to 10 % in series of silt and water and about 9% in series of sand and viscous fluid.

5.4. INFLUENCE OF INITIAL RELATIVE DENSITY OF SOIL

The influence of initial relative density of soil is considered in this section through 11 test series of four initial relative densities of 36, 45, 54 and 65%. Those 11 test series form 4 groups, within each group all properties except the initial relative density are kept the same. It is expected that the initial relative density has a certain effect on the static force

through the influence on the soil friction angle, as well as the increase of the rapid force over the static force due to the influence on the shear modulus and the dilatancy of the soil materials.

5.4.1. STATIC RESISTANCE

Table 5.7 summarises the maximum and scattering of the static head force and a contribution percentage of the tip force to the head force in each test series.

Table 5.7: Influence of relative density of soil on static force

Group	Series	Properties	Max. head [kN]	Scatter [%]	Tip [%]
Group 1	21	Sa 65 Vi, J C 16	3.56	1-3	78-80
	25	Sa 65 Vi, J C 16	3.63	1-3	80-82
	23	Sa 45 Vi, J C 16	2.07	2	80-81
Group 2	27	Si 65 Wa, J C 16	3.70	4	80-82
	28	Si 45 Wa, J C 16	1.62	3	73-74
Group 3	22	Sa 65 Vi, E C 16	1.88	22-30	85-89
	26	Sa 65 Vi, E C 16	2.02	27-33	84-87
	24	Sa 45 Vi, E C 16	1.36	19	71-77
Group 4	3	Sa 36 Vi, J C 11.3	0.62	14	72-76
	2	Sa 54 Vi, J C 11.3	0.84	2	81-82
	11j	Sa 65 Vi, J C 11.3	0.73	1-3	

It is clear from Table 5.7 that the initial relative soil density has a significant influence on the maximum static force. The general trend is that a decrease of the initial soil density leads to a decrease of the maximum head force (in all groups) and the contribution of tip force (in groups 2, 3 and 4). The main explanation for this trend is the relationship between the relative density and the cone resistance (and thus the pile capacity) as an increase of the relative density results in an increase of the cone resistance as recommended by numerous authors [170, 171, 243] for granular materials. As Lunne and Christoffersen [170] or Schmertmann [243] suggested, when the relative density increases from 36% to 65%, the cone resistance can increase up to 300%. The differences of the head force in all groups stay within the suggested range in the literature [170, 171, 243].

In group 1 of the series in sand and viscous fluid, the difference in the maximum head force between the soil beds of 65% and 45% relative density is 75%; this difference is even bigger, 128%, in group 2 for the series in silt and water. This suggests that the cone resistance of the silt bed is more sensitive to the change of the initial relative density than that of the sand bed. The difference in the maximum head force is only 48% in group 3 in which the pile was pre-embedded. The influence of the installation method will be discussed later. Finally, in group 4 the difference is 35% between the soil bed of 54% relative density and 36% relative density.

5.4.2. RATIO OF RAPID FORCES OVER STATIC FORCES

Tables 5.8 summarizes the ratios of the maximum of the head, tip and shaft rapid forces over the corresponding static forces at the same displacement of 10% D (R_{max}); and Table 5.9 summarizes the ratios of the unloading point head, tip and shaft forces over the static forces at the same displacement (R_{up}). The dynamic drainage factors for each test are also given. In general, a soil bed of a lower relative density has a lower value of the shear modulus and therefore a lower value of the drainage factor. Consequently, test series in the soil bed with a lower relative density have a higher increase of the rapid force over the static force following the general trends mentioned in section 5.2.4.

GROUP 1 OF JACKED 16 MM DIAMETER CEP IN SAND AND VISCOUS FLUID

Figure 5.14 shows the dependency of the ratio of the rapid forces over the static force on the drainage factor and the loading rate for series in sand and viscous fluid with different initial relative densities of 65% (series 21 and 25) and 45% (series 23).

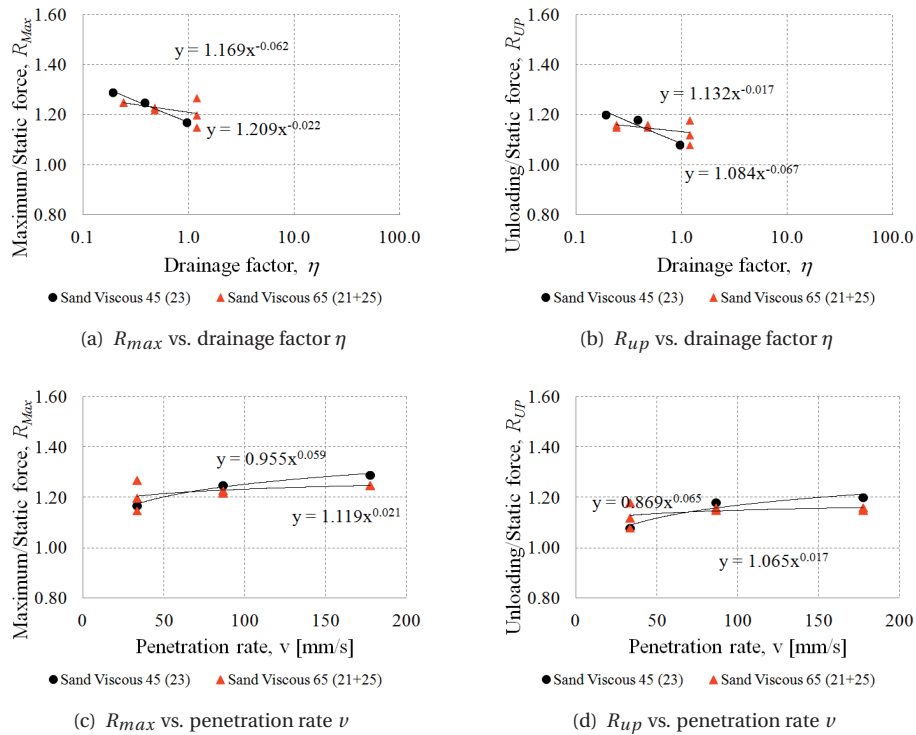


Figure 5.14: Influence of initial density in group 1

Table 5.8: Influence of initial densities on R_{max}

Group	Test	Properties	Drainage factor			Head			Tip			Shaft		
			Slow	Average	Fast	Slow	Average	Fast	Slow	Average	Fast	Slow	Average	Fast
Group 1	21	Sa 65 Vi, J C 16	1.19	0.45	0.24	1.21	1.22	1.27	1.27	1.23	1.25	1.15	1.30	1.55
	25	Sa 65 Vi, J C 16	1.19	0.45	0.24	1.15	1.25	1.29	1.15	1.22	1.25	1.21	1.44	1.65
	23	Sa 45 Vi, J C 16	0.94	0.38	0.19	1.16	1.33	1.4	1.17	1.25	1.29	1.28	1.94	2.10
Group 2	27	Si 65 Wa, J C 16	55.02	22.01	11.00	1.03	1.08	1.12	1.00	1.05	1.04	0.97	1.03	1.31
	28	Si 45 Wa, J C 16	41.34	16.53	8.27	1.05	1.16	1.26	1.09	1.16	1.21	1.05	1.28	1.67
Group 3	22	Sa 65 Vi, E C 16	1.19	0.45	0.24	1.15	1.53	1.46	1.13	1.42	1.33	1.59	2.36	2.82
	26	Sa 65 Vi, E C 16	1.19	0.45	0.24	1.09	1.35	1.42	0.96	1.28	1.30	1.83	2.14	2.33
	24	Sa 45 Vi, E C 16	0.94	0.38	0.19	1.35	1.66	1.67	1.18	1.57	1.50	2.03	2.26	2.52
Group 4	3	Sa 36 Vi, J C 11.3	1.48	0.59	0.30	1.67	missed	2.36	1.23	missed	1.38	3.09	missed	4.86
	2	Sa 54 Vi, J C 11.3	2.48	0.99	0.94	1.38	1.58	2.14	1.24	1.35	1.43	2.84	2.63	4.92
	11j	Sa 65 Vi, J C 11.3	2.38	0.95	0.45	1.46	1.63	1.61						

Table 5.9: Influence of initial densities on R_{up}

Group	Series	Properties	Drainage factor			Head			Tip			Shaft		
			Slow	Average	Fast	Slow	Average	Fast	Slow	Average	Fast	Slow	Average	Fast
Group 1	21	Sa 65 Vi, J C 16	1.19	0.45	0.24	1.10	1.14	1.16	1.18	1.16	1.15	0.86	1.05	1.19
	25	Sa 65 Vi, J C 16	1.19	0.45	0.24	1.05	1.16	1.18	1.08	1.15	1.16	0.96	1.19	1.24
	23	Sa 45 Vi, J C 16	0.94	0.38	0.19	1.04	1.18	1.24	1.08	1.18	1.20	0.86	1.21	1.42
Group 2	27	Si 65 Wa, J C 16	55.02	22.01	11.00	0.98	1.02	1.02	1.00	1.05	1.04	0.88	0.90	0.93
	28	Si 45 Wa, J C 16	41.34	16.53	8.27	0.97	1.02	1.13	1.01	1.08	1.11	0.86	0.88	1.21
Group 3	22	Sa 65 Vi, E C 16	1.19	0.45	0.24	1.04	1.36	1.31	1.06	1.32	1.23	0.88	1.54	1.84
	26	Sa 65 Vi, E C 16	1.19	0.45	0.24	0.98	1.22	1.26	0.91	1.20	1.21	1.24	1.31	1.55
	24	Sa 45 Vi, E C 16	0.94	0.38	0.19	1.14	1.50	1.49	1.11	1.47	1.39	1.23	1.58	1.85
Group 4	3	Sa 36 Vi, J C 11.3	1.48	0.59	0.30	1.48	missed	1.54	1.11	missed	1.25	1.27	missed	2.28
	2	Sa 54 Vi, J C 11.3	2.48	0.99	0.94	1.15	1.33	1.46	1.13	1.26	1.30	1.24	1.61	2.08
	11j	Sa 65 Vi, J C 11.3	2.38	0.95	0.45	1.26	0.90	0.45						

It can be seen from Figure 5.14 that the data points follow almost the same trend, which suggests that the difference between these series is minor and therefore, in group 1, the initial relative density has little influence on the increase of the rapid force over the static force. It is worth mentioning that, although the two trend lines in each subfigure of Figure 5.14 have different gradients, it does not imply different trends. In fact, the difference of the gradients comes from the extra loadings in series 21 which is performed at the end of the loading process. Without these extra loadings, the data points are better concentrated.

Except for the slow loading tests in series 21, the increase of the rapid tip force over the static tip force slightly increases (a few percent) with a decrease of the relative density. The highest increase of the maximum force over the static force is 29%, and the highest increase of the unloading force over the static force is 20%. These two highest increases appear in series 23 in the 45% relative density soil bed.

GROUP 2 OF JACKED 16 MM DIAMETER CEP IN SILT AND WATER

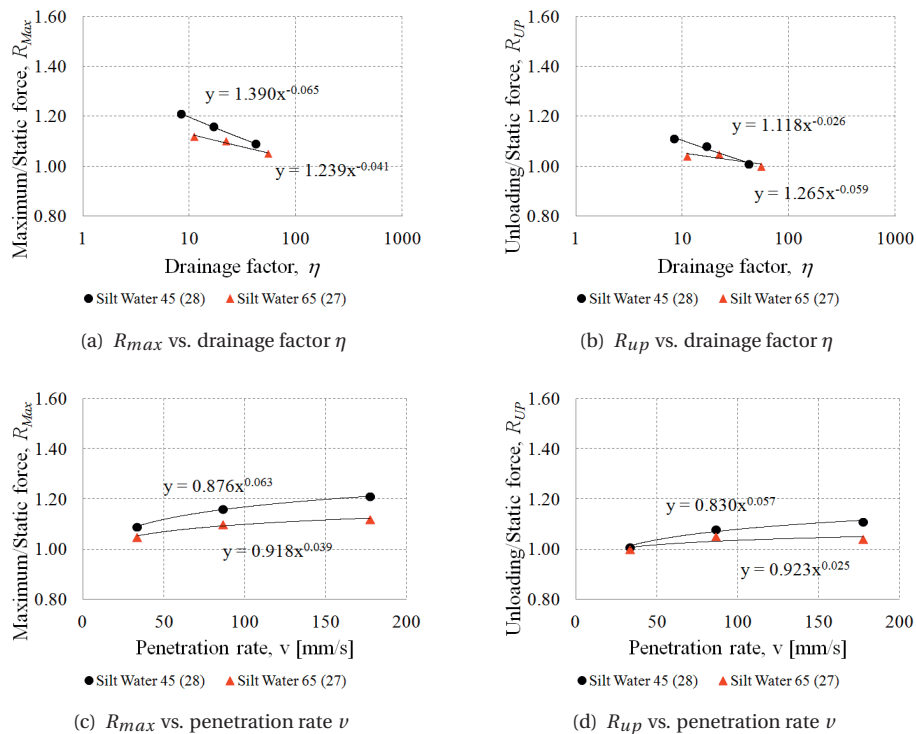


Figure 5.15: Influence of initial density in group 2

Figure 5.15 shows the dependency of the ratios of the rapid forces over the static force on the drainage factor and the loading rate for series in silt and water with different initial relative densities of 65% (series 27) and 45% (series 28). The two general trends

mentioned in section 5.2.4 hold for head force, tip resistance and shaft friction in most of loadings. At any given loading rates, the values of both R_{max} and R_{up} of series 28 are slightly higher than those of series 27, Figure 5.15(a,c), due to the fact that at the same loading rate the drainage factor of series 28 is lower than that of series 27, Figure 5.15(b,d). The gradients of the trend lines in Figure 5.15 imply that the differences in the values of R_{max} and R_{up} between series 27 and 28 are more profound at the higher loading rate and/or at the lower drainage factor.

The maximum increases of the maximum and unloading rapid force over the static force in series 27 are 12% and 5% respectively; while those values in series 28 are 21% and 11%.

GROUP 3 OF PRE-EMBEDDED 16 MM DIAMETER CEP IN SAND AND VISCOUS FLUID

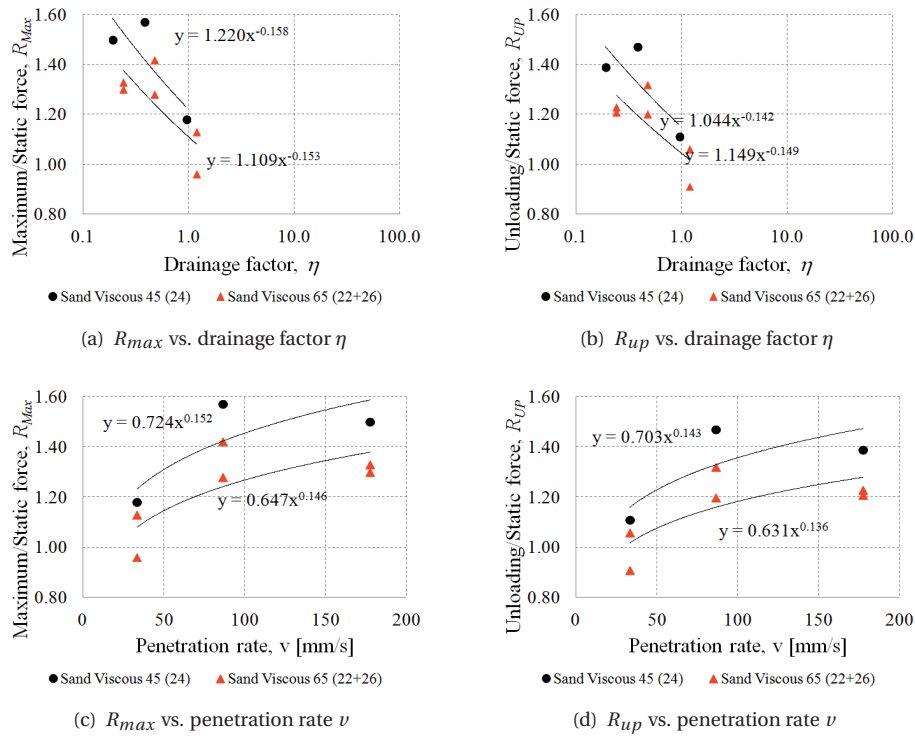


Figure 5.16: Influence of initial density in group 3

Figure 5.16 shows the dependency of the ratios of the rapid forces over the static force on the drainage factor and the loading rate for series in sand and viscous fluid with different initial relative densities of 65% (series 22 and 26) and 45% (series 24). At any given loading rates, the values of both R_{max} and R_{up} of series 24 are significantly higher than those of series 22 and 26. The differences in the values of R_{max} and R_{up} between series in the soil bed of 45% and 65% initial relative density are slightly more profound at the

higher loading rate and/or at the lower drainage factor, Figure 5.16. It should be noted that in three series 22, 24 and 26, the highest values of R_{max} and R_{up} are normally found in the loadings with average penetration rate and/or drainage factor. The reason for this phenomenon is still unclear.

The maximum increases of the maximum and unloading rapid force over the static force in series in the soil bed of 45% are 57% and 47% respectively; while those values in series 28 are 42% and 32%.

GROUP 4 OF JACKED 11.3 MM DIAMETER CEP IN SAND AND VISCOUS FLUID

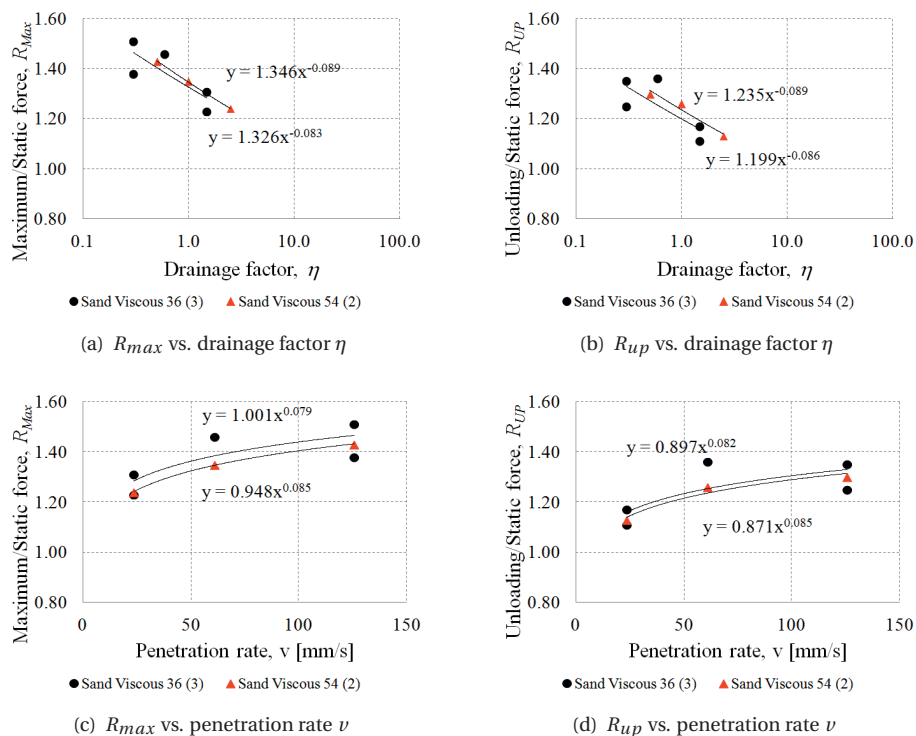


Figure 5.17: Influence of initial density in group 4

Figure 5.17 shows the dependency of the ratios of the rapid forces over the static force on the drainage factor and the loading rate for series in sand and viscous fluid with different initial relative densities of 54% (series 2) and 36% (series 3). It can be seen that the trend lines in Figure 5.17 are very close to each other with almost the same gradient which indicates that the difference in the increase of the rapid force over the static force between the two series in 36% and 54% relative density is minor. Consequently, the influence of the relative density in group 4 is insignificant. This observation is similar to the one in group 1 of jacked CEP in sand and viscous fluid which may imply the domination of the

installation method over the initial relative density on the influence on R_{max} and R_{up} . Nevertheless, the installation method is considered in the later section.

5.4.3. SUMMARY

Table 5.10, which is created in a similar way as Table 5.6, summarises the influence of the relative density on the static force and on the ratio of the rapid force over the static force. In the second column of Table 5.10, the static force of series in the 36% relative density soil bed is compared with that of series in the 45%, 54% and 65% relative density soil bed. In the third and fourth column of Table 5.10, the influence of the initial relative density is related to the increase of the maximum force and the unloading point force over the static force in term of a percentage of increase.

Table 5.10: Influence of initial relative densities

Initial relative densities	F_static %	F_max/F_static % of increase	F_up/F_static % of increase
Sand 36%	100	23 - 51	11 - 36
Sand 45%	107 - 164	17 - 50	8 - 47
Sand 54%	135	23 - 43	13 - 30
Sand 65%	118 - 287	13 - 42	6 - 32
Silt 45%	100	9 - 21	1 - 11
Silt 65%	228	6 - 12	0 - 5

It is clear from Table 5.10 that the initial relative density has a strong influence on the static tip resistance. An increase of the initial relative density from 36% to 65% can result in an increase of up to 187% of the head force. Two agents which can explain this increase. The main factor is the increase of the relative density leads to the increase of the cone resistance [23, 141, 170, 243]. Another factor is the increase of the soil friction angle associated with the increase of the initial relative density, which could lead to the increase of the shaft friction [23, 34, 141, 196].

The initial relative density has a certain influence on the increase of the rapid force over the static force, as the initial relative density decreases the values of R_{max} and R_{up} increase. However, it might be possible that the influence of the relative density is not significant since Table 5.10 showed the overlap of the range of R_{max} and R_{up} , or Figure 5.14 and 5.17 illustrated a similar trend of the relationship $R_{max} - \eta$ and $R_{up} - \eta$ in the comparison of series 21 & 25 ($D_r = 65\%$) versus series 23 ($D_r = 45\%$) and the comparison of series 2 ($D_r = 54\%$) versus series 3 ($D_r = 36\%$), respectively. Nevertheless, the values of R_{max} and R_{up} in the last two rows in Table 5.10 suggested that the decrease of the initial relative density leads to the minor increasing influence of both the excess pore pressure effect (R_{up}) and the rate effect ($R_{max} - R_{up}$) in the test series in silt and water. In particular, when the initial relative density of the sand bed reduces from 65% to 36%, the excess pore pressure effect contributes to 4% increase more, and the rate effect contributes to 5% increase more or when the initial relative density of the silt bed reduces from 65% to 45%, the excess pore pressure effect contributes to 6% increase more, and the rate effect contributes to 3% increase more.

The additional influence of the excess pore pressure as the relative density decreases is rather unexpected in the normal sense. In general, it is expected that, in loose sand, there might be a positive excess pore pressure due to compaction during shearing; whereas, in dense sand, there might be a negative excess pore pressure due to dilatancy during shearing. Consequently, it is supposed that the increase of the rapid resistance over the static resistance due to the excess pore pressure effect is more for dense sand than for loose sand. However, Table 5.10 suggested the opposite. On the other hand, following Equation 3.1, it is logical that as the initial relative density decreases, the soil shear stiffness reduces which leads to a reduction of the drainage condition. Because of this, the excess pore pressure effect is more for loose sand than for dense sand which is now in agreement with the observation from the experiments.

The mechanism for the additional influence of the rate effect is unclear. It is expected that when the initial relative density reduces, the friction angle or the interlocking of soil grains should reduce and consequently the constitutive rate effect hence the rate effect should decrease. This behaviour in sand and viscous fluid is not as obvious as in silt and water.

5.5. INFLUENCE OF PILE INSTALLATION METHODS

The pile in this study was installed either by static pushing (jacked) into the soil from the depth of $10 D$ to the depth of $20 D$ or by directly placing it at the depth of $20 D$. This variation is considered to investigate two typical types of pile installation methods, which are the jacked being similar for a displacement pile and the pre-embedded being similar to a bored pile. The installation method has a significant influence on the static tip resistance as reported by numerous papers [67, 217, 225, 250]. For the rapid pile load test, although the test with the jacked pile and the test with the pre-embedded pile, in principle, have the same drainage factor, it turns out that the increase of the maximum or unloading point force over the static force are not the same. The installation method has a considerable influence on the increase of the rapid forces over the static force which will be discussed in more detail later. In this section, 10 test series with a close-ended pile in sand and viscous fluid are investigated to study the influence of the installation method.

5.5.1. STATIC RESISTANCE

Table 5.11 summarises the maximum and scattering of the static head force and a contribution of the tip force to the head force in each test series. It clearly shows the significant influence of the installation method on the maximum static force. The maximum head force of the jacked pile is always higher than that of the pre-embedded pile. The scattering of measured maximum force in the jacked-pile test is also much smaller than that in the pre-embedded pile test. The strong influence of the installation method on the maximum pile force is expected because the jacked installation process significantly changes the state of the surrounding soil of a pile. In particular, the soil along the shaft is loosened thus the lateral earth pressure increases and the shaft friction is improved greatly; on the other hand, the soil under the pile tip is densified, therefore the internal friction angle as well as the stress of the soil increases and the tip resistance is enhanced significantly [67, 217]. The static head force of the jacked pile can be higher than that of the

pre-embedded pile about 18% (group 4) to 52% (group 2) and even up 93% (group 1). In group 3 of a pile pre-embedded at the depth $10 D$ (test 11b) and a pile pre-embedded at the depth $20 D$ (test 15), the maximum head force of test 15 is 93% higher than that of test 11b. This big difference originates from the twofold difference in the stress level at the pile tip of these two tests.

Table 5.11: Influence of installation methods on static force

Group	Series	Properties	Max. head [kN]	Scatter [%]	Tip [%]
Group 1	21	Sa 65 Vi, J C 16	3.56	1-3	78-80
	25	Sa 65 Vi, J C 16	3.63	1-3	80-82
	22	Sa 65 Vi, E C 16	1.88	22-30	85-89
	26	Sa 65 Vi, E C 16	2.02	27-33	84-87
Group 2	23	Sa 45 Vi, J C 16	2.07	2	80-81
	24	Sa 45 Vi, E C 16	1.36	19	71-77
Group 3	11b	Sa 65 Vi, E C 11.3	0.32	40-47	
	15	Sa 65 Vi, E C 11.3	0.62	42-46	
Group 4	11j	Sa 65 Vi, J C 11.3	0.73	1-3	
	15	Sa 65 Vi, E C 11.3	0.62	42-46	

5.5.2. RATIO OF RAPID FORCES OVER STATIC FORCES

Tables 5.12 summarises the ratios of the maximum of the head, tip and shaft rapid forces over the corresponding static forces at the same displacement of $10\% D$ (R_{max}); and Table 5.13 summarises the ratios of the unloading point head, tip and shaft forces over the static forces at the same displacement (R_{up}). The drainage factors for each test are given. In Table 5.12 and 5.13, the drainage factors of test series in each group are identical since they are determined from the equal initial shear modulus of the soil bed together with other exact parameters, Equation 3.1. However, there is a difference in the increase of the rapid force over the static force between two series with the jacked pile and series with the pre-embedded pile. In general, series with the jacked pile have a lower increase of the rapid force over the static force than series with the pre-embedded pile. The difference in the increase of the rapid force over the static between those two types of test series also depends on pile diameter and relative density of a soil bed.

Table 5.12: Influence of installation method on R_{max}

Group	Series	Properties	Drainage factor			Head			Tip			Shaft		
			Slow	Average	Fast	Slow	Average	Fast	Slow	Average	Fast	Slow	Average	Fast
Group 1	21	Sa 65Vi, J C 16	1.19	0.45	0.24	1.21	1.22	1.27	1.27	1.23	1.25	1.15	1.30	1.55
			1.18			1.18			1.20				1.17	
			1.19	0.45	0.24	1.15	1.25	1.29	1.15	1.22	1.25	1.21	1.44	1.65
Group 2	23	Sa 45Vi, J C 16	0.94	0.38	0.19	1.16	1.33	1.40	1.17	1.25	1.29	1.28	1.94	2.10
			0.94	0.38	0.19	1.35	1.66	1.67	1.18	1.57	1.50	2.03	2.26	2.52
			1.19	0.45	0.24	1.15	1.33	1.42	0.96	1.28	1.3	1.83	2.14	2.33
Group 3	11b	Sa 65Vi, E C 11.3	2.38	0.95	0.45	1.98	2.53	2.34						
			2.38	0.95	0.45	1.54	1.83	1.78						
			1.19	0.45	0.24	1.09	1.35	1.42	1.17	1.25	1.29	1.28	1.94	2.10
Group 4	11j	Sa 65Vi, J C 11.3	2.38	0.95	0.45	1.46	1.63	1.61						
			2.38	0.95	0.45	1.54	1.83	1.78						
			1.19	0.45	0.24	1.09	1.35	1.42	1.17	1.25	1.29	1.28	1.94	2.10

Table 5.13: Influence of installation method on R_{up}

Group	Series	Properties	Drainage factor			Head			Tip			Shaft		
			Slow	Average	Fast	Slow	Average	Fast	Slow	Average	Fast	Slow	Average	Fast
Group 1	21	Sa 65Vi, J C 16	1.19	0.45	0.24	1.10	1.14	1.16	1.18	1.16	1.15	0.86	1.05	1.19
			1.09			1.09			1.12				0.95	
			1.19	0.45	0.24	1.05	1.16	1.18	1.08	1.15	1.16	0.96	1.19	1.24
Group 2	23	Sa 45Vi, J C 16	0.94	0.38	0.19	1.04	1.18	1.24	1.08	1.18	1.20	0.86	1.21	1.42
			0.94	0.38	0.19	1.14	1.50	1.49	1.11	1.47	1.39	1.23	1.58	1.85
			1.19	0.45	0.24	1.04	1.18	1.22	0.91	1.20	1.21	1.24	1.31	1.55
Group 3	11b	Sa 65Vi, E C 11.3	2.38	0.95	0.45	1.88	1.30	0.45						
			2.38	0.95	0.45	1.46	1.12	0.38						
			1.19	0.45	0.24	1.04	1.18	1.22	0.91	1.20	1.21	1.24	1.31	1.55
Group 4	11j	Sa 65Vi, J C 11.3	2.38	0.95	0.45	1.26	0.90	0.45						
			2.38	0.95	0.45	1.46	1.12	0.38						
			1.19	0.45	0.24	1.04	1.18	1.22	0.91	1.20	1.21	1.24	1.31	1.55

GROUP 1 WITH THE 16 MM DIAMETER CEP IN 65% RELATIVE DENSITY SOIL BED

Figure 5.18 shows the dependence of the ratios of the rapid forces over the static force on the drainage factor and the loading rate for series in sand and viscous fluid of 65% relative density with the jacked pile (series 21 and 25) and with the pre-embedded pile (series 22 and 26). In the first rapid loading cycle in the slow loading rate, the values of R_{max} and R_{up} of the series with the pre-embedded pile are lower than the values of R_{max} and R_{up} of the series with the jacked pile. On the other hand, the loading cycles with average and fast loading rates show that the series with the pre-embedded pile have the higher values of R_{max} and R_{up} than those of the series with the jacked pile.

The highest increases of the maximum and unloading rapid forces over the static force are 27% and 18% in the series with the jacked pile, which are found at the slow loading rate. In the series with the pre-embedded pile, those values are 42% and 32%, which occur at the average loading rate.

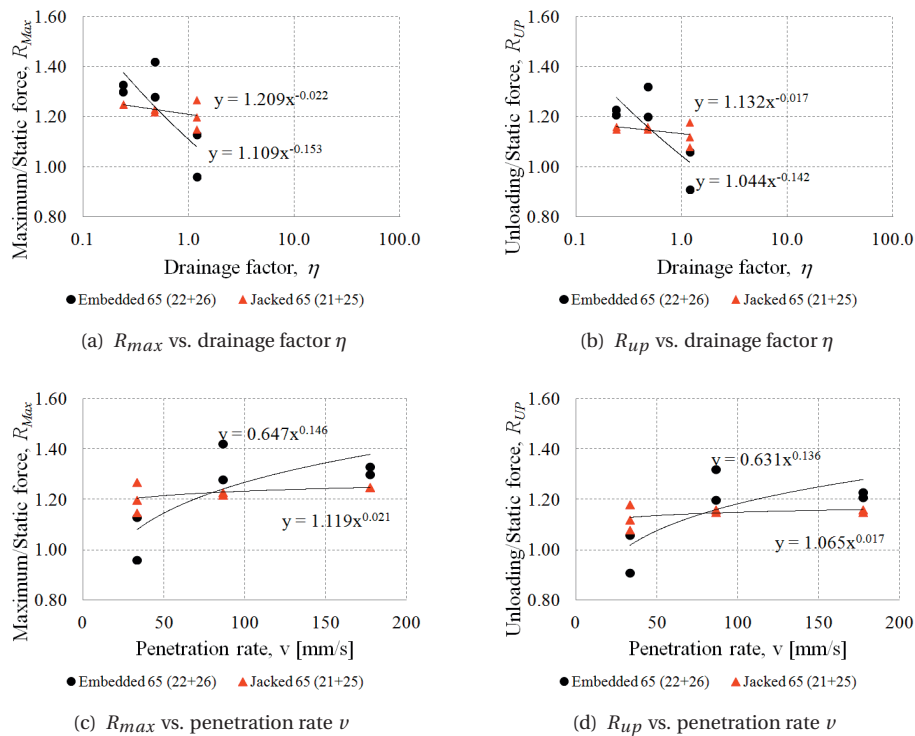


Figure 5.18: Influence of installation method in group 1

GROUP 2 WITH THE 16 MM DIAMETER CEP IN 45% RELATIVE DENSITY SOIL BED

Figure 5.19 shows the dependence of the ratios of the rapid forces over the static force on the drainage factor and the loading rate for series in sand and viscous fluid of 45% relative density with the jacked pile (series 23) and with the pre-embedded pile (series 24). The values of R_{max} and R_{up} in series with the pre-embedded pile are always higher

than the values of R_{max} and R_{up} in series with the jacked pile at any equal penetration rate or drainage factor. This difference is more significant when the drainage factor reduces or when the penetration rate increases, Figure 5.19. It is therefore reasonable to conclude that the influence of the installation method on the values of R_{max} and R_{up} in series with the 45% relative density soil bed is significant.

The highest increases of the maximum and unloading rapid forces over the static force are 29% and 20% in the series with the jacked pile, which are found at the fast loading rate. In the series with the pre-embedded pile, those values are 57% and 47%, which occur at the average loading rate.

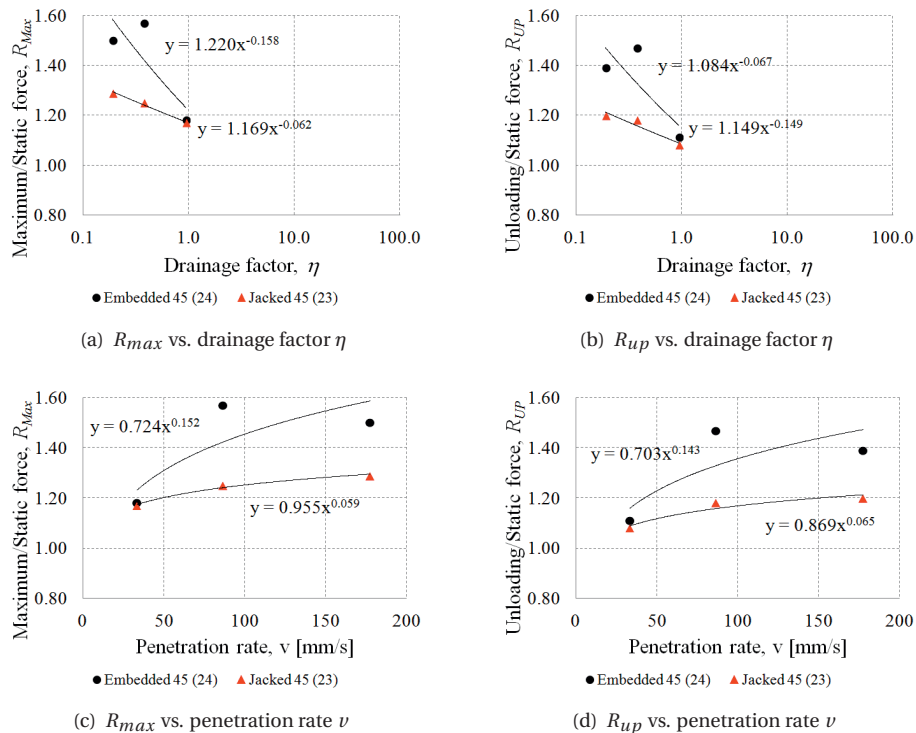


Figure 5.19: Influence of installation method in group 2

GROUP 3 AND 4 WITH THE 11.3 MM DIAMETER CEP IN 65% RELATIVE DENSITY SOIL BED

Figure 5.20 shows the dependence of the ratios of the rapid forces over the static force on the drainage factor and the loading rate for series in sand and viscous fluid of 65% relative density with the jacked pile pre-embedded in the depth of $10 D$ (series 11b) and in the depth of $20 D$ (series 15) - group 3. Figure 5.21 shows the dependence of the ratios of the rapid forces over the static force on the drainage factor and the loading rate for series in sand and viscous fluid of 65% relative density with the jacked pile (series 11j) and with the pre-embedded pile (series 15) - group 4. Because of the problem with the control servo system, the tip measurement was missing in those three series. Moreover,

because of the loading pattern, the ratio of the unloading point force over the static force decreases with a decrease of the drainage factor, and it is far smaller than unity.

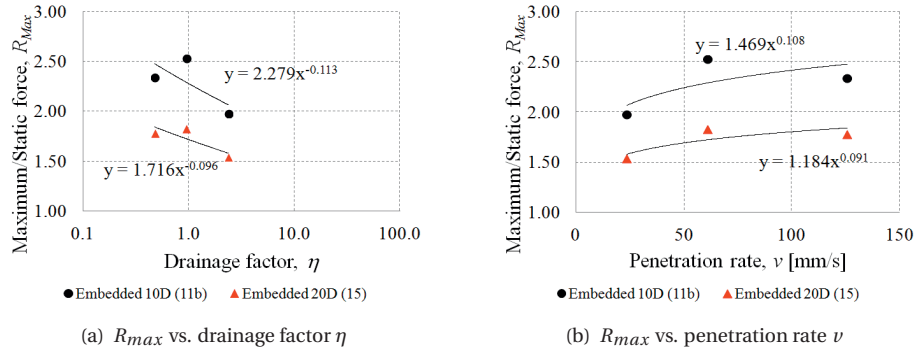


Figure 5.20: Influence of installation method in group 3

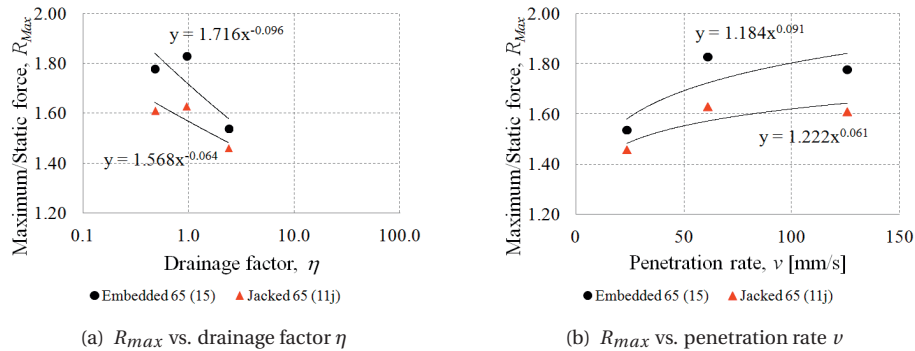


Figure 5.21: Influence of installation method in group 4

5.5.3. SUMMARY

Table 5.14, which is created similarly to Table 5.6, summarises the influence of the installation method on the static force and the ratios of the rapid forces over the static force.

The installation method has a strong influence on the static force with the static force of the jacked pile is 52 to 93% higher than that of the pre-embedded pile. This is understandable from the fact that the stress state of the surrounding soil of the pile in the jacked pile test and the pre-embedded pile test is significantly different due to the installation process occurs when the pile was jacked into the designed level of 20 D .

Table 5.14 clearly shows a strong influence of the installation method on the increase of the rapid force over the static force. The increase of the rapid force over the static force in the series with the pre-embedded pile also varies in a wider range than the increase in the series with the jacked pile. With the pre-embedded pile, R_{max} and R_{up} vary from -4

up to 57% and from -9 up to 47%, respectively; whereas with the jacked pile, R_{max} and R_{up} vary from 15 to 29% and from 8 to 20%, respectively.

Table 5.14: Influence of the installation method

Installation methods	F_static %	F_max/F_static % of increase	F_up/F_static % of increase
Pre-embedded pile	100	-4 - 57	-9 - 47
Jacked pile	152 - 193	15 - 29	8 - 20

It is interesting to see that the rate effect contributes similar portion (about 10%) of the increase of the rapid force over the static force in the two series. However, the excess pore pressure effect accounts for only 20% of the increase of the rapid force over the static force in series with the jacked pile, but it contributes up to 47% of the increase in series with the pre-embedded pile. It seems that the excess pore pressure effect is much more significant in the pile load test with the pre-embedded pile.

During the installation process, the soil along the pile shaft is loosen whereas the soil under the pile is densified [67, 277]. Accordingly, the horizontal stress long the pile shaft and under the pile tip significantly increases [67, 217]. As the confinement of the soil increases, there are two possibilities. The first one is the increasing confinement reduces the mobility, or the capacity of shear deformation, of soil grains. As a consequence, the failure surfaces, which occur during the rapid pile load test and account for the excess pore pressure effect [206], may be limited in size and time or even cannot be created. This possibility agrees well with Equation 3.1 which implies that as the shear modulus increases, the drainage factor increases. Moreover, it can explain the higher influence of the excess pore pressure effect on R_{max} and R_{up} . On the other hand, the second possibility is that as the behaviour of the soil under the pile tip changes from significantly compressive inside the "nose cone" to considerably dilative up to the distance of $2 D$ under the pile tip and $2 D$ from the pile shaft [207, 279] during the installation process, the negative excess pore pressure occurs more in the pile load test with the jacked pile. In that case, it is expected that the excess pore pressure effect is more significant in the pile load test with the jacked pile which contrasts with what is observed here. While the second possibility is reasonable in relationship to the contractive/dilative behaviour of granular soils, the first possibility can actually explain the results on Table 5.14.

The results from this section pointed out that the installation method has a strong influence on the increase of the rapid force over the static force by changing the drainage condition. However, it is clearly not an easy task to quantify the influence of the installation method in this study. Firstly, the measurements in the pre-embedded pile test are not as repeatable as the measurements in the jacked pile test. Secondly, it is still impossible to make a detail quantitative measurement of the change of relative density (and the shear modulus) of the soil around the pile during installation or on the creation of the failure surface during the rapid load test.

5.6. INFLUENCE OF PILE TYPES

Three pile types are used in this study namely open-ended pile (OEP) with the diameter of 11.3 mm, close-ended pile (CEP) with the diameter of 11.3 mm and CEP with the diameter of 16 mm. In this section, 10 test series are investigated to study the influence of the pile types.

It should be noted that the stress levels at the pile tip of the 11.3 mm-diameter pile and of the 16 mm-diameter pile are quite different since the tip is at a different depth (20 D). Consequently, A pile load test with the 11.3 mm diameter CEP and a pile load test with 16 mm diameter pile CEP clearly have different maximum static force as well as different increase of the rapid forces over the static force.

A static pile load test with CEP and a static pile load test with OEP may have identical, similar or different maximum force, which depends on the plugging mode and the length of the plug of the OEP. If the OEP is fully plugging and the plug length is equal to the penetration depth, then the response and the force of the OEP are identical to those of the CEP. In general, the plug length is shorter than the penetration depth [208]; therefore the force of the OEP is smaller to that of the CEP due to less densification of the surrounding soil. In a rapid pile load test, although the CEP and the OEP have the same drainage factor calculated following Equation 3.1, it turns out that the increases of the rapid force over the static force in those tests are quite different.

5.6.1. STATIC RESISTANCE

Table 5.15 summarises the maximum and scattering of the static head force and a contribution percentage of the tip force to the head force in each test series.

Table 5.15: Influence of pile types on static force

Group	Series	Properties	Max. head [kN]	Scatter [%]	Tip [%]
Group 1	11j	Sa 65 Vi, J C 11.3	0.73	1-3	
	21	Sa 65 Vi, J C 16	3.56	1-3	78-80
	25	Sa 65 Vi, J C 16	3.63	1-3	80-82
Group 2	15	Sa 65 Vi, E C 11.3	0.62	42-46	
	22	Sa 65 Vi, E C 16	1.88	22-30	85-89
	26	Sa 65 Vi, E C 16	2.02	27-33	84-87
Group 3	12	Si 65 Wa, J O 11.3	0.61	6	
	14	Si 65 Wa, J C 11.3	0.66	1	
Group 4	4	Sa 65 Wa, J C 11.3	1.40	6	
	16	Sa 65 Wa, J O 11.3	0.96	3	

Group 1 and 2 show the comparison of the maximum static head forces between the series with the 11.3 mm diameter pile (series 11j and series 15) and the series of the 16 mm diameter pile (series 21+25 and 22+26) with two pile installation methods, jacked (group 1) and pre-embedded (group 2). It is as expected that the series with a larger pile have much larger head force. In group 1 with the jacked piles, the difference in the maximum static unit force of the series 11j (11.3 mm diameter pile) and that of the series 21+ 25 (16 mm diameter pile) is about 2.44 times. In group 2 with the pre-embedded

piles, this difference is about 1.59 times. The difference between the small pile (11.3 mm diameter) and the large pile (16 mm diameter) comes directly from the different stress level at the pile tip as mentioned above. Further different between group 1 and 2 may come from the influence of the installation method, group 1 is the jacked pile whereas group 2 is the pre-embedded pile.

Group 3 and 4 show the comparison between the series of CEP (series 14 and 4) and the series of OEP (series 12 and 16) in two different sets of materials, namely: silt and water (group 3) and sand and water (group 4). In group 3 of the series in silt and water, the maximum head force of CEP (0.66 kN) and OEP (0.61 kN) is less than 10% different. However, in group 2 of the series in sand and water, the maximum head force of CEP (1.40 kN) is 45% higher than that of OEP (0.96kN). This big difference in two sets of materials may suggest that the OEP in silt was plugging and its behaviour or, more precisely, the maximum force is similar to that of the CEP. On the contrary, the OEP in sand was probably unplugged, the sand plug inside the OEP was continuously pushed further as more sand comes inside the pile and therefore its capacity is significantly lower than the capacity of the CEP.

5.6.2. RATIO OF RAPID FORCES OVER STATIC FORCES

Tables 5.16 summarizes the ratios of the maximum of the head, tip and shaft rapid forces over the corresponding static forces at the same displacement of 10% D (R_{max}); and Table 5.17 summarizes the ratios of the unloading point head, tip and shaft forces over the static forces at the same displacement of 10% D (R_{up}). In addition, the drainage factors for each series are given. It should be noted that, as mentioned before, there was a problem with the servo control system and there was no information for tip measurements in the series from 11 to 16. Because series 11-16 have a decrease of the increase of the unloading point force over the static force with a decrease of the drainage factor whilst other series, which is used to compare with series 11-16, have an opposite trend, comparison between series 11-16 and the other series on R_{up} is not reasonable and has no practical meaning.

In group 1 and 2, the drainage factor of the series with the smaller pile (series 11j and series 15) is higher than that of the series with the bigger pile (series 21+25 and 22+26) hence the general trends mentioned in section 5.2.4 are supposed. However, the increases of the maximum head force over the static head force in the series 11j and 15 are significantly larger than the increases in the series 21+25 and 22+26, respectively. This is contradictory to what expected. One possible explanation is the dependency of the shear modulus on the stress level which is reported in the literature [130, 222] but is not taken into account here. The shear modulus used to calculate the drainage factor in the series 11-15, 21-22 and 25-28 are the same. Another uncertainty is a loading and servo control system: the series 11-16 were conducted with a different loading and servo control system, which created a very high acceleration and a strange loading pattern. Because of this, the increase of the rapid force over the static force in the series 11-16 is questionable.

Table 5.16: Influence of pile type on R_{max}

Group	Series	Properties	Drainage factor			Head			Tip			Shaft			
			Slow	Average	Fast	Slow	Average	Fast	Slow	Average	Fast	Slow	Average	Fast	
Group 1	11j	Sa 65 Vi, J C 11.3	2.38	0.95	0.45	1.46	1.63	1.61	1.27	1.23	1.25	1.15	1.15	1.30	1.55
	21	Sa 65 Vi, J C 16	1.19	0.45	0.24	1.21	1.22	1.27	1.27	1.23	1.25	1.15	1.21	1.44	1.65
	25	Sa 65 Vi, J C 16	1.19	0.45	0.24	1.15	1.25	1.29	1.15	1.22	1.25	1.15	1.21	1.44	1.65
Group 2	15	Sa 65 Vi, E C 11.3	2.38	0.95	0.45	1.54	1.83	1.78	1.13	1.42	1.33	1.59	2.36	2.82	
	22	Sa 65 Vi, E C 16	1.19	0.45	0.24	1.15	1.53	1.46	0.96	1.28	1.30	1.83	2.14	2.33	
	26	Sa 65 Vi, E C 16	1.19	0.45	0.24	1.09	1.35	1.42	0.96	1.28	1.30	1.83	2.14	2.33	
Group 3	12	Si 65 Wa, J O 11.3	110.30	44.12	22.06	1.10	1.20	1.14							
	14	Si 65 Wa, J C 11.3	110.30	44.12	22.06	1.10	1.22	1.26							
Group 4	4	Sa 65 Wa, J C 11.3	714.24	285.70	142.85	0.97	1.10	1.41	0.85	1.04	1.08	1.61	1.68	3.11	
	16	Sa 65 Wa, J O 11.3	714.24	285.70	142.85	1.15	1.14	1.00	1.09	1.10		1.69	1.56		

Table 5.17: Influence of pile type on R_{tip}

Group	Series	Properties	Drainage factor			Head			Tip			Shaft		
			Slow	Average	Fast	Slow	Average	Fast	Slow	Average	Fast	Slow	Average	Fast
Group 1	11j	Sa 65 Vi, J C 11.3	2.38	0.95	0.45	1.26	0.90	0.45	1.18	1.16	1.15	0.86	1.05	1.19
	21	Sa 65 Vi, J C 16	1.19	0.45	0.24	1.10	1.14	1.16	1.18	1.15	1.16	0.96	1.19	1.24
	25	Sa 65 Vi, J C 16	1.19	0.45	0.24	1.05	1.16	1.18	1.08	1.15	1.16	0.96	1.19	1.24
Group 2	15	Sa 65 Vi, E C 11.3	2.38	0.95	0.45	1.46	1.12	0.38	1.06	1.32	1.23	0.88	1.54	1.84
	22	Sa 65 Vi, E C 16	1.19	0.45	0.24	1.04	1.36	1.31	0.91	1.20	1.21	1.24	1.31	1.55
	26	Sa 65 Vi, E C 16	1.19	0.45	0.24	0.98	1.22	1.26	0.91	1.20	1.21	1.24	1.31	1.55
Group 3	12	Si 65 Wa, J O 11.3	110.30	44.12	22.06	1.02	0.87	0.63						
	14	Si 65 Wa, J C 11.3	110.30	44.12	22.06	1.04	0.69	0.52						
Group 4	4	Sa 65 Wa, J C 11.3	714.24	285.70	142.85	0.83	0.98	1.02	0.81	0.97	0.98	0.97	1.04	1.24
	16	Sa 65 Wa, J O 11.3	714.24	285.70	142.85	1.01	0.99	0.77	1.01	1.01	1.02	1.02	1.88	

In groups 3 and 4 of the series with the CEP and the series with the OEP, although having the same drainage factor as defined in Equation 3.1, the series with the CEP have a higher increase of the maximum force over the static force than that of the series with the OEP regardless of the soil types. The possible explanation for this difference is the drainage condition. In the series with the OEP, the pore water can be drained not only under the pile tip and along the outer pile shaft as in the series with the CEP but also along the inner pile shaft and on the free surface of the soil plug. As the drainage ability of the series with the OEP is higher than that in the series with CEP, the influence of excess pore pressure is expected to be less significant, and therefore the increase of the maximum force over the static force is less.

GROUP 1 AND 2 OF THE JACKED PILE IN SAND AND VISCOUS FLUID

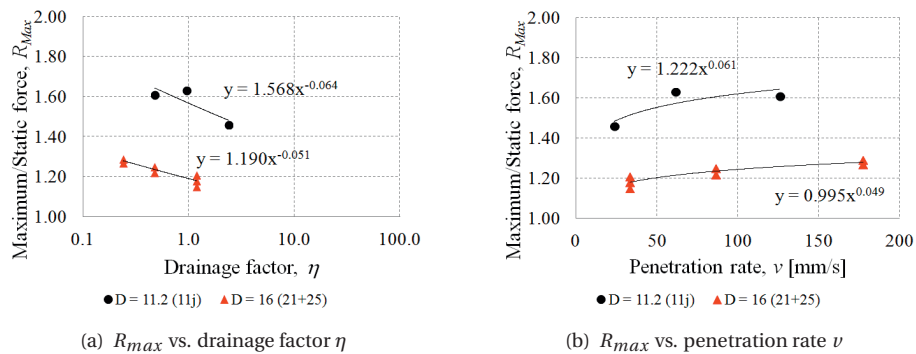


Figure 5.22: Influence of pile tip level in group 1

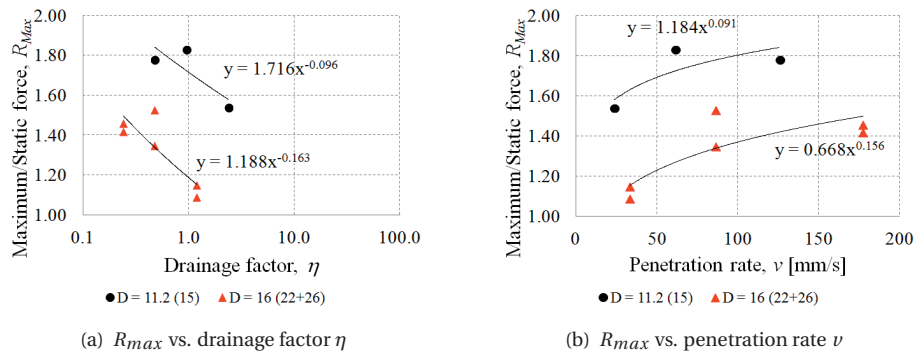


Figure 5.23: Influence of pile tip level in group 2

Figure 5.22 shows the relations between the increase of the maximum head force over the static head force with the loading rate (a) and the drainage factor (b) for the series with

the 11.3 mm pile (series 11j) and the series with the 16 mm pile (series 21+25). The pile was jacked in the soil bed of sand and viscous fluid. The trend lines following the power relationship between R_{max} and the loading rate/the drainage factor are included. Similarly, Figure 5.23 shows the relations between R_{max} and the loading rate/the drainage factor for the series with the 11.3 mm pile (series 15) and the series with the 16 mm pile (series 22+26). The pile mentioned in Figure 5.23 was pre-embedded.

In each individual series, it is obvious that the test with the higher penetration rate or, the lower drainage factor has the higher increase of the maximum head force over the static head force. The only exception is in the series 11j and the series 15 where the average loadings with the medium drainage factor have a slightly higher value of R_{max} than the R_{max} value of the series 21+25 and 22+26, respectively. Both Figure 5.22 and 5.23 clearly show that the series with a smaller pile has a higher increase of the maximum head force over the static head force than that of the series with a bigger pile.

The difference in the increase of the head force can be up to more than 40% (an increase of 63% for series 11j versus 22% for series 21 and an increase of 83% for series 15 versus 35% for series 26).

GROUP 3 IN SILT AND WATER AND GROUP 4 IN SAND AND WATER

Figure 5.24 shows the relations between the increase of the maximum head force over the static head force with the loading rate (a) and the drainage factor (b) for the series with the OEP (series 12) and the series with the CEP (series 14) in silt and water. Figure 5.25 shows the relations between R_{max} of the head force with the loading rate (a) and the drainage factor (b) for the series with the OEP (series 16) and the series with the CEP (series 4) in sand and water.

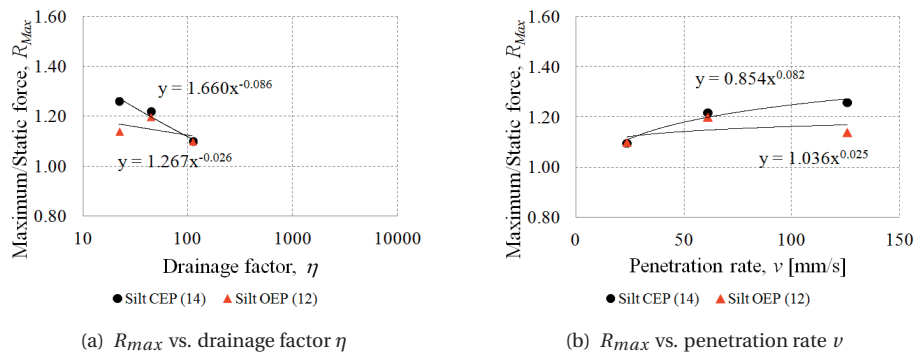


Figure 5.24: Influence of pile types in group 3

The series with the CEP always has a higher increase of the maximum head force over the static force than the series with the OEP does; the difference is more evident when the loading rate increases or the drainage factor decreases. The difference in the increase of the head force between the series with the CEP and the series with the OEP is up to 12% for the series in silt and water and up to 41% for the series in sand and water. It is noticed that in series 16 of the OEP in sand and water, there is almost no increase

of the rapid maximum head force over the static head force which suggests a negligible influence of both the rate effect and the excess pore pressure effect in this series.

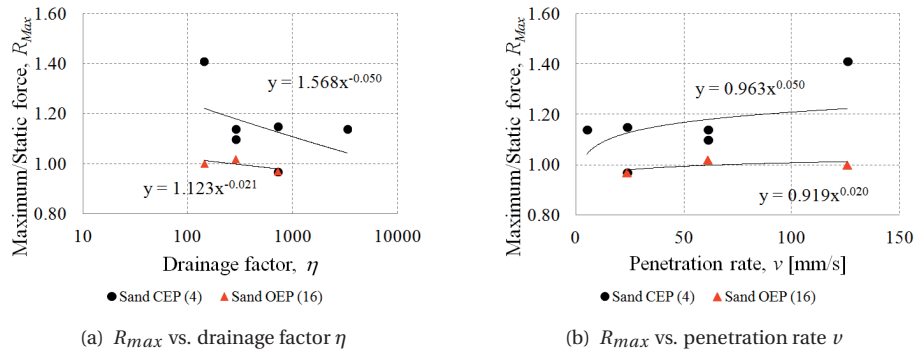


Figure 5.25: Influence of pile types in group 4

5.6.3. SUMMARY

Table 5.18 summarises the influence of the pile type on the static force. Table 5.18 is created in a similar way with Table 5.6 but for the static head force only due to the limited data and a question on the validity of the measurement on the tests 11 to 16.

Table 5.18: Influence of the pile type

Pile types (head force)	F_static %	F_max/F_static %
Open-ended pile	100	-3 - 20
Close-ended pile	152 - 193	-3 - 41
$D = 11.3$ mm	100	46 - 83
$D = 16$ mm	148 - 243	9 - 53

The pile type and the pile diameter strongly influence the static pile head force. The difference in the static pile head force of the close ended pile and the open-ended pile is from 10 to 50%. This difference depends on the plugging mode of the open-ended pile. If the OEP is plugged then its capacity is comparable to the capacity of the CEP; otherwise, if the OEP is unplugged, its capacity is significantly lower than the capacity of the CEP since the sand continuously moves into the hollow pile.

The static head force of the series with the 16 mm diameter pile is a factor 3-5 larger than that of the series with the 11.3 mm diameter pile. There are three geometry characteristics, which contribute to the difference in the maximum static forces of the series with 11.3 mm pile and of the series of 16 mm pile. They are (for the 16 mm pile series): the stress level along the pile shaft and at the pile base that is 1.43 times higher, the area of the shaft friction that is 2.05 times higher and the tip area that is 2.05 times higher. These geometry characteristics may account for the factor 3 of the difference in

the maximum static forces of the series with the pre-embedded pile. But they do not fully explain the factor 5 of the force difference in the series with the jacked pile. Again, the jacked installation process can be considered as an explanation since this process significantly enhances the bearing capacity of the pile. However, it is ambiguous without quantitative reasoning.

The pile type and the pile diameter have a strong influence on the increase of the rapid head force over the static head force. The rapid test with the CEP has a higher value of the normalised head force than the rapid test with the OEP does which may be due to the fact that the OEP has an extra drainage path inside the hollow pile. The rapid test with the small pile has a higher value of the normalised head force than the rapid test with the large pile does; this observation has not yet been explained in this study.

5.7. CONCLUSIONS

In this chapter, analysis on the results of the centrifuge pile load testing series is given. The influence of the constitutive rate effect and the excess pore pressure effect are studied by variations of the loading rate and the drainage condition of the soil. Moreover, the influence of the soil and fluid type, the initial relative density, the installation method and the pile type are also considered. The following conclusions are deduced from the interpretation of the experimental results of the centrifuge pile load series from Nguyen [206] and this study [169, 205].

For an interpretation of a rapid load test, it is well-known that the resistance during rapid loading is considerably higher than the corresponding static resistance, which is due to the penetration rate effect. After excluding the inertia term, the penetration rate effect can be divided into the excess pore pressure effect and the rate effect. The excess pore pressure effect comes from the increase of the effective stress due to the negative pore pressure which strongly depends on the drainage condition of the test. The rate effect can include the constitutive term relating to the interlocking of soil particles and the damping term. Those terms, in general, can not be separated. The generalisation of the penetration rate effect is: (1) within the same material, a rapid loading test with a higher loading rate corresponding to a lower drainage factor has a higher increase of the rapid force over the static force (factor R_{max} and R_{up}); and (2) for rapid loading tests of the same loading rate, a test with a smaller drainage factor has a higher value for R_{max} and R_{up} . Dependencies of R_{max} and R_{up} on the loading rate and the drainage factor can be found in Figure 5.1 and 5.2.

In the fully drained soil bed, there is no pore pressure effect for the rapid pile test. The excess pore pressure effect increases up to 10% of the tip resistance for the pile test in the partially drained soil bed, and about 6 to 47% for the pile test in a nearly undrained soil bed. The magnitude of the increase depends on the loading rate.

The constitutive rate effect increases about 10% of the maximum tip resistance for the rapid pile test in the fully drained soil (series 4). It should be noted that in series 4, it is likely that other rate effects rather than the constitutive rate effect are missing since the rate effect observed in Figure 5.3 is constant for the loading rate between 5-125.6 mm/s. For the rapid pile test in a partially drained and nearly undrained soil bed, the rate effect increases about 5 to 15% of the tip resistance depending on the loading rate between 5-125.6 mm/s. In comparison with the fully drained soil (series 4), it is likely

that not only the constitutive rate effect influences the value of R_{max} .

The material (soil and fluid) type has a significant influence on both the static resistance and the increase of the rapid resistance over the static resistance. In general, the static resistance of the pile test in sand and viscous fluid is the highest, then the one in sand and water is the second and the one in silt and water is the lowest. The main reason for the difference in the static resistance is the difference in the friction angle of the soil and the ratio of the pile diameter/thickness over the mean soil grain size. In a rapid load test, the increase of the rapid resistance over the static resistance is the highest in the sand and viscous fluid, the second in the silt and water and the lowest in the sand and water. This order relates directly to the magnitude of the drainage factor for each material types.

The initial relative density strongly influences the tip resistance of the static pile load test, an increase of about 20% in the initial relative density can lead to an improvement of 35 to 74% of the tip resistance. The initial relative density has a certain influence on the increase of the rapid tip resistance over the static tip resistance, as the initial relative density reduces the increase is more apparent. Limited data from the centrifuge series suggests that the decrease of the initial relative density leads to the increasing influence of the excess pore pressure effect because when the relative density reduces, the shear modulus decreases and consequently the drainage condition reduces.

The installation method has a strong influence on the static tip resistance, the tip resistance of the jacked pile is 52 to 93% higher than that of the pre-embedded pile. The installation method has a considerable influence on the increase of the rapid tip resistance over the static resistance; the maximum increase is only about 29% for the jacked pile, but it is about 57% for the pre-embedded pile. Besides, it seems that the higher increase observed for in the rapid pile load test with the pre-embedded pile mainly originates from the higher contribution of the excess pore pressure effect. This can be explained from the increasing confinement associated with the installation process which causes the increase of the shear modulus and hence the drainage condition increases in the soil around the jacked pile.

The pile type strongly influences the static head force; the head force of a close-ended pile test is about 10 to 50% higher than that of an open-ended pile test depending on the plugging mode of the open-ended pile. The pile type also has a strong influence on the increase of the rapid head force over the static head force. In general, the rapid test with the CEP has a higher value of the normalised head force than the rapid test with the OEP does; the rapid test with the small pile has a higher value of the normalised head force than the rapid test with the large pile does.

6

NUMERICAL MODELLING

6.1. INTRODUCTION

As mentioned in Chapter 1, numerical modelling of the static and rapid pile load tests in the saturated granular soil bed is performed in this thesis. In order to assess the excess pore pressure effect in the rapid pile load test, it is required that the numerical model can simulate the interaction between the soil skeleton and the fluid inside the pores of the soil skeleton. In other words, the numerical model can couple the dynamic analysis and the consolidation analysis. For this purpose, the Finite Element software Plaxis with the module Plaxis-PTU is employed.

This chapter, first, presents a brief review of the mechanics of porous media in section 6.2. Then the formulation and discretisation techniques in the Plaxis-PTU are shortly described in section 6.3. Finally, section 6.4 presents several preliminary calculations to verify and validate the module Plaxis-PTU.

6.2. BRIEF REVIEW OF MECHANICS OF POROUS MEDIA

The mechanics of porous media, in particularly saturated soils, is complicated because of the coupled responses of their individual components, the soil skeleton (the solid phase) and the fluid inside the pores of the soil skeleton (the fluid phase). Two mechanisms play an essential role in the interaction between the fluid and the soil skeleton if the fluid does not have enough time to escape the pore network. The first mechanism is an increase of pore pressure induced by a compression of the soil skeleton; the second mechanism is a decrease of pore pressure caused by a dilation of the soil skeleton. When the permeability is high, and the load is slowly applied, the coupling may be negligible since the overall behaviour is close to a drained one. However, the coupling can be significantly strong in the case of low permeability and fast transient loading (partially drained to undrained cases). Accurate prediction of the behaviour of porous media, therefore, requires taking into account this coupling in the analysis.

The study of porous media can be dated back to the original work of Woltman [287] who introduced the concept of volume fraction for describing multiphase media. Darcy [62] studied the motion of a water flow through sands and introduced the notation of permeability. Fillinger investigated the uplift problem in a liquid-saturated porous me-

dia and pioneered the porous media theory by introducing the concept of mixture theory [78], the friction force caused by the fluid flow on the porous solid [76] and the effect of effective stresses [77]. Terzaghi studied the non-viscous fluid flow through a deformable porous solid and published the well-known consolidation theory [268], later he introduced the capillary force in porous media [269] and formulated the effective stress for unsaturated soils which is widely used in modern soil mechanics [270]. Rendulic [231] generalised the Terzaghi one-dimensional consolidation theory to the three-dimensional one. Biot extended Terzaghi's concept to the consolidation theory for linear elastic and viscoelastic anisotropic porous solid [28, 29] by introducing the concepts of mass and viscous coupling in the fluid-solid interaction. The same theory has been reformulated by Biot [30–32] based on the concepts of partial solid stress and partial fluid pressure; finally, the fully coupled fluid-solid formulation for quasi-static and dynamic analysis of a saturated porous medium was developed [30, 31]. This formulation is derived from the momentum balance equation of the mixture, the momentum balance equation of the fluid and the mass conservation of the fluid flow. The solution provided by Biot consists of two dilatational waves and one rotational wave propagating in the porous medium with frequency dependent damping factors. The theory of poroelasticity is also formulated by Verruijt [263] in a specific version for soil mechanics, and Rice and Cleary [232] emphasises the two limiting behaviours, drained and undrained, of a fluid-filled porous material.

Zienkiewicz et al. [51, 167, 303–305, 305, 306] was the first to implement the Biot's two-phase mixture theory in the Finite Element Method (FEM) to account for inelastic behaviour and large deformation. Various finite element implementations of the Biot theory have also been carried out by Ghaboussi and Dikman [94] and Pervost [223, 224] with different primary variables and different arrangement of the variables. Zienkiewicz et al. [304] summarised three simplified formulations for the implementation of the Biot governing equations namely: $u-p$, $u-w-p$ and $u-U$ (with u is the solid displacement, p is the pore pressure, U is the fluid displacement, and w is the relative fluid displacement). In the $u-p$ formulation, inertial effects associated with the relative fluid motion are negligible therefore this formulation is suitable for low frequency loading in porous media (such as landslides, earthquakes or liquefaction phenomena) or quasi-static analysis. In the $u-w$ or $u-w-p$ formulations, all inertial effects are included therefore they are applicable for high-frequency phenomena such as blast loading or dynamic/rapid pile loading in porous media. In the case when the material response is incompressible then only the full $u-w-p$ formulation is capable of obtaining solutions [304].

Although the three formulations $u-p$, $u-w-p$ and $u-U$ are well-known and widely used, they are slightly different from that used in the earlier presentations of Biot [30, 31] which is easier to follow as it explores the physical meaning of each term [304]. Other finite element implementations of Ye et al. [299] and Al-Khoury et al. [5] are based directly on the original $u-U$ formulation of the Biot's fully coupled equations [30, 31]. These implementations are incorporated in research modules of commercial codes (Abaqus [299] and Plaxis [5], respectively). The Al-Khoury et al. implementation was included in the research module Plaxis-PTU and was applied successfully in the DC-COB project [179, 180] to simulate relatively high-frequency impacts (blast loading) on underground structures in porous media [5] with relatively coarse meshes. The implementation of Al-Khoury et

al. [5] is briefly described in the next section.

6.3. GOVERNING EQUATIONS AND FE FORMULATION

This section briefly summarised the governing equations of porous media described by Biot [30, 31] and their FE formulations implemented by Al-Khoury et al. [5] in the commercial code Plaxis.

6.3.1. GOVERNING EQUATIONS

Before proceeding with the general equations, some general notations are introduced for clarity:

- σ_s : the partial solid stress vector which is the average force supported by the solid portion of an infinitesimal cubic face;
- σ_w : the fluid stress;
- $\mathbf{u}_s, \mathbf{u}_w$: the displacement of the solid skeleton and the fluid phase, respectively;
- p : the pore fluid pressure;
- n : the porosity;
- ρ, ρ_s, ρ_w : the densities of the mixture, the solid phase and the fluid phase respectively; they are connected by a relation: $\rho = (1 - n)\rho_s + n\rho_w$.

The most fundamental principle in porous media might be the effective stress principle which is first formulated by Terzaghi [257]. This principle states that the fluid pressure causes only a uniform, volumetric strain by compressing the grains and that the major deformation of the porous skeleton is governed by the effective stress:

$$\sigma_s = \sigma'_s - \alpha \mathbf{I} p \quad (6.1)$$

where α is a compressibility parameter and \mathbf{I} is equal to unity for the normal stress components and zero for the shear stress components. For most of the geotechnical application, α is set to 1.0 [180]; consequently, the familiar relationship between the total stress, the effective stress and the pore pressure is found $\sigma_s = \sigma'_s - \alpha \mathbf{I} p$. In this thesis, the value of 1.0 is assigned to α .

The original Biot formulation, which incorporates the mass and viscous coupling effects in the stress equilibrium for both the solid skeleton and fluid phases, can be written as:

$$\nabla \cdot \sigma_s - \rho_{11} \ddot{\mathbf{u}}_s - \rho_{12} \ddot{\mathbf{u}}_w - b(\ddot{\mathbf{u}}_s - \ddot{\mathbf{u}}_w) = 0 \quad (6.2a)$$

$$\nabla \sigma_w - \rho_{21} \ddot{\mathbf{u}}_s - \rho_{22} \ddot{\mathbf{u}}_w + b(\ddot{\mathbf{u}}_s - \ddot{\mathbf{u}}_w) = 0 \quad (6.2b)$$

It is noted that the viscous damping and inertial effects are explicitly incorporated into Equations 6.2 through the viscous coefficient b and the mass densities $\rho_{..}$.

Inertial effect The inertial effect includes induced mass coupling effects arising from relative motion between the two phases: $\rho_{11} = \rho + n\rho_w(\bar{a} - 2)$ and $\rho_{22} = \bar{a}n\rho_w$ can be considered as the intrinsic density coefficients; $\rho_{12} = \rho_{21} = n\rho_w(1 - \bar{a})$ can be regarded as a measure of the coupled inertial effect that is reflected by the additional inertial coupling induced by the relative motion between the solid and fluid phases. Parameter \bar{a}

is the Biot tortuosity parameter which takes into account the fact that the water flow in the granular soil follows a twisting path through the pores. In the implementation of Plaxis-PTU, \tilde{a} is calculated as a function of the porosity: $\tilde{a} = 0.5 \times (1 + \frac{1}{n})$ [180].

Viscous damping effect The viscous coefficient b represents the viscous drag imposed to each constituent per unit volume when the fluid flows by the walls of the pores due to external loading which controls the relative motion between fluid and solid. It can be calculated as:

$$b = \frac{\gamma}{kn^2} \quad (6.3)$$

with γ is the fluid unit weight and k is the hydraulic permeability. The hydraulic permeability is a combination of properties of the fluid (the viscosity) and the solid (the intrinsic permeability).

The stress of the fluid is related to the volumetric strain of fluid and the volumetric strain of solid skeleton, as follows:

$$\sigma_w = -np = \tilde{Q}\mathbf{m}\nabla^T \mathbf{u}_s + \tilde{R}\nabla^T \mathbf{u}_w \quad (6.4)$$

with $\tilde{Q} = \tilde{M}n(\tilde{\beta} - n)$ and $\tilde{R} = \tilde{M}n^2$ in which \tilde{M} is the Biot coefficient of compressibility of the two-phase material, and $\tilde{\beta}$ is the Biot coefficient for the fluid flow. Details of parameters $\tilde{\beta}$ and \tilde{M} can be found in the paper of Biot and Willis [33]. As mentioned by Meijers [180], most granular soils consists of stiff particles with a high compression modulus therefore \tilde{M} can be simplified as $\tilde{M} = \frac{K_w}{n}$ and, subsequently, $\tilde{\beta}$ becomes unity.

6.3.2. SPATIAL DISCRETISATION

The governing equations are rewritten as:

$$\nabla \cdot \left[\boldsymbol{\sigma}'_s + \frac{\alpha}{n} \mathbf{m} (\tilde{Q}\mathbf{m}\nabla^T \mathbf{u}_s + \tilde{R}\nabla^T \mathbf{u}_w) \right] - \rho_{11}\ddot{\mathbf{u}}_s - \rho_{12}\ddot{\mathbf{u}}_w - b(\ddot{\mathbf{u}}_s - \ddot{\mathbf{u}}_w) = 0 \quad (6.5a)$$

$$\nabla (\tilde{Q}\mathbf{m}\nabla^T \mathbf{u}_s + \tilde{R}\nabla^T \mathbf{u}_w) - \rho_{21}\ddot{\mathbf{u}}_s - \rho_{22}\ddot{\mathbf{u}}_w + b(\ddot{\mathbf{u}}_s - \ddot{\mathbf{u}}_w) = 0 \quad (6.5b)$$

The associated boundary conditions are the natural boundary condition for stresses with $\hat{\mathbf{t}} = \mathbf{n} \cdot \boldsymbol{\sigma}$ and $\hat{\mathbf{t}}_p = \mathbf{n}p$ are external traction forces on Γ_t and Γ_p , respectively; and the essential boundary conditions with $\hat{\mathbf{u}}_s$ and $\hat{\mathbf{u}}_w$ are prescribed displacements in solid and water on Γ_s and Γ_w , respectively. \mathbf{n} is a unit normal vector.

By applying the Finite Element techniques and using the Galerkin's method [307], the matrix form of Equations 6.5 is obtained as following:

$$\begin{bmatrix} \mathbf{M}_{ss} & \mathbf{M}_{sw} \\ \mathbf{M}_{ws} & \mathbf{M}_{ww} \end{bmatrix} \begin{Bmatrix} \ddot{\mathbf{u}}_s \\ \ddot{\mathbf{u}}_w \end{Bmatrix} + \begin{bmatrix} \mathbf{C}_{ss} & \mathbf{C}_{sw} \\ \mathbf{C}_{ws} & \mathbf{C}_{ww} \end{bmatrix} \begin{Bmatrix} \dot{\mathbf{u}}_s \\ \dot{\mathbf{u}}_w \end{Bmatrix} + \begin{bmatrix} \mathbf{K}_{ss} & \mathbf{K}_{sw} \\ \mathbf{K}_{ws} & \mathbf{K}_{ww} \end{bmatrix} \begin{Bmatrix} \bar{\mathbf{u}}_s \\ \bar{\mathbf{u}}_w \end{Bmatrix} = \begin{Bmatrix} \bar{\mathbf{F}}_s \\ \bar{\mathbf{F}}_w \end{Bmatrix} \quad (6.6)$$

where the various matrices/vectors are defined as:

$$\begin{aligned}
\mathbf{M}_{ss} &= \int_{\Omega} \mathbf{N}_u^T \rho_{11} \mathbf{N}_u d\Omega & \mathbf{C}_{ss} &= \int_{\Omega} \mathbf{N}_u^T b \mathbf{N}_u d\Omega & \mathbf{K}_{ss} &= \int_{\Omega} \mathbf{B}_u^T \mathbf{D} \mathbf{B}_u d\Omega + \int_{\Omega} \mathbf{B}_u^T \frac{\alpha}{n} \tilde{\mathbf{Q}} \mathbf{B}_u d\Omega \\
\mathbf{M}_{sw} &= \int_{\Omega} \mathbf{N}_u^T \rho_{12} \mathbf{N}_p d\Omega & \mathbf{C}_{sw} &= \int_{\Omega} \mathbf{N}_u^T b \mathbf{N}_p d\Omega & \mathbf{K}_{sw} &= \int_{\Omega} \mathbf{B}_u^T \frac{\alpha}{n} \tilde{\mathbf{R}} \mathbf{B}_p d\Omega \\
\mathbf{M}_{ws} &= \int_{\Omega} \mathbf{N}_p^T \rho_{21} \mathbf{N}_u d\Omega & \mathbf{C}_{ws} &= \int_{\Omega} \mathbf{N}_p^T b \mathbf{N}_u d\Omega & \mathbf{K}_{ws} &= \int_{\Omega} \mathbf{B}_p^T \tilde{\mathbf{Q}} \mathbf{B}_u d\Omega \\
\mathbf{M}_{ww} &= \int_{\Omega} \mathbf{N}_p^T \rho_{22} \mathbf{N}_p d\Omega & \mathbf{C}_{ww} &= \int_{\Omega} \mathbf{N}_p^T b \mathbf{N}_p d\Omega & \mathbf{K}_{ww} &= \int_{\Omega} \mathbf{B}_p^T \tilde{\mathbf{R}} \mathbf{B}_p d\Omega \\
\bar{\mathbf{F}}_s &= \int_{\Gamma_t} \mathbf{N}_u \mathbf{n} p d\Gamma & \bar{\mathbf{F}}_w &= \int_{\Gamma_p} \mathbf{N}_p \mathbf{n} n p d\Gamma
\end{aligned}$$

in which $\bar{\mathbf{u}}_s$ and $\bar{\mathbf{u}}_w$ are the nodal displacements of the solid skeleton and the pore fluid, \mathbf{N}_u and \mathbf{N}_p are the shape functions for the solid and fluid parts and \mathbf{D} is a fourth order tensor defining a constitutive law for the solid skeleton.

6.3.3. TIME DISCRETIZATION: PARTITION OF TIME UNITY SCHEME

The explicit time integration schemes are commonly used to solve Equation 6.6 as done by [299] or the similar $u - U$ form of the Biot equation as done by [52, 304]. These algorithms are conditionally stable and the time step is restricted by a critical value which is related to the constitutive law as well as the spatial discretization. For the practical geotechnical application of a soil-pile problem with a high-nonlinear soil material and a very fine mesh in the soil-pile interaction zones, using the explicit time integration scheme leads to a huge number of time steps which is not practical. It is therefore important to use an implicit time integration scheme that is suitable for high-frequency wave propagation.

In the literature, there are many implicit time integration schemes which are unconditionally stable and second order accurate. Argyris and Mlejnek [14], Gladwell and Thomas [97], Hardy [111], Hughes [136] and Kontoe [153] performed numerical tests in structural problems and the spectral stability analysis for several schemes and summarised that:

- the Houbolt method [128], the Park multistep method [214] are unconditionally stable and second order accurate, but they require a special starting procedure and do not allow parametric control of the amount of numerical dissipation;
- the Newmark method [204] is the most commonly used family of algorithms with unconditionally stable and numerical damping possession for a proper choice of parameters;
- the Wilson- θ method [285] is also unconditionally stable with a suitable value for θ , however this method not favourable due to its characteristic to overshoot;
- the α -method (HHT method) of Hilber, Hughes and Taylor [116] and the WBZ method of Wood, Bossak and Zienkiewicz [288] are a generalization of the Newmark method to achieve controllable algorithmic dissipation of the high-frequency modes or, in other words, offers a selective filtering of the inaccurate high frequency modes;

- the generalized α -method (CH method) of Chung and Hulbert [56] combines features of the HHT and WBZ algorithms therefore with proper choice of parameters it is unconditionally stable, second order accurate and can achieve optimal high-frequency dissipation with minimal low-frequency impact;
- the general Single Step method SSPj of Zienkiewicz et al. [308] and the generalized Newmark method (GNpj) of Katona and Zienkiewicz [150] employ higher order polynomials to maximise accuracy and still maintain the unconditionally stable.

Al-Khoury et al. [5] pointed out that in wave propagation problems, the velocity and stress fields exhibit a jump at the wavefront and this discontinuity results in spurious oscillations if the Newmark, HHT, WBZ or CH methods are used. Therefore, in order to reduce this spurious oscillation, Al-Khoury et al. proposed the partition of time unity (PTU) method to describe the velocity discontinuity. This method bases on enhancing the shape function such that a field discontinuity can be introduced within the element. Details of this method can be found in the paper of Al-Khoury et al. [5], this section only summarises the main features of the method.

The second-order equation 6.6 is decomposed into two first-order equations as:

$$\mathbf{M}\dot{\bar{\mathbf{v}}} + \mathbf{C}\bar{\mathbf{v}} + \mathbf{K}\bar{\mathbf{u}} - \mathbf{F} = 0 \quad (6.8a)$$

$$\dot{\bar{\mathbf{u}}} - \bar{\mathbf{v}} = 0 \quad (6.8b)$$

with $\bar{\mathbf{v}} = [\bar{\mathbf{v}}_s \bar{\mathbf{v}}_w]^T$ and $\bar{\mathbf{u}} = [\bar{\mathbf{u}}_s \bar{\mathbf{u}}_w]^T$ are the nodal velocity and displacement. The displacement field can be described as:

$$\bar{\mathbf{u}}(t) = \lambda_n \bar{\mathbf{u}}_n + \lambda_{n+1} \bar{\mathbf{u}}_{n+1} \quad (6.9)$$

where $\lambda_n = 1 - \frac{\tau}{\Delta t}$, $\lambda_{n+1} = \frac{\tau}{\Delta t}$, $\tau = t - t_n$ and $\Delta t = t_{n+1} - t_n$. The velocity exhibits a jump at [5] Γ and this discontinuity is introduced using the partition of unity method as:

$$\bar{\mathbf{v}}(t) = \bar{\mathbf{v}}^c + \bar{\mathbf{v}}^e \quad (6.10a)$$

$$\bar{\mathbf{v}}^c = \lambda_n \bar{\mathbf{v}}_n^c + \lambda_{n+1} \bar{\mathbf{v}}_{n+1}^c \quad (6.10b)$$

$$\bar{\mathbf{v}}^e = \lambda_n H(\Gamma) \bar{\mathbf{v}}_{n+1}^e \quad (6.10c)$$

where c and e represent the conventional and enhanced finite elements and H is a Heaviside function. The time derivatives of $\bar{\mathbf{u}}(t)$ and $\bar{\mathbf{v}}(t)$ are:

$$\dot{\bar{\mathbf{u}}} = -\frac{1}{\Delta t} \bar{\mathbf{u}}_n + \frac{1}{\Delta t} \bar{\mathbf{u}}_{n+1} \quad (6.11a)$$

$$\dot{\bar{\mathbf{v}}}(t) = \dot{\bar{\mathbf{v}}}^c + \dot{\bar{\mathbf{v}}}^e \quad (6.11b)$$

$$\dot{\bar{\mathbf{v}}}^c = -\frac{1}{\Delta t} \bar{\mathbf{v}}_n^c + \frac{1}{\Delta t} \bar{\mathbf{v}}_{n+1}^c \quad (6.11c)$$

$$\dot{\bar{\mathbf{v}}}^e = -\frac{1}{\Delta t} H(\Gamma) \bar{\mathbf{v}}_{n+1}^e \quad (6.11d)$$

On the basis of the partition of unity method, and by using the weighted residual method, Equation 6.8 can be described in time as:

$$\begin{bmatrix} \mathbf{M} + \theta^c \mathbf{C} + (\theta^c)^2 \mathbf{K} & -\theta^{ce} \mathbf{M} + (\Delta t \theta^{ce} - \theta^{cet}) \mathbf{C} + \theta^c (\Delta t \theta^{ce} - \theta^{cet}) \mathbf{K} \\ \mathbf{M} + \theta^e \mathbf{C} + \theta^e \theta^c \mathbf{K} & -\mathbf{M} + (\Delta t - \theta^e) \mathbf{C} + \theta^e (\Delta t \theta^{ce} - \theta^{cet}) \mathbf{K} \end{bmatrix} \begin{Bmatrix} \bar{\mathbf{v}}_{n+1}^c \\ \bar{\mathbf{v}}_{n+1}^e \end{Bmatrix} = \begin{bmatrix} \mathbf{M} - (\Delta t - \theta^c) \mathbf{C} - \theta^c (\Delta t - \theta^c) \mathbf{K} & -\Delta t \mathbf{K} \\ \mathbf{M} - (\Delta t - \theta^e) \mathbf{C} - \theta^e (\Delta t - \theta^c) \mathbf{K} & -\Delta t \mathbf{K} \end{bmatrix} \begin{Bmatrix} \bar{\mathbf{v}}_n^c \\ \bar{\mathbf{u}}_n \end{Bmatrix} - \begin{Bmatrix} (-\Delta t + \theta^c) \mathbf{F}_n - \theta^c \mathbf{F}_{n+1} \\ (-\Delta t + \theta^e) \mathbf{F}_n - \theta^e \mathbf{F}_{n+1} \end{Bmatrix} \quad (6.12a)$$

$$\bar{\mathbf{u}}_{n+1} = \bar{\mathbf{u}}_n + (\Delta t - \theta^c) \bar{\mathbf{v}}_n^c + \theta^c \bar{\mathbf{v}}_{n+1}^c + (\Delta t \theta^{ce} - \theta^{cet}) \bar{\mathbf{v}}_{n+1}^e \quad (6.12b)$$

with θ^{\dots} are algorithmic parameters which can be given as:

$$\theta^c = \Gamma \quad \theta^{ce} = \frac{\Gamma}{\Delta t} \quad \theta^{cet} = \frac{\Gamma^2}{\Delta t} \quad \theta^e = \Gamma \quad (6.13)$$

in which Γ is taken as a varying fraction of Δt . The time-like parameter Γ has no physical meaning but provides the means for partitioning the time step according to the required amount of numerical dissipation. Al-Khoury et al. [5] proved that Γ can efficiently control the numerical dissipation in the high frequency range; they recommended using a large value of Γ in the high-frequency range and a low value in the low-frequency range. In this thesis, the value of 0.95 is assigned for Γ as recommended by Meijers [180].

Finally, Equation 6.12a is used to solve $\bar{\mathbf{v}}_{n+1}^c$ and $\bar{\mathbf{v}}_{n+1}^e$ and Equation 6.12b is employed to solve $\bar{\mathbf{u}}_{n+1}$.

6.4. PERFORMANCE OF PLAXIS-PTU

Al-Khoury et al. [5] implemented the Partition of Time Unity algorithm into the commercial software Plaxis under the research module Plaxis-PTU version 9.02. This section gives the results from several calculations made to verify and validate the Plaxis-PTU. The problems under consideration are one-dimensional single-phase, one-dimensional two-phase and two-dimensional two-phase problem.

6.4.1. ONE-DIMENSIONAL BAR TEST

In order to illustrate the solution of the wave propagation problem in a uniform steel bar with the length of 20 meters and the width of 0.5 meters. The material properties and loading history are given in Table 6.1. This problem is a typical wave propagation problem in one-dimensional space, the exact solution for this problem is well defined. The bar is initially at rest and is subjected to an instantaneous tip loading. Plaxis-PTU simulation uses 6-node triangle element to discretize the problem with the right end fixed, the top and bottom ends vertically fixed, Figure 6.1(a).

Table 6.1: Characteristics of the problem

Material properties				Loading history		
Young modulus	E	$30 \cdot 10^6$	kN/m ²	Magnitude at 0 ms	100	kN
Density	ρ	$7.4 \cdot 10^{-4}$	kg/m ³	Magnitude at 2 ms	100	kN
Poisson ratio	ν	0		Time step Δt	$1.6 \cdot 10^{-5}$	ms

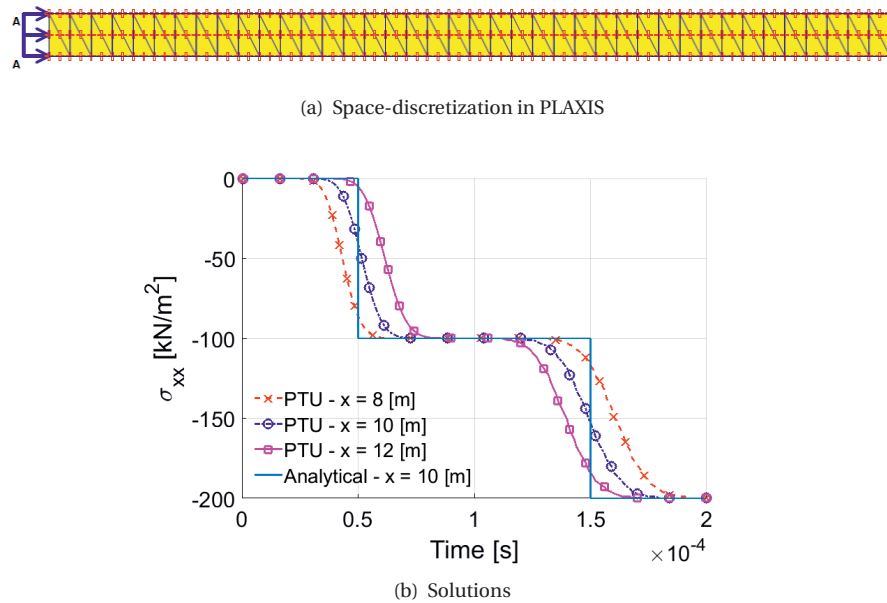


Figure 6.1: The wave propagation problem in one-dimensional space

The stress evolution in time at location $x = 8.0, 10.0, 12.0$ m for a model of the 20-m bar simulated in Plaxis are presented in Figure 6.1(b). It can be seen that the Plaxis-PTU show smooth and practically non-oscillatory solution. In comparison with the exact solution, the Plaxis-PTU solution is in good agreement on the magnitude of the origin and reflected stresses and the propagation of the stress wave from the loaded tip to the bar midpoint. However, the Plaxis-PTU solution exhibits an excessive smoothness at the sharp edges. This phenomenon, as pointed out by Al-Khoury et al. [5], also occurs in most practical time discretization schemes. The over smoothing can be originated from the facts that some of the physical frequencies are eliminated in the computational process; and therefore, frequencies generated from the rise of the load, in the numerical calculation, are never as high as those arising from the theoretical step load.

6.4.2. SATURATED SANDSTONE SAMPLE TEST OF GRINTEN

Van der Grinten et al. [100, 100–102] performed the shock-tube experiments to qualitatively measure the stress wave propagation in a porous medium. The shock-tube consists of a high-pressure air chamber above a low-pressure air chamber with a saturated sandstone sample inside. When the separation sheet between two chambers was removed suddenly, a pressure wave was generated, propagated into the water in the low-pressure chamber and loads the sample. During the test, the pore water pressure and effective stress were measured. Smeulders [251] provided the analytical solution based on Fourier transform of the problem and Hölscher [117] presented the numerical solution based on $u - p$ formulation of the Biot equation. The experimental setup of Grinten and the geometrical description of Hölscher are given in Figure 6.2. The Plaxis-PTU sim-

ulation uses the same geometrical of Hölischer and discretises the problem with 6-node triangle elements. The material properties used by Hölischer [117] are given in Table 6.2.

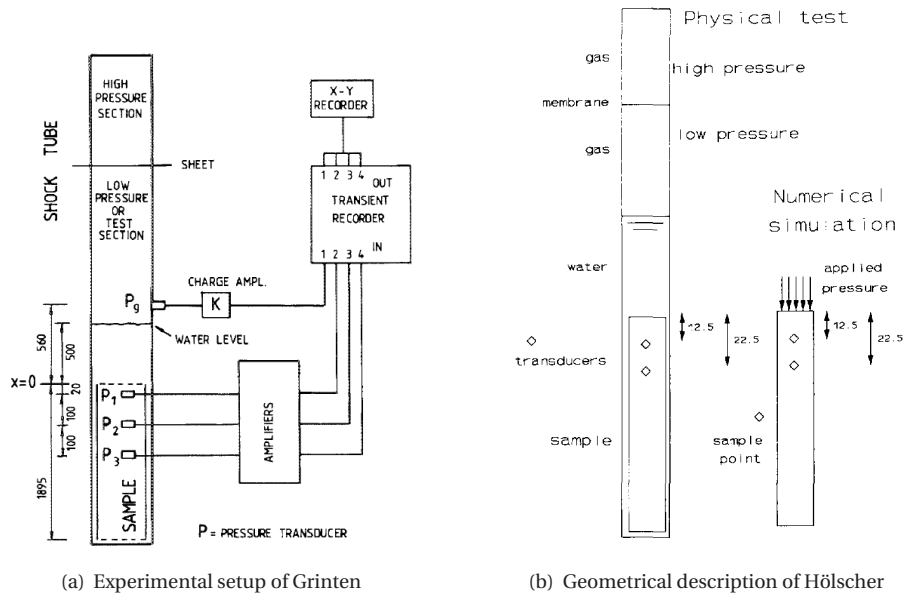


Figure 6.2: Shock-tube test of Griten

Table 6.2: Characteristics of simulations of Griten experiment

Material properties				Loading history		
Bulk modulus solid	K_s	2790	MPa	Magnitude at $0 \mu s$	1000	kPa
Shear modulus solid	G_s	1286	MPa	Magnitude at $40 \mu s$	1000	kPa
Young modulus solid	E	3345	MPa	Magnitude at $400 \mu s$	1000	kPa
Porosity	n	0.3		Time step Δt	$1.6 \cdot 10^{-5}$	ms
Permeability	k	$0.55 \cdot 10^{-3}$	m/s			
Bulk modulus fluid	K_f	2000	MPa			
Volumetric mass solid	ρ_s	2600	kg/m^3			
Volumetric mass fluid	ρ_f	1000	kg/m^3			

The calculated pore pressure and the effective stress from Plaxis-PTU simulations at two points, $x = 0.125$ and $x = 0.225$ m, are given in Figures 6.3(a) and (b). It is clear from Figure 6.3 that the pore pressure first increases to 40% (400 kN), maintains this value for a while, and then decreases to less than 10% (100 kN) of the applied load (1000 kN); simultaneously, the effective stress first increases to 60% of the applied load, maintains this value and then increases to more than 90% of the applied load. The sum of the pore pressure and the effective stress is equal to the applied load.

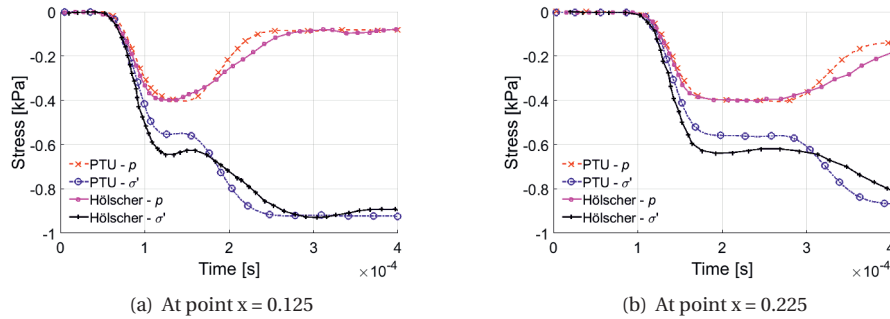


Figure 6.3: Simulations of Grinten's experiment [100, 117]

The calculated pore pressure and the effective stress from simulations of Holscher are also given in Figure 6.3. The development and magnitude of the pore pressure and the effective stress in Plaxis-PTU simulations agrees well with the results from Holscher's simulations.

6.4.3. SHALLOW FOUNDATION TEST OF HOANG AND ZIENKIEWICZ

Huang and Zienkiewicz [134] proposed new time-stepping algorithms for coupled soil-pore fluid dynamic problems and demonstrated the stability and accuracy of these schemes for some problems in one- and two-dimension. The example of a foundation on an elastic soil subjected to a surface step loading is taken out to verify the Plaxis-PTU. Description of the problem, locations of three monitored points at three depths of 15 m (point C), 18 m (point B) and 24 m (point A) are given in Figure 6.4. The material properties used by Huang and Zienkiewicz [134] and the applied load profiles are given in Table 6.3.

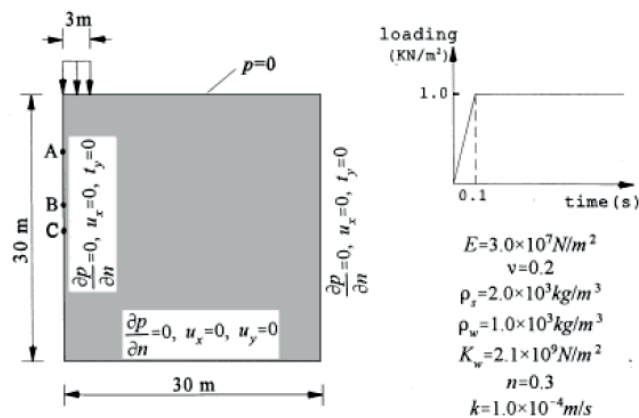


Figure 6.4: An elastic soil foundation subjected to a surface step loading [134]

Table 6.3: Characteristics of simulations of Huang and Zienkiewics

Material properties				Loading history		
Young modulus solid	E	$30 \cdot 10^6$	N/m ²	Magnitude at 0 s	0	kPa
Poisson ratio	ν	0.2		Magnitude at 0.1 s	100	kPa
Porosity	n	0.3		Magnitude at 1 s	100	kPa
Permeability	k	10^{-4}	m/s	Time step Δt	$1.6 \cdot 10^{-5}$	ms
Volumetric mass solid	ρ_s	2000	kg/m ³			
Volumetric mass fluid	ρ_f	1000	kg/m ³			
Bulk modulus fluid	K_f	$2.1 \cdot 10^9$	N/m ²			

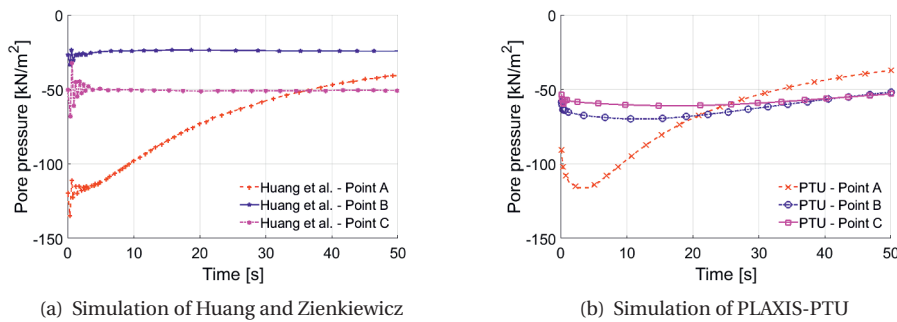


Figure 6.5: Solutions for Huang and Zienkiewicz problem

The simulation results of Huang and Zienkiewicz are presented in Figure 6.5(a) with significant spurious oscillations at the beginning time when the load rises from 0 to 100 kPa in 0.1 seconds. The simulation results from Plaxis-PTU are presented in Figure 6.5(b) without any oscillation. At point A, there is an agreement between two results. The pore pressure reaches a maximum value of 120 kN around the 5th seconds then gradually dissipates to 40 kN at the 50th seconds. At point B and point C, Huang and Zienkiewicz's result shows pore pressures of 25 kPa and 50 kPa respectively. It should be noted that the calculated pore pressure of point B (located between point A and point C) is smaller than those of point A and point C from the initial time till the 35th second. It is not reasonable as pointed out by Meijers [180]; therefore, there might be a mistake in presenting the data in Huang and Zienkiewicz paper [180]. Plaxis-PTU result shows pore pressures at point B and C of 70 and 60 kPa respectively (at peak), and the pore pressure of B is somewhere between those of A and C, which is reasonable.

6.4.4. PLAXIS-PTU WITH INTERFACE ELEMENTS

In this section, the performance of PLAXIS-PTU in a numerical simulation with the virtual thickness interface element is examined since the interface element is required in modelling the problem including the inter-facial behaviour at the pile-soil interface presented in the next chapter. The interface element in this numerical test is located between the permeable medium (the sandstone sample) and the impermeable medium

(the solid block).

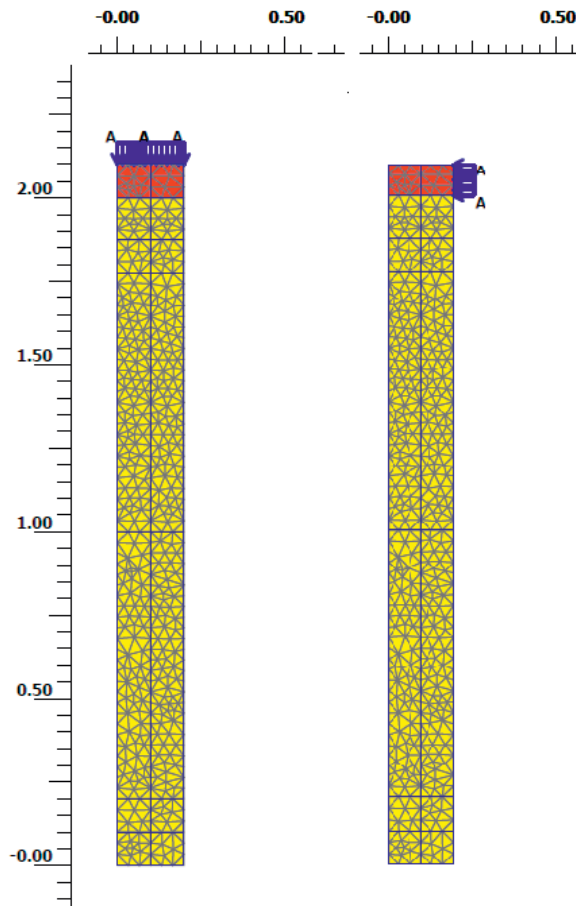


Figure 6.6: Problems of a soil column test with an interface element

Figure 6.6 presents the discretisation of two problems. In the first problem, Figure 6.6(a), the mesh boundary is horizontally fixed, the applied load is placed vertically on the solid block. In this slender configuration, the compression behaviour is dominant which is similar to what happens at the pile tip. In the second problem, Figure 6.6(b), the mesh boundary is vertically fixed, the applied load is placed horizontally on the solid block. It is expected that the shear behaviour is dominant in this problem which resembles what happens along the pile shaft. For each problem, two simulations with and without the interface elements are performed.

The material properties for the sandstone sample are similar to those of the Grinten test. The interface elements have the same properties as the sandstone sample. The solid block is impermeable in which the stiffness of the solid block is 1000 times higher than that of the sandstone sample.

The solutions of the effective stress and the excess pore pressure for a point located 0.25 m from the top obtained by Plaxis-PTU for those two problems are given in Figure 6.7. It is clear that the solutions of the case with the interface element and those of the case without interface element are identical. Consequently, it can be concluded that the virtual thickness interface element can normally work within the Plaxis-PTU without any influence on the transmission of loading stress from the block to the soil medium.

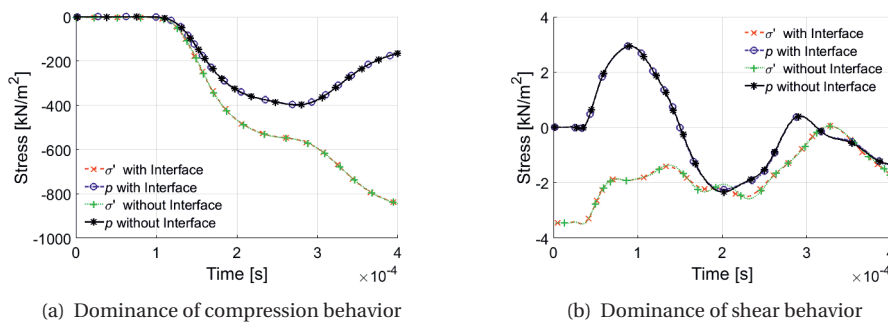


Figure 6.7: Solutions for a soil column test with an interface element

6.5. CONCLUSIONS

Al-Khoury et al. [5] proposed the Partition of Time Unity scheme to solve the $u - U$ formulation of the Biot dynamic consolidation problem. As proven by Al-Khoury et al., the PTU algorithm is unconditionally stable and second order accurate; it can eliminate the spurious oscillation in numerical results. Later, PTU algorithm was implemented in the Finite Element software Plaxis as the research module Plaxis-PTU [5] and is applied to the DC-COB project at Deltares [179, 180].

Through some numerical tests in this chapter, it is demonstrated that Plaxis-PTU gives a qualitatively and quantitatively good agreement with experimental results, analytical and numerical solutions for the single-phase problem and the two-phase problems. Plaxis-PTU works well when the interface element is placed between the permeable and impermeable media which is a big advantage in a simulation of a typical soil-structure interaction problem in geotechnical applications. Therefore, Plaxis-PTU is suitable for the simulation of the pile load test in porous media and will be used in the next chapter.

7

NUMERICAL MODELLING - RESULTS

7.1. INTRODUCTION

As mentioned in the previous chapters, the Finite Element software Plaxis is used for the numerical modelling of the pile load test in which the module Plaxis-PTU [5] is used specifically for the rapid load test. The main ideas of the numerical modelling are: (1) to calculate the ratio R of the static pile force over the rapid pile force at the same displacement and (2) to investigate the behaviour of the excess pore pressure and its influence on the value of R . It should be noted that the term "rapid" is used instead of "dynamic" in reference to the non-static pile load test in order to be consistent with the experiments and to correspond with the relative long loading duration of 50-400 ms of the prototype rapid tests, which is longer than that of a typical dynamic pile load test.

Although the physical modelling counterparts are available, a comprehensive comparison between the simulation results and the experimental results is not the direct interest of this thesis because the pile load tests in the experiment are strongly influenced by the processes prior to the load tests such as sample preparation, centrifuge spinning up, and especially installation process. Consequently, a direct comparison between numerical results and experimental tests is dominated by the difficulties to simulate the pile behaviour with numerical methods realistically due to the difficulties to cope properly with the installation effects of the jacked pile tests [39, 68]. The focus of the comparison here is rather on the general features such as the total pile capacity, the distribution of the tip resistance and the shaft friction and the general trend of the excess pore pressure as well as its influence on the rapid pile capacity. Therefore, instead of using complicated numerical methods and techniques, this thesis uses a robust schemes (similar to ones proposed by Broere and van Tol [39]) for the simulation of the initial condition in order to partially incorporate the effects of the preparation processes on the pile capacity. These schemes, as well as their background theory, will be described in section 7.2. Other features of numerical simulations such as modelling cases, constitutive model, calculation phases are also presented in section 7.2. The simulation results of the static and rapid pile load tests are given in sections 7.3 and 7.4, respectively; comparison between simulations and the experiments are presented and discussed in section 7.5.

7.2. PROBLEM DESCRIPTION

7.2.1. MODELLING CASES

The simulations are based on the geometry of the Deltares geotechnical centrifuge pile load test series which is described in Chapter 3. In the series, a prototype of a 0.64 m diameter pile in a fully saturated sand bed was modelled by a 16 mm model scale pile at an acceleration of 40-g. In the numerical modelling, the geometry and results are scaled to prototype scale and used in simulations instead of applying an artificial acceleration field of 40-g.

There are two series centrifuge pile tests which are used for the simulations in this chapter. They are series 23 of the pre-embedded pile in saturated sand with a relative density of 45% and series 24 of the jacked pile in saturated sand with the same relative density. In order to judge the quality of the simulations, several comparisons between the simulations and the centrifuge results are made:

- the total load capacity of the pile at 10% D vertical displacement of the pile head;
- the distributions of the tip capacity and the shaft friction to the total load capacity of the pile at 10% D displacement, which is roughly 80% and 20% respectively.

It should be noted that the tip force and thus the capacity in the simulations are calculated from the average stress of all integration stress points inside the pile and closed to the pile tip times the area of the pile tip.

7.2.2. CALCULATION GEOMETRY

An axisymmetric configuration is used for the calculation. The radius and height of the domain are 25 and 40 m, respectively. The pile with a length of 12 m and a radius of 0.32 m is located on the symmetry axis. The left and right boundaries of the domain are horizontally fixed while the bottom boundary is entirely fixed; all boundaries are impermeable.

A basic mesh with 2308 6-node triangular elements is used for simulations; each element contains 3 integration points. The pile is modelled as a cluster of elements having the dimensions and the location of the prototype pile. The soil around and below the pile is also modelled as a cluster of elements. At the interface between the pile cluster and the soil cluster, there will be either special interface elements or prescribed displacements which are clearly defined and announced when used. On top of the pile, a prescribed displacement is optionally imposed to model the initial conditions required and a prescribed load is applied to model the loading condition similar to the experiment. A mesh sensitivity analysis was performed and, finally, the mesh is refined in the zone of the distance D from the pile center and D under the pile tip; within this zone, there are 8 and 6 elements per the distance of D in the horizontal and vertical directions, respectively. This density of mesh is reasonable to provide enough details on the stress/strain information around the pile area and yet not time-consuming. The calculation mesh is illustrated in Figure 7.1.

7.2.3. CONSTITUTIVE MODEL

The Hardening Soil model is considered as an advanced constitutive model for soil since the model recognises the stiffness dependency on the stress level as well as the loading

path. The model has a hyperbolic stress-strain relationship in virgin loading, and a linear unloading-reloading behaviour; more detail of the model can be found in Brinkgreve et al. [38]. The stiffness-dependency feature is important not only for the proper simulation of the static pile load test as shown by Wehnert and Vermeer [273] but also for the dynamic simulation when loading and unloading are expected. Therefore the soil behaviour in this thesis is modelled by the Hardening Soil model.

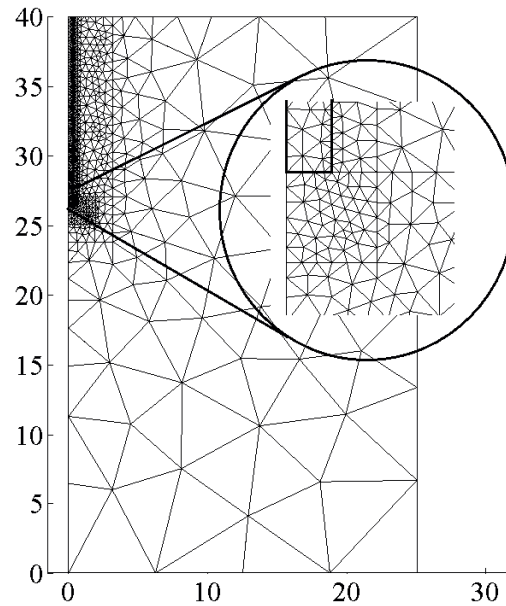


Figure 7.1: Calculation mesh with refinement under the pile tip

Table 7.1: Parameters of soil and pile for simulations

Parameter	Symbol	Unit	Sand			Pile
Material model			Hardening-Soil			Linear-Elasticity
Behavior			Drained			Non-porous
Type			Loose	Medium	Dense	-
Unsaturated unit weight	γ_{unsat}	kN/m ³	16	16	16	24
Saturated unit weight	γ_{sat}	kN/m ³	20	20	20	-
Young modulus	E_{ref}	kN/m ²	36*10 ³	45*10 ³	54*10 ³	2*10 ⁷
Oedometer modulus	E_{oed}	kN/m ²		= E_{ref}		-
Unloading/Reloading modulus	E_{ur}	kN/m ²		= 3* E_{ref}		-
Power	m			0.5		-
Poisson ratio	ν			0.3		0.0
Cohesion	c	kN/m ²		0.1		-
Friction angle	ϕ	°	37.0	42.5	42.5	-
Dilation angle	ψ	°	7.5	10	11.0	-
Permeability	k	m/s		8.9*10 ⁻⁵		-

The Baskarp sand, used in the centrifuge test that will be simulated, is reported to have a total unit weight of 20 kN/m^3 , a stainless steel-soil interface friction angle is about 30° . The triaxial test of a 41.9% relative density sample of Baskarp sand is performed at Deltares [8], the test results indicate a loading stiffness E_{50} of 45 MPa, a friction angle of $40\text{-}42.5^\circ$, a dilation angle of approximately $9\text{-}12^\circ$. The pile, which is a hollowed steel instrumented, is assumed to have a unit weight of 24 kN/m^3 and a Poisson's ratio of 0. The pile is modelled as a linear elastic material. Further soil and pile properties are estimated as listed in Table 7.1. It should be mentioned that, later, the permeability is varied to investigate the influence of the drainage condition on the increase of the rapid force over the static force.

7.2.4. SOIL-PILE INTERFACE

The load-deformation of the soil-structure system is significantly affected by the behaviour of the soil-structure interface and its stress-displacement relationship. This is especially true for the axially loaded pile-soil system, where the shaft resistance is given by frictional resistance between the pile and the soil. Much experimental evidence [10, 80, 86, 165, 185, 286] shows that this frictional resistance is developed in a thin layer, called the soil-structure interface, formed by soil grains with a thickness of about 8-15 times the mean grain size of the soil [185, 286]. During loading, the soil grains rotate and slide and make the interface undergo large strain resulting in less confining stress and hence smaller friction is achieved along the shaft. Using continuum elements in the boundary between the pile and the soil fails to capture this relative movement because the nodal compatibility of the finite element method constrains the adjacent elements to move together.

In the literature, many methods have been used to model the discontinuous behaviour at the soil-structure interface: use of thin continuum elements with standard constitutive laws [99, 213], use of springs to connect opposite nodes of adjacent elements [87], employment of interface elements with virtual thickness [26, 95], and hybrid methods where the soil and structure are modelled separately and linked through constraint equations to maintain compatibility at the interface [149, 237]. The method of using interface elements with a virtual thickness is probably the most popular method of all due to its simplicity as well as flexibility on regulating the interaction behaviour through the strength reduction factor which is the ratio between the strength of the soil and the strength of the interface [38] or the soil-structure normalised roughness which is the ratio of the maximum asperities of the pile surface and the soil mean grain size [218, 260, 261]. By using the interface element with virtual thickness, Langen and Vermeer [161] indicated that unrealistic high-stress concentration around a sharp corner could be avoided, Wehnert and Vermeer [273] showed that the mesh dependency of the shaft resistance in the pile-soil interaction simulation is removed, and Aguiar et al. [3] pointed out that the soil-pile interface behaviour observed experimentally are well reproduced.

As mentioned that the distribution of the tip and shaft capacity in the experiments is roughly 80% and 20%, respectively, of the total load capacity, two possibilities of modelling the interface behaviour are investigated to achieve a similar proportion in the simulations. Those two approaches are: (1) using an elastic thin layer with different stiffness

ranging from 0.05% to 50% E_{50} of the soil, and (2) using virtual-thickness interface elements with different strength reduction factors ranging from 0.5 (half-strength) to 1.0 (no strength reduction). Several trial simulations of the static and rapid pile load tests following these two approaches were performed to evaluate their influence on the proportion of the tip and shaft capacities. Results of the static and rapid simulations following the two approaches mentioned are given in detail in Appendix B.1.

Figure 7.2 presents the force-displacement curves in two static simulations with the interface elements in Figure 7.2(a) and with the elastic elements in Figure 7.2(b). The proportion of 80% tip resistance and 20% shaft friction can be achieved if the strength reduction factor of 0.5 is assigned for the interface elements, or if the stiffness of 0.05% E_{50} is assigned for the thin elastic elements.

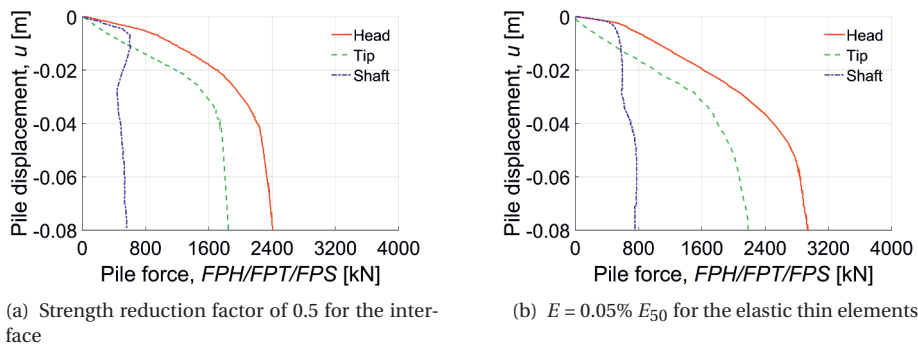


Figure 7.2: Influence of interface types in the static pile load test simulation

Further investigation, Appendix B.1, suggested that using the interface elements re-distributes the shear stress along the pile shaft and in the simulation of the rapid load test and the proportion of 80% tip - 20% shaft can be achieved easily. On the other hand, when using the thin elastic elements with a very small stiffness assigned to those thin elements, the enormous difference between the stiffness of the pile, the soil and the thin elements leads to the numerical problem of ill-conditioning in the rapid simulation. Consequently, this approach is not suitable for the rapid simulation. It is therefore decided to use the virtual thickness interface elements to model the interface behaviour in both the static and rapid pile load test simulations.

7.2.5. INITIAL CONDITIONS

In order to have a proper simulation of the pile capacity, a proper initial state prior to loading is very important [240]. Without any influence from the presence of the pile, the soil state can be reasonably assumed to follow the K_0 procedure. This is apparently not the case for the centrifuge pile load tests of the jacked-in pile since the soil density and stress state are strongly altering during the installation process [67]. It is also not the case even for the centrifuge pile load tests of the pre-embedded pile as the spinning up process of the centrifuge, and several earlier conducted tests had also changed the soil state [67]. The importance of the initial state will be discussed in this section.

INFLUENCE OF THE PREPARATION PROCESS AND INSTALLATION PROCESS

During spinning up of the centrifuge, an increase in the gradient of the confining stress occurs and which can create a non-uniform density in an initially uniform density model [47, 215]. The amount of stress densification depends on the amount of stress gradient change, sand type and initial relative density which could be significant for a relatively loose soil sample and high centrifugal gravity [47]; Park and Byrne [215] found an increase from 50% relative density up to 57% to 60% relative density depending on the sand type. Dijkstra [67] performed a centrifugal pile installation test in Baskarp sand in a three-dimensional configuration and used an electrical analogue to measure the change in electrical resistance and therefore determined the density change of the soil around the pile. Dijkstra [67] showed that a density increase of the soil occurs near the pile during spin-up of the centrifuge for both loose and dense soil sample; for the dense soil sample of 69% relative density, Dijkstra reported a densification of 4% to 6% along the pile shaft and at the pile base during the spinning up of the centrifuge and the initial unloading prior to pile load tests.

It is widely accepted that a difference in bearing capacity between pre-embedded piles and jacked piles exists thank to the installation process. More precisely, the installation process alters the density and stress of the soil surrounding the pile, hence modifies the strength and stiffness of the soil and, consequently changes the bearing capacity of the pile.

Robinsky et al. [234, 235] were the first authors to investigate the soil behaviour around a jacked pile in dry sand with a relative density of 37% to 57% during the installation process in the three-dimensional configuration. By using the X-ray method with radiographic equipment, they showed that during installation the soil below the pile base compacted while the soil along the pile shaft loosened for both dense and loose tests. The influence zone of the installation process extends up to 5.5 pile diameters from the pile shaft and 4.5 pile diameters under the pile base. Kobayashi and Fukagawa [152] used X-ray technique and image technique to characterise soil displacements during penetration of a CPT in dry sand and suggested that the soil below the pile base loosened and the soil along the pile shaft densified for both dense and loose tests. Observation of Kobayashi and Fukagawa contradicts with that of Robinsky et al. due to the difference in failure mechanism. The CPT in Kobayashi and Fukagawa tests is short and stiff with the ratio of the length over the diameter (L/D) is only 6, therefore, the failure mechanism is similar to shallow foundation; while this ratio is about 16 in Robinsky et al. and the failure mechanism is similar to that of the deep foundation. Chong [55] and Shublaq [250] used thermal conductivity measurement to investigate the density evolution during the pile/CPT penetration in dry sand ($L/D = 20$) with a relative density of 40% to 80%. The soil under the pile tip is loosened for initial dense sand (dilative behaviour), but it is densified for initial loose sand (compacted behaviour); the soil around the pile shaft is reported to be loosening regardless of the initial density. Dijkstra [67] used an electrical analogue to measure the porosity of the soil with a relative density of 35% to 76% around the pile ($L/D = 30$) during the centrifuge modelling of pile penetration. Dijkstra showed that during the pile installation phase the soil near the pile shaft loosens in the medium dense and dense tests; and during the pile load test, the soil porosity does not change significantly but the initial unloading after installation prior to any pile load tests always

leads to densification. Dijkstra reported a loosening of 8% at the pile base during the installation phase for the dense soil sample of 69% relative density.

In a plane-strain configuration, White et al. [277–280], gave very detailed information on soil displacements during the installation of a jacked pile ($L/D = 22$) in dry sand with a relative density of 34% to 55% by using the Particle Image Velocimetry technique. White et al. observed densification in the pile-soil interface with a clear nose cone under the pile base. This volume reduction is explained by redistribution and crushing of the grains. The calculated soil strains suggested that compressive volumetric strains are found under and around the pile base whereas expansive volumetric strains are found along the pile shaft. Dijkstra [67] experimentally investigated the pile installation in granular medium with the photoelasticity technique to observe the stress evolution of broken glass and with the Digital Image Correlation technique to examine the strain evolution of coarse sand during pile penetration. From the tests in broken glass, it is indicated that about 70% of the pile head force is transmitted to the pile base, the stresses at the pile base at the steady state increase several times relative to the initial stress.

Besides experimental approaches, numerical methods are widely employed to study the pile/cone penetration problem since they can provide great detail and, at the same time, various loading and boundary conditions can be easily imposed. Henke and Grabe [115] used the Finite Element Method with the kinematic contact formulation to model the pile penetration into the Karlsruhe soil continuum in a three-dimensional space. Henke and Grabe indicated a dilation zone along the pile shaft up to a distance of approximately 0.5 - 1.0 times the diameter of the pile and a zone of compaction close to the tip for medium dense soil with a relative density of 45%. High radial stresses are observed around the pile toe with an increase relative to the initial radial stress of approximately 10 times for the dense case (relative density of 80%). The maximum vertical stress as well as the highest radial stress are found at the bottom of the pile which leads to a compaction of the surrounding soil directly at the pile toe. Mahutka et al. [173] employed the adaptive meshing technique to model the pile driving process on the axisymmetric finite element mesh. In the case of the jacked pile in dense Karlsruhe sand simulations, an increase in the void ratio close to the shaft is observed, very high stresses are seen at the pile toe and do not dissipate after the jacking process is terminated. The zone of high stresses can extend up to 5 pile diameters from the pile toe. Qiu et al. [226] applied the Coupled Eulerian-Lagrangian method to simulate the jacking of a pile into dry Mai-Liao sand in the three-dimensional configuration. Qiu et al. found that the void ratio directly at the pile shaft increases due to dilatancy and that the stresses increase significantly around the pile toe which is in good accordance with [115, 173]. Dijkstra et al. [68] modelled the centrifugal pile jacking in saturated sand by using both full Eulerian and Arbitrary Lagrangian-Eulerian schemes on an axisymmetric finite element mesh. The simulation results following both schemes showed a loosening of the soil near the shaft and a slight densification below the pile base. Dijkstra et al. indicated that although the results are qualitatively good, they are not good quantitatively because of the limitation in the determination of the constitutive model parameters at the very high stress, strain levels and gradients.

INCLUDING THE EFFECTS OF THE PREPARATION PROCESS AND INSTALLATION PROCESS

From the above section, it is clear that the preparation and installation phases strongly affect the state (the density and the stress) of the soil surrounding the pile. Therefore, it is necessary to numerically incorporate the effects of those processes in order to have a realistic simulation of the pile load test behaviour. It is apparent that the most proper way to simulate the influence of the installation process is modelling the installation process itself by advanced methods such as Arbitrary Lagrangian-Eulerian method [16, 68, 259], contact mechanics and Finite Element Method [81, 249], Coupled Eulerian-Lagrangian method [107, 225, 227], Material Point Method [217]. However, simulation of the installation process is also a complicated topic and requires significant work. An alternative option is incorporating the effects of preparation and installation phases by making a modification of the material parameters based on the change of the density or the stress level and/or pre-stressing the soil surrounding the pile. The section below discusses those two possibilities.

There are many experimental proofs for the dependency of the strength of the sandy soil on the stress level as well as on the relative density. Scheme 3 is proposed based on the related literature. Lee et al. [164] presented triaxial data from dense Ottawa sand and dense Sacramento River sand and showed that there is a decrease in friction angle associated with an increase in confining pressure. This observation is in agreement with the observation of Gan et al. [89] on Monterey sand and Danish Normal sand. Bolton [34] collected data from triaxial and plane strain shear tests for 17 types of sand and proposed simple equations for triaxial and plane strain tests which correlate the maximum mobilised friction angle with the relative density at different mean stress levels. In general, the friction angle reduces about 2° to 4° when the relative density reduces 10% from 65 to 55% depending on the confining stress level. Similarly, Schmertman [243] implied that the friction angle decreases from 43° to 38° when the relative density falls from 65 to 55% for fine sand with $d_{50} = 75 - 420 \mu\text{m}$. Clark [58] indicated that both the peak friction angle and the critical state friction angle decrease with the stress level, i.e. when the confining pressure increases from 25 to 2500 kPa, the peak angle decreases from 49° to 39° while the critical state angle changes from 40° to 34° . Andersen and Schjetne [11] provided a comprehensive database of the strength parameters and consolidations characteristics of sand, silt and clay based on the Norwegian Geotechnical Institute files and published literature. For sands of $d_{50} = 126 - 135 \mu\text{m}$, Andersen and Schjetne reported that the dilation angle decreases from 12 to 8° and the friction angle decreases from 40° to 35° when the relative density falls from 65 to 55%. The observations from the experimental studies mentioned above will be employed later in this study.

In the simulations of the pile-soil interaction problem using the small-strain Finite Element framework, several techniques have been proposed to initiate an appropriate initial condition for the soil. Russo [236] used the back-analysed K -value from a field test as a K_0 -value to initialise the appropriate stress field around the pile. However, by using this method, the horizontal stress is increased in the entire soil which does not represent a cavity expansion due to pile penetration. Satibi [240] employed the K_0 -pressure method in which stress-controlled expansion of a cylindrical cavity is imposed to the interface between the pile shaft and the soil with the value of K_0 is taken from back-calculation of measured load-settlement curves. The K_0 -pressure method provides a

load-settlement curve which is in good agreement with one from the pile load test in Wijchen [115]. However, it should be noticed that this is a shaft-dominant case where the shaft friction is about 90% of the total bearing capacity. Broere and van Tol [39] proposed two schemes to incorporate the installation effect in modelling the bearing capacity of displacement piles. In the first scheme, a certain amount of volumetric strain is imposed in the area representing the pile; and in the second scheme, displacement-controlled expansion is applied on the interface between either the pile shaft or the pile tip and the soil. The estimated total capacity following the first scheme is close to the observed value from the results of a centrifuge test that was used for calibration. However, the shaft friction is too high whereas the tip resistance is too low. On the other hand, the calculated total capacity as well as the distribution of the total load over shaft friction and tip resistance is more satisfactory following the second scheme.

Several trial simulations of the static pile load tests following two schemes proposed by Broere and van Tol [39] were performed to further evaluate their effectiveness to achieve a required total load capacity with a certain proportion of the tip and shaft resistances. Results of the static simulations following the two schemes are given in detail in Appendix B.2. It is confirmed that the techniques of prescribing volumetric expansion and prescribing horizontal displacements have much stronger influence on the shaft friction than on the tip resistance. When applying one of these two techniques, the tip resistance actually reduces due to the stress relaxing under the pile tip while the shaft friction increases; consequently, when the tip resistance reaches the value required, the shaft contributes to the total capacity in a much higher proportion than that of the tip. The technique of prescribing vertical displacement improves the tip resistance significantly while it increases the shaft friction slightly, i.e. prescribed displacement of $1 D$ increases the tip resistance 300% and the shaft friction 75%. It is however not desirable to apply a large prescribed vertical displacement, i.e. larger than $1.5 D$; otherwise, the elements under the pile tip area are so severely distorted that the Jacobian of the deformation matrix becomes negative. However, with a rather small prescribed displacement, a required total capacity can be achieved with a good proportion of the shaft friction and the tip resistance. Therefore, the technique of prescribing vertical displacement will be used in this study.

7.2.6. SIMULATION SCHEMES AND CALCULATION PHASES

Based on the literature review and trial simulation tests from the previous section, four simulation schemes are employed in this study to model the pile load test.

Scheme 1 is the most basic one in which the pile and the soil are modelled as two nearby clusters without any specific treatment in the boundary between them; the soil elements are rigidly connected to the pile, and they move together with the pile. Therefore, the pile shaft is subjected to large normal stress and a high shaft capacity is expected.

Scheme 2 uses the virtual thickness interface elements to properly model the interfacial behaviour which is the essential importance of the pile-soil interaction problem. The strength reduction factor of the interface elements is derived from the friction angle of the soil and the friction angle between the soil and the pile surface as formulated in

the Plaxis manual [38]:

$$R_{inter} = \frac{\tan \phi_{inter}}{\tan \phi} \quad (7.1)$$

in which ϕ is the friction angle of the soil and ϕ_{inter} is the friction angle between the soil and the pile surface.

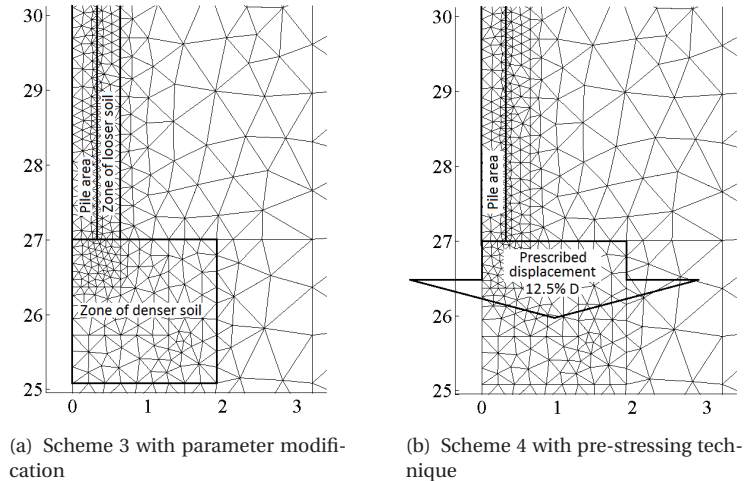


Figure 7.3: Illustration of simulation scheme 3 and 4

Scheme 3 utilises the virtual-thickness interface elements and an adaption for the material properties to take into account the influence of the preparation phase. This scheme aims to model the pile load test with the pre-embedded pile. Following the indication of Grabe et al. [115, 173, 226] and Dijkstra et al. [67, 68] on the change of void ratio and stress state around the pile and the indication of Bolton [34], Clark [58] and Andersen and Schjetne [11] on the change of stiffness and strength parameters of soil due to the change of void ratio and stress state, modification of soil parameters are proposed for scheme 3: the soil is considered to be looser in a slice of the width of R along the pile shaft, and the soil is adapted to be denser in a square of $3D \times 3D$ right under the pile tip. The corresponding parameters of the soil in these two zones are given in Table 7.1. Zone of modified parameters is illustrated in Figure 7.3(a).

Scheme 4 utilises the virtual thickness interface elements, an adaption for the material properties and the technique of prescribing vertical displacement to take into consideration the influence of the preparation and installation phases. This scheme aims to model the pile load test with the jacked-in pile. As indicated by Grabe et al. [115, 173, 226] and Dijkstra et al. [67, 68] the zone of high stress under the pile tip after the installation process can extend $3-5 D$ from the pile tip. Several trial simulations indicated that applying the prescribed vertical displacement as recommended by Broere and van Tol [39] on this zone, smaller displacement is required and the problem of severe distortion can be avoided. The pre-stressing technique used in scheme 4 is the prescribing of 12.5%

D along the line up to $3D$ under the pile tip. Illustration of the pre-stressing method is shown in Figure 7.3(b).

With the basis that the pile and the soil are modelled as the two separate clusters of elements without any specific treatment, summary of the four calculation schemes can be briefly described as follows:

- Scheme 1: the basis;
- Scheme 2: scheme 1 with the virtual thickness interface elements are used along the interface between the pile and the soil clusters;
- Scheme 3: scheme 2 with the adaption for the material properties along the pile shaft and under the pile tip;
- Scheme 4: scheme 3 with the pre-stressing under the pile tip.

Details of all calculation phases for each simulation scheme can be found in Appendix C. Twenty four simulations in total are performed including: 1) four static simulations following scheme 1 to 4; 2) two rapid simulations following scheme 1 and 2; 3) nine rapid simulations following scheme 3 with different permeability of 8.9×10^{-8} to 8.9×10^{-2} m/s; and 4) nine rapid simulations following scheme 4 with different permeability of 8.9×10^{-8} to 8.9×10^{-2} m/s.

7.3. SIMULATION OF STATIC PILE LOAD TESTS

In the static simulations, the displacement of 20% D (0.12 mm) was imposed in about 30 up to 120 calculation steps, the difference in the number of the calculation step due to the fact that the are-length controlled is used in Plaxis to automatically determine the step size for the best performance. The results of four static simulations following four schemes listed in the previous section are presented in this section. The comparison between the simulation results with the results of static tests of centrifuge test series 23 and 24 is also given in term of the total pile capacity and the distribution of the tip resistance and the shaft friction.

7.3.1. PILE CAPACITY AT 10% D

The static load-displacement relations of four simulation schemes are plotted in Figure 7.4 together with the measurements from the centrifuge tests. The results showed in Figure 7.4 indicate a significant influence of the interface element as well as the preparation and installation processes.

In scheme 1 (without using the interface elements), the total capacity is much higher than those of other schemes (using the interface elements) in which the main contribution comes from the enormous shaft friction. As the shaft friction contributes more than 80% of the total capacity, the pile in scheme 1 is similar to the shaft-dominance pile foundation. Moreover, there is no clear failure of the shaft friction even up to the displacement of 10% D which is due to the high dilation of the soil. By modelling the interfacial behaviour between the pile shaft and the soil in schemes 2, 3 and 4, there is a clear failure of the shaft friction as expected. The shaft friction is fully mobilised at the very small displacement, of less than 1% D , which is because the dilation of the interface element is implicitly neglected. At the displacement of 10% D , the shaft friction of scheme 2 is equal to 40-50% of those of the centrifuge tests, in scheme 3 the shaft friction

is 10% higher than the shaft friction of the pre-embedded pile test and in scheme 4 the shaft friction is almost equal to that of the driven pile test.

Although the interface element helps to improve the tip resistance by redistributing the stress field close to the pile tip, only using the interface element is not enough to achieve a higher tip resistance since both scheme 1 and 2 underestimate the tip resistance in comparison with the experiments. On the other hand, the modification of soil parameters in scheme 3 and the combination of the modification of soil parameters and the pre-stressing techniques in scheme 4 solve this problem. At the displacement of 10% D , the tip resistances of scheme 3 and 4 are slightly higher than those of the pre-embedded pile tests and the driven pile tests, respectively. It is noted that without the modification of soil parameters, the pre-stressing technique is enough to increase the pile tip resistance; however the shaft friction also increases significantly due to pre-stressing, as shown in Appendix B.2, and therefore the distribution of the tip resistance and the shaft friction in numerical simulations is not similar to the distribution in experiments anymore.

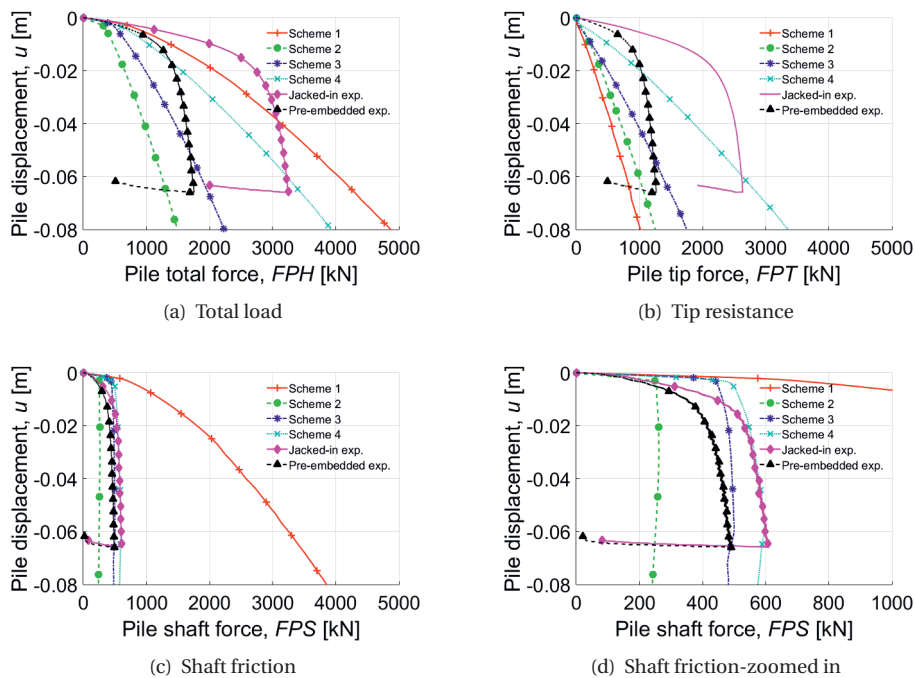


Figure 7.4: Load-Displacement curves of static tests

A clear shortcoming of all four schemes is the underestimation of the initial stiffness of the load-displacement results; even if the unloading/reloading stiffness of the soil is employed, the stiffness of the pile response only increases slightly within less than 0.5% D displacement. Another shortcoming is that the clear failure of the pile, or more precisely of the tip resistance, in the experiment is not represented. The overprediction of

the volumetric expansion may be the main reason for this as the strength parameters are kept constant (with the dilatancy cutoff option) and a suitable constitutive model with the strength parameters dependent on the stress/strain state may overcome this problem. Advanced numerical methods and techniques [68, 217, 227, 249] may solve above shortcoming, but they are not the main interest of this study. Nevertheless, schemes 3 and 4 provide satisfactory results when comparing with the experimental results in term of the pile capacity at the pile displacement of 10% D and the high contribution of the end bearing capacity to the total capacity which is about 70-80% (a typical end-bearing pile).

7.3.2. STRESS STATE

The mean effective stress and the deviatoric stress of the four schemes are plotted for the situation before static loading in Figures 7.5 and 7.6 and for the moment at a displacement of 10% D in Figures 7.7 and 7.7. Apparently, different simulation schemes result in significant different stress states.

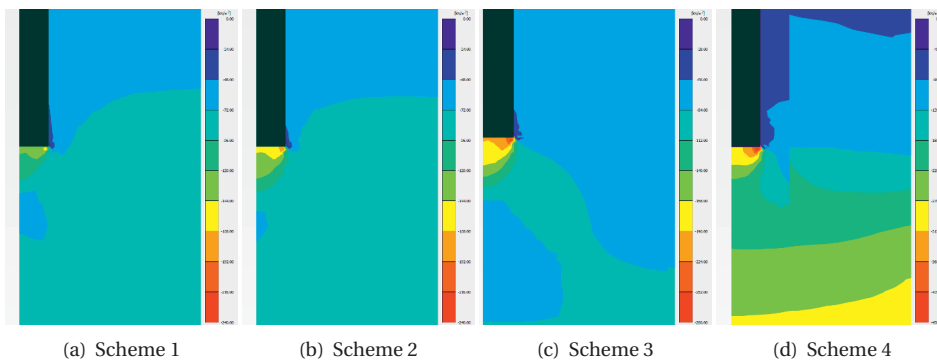


Figure 7.5: Mean effective stress before static loading

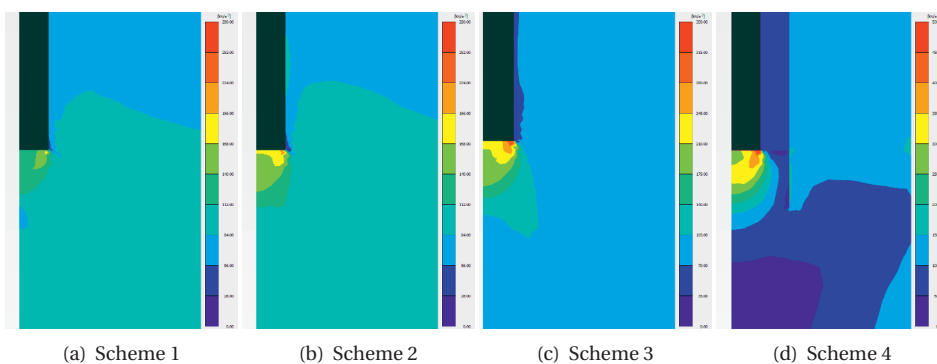


Figure 7.6: Deviatoric stress before static loading

Before static loading, the stress states of three scheme 1, 2 and 3 are quite similar; the slight difference is the presence of the interface element during the gravity loading of the pile. In scheme 4 with the vertical pre-stressing, both the mean effective stress and the deviatoric stress are larger in magnitude and spatial distribution about 2-3 times (taking into account the difference of the scale) than those of the other schemes.

For the situation at a displacement of $10\% D$, there is a big difference between the stress state among four schemes. In scheme 1, the stress state (the mean and deviatoric stresses) increases about three times under the pile tip and about ten times along the pile shaft (in comparison with the initial stress state). In scheme 2, with the presence of the interface element, the shaft friction decreases significantly hence the stress state under the pile tip builds up to a level that is about three times higher than that of scheme 1. In scheme 3 and 4, with the parameter modification and the pre-stressing, the stress is about five times and eight times higher, respectively, than the stress achieved with scheme 1. With such a higher stress level, the tip resistance is significantly improved with scheme 3 and 4.

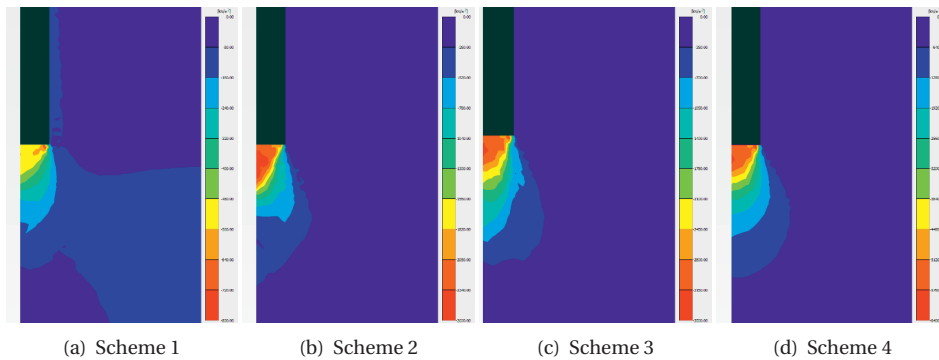


Figure 7.7: Mean effective stress at displacement of $10\% D$

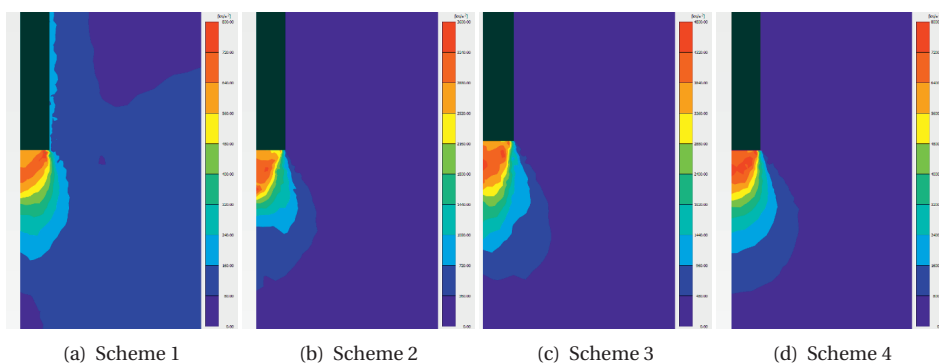


Figure 7.8: Deviatoric stress at displacement of $10\% D$

7.3.3. SUMMARY

In order to achieve a proper prediction of the total pile load and a similar distribution of the tip resistance and the shaft friction in comparison with those of the experiment (at the displacement of 10%D), a special treatment is required. The interface elements are necessary to model the interfacial behaviour. A modification of the soil parameters is appropriate to take into account the influence of the preparation process and hence successfully model the pre-embedded pile. The pre-stressing technique can significantly improve the stress under the pile to achieve a high tip resistance and a reasonable shaft friction; consequently, the jacked piles can be simulated. It is worth mentioning that judgement on the quality of the simulations is based on the total load capacity and the distribution of the tip resistance and the shaft friction at the displacement of 10%D.

7.4. SIMULATION OF RAPID PILE LOAD TESTS

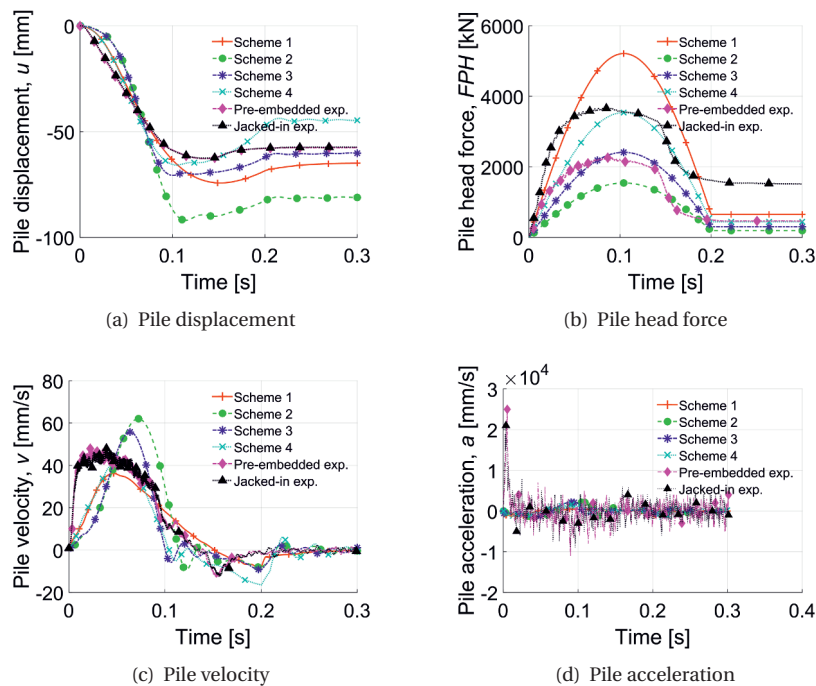


Figure 7.9: Loading pulse

In this section, the results of the simulations of the rapid load tests following four schemes are given and compared with the experiment in terms of the load capacity and the tip resistance-the shaft friction proportion. It will be shown in Section 7.4.1 that, regarding the load capacity and the contribution of the tip resistance or the shaft friction to the total pile capacity, scheme 3 and scheme 4 can simulate well the pre-embedded pile and the jacked-in pile, respectively. Then, the detail results on the strains and pore pres-

ures field from the test simulation following scheme 4 with the default permeability of 8.9×10^{-5} m/s are shown and compared with the results of a rapid test of the centrifuge test series 24 in Section 7.4.2. The reason for the choice of the simulation following scheme 4 is that the results of simulations following scheme 3 and 4 are of the same trend.

The applied load on the pile head and the displacement, velocity and acceleration as a function of time are plotted in Figure 7.9 for the simulations following Scheme 1 to 4 and for the experimental rapid load test with the pre-embedded pile and the jacked-in pile. It can be seen from Figure 7.9 that although the maximum displacement is comparable, the applied force in Scheme 1 and Scheme 4 are much different than the remaining two schemes and the two experiments which shows the strong influence of the modelling techniques as mentioned in Section 7.3. The velocity profiles in the experiments are much stiffer than those in the simulations; similarly, the acceleration profiles in the experiments are much higher than those in the simulations. The differences in the velocity profile and the acceleration profile can result in the difference in the stiffness of the load-displacement response between the experiments and the simulations.

7.4.1. PILE CAPACITY AT 10% D

The rapid load-displacement relationships of four simulation schemes are plotted in Figure 7.10 together with the measurements from the centrifuge tests.

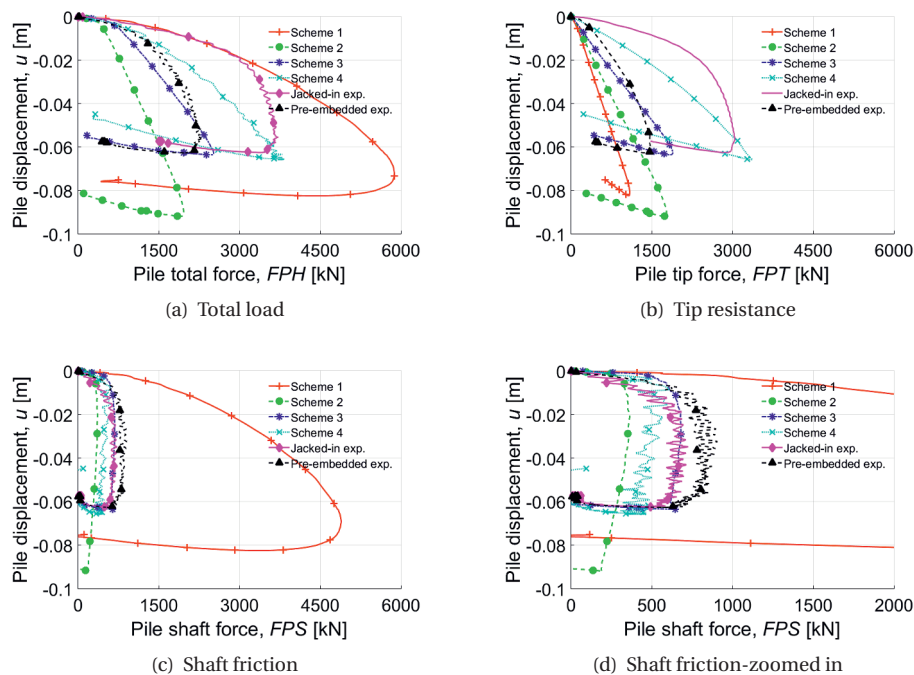


Figure 7.10: Load-Displacement curves of dynamic tests

Scheme 1 overestimates the pile capacity, in particular, the shaft friction is several times higher than the tip resistance; moreover, the shaft friction, as well as the tip resistance, are not fully mobilised. With the presence of the interface elements, the shaft friction following scheme 2, 3 and 4 are fully mobilised after the pile has been displaced by about $2\%D$. The shaft friction of scheme 2 is lower while the shaft friction of scheme 3 and 4 are comparable with those of the centrifuge tests. Scheme 1 and 2 significantly underestimate the tip resistance whereas scheme 3 and scheme 4 predict well the tip resistance of the pre-embedded pile test and the driven pile test, respectively. However, the tip resistance in all schemes is still not fully mobilised at a displacement of $10\% D$ because of the high dilation angle.

7.4.2. STRAIN AND PORE PRESSURE

As the results of the pile capacity in the simulations following scheme 1 and 2 are far from those of the experiment, their results are not investigated further. As the results of simulations following scheme 3 and 4 are of the same trend, in this section, only the results from the simulation following scheme 4 are presented.

The changes of the volumetric strain, the deviatoric strain and the pore pressure along the pile shaft are plotted in Figure 7.11; the changes of the volumetric strain, the deviatoric strain and the pore pressure at three different depths under the pile tip, i.e. $R/2$, R and $2R$, are plotted in Figure 7.12. Different lines present the values of the volumetric strain or the pore pressure at different times from 0.02 seconds to 0.3 seconds.

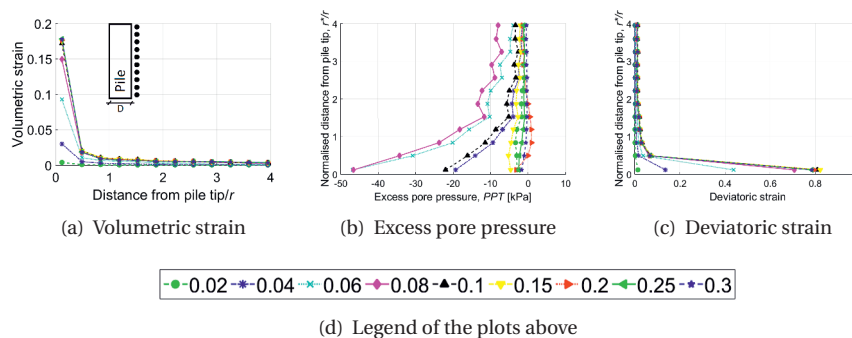


Figure 7.11: Volumetric strain and pore pressure along the shaft at different times

Figure 7.11 clearly suggests that along the pile shaft the soil only experience extension with positive volumetric strain, the shearing behaviour is also dominant in this zone and the respective excess pore pressure is negative most of the time.

It can be seen from Figure 7.12 that the soil directly under the pile tip (with the distance from the pile centre smaller than $r = 0.32$ m) is mainly in compression with negative volumetric strain and positive excess pore pressure. Moreover, the closer the soil is to the pile centre, the more compression the soil sustains; the maximum compression is achieved at around 0.1 seconds. On the other hand, the soil on the pile shoulder (with the distance from the pile centre smaller than $r = 0.32$ m) is mainly in extension with

positive volumetric strain and negative excess pore pressure. The maximum extension is achieved at around 0.1 seconds when the loading reaches its maximum value.

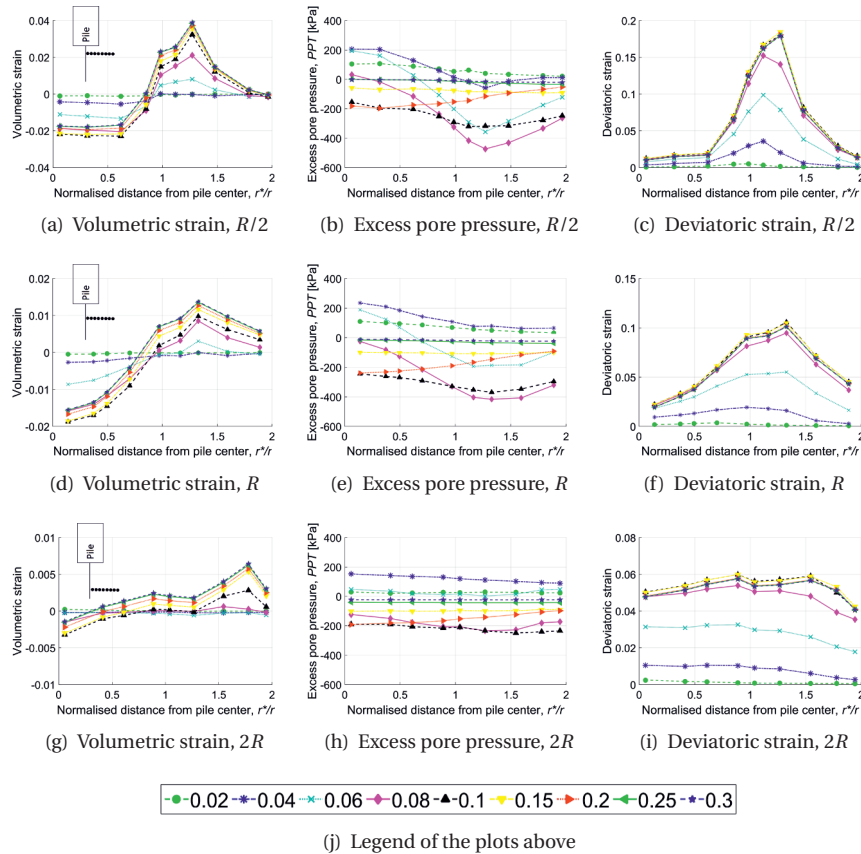


Figure 7.12: Volumetric strain and pore pressure at different depths under the pile tip at different time

Based on the horizontal and vertical distributions of the volumetric strain, the existence of the nose cone under the pile tip, as observed by Robinsky et al. [234] and White [278], is confirmed; the nose cone is presented in Figure 7.13 by the bold line. The presence of the nose cone under the pile tip can be seen clearly in the plot of the volumetric strain at three different times in Figure 7.14. In Figure 7.13, there are seven points of interest which locate in or next to the locations of PPTs in the experiments. The evolution of the pore pressure with time at those locations is presented in Figure 7.15.

The soil inside the nose cone is compressed during pile penetration to the maximum negative volumetric strain and unloaded, Figure 7.12(a). The correlated excess pore pressure inside the nose cone first increases to the maximum positive then reduces to maximum negative (even before the applied load reaches the maximum value) and dissipates as shown in both Figures 7.12(b, e and h) and 7.15(a). This behaviour of the

excess pore pressure is similar to the observations of Nguyen [206] in his centrifuge test and the field test measurement of Hölischer et al. [122].

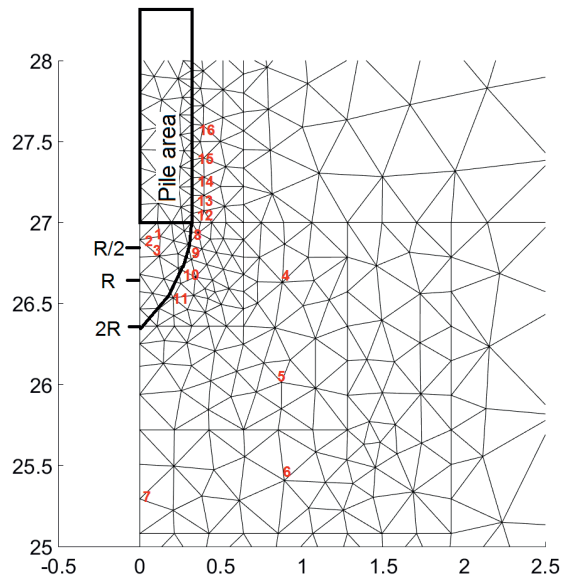


Figure 7.13: Pile corner with the soil-cone. Points 4-5 are the locations of the PPT-1 and PPT-2, respectively, in the experiments.

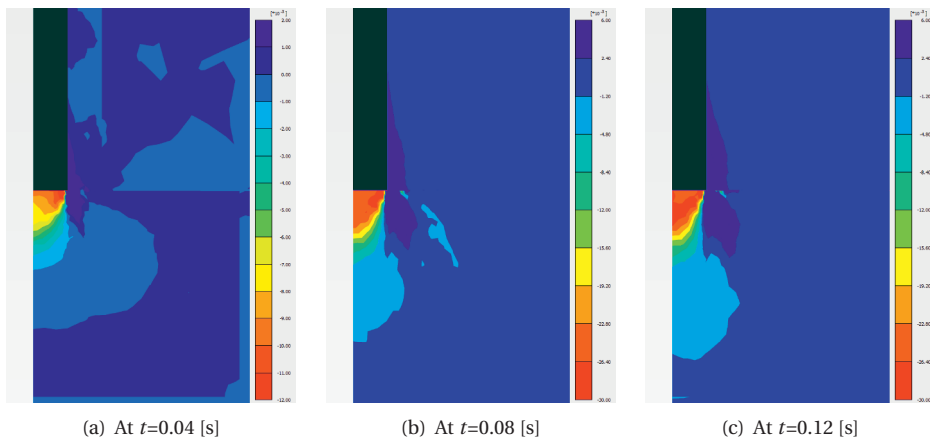


Figure 7.14: Volumetric strain under the pile tip

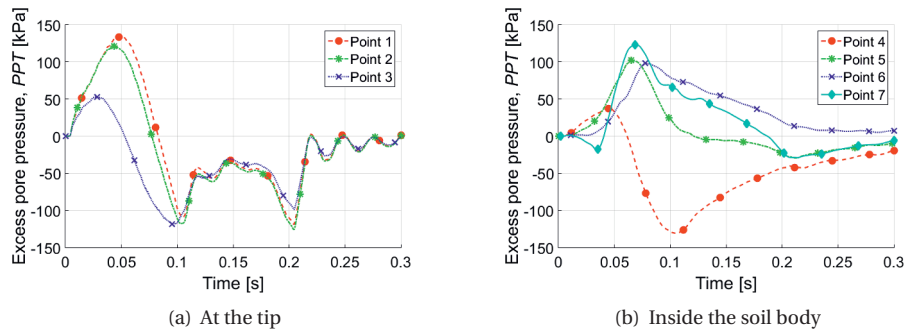


Figure 7.15: Pore pressure under the pile tip and inside the soil body

Along the edge of the nose cone, as pointed out by Robinsky and Morrison [235] and White [278], the soil particles slides as a flow and the shear behaviour is dominant over the compression behaviour. This is confirmed in Figure 7.12 by the fact that the magnitude of the deviatoric strain is about 5-10 times higher than the magnitude of the volumetric strain. Because of the dominance of the shear behaviour along the edge of the nose cone, the excess pore pressure in this zone is negative during most of the loading duration as shown in Figure 7.12.

At point 4 inside the soil body, Figure 7.13, which is located at $1 D$ from the pile shaft and $0.5 D$ under the pile tip, the excess pore pressure first increases to maximum positive pore pressure then decreases to maximum negative pore pressure and then dissipates which is indicated that the soil at that point is first compressed and then sheared, Figure 7.15(b). Deeper under the pile tip, at point 5, 6 and 7 in Figure 7.13, the excess pore pressure is mainly positive which suggests that the soil is mainly in compression, Figure 7.15(b).

7.4.3. INFLUENCE OF PORE PRESSURE ON RAPID CAPACITY

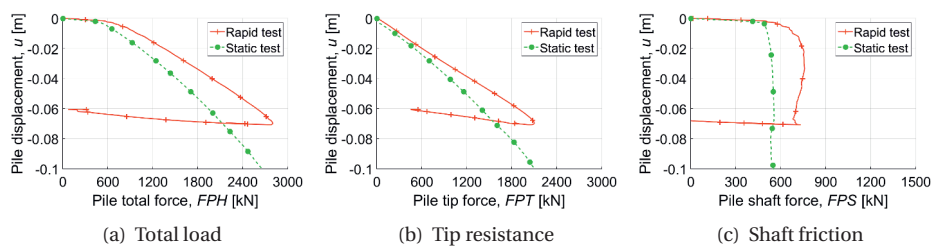


Figure 7.16: Reaction forces of simulations following scheme 4

The measured data in Chapter 4 indicates that the pile capacity at a certain displacement in the dynamic test is higher than that in the static test. This phenomenon is also observed as shown in Figure 7.16 in which both the tip resistance and the shaft friction of

the rapid load test simulation are higher than those of the static simulation, respectively, at any given displacement level.

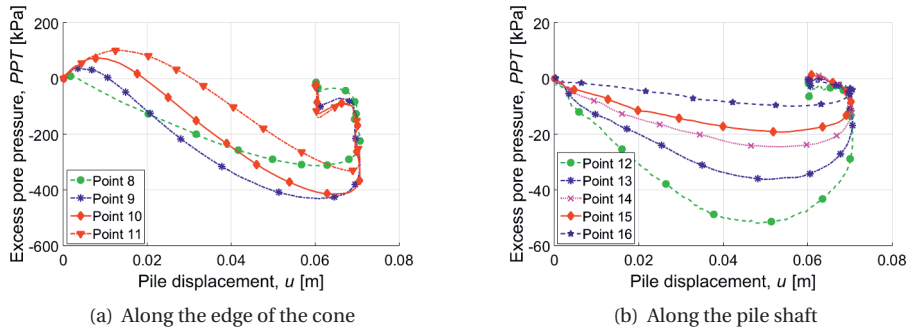


Figure 7.17: Excess pore pressure as a function of pile displacement

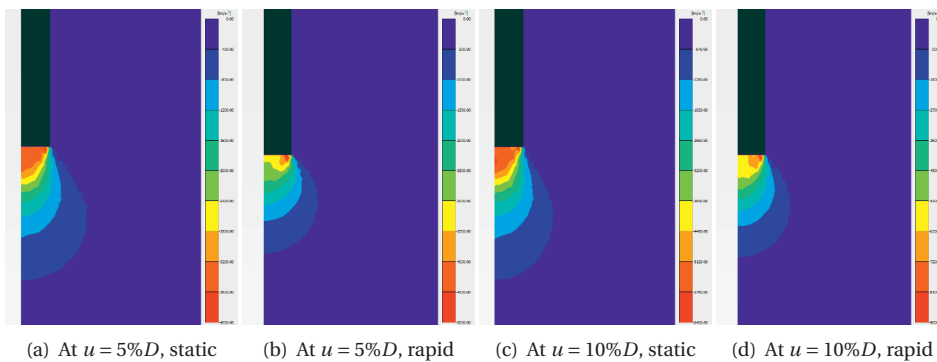


Figure 7.18: Effective isotropic stress, p [kPa]

Figure 7.16 indicates that not only the maximum pile capacity but also the pile capacity at the unloading point (the point at which the displacement is highest) of the rapid simulation is higher than the pile capacity of the static simulation. This agrees well with the experiment and implies an important influence of the excess pore pressure since, at the unloading point, the other rate effect is supposed to be trivial since the pile velocity is zero. Although the increase of the rapid pile capacity over the static pile capacity is due to the rate effect and the effect of negative excess pore pressure around the pile [206], this section focuses mainly on the effect of excess pore pressure.

The excess pore pressures at different locations as a function of the pile head displacement are plotted in Figure 7.17(a) for four points 8 to 11 along the edge of the cone; and Figure 7.17(b) for five points 12 to 16 along the shaft. Locations of point 8 to 16 are marked in Figure 7.13. At the tip shoulder (point 7) and along the pile shaft, the excess pore pressure is always negative. At point 8 and 9 along the nose cone, the excess pore

pressure is also negative after the displacement of 10% D and 20% D , respective. The dominant presence of the negative excess pore pressure during the downward movement of the pile in Figure 7.17 confirms the dominance of the shear behaviour along the pile shaft and along the edge of the cone during the rapid pile loading test. Because the negative excess pore pressure is generated, the effective stress in the rapid load test is higher than that in the static load test, Figure 7.18 which increases the strength of the soil and, consequently, both the tip resistance and the shaft friction increase.

7.4.4. SUMMARY

In terms of the total pile capacity and the distribution of the tip resistance and the shaft friction in a rapid pile load test, scheme 3 and scheme 4 are appropriate for the simulations of the pre-embedded pile and the jacked pile, respectively.

During a rapid pile load test, multiple zones around a pile which experience different behaviour are confirmed. Furthermore, by using the Plaxis-PTU, the response of the excess pore pressure in those zones is clarified. The soil along the pile shaft is sheared and expanded resulting in the negative excess pore pressure during most of the loading pulse. Right under the pile tip, the soil is compacted with a high compressive strain and therefore the excess pore pressure is positive. A nose cone of compacted soil is confirmed to exist under the pile tip. Along the boundary of this nose cone, the soil is sheared leading to high negative excess pore pressure. Further away from the pile, the soil zone under the influence of the P-wave experiences mainly compression and has the positive excess pore pressure. The soil under the influence of the shear wave or both body and shear waves experiences both the compression and shearing which results in the presence of both the positive and negative excess pore pressure.

The occurrence of the negative excess pore pressure in the shearing zone around the pile may associate with the increase of the pile capacity in the rapid load test in comparison with the pile capacity in the static load test as the negative excess pore pressure results in an increase of the effective stress and consequently an increase in the soil strength.

7.5. COMPARISON WITH EXPERIMENTS

This section presents a further comparison between the simulated rapid pile load tests and the experimental ones. As mentioned previously, there is a significant discrepancy in the stiffness of the load-displacement response between the calculations and the experiments due to the simple modelling technique. However, because of the similarity on the load capacity and therefore the stress level at and around the pile tip area, it is feasible and reasonable to make a comparison of the excess pore pressure response and on the ratio of the rapid capacity over the static capacity.

7.5.1. EVOLUTION OF THE EXCESS PORE PRESSURE

GENERAL BEHAVIOUR

Right under the pile tip, the excess pore pressure behaves differently in the experiment and the simulation.

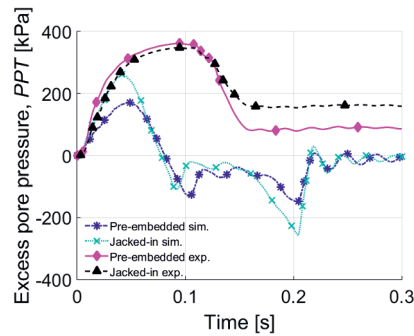


Figure 7.19: Comparison of the excess pore pressure at the pile tip

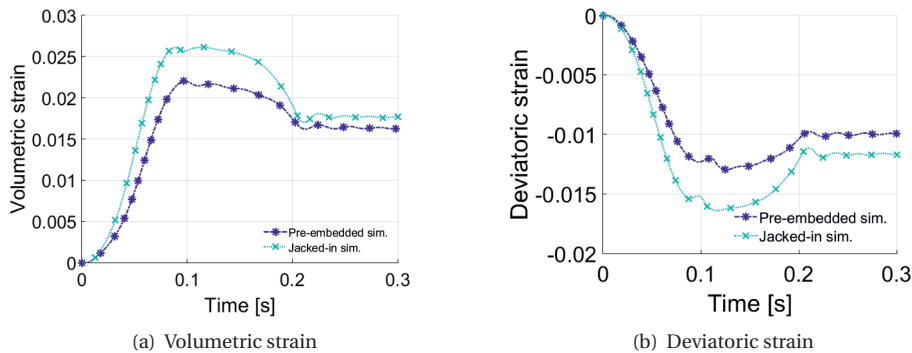


Figure 7.20: Volumetric and deviatoric strains at the pile tip from the numerical simulation

In the experimental observation of series 23 and 24, the excess pore pressure response consists of two phases of (1) an increase to the peak positive value and (2) a dissipation to the stationary value, Figure 7.19. On the other hand, the excess pore pressure response in the simulation consists of three phases of (1) an increase to the peak positive value due to compression, (2) a decrease to the peak negative value due to shear and (3) dissipation due to consolidation, Figure 7.19. The response of the excess pore pressure in the simulation corresponds well with the change of volumetric and deviatoric strains at the pile tip, Figure 7.20. The explanation for this difference, as mentioned in Chapter 4, is geometrical as the size of the sand cone under the pile tip in series 23 and 24 is almost two times the diameter of the pore pressure transducer, therefore, the PPT shows only the positive excess pore pressure due to the compaction in the sand cone.

Figure 7.21 presents the excess pore pressure responses in the experiment and in the simulation at the location $0.5 D$ below the pile tip and $1.5 D$ from the pile centre which is also named as level 1 in Chapter 4. The excess pore pressure responses in the experiment and the simulation show the same general trend of (1) increasing to the peak positive value, (2) decreasing to the peak negative value and (3) dissipating. The difference between the peak values of the excess pore pressure in the experiment and the simula-

tion is inevitable since the measurements at three axisymmetric locations are different as well as discussed in Chapter 4. It is also noticed from Figure 7.21 that, the duration of the compression phase in the experiment is comparable to that in the simulation.

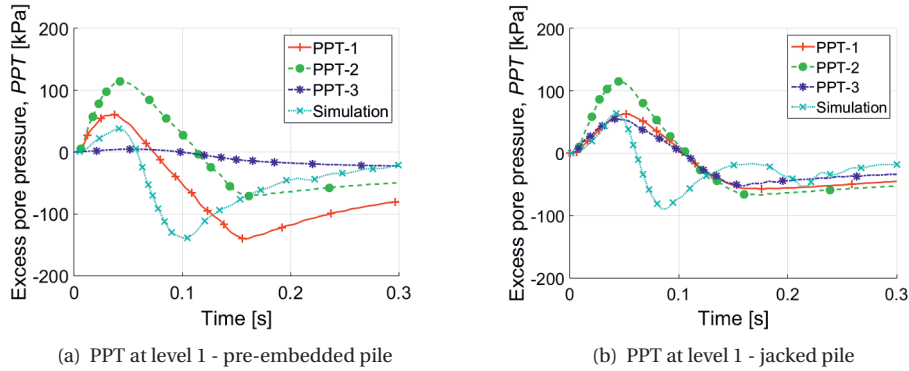


Figure 7.21: Comparison of the excess pore pressure at the location of PPT-1 to PPT-3

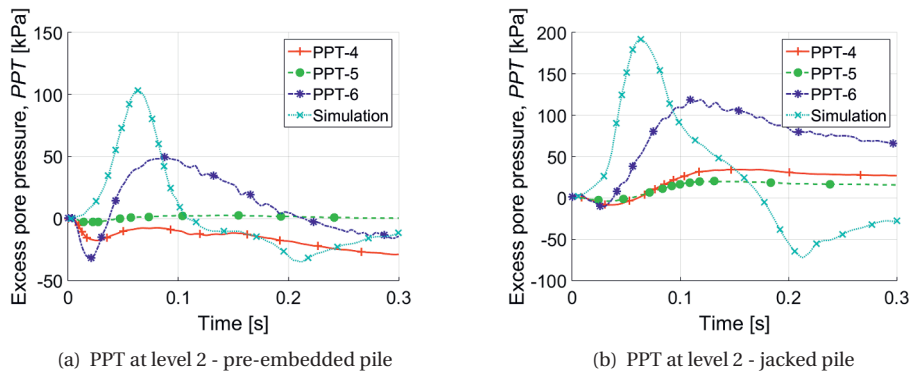


Figure 7.22: Comparison of the excess pore pressure at the location of PPT-4 to PPT-6

Figure 7.22 presents the excess pore pressure responses in the experiment and the simulation at the location $1.5 D$ below the pile tip and $1.5 D$ from the pile centre named as level 2 in Chapter 4. The excess pore pressure responses in the experiment and the simulation follow different trends. In the simulation, the same general trend as described in the previous paragraph is observed. However, the excess pore pressure response in the experiment features by (1) a (slight) decrease to a maximum negative value, (2) an increase to a maximum positive value and (3) dissipation. It means that at this location in the simulation there is compression first then shearing follows, whereas in the experiment there is shearing first then compression follows. It is not strange that a small difference in the stress and strain field might be the reason for this difference in the excess pore pressure response.

VARIATION OF PERMEABILITY

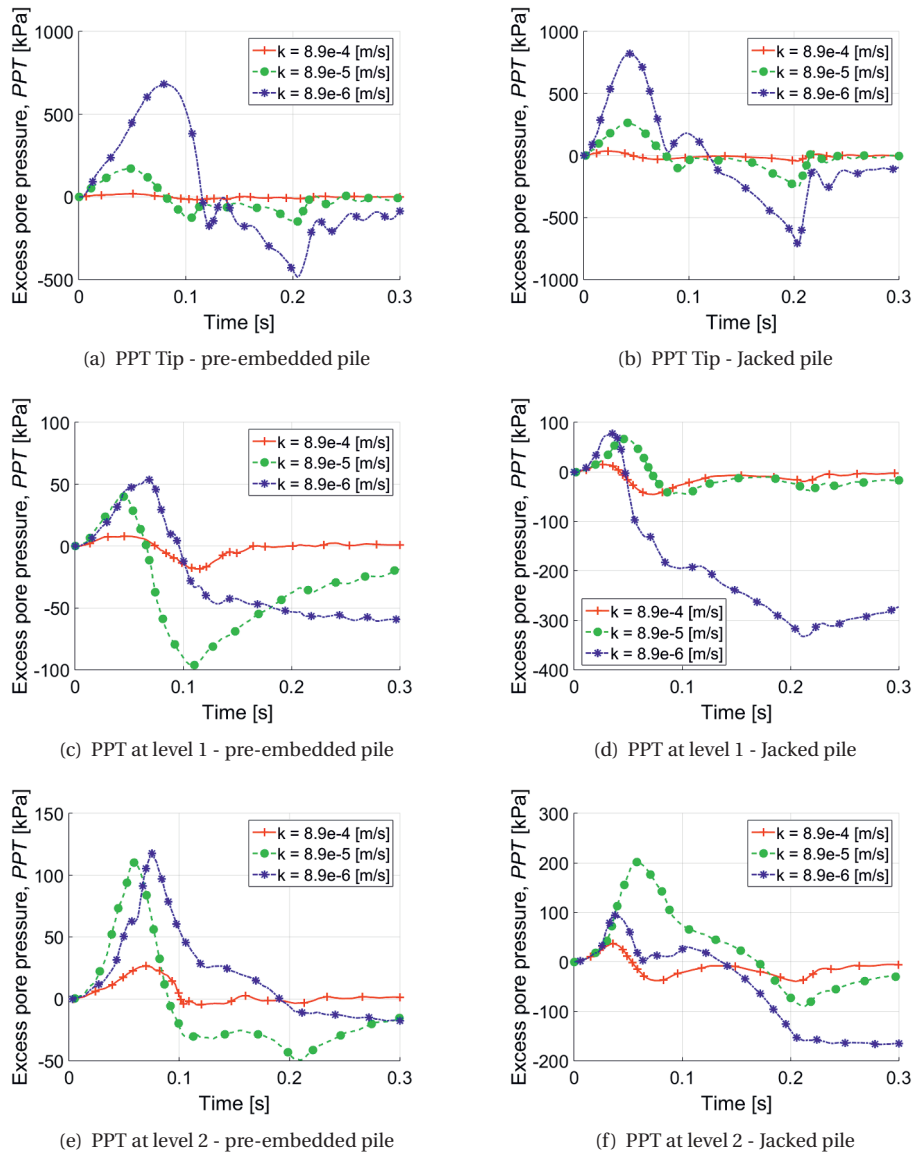


Figure 7.23: Influence of permeability on excess pore pressure responses

In this section, the influence of the permeability on the response of the excess pore pressure is investigated. Simulations of the rapid pile load test with three different permeability's of 8.9×10^{-6} , 8.9×10^{-5} and 8.9×10^{-4} are conducted; the excess pore pressure responses at the pile tip, at the location of PPT-1 and the location of PPT-4 are presented

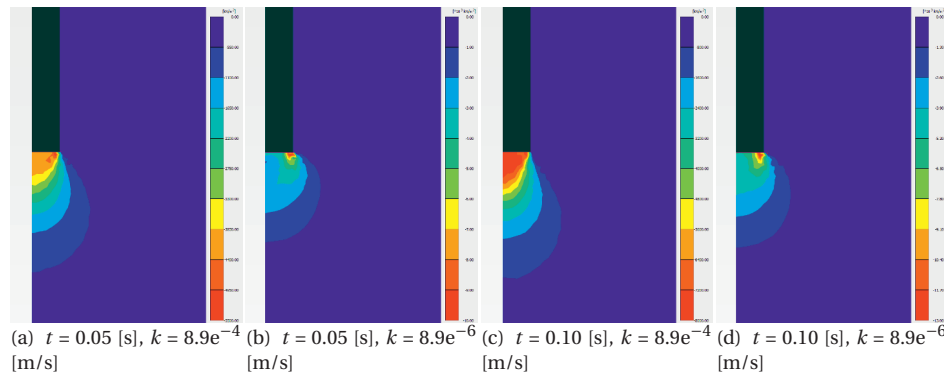
in Figure 7.23.

The permeability has no influence on the general trend of the excess pore pressure response in all locations in the simulations. Regardless of the permeability, the trend of the excess pore pressure response in all figures in Figure 7.23 features by three phases as described previously as (1) an increase to the peak positive value due to compression, (2) a decrease to the peak negative value due to shear and (3) dissipation due to consolidation.

On the other hand, the permeability has a certain effect on the magnitude of the maximum positive/negative excess pore pressure as well as the time of the peak values. This influence is more significant closer to the pile. At the pile tip, as the permeability reduces, the magnitude of the maximum positive and/or negative excess pore pressure increases drastically, the time of the peak values also lags slightly, and both the duration of the shearing phase and the dissipation time are lengthened. Further away from the pile, the difference of the excess pore pressure response between the simulation with the permeability of 8.9×10^{-4} and the simulation with the permeability of 8.9×10^{-5} is still significant, especially for the maximum positive/negative excess pore pressure values. However, the difference of the excess pore pressure response between the simulation with the permeability of 8.9×10^{-5} and the simulation with the permeability of 8.9×10^{-6} is mainly for the duration of the shearing phase and the dissipation time.

The significant influence of the permeability on the response of the excess pore pressure is expected since the permeability directly governs the drainage condition of the pore water. As the drainage condition, i.e. the permeability, reduces, the dissipation of the pore water will reduce during soil deformation but not the generation of the pore pressure. Consequently, the excess pore pressure inside the pores will build up higher during compression as it dissipates slower during shearing.

Figure 7.24: Influence of permeability on stress distribution



7.5.2. INFLUENCE OF THE DRAINAGE CONDITION ON THE RATIO OF RAPID OVER STATIC PILE FORCES

It is clear from the previous sections that the negative excess pore pressure contributes to the increase of the rapid pile force over the static pile force (section 7.4.3) and the

permeability or, more generally, the drainage condition significantly affects the building up and dissipation of the excess pore pressure (section 7.5.1). Therefore, by varying the permeability of the soil, different drainage conditions can be achieved and hence the influence of the excess pore pressure on the increase of the rapid pile force over the static pile force can be investigated.

Figure 7.25¹ presents the relationship between the drainage factor η and the ratio of the maximum/unloading rapid tip force over the static tip force at the same displacement (R_{max} and R_{up}) in the pre-embedded simulation and in the jacked simulation. It can be seen from Figure 7.25(a) that there is no clear difference between the value of R_{max} between the pre-embedded simulation and those with the jacked pile when the drainage condition is partially drained ($\eta \geq 80$). However, when the drainage condition changes closer to undrained, values of R_{max} of the pre-embedded simulation are higher than R_{max} of the jacked simulation. This observation from the simulation results agrees well with the observation from the experiment results in Chapter 5 - Section 5.5, Figures 5.18 to 5.21. The higher influence of the excess pore pressure on R_{max} in the pre-embedded simulation than in the jacked simulation is understandable since the difference in the excess pore pressure at and around the pile tip in the pre-embedded simulation and the jacked simulation is much smaller than the difference in the stress state. Figure 7.25(b) suggests that there is no difference on the influence of the drainage condition to the values of R_{up} in the pre-embedded simulation and the jacked simulation.

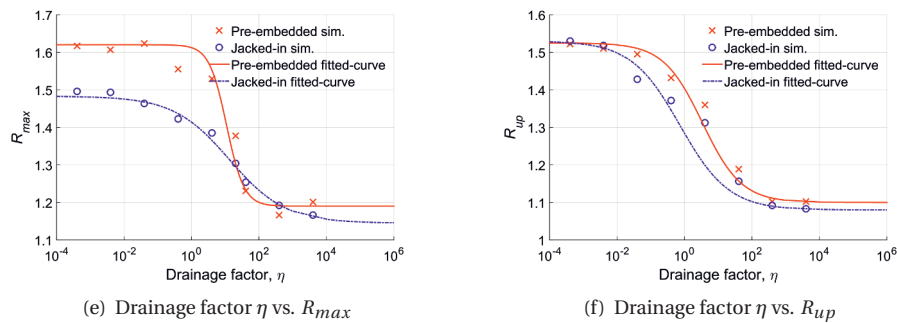


Figure 7.25: Relationship of drainage factor and normalised forces from simulations

Figure 7.26 presents the relationship between the drainage factor η and R_{max} and R_{up} for all experiments and simulations in this study; the backbone curves of the experimental results are also included for more convenient comparison between the experimental results and the simulated one. Figure 7.26 shows the similar trend for both the simulation and the experiment which is as expected since the underlying mechanisms of generating and dissipating of the excess pore pressure in the experiment, and therefore, the influences of the excess pore pressure in the rapid pile load test are well reproduced in the simulation thanks to the Hardening-Soil constitutive model.

¹In Figure 7.25, the points are simulated results, and the curves are trend-lines fitting of the points.

It is shown in Figure 7.26 that at the same drainage condition, the ratio R in the simulation is higher than R in the experiment, which might be due to the difference of the dilative behaviour. In the simulations, in order to have a load capacity at the displacement of $10\% D$ comparable to that in the experiment, the soil right under the pile tip is modelled denser by increasing a strength parameter which is the dilation angle (an increase of 1°). Consequently, the influence of the excess pore pressure is slightly exaggerated in the simulation.

In Figure 7.26(b), it can be seen that at the unloading point in the fully drained condition, the simulations still show some influence of the excess pore pressure ($R_{up} = 1.1$) whereas the experiments suggests no excess pore pressure effect ($R_{up} = 1.0$). In fact, it is expected that when the velocity of the pile is zero, and the permeability of the soil is very high, the load rate effect should vanish, and therefore, the unloading tip resistance should equal the static tip resistance. This is observed in the experiment but not in the simulation.

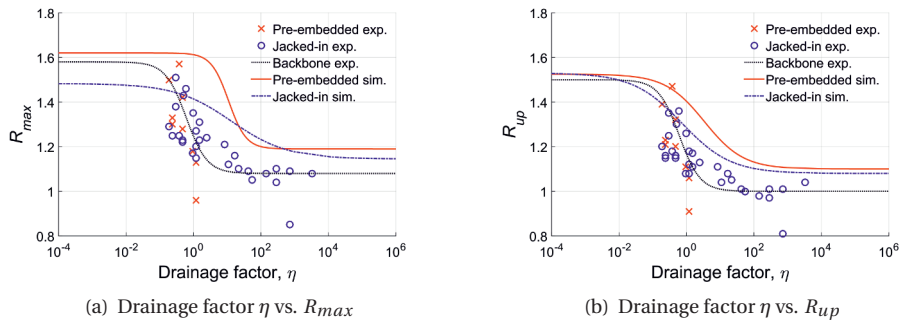


Figure 7.26: Relationship of drainage factor and normalised forces

7.6. CONCLUSIONS

Focusing on the pile capacity at a certain displacement and the overall behaviour of the excess pore pressure, the static and rapid pile load test in saturated sand can be reasonably modelled in the numerical FEM software Plaxis which is capable of modelling the coupled dynamic-consolidation phenomenon with robust techniques.

Four simulation schemes are examined in an attempt to simply incorporate the effects of prior loading activities such as sample preparation, centrifuge spinning up, pile installation in order to achieve comparable pile tip and shaft capacities in both the static and rapid simulations to the tip and shaft capacities of the corresponding experiments. It is shown that scheme 3 (using interface elements, adaption of soil parameters) and scheme 4 (using interface elements, adaption of soil parameters and pre-stressing in the soil zone under the pile tip) are suitable for the simulation of the pile load test with the pre-embedded pile and for the pile load test with the jacked pile, respectively. On the other hand, the simulations underestimate the initial stiffness of the load-displacement results and do not show a clear failure of the pile. The stiffness of the load-displacement response, on the other hand, cannot be captured with conventional techniques used in scheme 3 and 4 and the Hardening-soil constitutive model.

By using the Hardening-soil model and the Plaxis-PTU scheme, the contractive and/or dilative behaviour of the soil during the rapid pile load test and the corresponding excess pore pressure response can be realistically simulated. During a rapid pile load test, multiple zones along the pile shaft and under the pile tip are confirmed to undergo different compression and shearing. Consequently, positive and negative excess pore pressures develop in those zones and influence the rapid pile capacity. In particular, the dominant presence of the negative excess pore pressure during the downward movement of the pile increases the effective stress of the soil and hence the strength of the soil and the pile capacity increases.

The evolution of the excess pore pressure in the simulation has a similar trend to that of the experiment. There are, however, some minor discrepancies on the values of the maximum positive and/or negative excess pore pressure, the duration of the shearing phase and the duration of the dissipation phase. In some specific zones, i.e. at the distance of PPT-4, there are also some differences in the general trend of the excess pore pressure response. The permeability has a significant influence on the response of the excess pore pressure during the rapid pile load test since it governs the drainage condition of the pore water. Closer to the pile, the influence is more significant.

The simulations and the experiments have the same general trend of the influence of the drainage condition on the ratio of the rapid pile capacity over the static pile capacity. However, the ratio of the rapid pile capacity over the static pile capacity of the simulation is higher than that of the experiment at the same drainage conditions. The reason is the higher dilatancy angle is used in the simulation than the dilatancy angle in the experiment in order to partially incorporate the prior loading effect and have a comparable stress state at the pile tip in the simulation to the stress level in the experiment; consequently, the influence of the excess pore pressure is exaggerated in the simulation. A more sophisticated technique or numerical method to fully take into account the prior loading and installation effect may solve this problem.

8

CONCLUSIONS

8.1. CONCLUSIONS

This thesis presents experimental and numerical modelling of pile load tests in saturated granular soils in order to assess the rate effect and the excess pore pressure effect on the interpretation of a rapid pile load test. Based on this research, the following conclusions are drawn.

8.1.1. RESPONSES OF EXCESS PORE FLUID PRESSURE

The evolution of excess pore pressure is firmly related to the soil behaviour during the rapid load test. The results of the measurement of excess pore pressure in Section 4.5 confirm and clarify the responses generally observed in the literature. Briefly speaking, three most common responses can be distinguished: (1) a gradual increase to a maximum positive value and a gentle dissipation to a stationary value; (2) a rapid increase to a maximum positive value, a rapid decrease to a maximum negative value and a gradual dissipation; and (3) a rapid decrease to a maximum negative value, a rapid increase to a maximum positive value and a gradual dissipation. The first behaviour is representative for the soil right under the pile tip center (inside the "nose cone") regardless of the loading duration or the imposed displacement magnitude or for the soil under the pile tip, in general, when the rapid load test has a slow-rate loading (larger than 50 ms) and a small (not larger than 2.5% D) imposed displacement. The other two responses are common for the soil under the pile tip which experiences both compression and shearing during the rapid loading tests with an average- to fast-rate loading (no larger than 20 ms) and a medium to large (from 5% D) prescribed displacement. It is likely that the second behaviour occurs in the soil zone where the contractive behaviour dominates, whereas the third behaviour happens in the soil zone where the dilative behaviour prevails.

In the experimental modelling, axisymmetric installation of PPTs around the penetrated pile reveals the asymmetry of the responses of excess pore pressure. The excess pore pressure response exhibits an initial elastic symmetric behaviour followed by asymmetric behaviour. The asymmetry of the excess pore pressure responses can be caused by physical reasons, e.g. (1) the asymmetry of failure or, more precisely, of the failure surfaces induced by pile penetration; and (2) the heterogeneity of the soil bed. But it can

also have an experimental reason, e.g. when it is caused by the difference of distances of each PPT from the pile centre line and/or the misalignment of the pile during loading. This may cause considerable deviations of the magnitude of the maximum value due to the high gradient (with distance) of the excess pore pressure during rapid loading.

The response of the excess pore pressure in the soil surrounding the pile during rapid pile loading is also researched with numerical modelling. From the numerical simulations, it appears that along the pile shaft, the soil is sheared and expands resulting in negative excess pore pressure. Under the pile tip, a nose cone of compacted soil occurs. Along the boundary of this nose cone, the soil is sheared leading to high negative excess pore pressure.

It is confirmed that the permeability has no influence on the general trend of the excess pore pressure response, but it has a significant effect on the magnitude of the maximum positive/negative excess pore pressure as well as the time that the peak values are reached.

8.1.2. RATE EFFECT

During the rapid pile load test, important effects related to the loading velocity of the pile occur namely: (1) damping effect, (2) constitutive-rate effect, and (3) excess pore pressure effect. The first part of this section focus on the first two effects. These effects are derived from fully drained tests (in sand/water) in which the excess pore pressure effect does not play a role. The excess pore pressure effect is presented in more detail in the second part of this section. It should be noted that the rate effect is evaluated from the experimental modelling. The constitutive rate effect is not incorporated in the numerical modelling.

CONSTITUTIVE RATE EFFECT AND INFLUENCE OF DAMPING

Analysis of the fully drained experimental results (in sand/water tests) shows that the damping effect is insignificant. In the unloading point (to assess the equivalent static capacity), the influence of the constitutive rate effect on tip resistance is negligible. An increase of 10% for the maximum pile tip resistance in the rapid test over the static value is solely due to the constitutive-rate effect. These conclusions are in agreement with the results of Nguyen [206].

In the partially drained tests (in sand/viscous fluid or silt/water), the ratio of the maximum rapid pile tip resistance over the static pile tip resistance increases with an increase of the loading velocity, which suggests that the damping effect coexists with the constitutive rate effect. The constitutive rate effect together with the damping effect increase with the loading velocity and have a maximum value of about 10%.

EXCESS PORE PRESSURE EFFECT

The main mechanism of the excess pore pressure effect is the presence of negative pore pressure due to the shear-induced dilatancy of the soil which increases the effective stress in the soil, hence, the soil strength and, therefore, the pile resistance. The excess pore pressure effect depends on the drainage factor which can be determined from the soil properties, the pile radius and the loading duration or the loading velocity of the test.

In the experimental modelling, increases of up to 47% for the unloading point tip resistance and up to 57% for the maximum tip resistance in the rapid test over the static

value are indicated. The relationship between the drainage factor η and the normalised tip resistance R (the ratio between the rapid resistance over the static resistance), initiated by Nguyen [206], are extended experimentally for partially drained conditions using a silt water mixture. These measurements confirm the curve initiated by Nguyen [206]. This curve can be formulated by a trend-line following an equation of the form $R = \hat{a} + \frac{\hat{b}}{1 + \hat{c} \times \eta^{\hat{d}}}$ with \hat{a} , \hat{b} , \hat{c} and \hat{d} are constants.

A relationship between the drainage factor and the normalised tip resistance from the numerical modelling is found to have the same trend with that relationship from the experimental modelling. An increase of up to 52% for the unloading point tip resistance and up to 62% for the maximum tip resistance at the displacement of 10% D is found. The excess pore pressure effect is slightly exaggerated in the numerical modelling, probably because of the high and constant value of the dilatancy angle which is used to model the installation effect.

8.1.3. OTHER EFFECTS

Variations of soil/fluid type, soil relative density, installation method and pile type allow assessment of the influence of those variations on the normalised tip resistance. In general, the normalised tip resistances of both the maximum and unloading resistance are higher than one, i.e. the rapid pile load test gives a higher resistance than the static pile load test.

EFFECTS OF THE TYPE AND PERMEABILITY OF THE SOIL

The influence of soil permeability can be described by the drainage factor. This factor must be considered in the interpretation of the rapid pile load test results. The normalised tip resistance increases with a decrease of the soil permeability. The soil permeability has a strong influence on the normalised tip resistance.

EFFECTS OF THE RELATIVE DENSITY OF THE SOIL

The normalised tip resistance increase with initial relative density due to a decrease of the soil shear strength and hence the drainage factor. However, the soil relative density has a limited influence on the normalised tip resistance.

EFFECTS OF THE INSTALLATION METHOD

The normalised tip resistance of the pre-embedded pile tests is significantly higher than that of the jacked pile tests due to the higher shear modulus of the soil and therefore the higher drainage factor of the jacked pile tests than that of the pre-embedded pile tests. The installation method has a strong influence on the normalised tip resistance.

In the numerical modelling, not the installation process itself but the influence of the installation process on the stress around the pile is simulated. Consequently, only the bearing capacity of the pile at the displacement of 10% D and the tip-dominance pile is simulated. The pre-embedded pile can be modelled by adapting the soil parameters in an R-width slice along the pile shaft (looser) and a $3D \times 3D$ -block under the pile tip (denser). The jacked pile can be simulated by prescribing a displacement of 12.5% D along the line up to $3D$ under the pile tip. The simulations also suggest the strong influence of the installation method is similar to what is observed in the experiments.

EFFECTS OF THE TYPE OF THE PILE

The pile properties have a limited influence on the normalised head resistance. Regarding the pile type, the normalised head resistance of the close-ended pile is higher than that of the open-ended pile. Regarding the pile diameter, the normalised head resistance of the small pile is higher than that of the large pile.

PLAXIS-PTU MODEL

Plaxis-PTU model is capable of modelling the coupled dynamic-consolidation phenomenon by solving the Biot two-phase equations with robust techniques. The static and rapid pile load tests in granular soil are modelled reasonably well with Plaxis-PTU. The calculated trend of the excess pore pressure response is in reasonable agreement with the experimental trend. At some locations, there is a difference in the excess pore pressure response which may be due to the difference in the stress and strain fields.

The relationships between the drainage factor and the normalised tip resistance of the simulation and the experiment have the same tendency. However, the simulated normalised tip resistance is slightly higher than the experimental one due to the higher influence of the excess pore pressure. The probable reason is that a higher dilatancy angle is used in the simulation than the dilatancy angle in the experiment in order to partially incorporate the installation effect.

8.1.4. THE UNLOADING POINT METHOD

The original unloading point method assumes that at the unloading point, the rapid force minus the inertia force equals the equivalent static soil force at that point. This assumption makes the unloading point method directly applicable to the drained test without any influence from the excess pore pressure. A value of the drainage factor equal to 55 is recommended (from the experimental modelling) to distinguish between the drained (higher than 55) and partially drained pile load tests. In the partially drained tests, the excess pore pressure effect should be taken into account following the drainage factor of the tests. The backbone curve in Figure 5.2, which is experimentally derived, gives an indication of the correction factor of the static pile tip resistance from the rapid pile tip resistance.

8.2. RECOMMENDATIONS

As the generation/dissipation of the excess pore pressure is closely related to the creation of the failure surfaces, it is recommended to investigate this phenomenon more intensively. There are two possible numerical approaches to study the symmetry of the failure surfaces. The first approach is using the Discrete Element Method in three-dimensional configuration in which the particle size follows a realistic grain size distribution; this approach can well reproduce the particle nature of the granular soil. The second method is using the Finite Element Method in a three-dimensional configuration incorporating the variation of $\pm 0.5\%$ relative density, i.e. with random fields.

In this thesis, not the installation process but the installation effect is included; therefore the numerical simulation only has a comparable total pile capacity and a similar distribution of the tip resistance and the shaft friction to those in the experimental modelling. It is, however, possible to simulate the influence of the installation process by

modelling the installation process itself and then mapping the stress and strain fields as well as the state parameters into a simulation in Plaxis, an example of such mapping was done by Engin [72]. A full simulation of the installation process or a comprehensive mapping procedure as mentioned above is recommended to improve the simulation of this thesis, especially the stiffness of the load-displacement behaviour and the stress and strain states of the soil around the pile.

An advanced soil model in which soil behaviour, especially the dilative behaviour, is dependent on the stress/strain state is highly recommended. By incorporating such property, the dilatancy behaviour can better be modelled which may improve the prediction of the excess pore pressure effect which is slightly exaggerated in the simulation of this thesis.

A

LOADING SCHEMES

This section presents the loading schemes in three pile loading test programs in 2007 [206], 2009 [169] and 2011 [205].

Table A.1: Loading scheme for the experiment in 2007

Loading program		
Steps	Phases	Remarks
1	Installation • Jacked-in pile • Pre-embedded pile	Final embedded depth of $20 D$ Place at $10 D$, push in more $10 D$ Place at $20 D$
2	Rapid loading 1 • $1\%D$ • $2\%D$ • $5\%D$ • $10\%D$	Slow-rate (loading duration for each disp. level is 0.048 sec) Disp. ↓ $1\%D = 0.113$ mm with $v = 2.35$ [mm/s] Disp. ↑ $0.5\%D = 0.0565$ mm with $v = 2.35$ [mm/s] Unloading of the pile to approx. 0 kN Disp. ↓ $2\%D = 0.226$ mm with $v = 4.70$ [mm/s] Disp. ↑ $1\%D = 0.113$ mm with $v = 4.70$ [mm/s] Unloading of the pile to approx. 0 kN Disp. ↓ $5\%D = 0.565$ mm with $v = 11.77$ [mm/s] Disp. ↑ $1\%D = 0.113$ mm with $v = 11.77$ [mm/s] Unloading of the pile to approx. 0 kN Disp. ↓ $10\%D = 1.13$ mm with $v = 23.5$ [mm/s] Disp. ↑ $1\%D = 0.113$ mm with $v = 23.5$ [mm/s] Unloading of the pile to approx. 0 kN
3	Static loading 1	Disp. $10\%D = 1.13$ mm in 676.6 sec ($v = 0.00167$ [mm/s]) Unloading of the pile to approx. 0 kN
4	Rapid loading 2 • $1\%D$ • $2\%D$ • $5\%D$ • $10\%D$	Average-rate (loading duration for each disp. level is 0.0185 sec) Disp. ↓ $1\%D = 0.113$ mm with $v = 6.10$ [mm/s] Disp. ↑ $0.5\%D = 0.0565$ mm with $v = 6.10$ [mm/s] Unloading of the pile to approx. 0 kN Disp. ↓ $2\%D = 0.226$ mm with $v = 12.2$ [mm/s] Disp. ↑ $1\%D = 0.113$ mm with $v = 12.2$ [mm/s] Unloading of the pile to approx. 0 kN Disp. ↓ $5\%D = 0.565$ mm with $v = 30.5$ [mm/s] Disp. ↑ $1\%D = 0.113$ mm with $v = 30.5$ [mm/s] Unloading of the pile to approx. 0 kN Disp. ↓ $10\%D = 1.13$ mm with $v = 61.1$ [mm/s] Disp. ↑ $1\%D = 0.113$ mm with $v = 61.1$ [mm/s] Unloading of the pile to approx. 0 kN
5	Static loading 2	Disp. $10\%D = 1.13$ mm in 676.6 sec ($v = 0.00167$ [mm/s])

continued on the next page

Loading program (... continued)		
Steps	Phases	Remarks
Unloading of the pile to approx. 0 kN		
6	Rapid loading 3 • 1%D • 2%D • 5%D • 10%D	Fast-rate (loading duration for each disp. level is 0.009 sec) Disp. ↓ 1%D = 0.113 mm with $v = 12.55$ [mm/s] Disp. ↑ 0.5%D = 0.0565 mm with $v = 12.55$ [mm/s] Unloading of the pile to approx. 0 kN Disp. ↓ 2%D = 0.226 mm with $v = 12.2$ [mm/s] Disp. ↑ 1%D = 0.113 mm with $v = 12.2$ [mm/s] Unloading of the pile to approx. 0 kN Disp. ↓ 5%D = 0.565 mm with $v = 30.5$ [mm/s] Disp. ↑ 1%D = 0.113 mm with $v = 30.5$ [mm/s] Unloading of the pile to approx. 0 kN Disp. ↓ 10%D = 1.13 mm with $v = 125.6$ [mm/s] Disp. ↑ 1%D = 0.113 mm with $v = 125.6$ [mm/s] Unloading of the pile to approx. 0 kN
7	Static loading 3	Disp. 10%D = 1.13 mm in 676.6 sec ($v = 0.00167$ [mm/s]) Unloading of the pile to approx. 0 kN

The end

Table A.2: Loading scheme for the experiment in 2009

Loading program		
Steps	Phases	Remarks
1	Installation • Jacked-in pile • Pre-embedded pile	Final embedded depth of 20 D Place at 10 D , push in more 10 D Place at 20 D
2	Rapid loading 1 • 1%D • 10%D	Fast-rate (loading duration for each disp. level is 0.009 sec) Disp. ↓ 1%D = 0.113 mm with $v = 12.55$ [mm/s] Disp. ↑ 0.5%D = 0.0565 mm with $v = 12.55$ [mm/s] Unloading of the pile to approx. 0 kN Disp. ↓ 10%D = 1.13 mm with $v = 125.6$ [mm/s] Disp. ↑ 1%D = 0.113 mm with $v = 125.6$ [mm/s] Unloading of the pile to approx. 0 kN
3	Static loading 1	Disp. 10%D = 1.13 mm in 676.6 sec ($v = 0.00167$ [mm/s]) Unloading of the pile to approx. 0 kN
4	Rapid loading 2 • 1%D • 2%D • 5%D • 10%D	Average-rate (loading duration for each disp. level is 0.0185 sec) Disp. ↓ 1%D = 0.113 mm with $v = 6.10$ [mm/s] Disp. ↑ 0.5%D = 0.0565 mm with $v = 6.10$ [mm/s] Unloading of the pile to approx. 0 kN Disp. ↓ 2%D = 0.226 mm with $v = 12.2$ [mm/s] Disp. ↑ 1%D = 0.113 mm with $v = 12.2$ [mm/s] Unloading of the pile to approx. 0 kN Disp. ↓ 5%D = 0.565 mm with $v = 30.5$ [mm/s] Disp. ↑ 1%D = 0.113 mm with $v = 30.5$ [mm/s] Unloading of the pile to approx. 0 kN Disp. ↓ 10%D = 1.13 mm with $v = 61.1$ [mm/s] Disp. ↑ 1%D = 0.113 mm with $v = 61.1$ [mm/s] Unloading of the pile to approx. 0 kN
5	Static loading 2	Disp. 10%D = 1.13 mm in 676.6 sec ($v = 0.00167$ [mm/s]) Unloading of the pile to approx. 0 kN
6	Rapid loading 3 • 1%D • 2%D	Slow-rate (loading duration for each disp. level is 0.048 sec) Disp. ↓ 1%D = 0.113 mm with $v = 2.35$ [mm/s] Disp. ↑ 0.5%D = 0.0565 mm with $v = 2.35$ [mm/s] Unloading of the pile to approx. 0 kN Disp. ↓ 2%D = 0.226 mm with $v = 4.70$ [mm/s]

continued on the next page

Loading program (... continued)		
Steps	Phases	Remarks
	<ul style="list-style-type: none"> • 5%D • 10%D 	Disp. ↓ 1%D = 0.113 mm with $v = 4.70$ [mm/s] Unloading of the pile to approx. 0 kN Disp. ↓ 5%D = 0.565 mm with $v = 11.77$ [mm/s] Disp. ↓ 1%D = 0.113 mm with $v = 11.77$ [mm/s] Unloading of the pile to approx. 0 kN Disp. ↓ 10%D = 1.13 mm with $v = 23.5$ [mm/s] Disp. ↓ 1%D = 0.113 mm with $v = 23.5$ [mm/s] Unloading of the pile to approx. 0 kN
7	Static loading 3	Disp. 10%D = 1.13 mm in 676.6 sec ($v = 0.00167$ [mm/s]) Unloading of the pile to approx. 0 kN

The end

Table A.3: Loading scheme for the experiment in 2011

Loading program		
Steps	Phases	Remarks
1	Installation <ul style="list-style-type: none"> • Jacked-in pile • Pre-embedded pile 	Final embedded depth of 20 D Place at 10 D , push in more 10 D Place at 20 D
2	Rapid loading 1 <ul style="list-style-type: none"> • 1%D • 2.5%D • 5%D • 10%D • 25%D 	Slow-rate (loading duration for each disp. level is 0.048 sec) Disp. ↓ 1%D = 0.16 mm with $v = 3.33$ [mm/s] Disp. ↓ 0.5%D = 0.08 mm with $v = 3.33$ [mm/s] Unloading of the pile to approx. 0 kN Disp. ↓ 2%D = 0.40 mm with $v = 8.44$ [mm/s] Disp. ↓ 1%D = 0.16 mm with $v = 8.44$ [mm/s] Unloading of the pile to approx. 0 kN Disp. ↓ 5%D = 0.80 mm with $v = 16.66$ [mm/s] Disp. ↓ 1%D = 0.16 mm with $v = 16.66$ [mm/s] Unloading of the pile to approx. 0 kN Disp. ↓ 10%D = 1.6 mm with $v = 33.33$ [mm/s] Disp. ↓ 1%D = 0.16 mm with $v = 33.33$ [mm/s] Unloading of the pile to approx. 0 kN Disp. ↓ 25%D = 4.0 mm with $v = 83.33$ [mm/s] Disp. ↓ 1%D = 0.16 mm with $v = 83.33$ [mm/s] Unloading of the pile to approx. 0 kN
3	Static loading 1	Disp. 10%D = 1.6 mm in 676.6 sec ($v = 0.00236$ [mm/s]) Unloading of the pile to approx. 0 kN
4	Rapid loading 2 <ul style="list-style-type: none"> • 1%D • 2%D • 5%D • 10%D 	Average-rate (loading duration for each disp. level is 0.0185 sec) Disp. ↓ 1%D = 0.16 mm with $v = 8.65$ [mm/s] Disp. ↓ 0.5%D = 0.08 mm with $v = 8.65$ [mm/s] Unloading of the pile to approx. 0 kN Disp. ↓ 2%D = 0.32 mm with $v = 17.29$ [mm/s] Disp. ↓ 1%D = 0.16 mm with $v = 17.29$ [mm/s] Unloading of the pile to approx. 0 kN Disp. ↓ 5%D = 0.80 mm with $v = 43.24$ [mm/s] Disp. ↓ 1%D = 0.16 mm with $v = 43.24$ [mm/s] Unloading of the pile to approx. 0 kN Disp. ↓ 10%D = 1.6 mm with $v = 86.49$ [mm/s] Disp. ↓ 1%D = 0.16 mm with $v = 86.49$ [mm/s] Unloading of the pile to approx. 0 kN
5	Static loading 2	Disp. 10%D = 1.6 mm in 676.6 sec ($v = 0.00236$ [mm/s]) Unloading of the pile to approx. 0 kN
6	Rapid loading 3 <ul style="list-style-type: none"> • 1%D 	Fast-rate (loading duration for each disp. level is 0.009 sec) Disp. ↓ 1%D = 0.16 mm with $v = 17.77$ [mm/s]

continued on the next page

Loading program (... continued)		
Steps	Phases	Remarks
		Disp. \uparrow 0.5%D = 0.08 mm with $v = 17.77$ [mm/s] Unloading of the pile to approx. 0 kN
	• 2%D	Disp. \downarrow 2%D = 0.32 mm with $v = 35.55$ [mm/s] Disp. \uparrow 1%D = 0.16 mm with $v = 35.55$ [mm/s] Unloading of the pile to approx. 0 kN
	• 5%D	Disp. \downarrow 5%D = 0.80 mm with $v = 88.89$ [mm/s] Disp. \uparrow 1%D = 0.16 mm with $v = 88.89$ [mm/s] Unloading of the pile to approx. 0 kN
	• 10%D	Disp. \downarrow 10%D = 1.6 mm with $v = 177.77$ [mm/s] Disp. \uparrow 1%D = 0.16 mm with $v = 177.77$ [mm/s] Unloading of the pile to approx. 0 kN
7	Static loading 3	Disp. 10%D = 1.6 mm in 676.6 sec ($v = 0.00236$ mm/s) Unloading of the pile to approx. 0 kN

The end

B

PRELIMINARY SIMULATIONS

B.1. INFLUENCE OF INTERFACE

A series of calculation is performed to examine the performance of two possibilities of modelling the interface behaviour. The first possibility is using the virtual-thickness interface elements with different strength reduction factors (R_{inter}) which allows the nodes belong to the pile and those belong to the soil move independently. The second option is using an elastic layer with a thickness of 0.04 m (6.25% D) along the pile shaft with different stiffness to represent the strength reduction.

All calculations in this part consists of six phases 1, 2, 3, 5, 6 and 7 or 8 (without taking into account the influence of pre-loading processes). The prescribed vertical displacement of 1 D is applied at the interface between the pile cluster and the soil cluster to increase the tip capacity.

The results of this section indicates that using the virtual thickness interface is much more efficient than using the elastic thin layer in term of reducing the shaft friction, redistributing the stress along the shaft and avoiding numerical difficulty due to the ill-conditioning.

B.1.1. ON STATIC SIMULATIONS

The pile loads as a function of the pile head displacement are plotted for different simulations in Figure B.1. It should be noted that all simulations have the prescribed vertical displacement of 0.64 m at the pile tip-soil interface to increase the tip capacity and the interface or the thin layer of elastic material is activated after the prescribing vertical displacement phase and before the loading phase to avoid numerical difficulties.

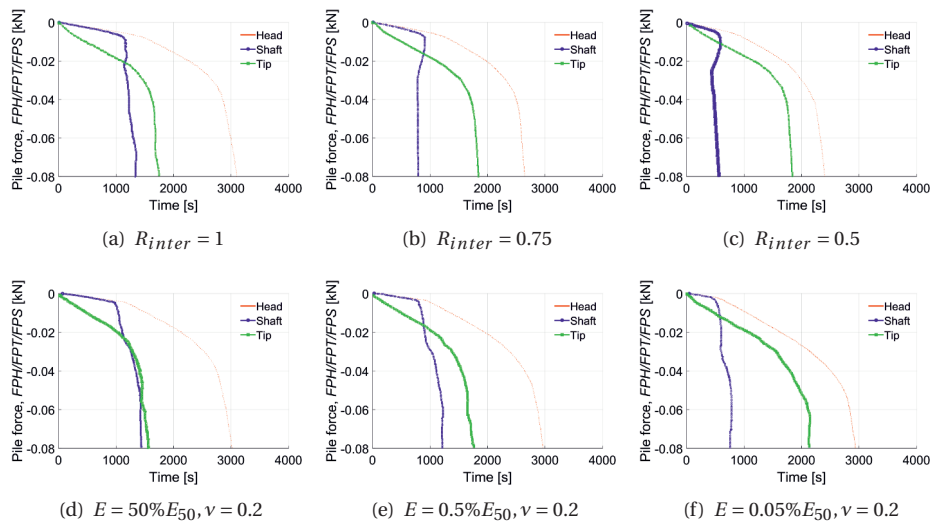


Figure B.1: Influence of interface types on static simulation

From Figure B.1, it is clear that using the interface elements in PLAXIS greatly reduces the shaft friction and keeps the tip resistance remained (or with only small reduction) and using the elastic thin layer along the pile shaft reduces the shaft friction and increases the tip resistance. Using the interface element, the shaft friction is fully mobilized at less than 0.5% D displacement and reduces to a stationary value. Using the thin layer of elastic material, the shaft friction is mostly mobilized at less than 0.5% D displacements and gradually increases to a fully mobilized value at between 5 and 10% D displacements. Further investigation on the usage of the interface elements reveals that using the reduction factor of $R_{inter} = 0.5$ the contribution of the tip capacity is 75-80% of the total capacity and the total capacity reduces about 20% without using the interface elements. On the usage of the elastic thin layer, with the stiffness as low as $E = 0.05\%E_{50}$, the contribution of the tip capacity rises to 70% of the total capacity and the total capacity reduces only 10% without using the elastic thin layer.

One of the big drawback when using the elastic thin layer with the stiffness as small as $E = 0.05\%E_{50}$ is a numerical problem of ill-conditioning due to the high magnitude difference of the stiffness between the pile, the soil and the elastic material. Therefore this method is not of interest anymore.

B.1.2. ON DYNAMIC SIMULATIONS

Several calculations are performed to investigate the influence of the interface elements on the dynamic simulation. The pile load-displacement curves from those calculations are plotted in Figure B.2.

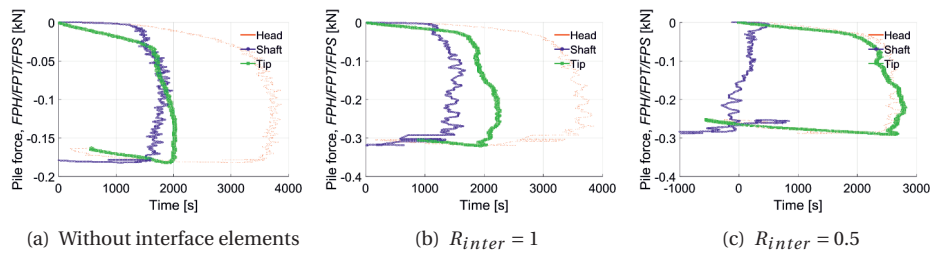


Figure B.2: Influence of interface types on dynamic simulation

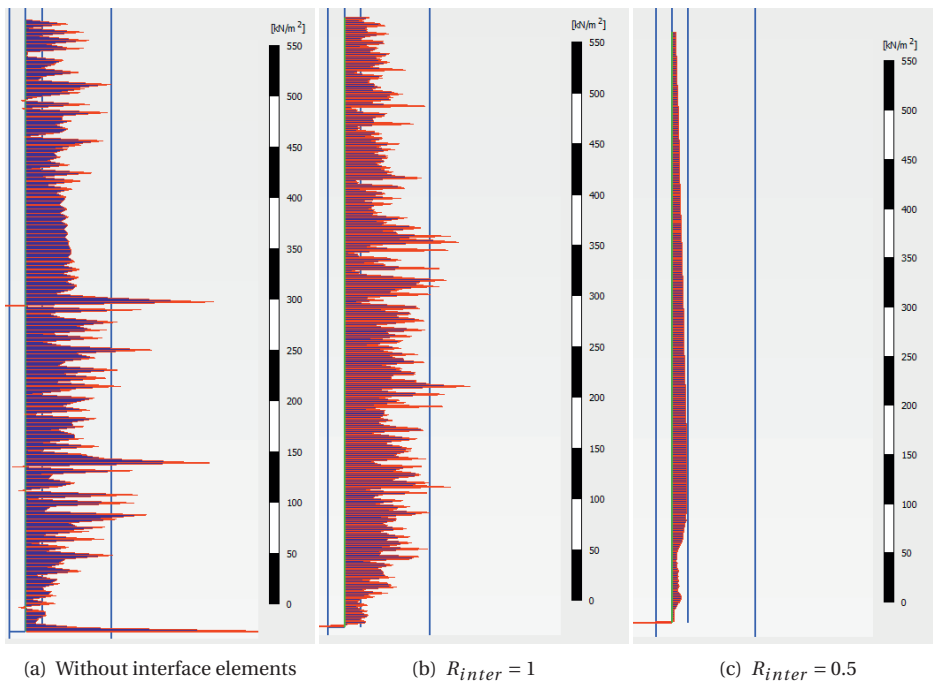


Figure B.3: Shear stress along the pile shaft

The influence of the interface elements on the contribution of the tip resistance and the shaft friction to the total capacity in the dynamic simulation is similar to that in the static simulation: without the interface the tip resistance is equal or smaller than the shaft friction, with the rigid interface the tip resistance is about 10-20% higher than the shaft friction and with the interface elements of $R_{inter} = 0.5$ the tip resistance contributes 80-90% for the total capacity. Similar to the static simulation, using of the interface elements of 50% strength reduction reduces the total capacity.

The shear stresses along the interface of three simulations are plotted in Figure B.3. It can be clearly seen that the interface elements greatly reduces as well as redistributes

the shear stress along the shaft.

B.2. INFLUENCE OF PRE-STRESSING

In this section, following the work of Broere and vanTol [39], three possibilities of pre-stressing to increase the pile capacity are examined, including: prescribing volumetric expansion, prescribing horizontal displacements and prescribing vertical displacements. Several series of calculation are performed. In the first series different amounts of volumetric strain is prescribed, in the second series different magnitudes of vertical displacement is applied and in the third series different magnitudes of horizontal displacement is applied whilst a vertical displacement is also prescribed.

The results of this section indicate that the techniques of prescribing volumetric expansion and prescribing horizontal displacement have a much stronger influence on the shaft friction than on the tip resistance which means the shaft friction increases rapidly whilst the tip resistance increases slowly or even decreases. The technique of prescribing vertical displacement improves the tip resistance significantly and has a little effect on the shaft friction. However this technique is also limited on the magnitude of the applied vertical displacement to avoid severe distortion under the pile tip.

B.2.1. PRESCRIBING VOLUMETRIC EXPANSION

This method is used by prescribing a volumetric strain in the area representing the pile. The calculation phases of the calculation following this method are the initial stresses are 1, 2, 3, 5 and 7. In phase 2, the soil cluster at the pile location is expanded with the predefined amount of volumetric strain.

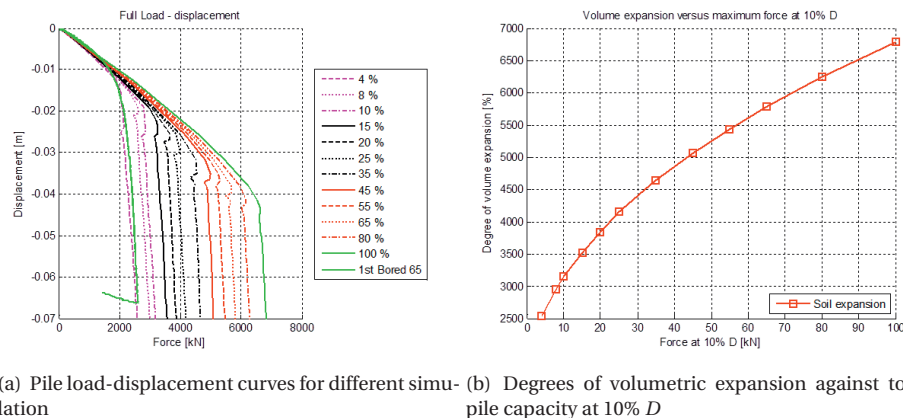


Figure B.4: Influence of the prescribing volumetric expansion technique

A series of calculation was performed to investigate the influence of the degree of prescribing volumetric expansion on the pile capacity. The load-displacement curves of simulation with different degrees of volumetric expansion ranging from 4% to 100% are presented in Figure B.4(a) and the relation curve between different degrees of volumetric

expansion and total pile capacity at 10% D is shown in Figure B.4(b). The distributions of the tip capacity and the shaft friction in all tests are quite similar and only the distributions taken from the simulations of 4% and 65% volumetric expansion are shown in Figure B.5.

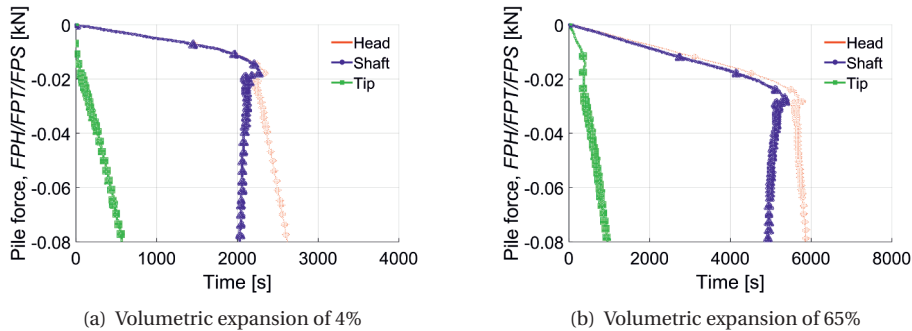


Figure B.5: Distribution of the tip resistance and shaft friction

It is clear from Figure B.4 that with a predefined degree of volumetric expansion applied to the soil cluster at the pile location, the total capacity ranging from 2500 kN up to 6800 kN can be achieved. Figure B.5 indicates that actually the improvement of the total capacity mainly comes from the shaft friction and the higher the degree of volumetric expansion, the larger the contribution percentage of the shaft friction for the total capacity. For example, in the simulation of 4% volumetric expansion the shaft friction is about 80% of the total capacity and in the simulation of 65% volumetric expansion the shaft friction is about 84% of the total capacity at the displacement of 10% D . It is clear that the shaft friction is much more sensitive to the volumetric expansion than the tip resistance and applying the volumetric expansion technique is only suitable for cases of the shaft-dominance pile.

B.2.2. PRESCRIBING VERTICAL DISPLACEMENTS

In this series, only vertical displacement (Δu_y) was applied on the interface between the pile cluster and the soil cluster under the pile tip. The pile load-displacement curves for three simulation with a vertical displacement of 0.5 D , D and 1.5 D are shown in Figure B.6.

It can be seen from Figure B.6 that by applying Δu_y at the pile tip-soil interface, both the shaft friction and the tip capacity improves. However, as the tip capacity continues to increase with the increase of Δu_y (roundly 500 kN per 0.5 D), the shaft friction does not increase anymore when Δu_y is higher than 1 D . However, a big draw back of this method is that the prescribed vertical displacement can not be too large, for example larger than 1.5 D , otherwise the elements under the pile tip area are severely distorted which may lead to divergence during nonlinear calculation.

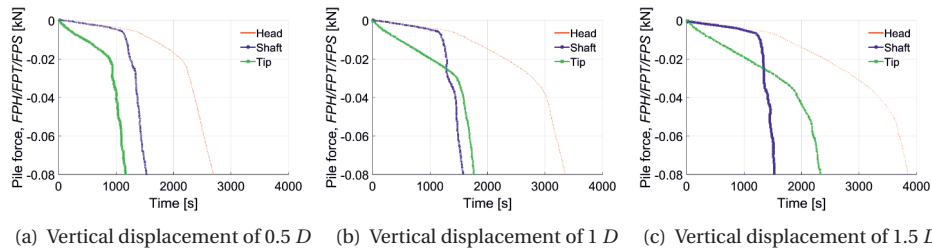


Figure B.6: Pile loads as a function of pile displacement

B.2.3. PRESCRIBING HORIZONTAL DISPLACEMENTS

In this series, several calculations are performed, each calculation has a vertical displacement of $\Delta u_y = D$ applied at the pile tip-soil interface and a certain amount of prescribed horizontal displacement (Δu_x) applied at the pile shaft-soil interface. The pile load-displacement curves for three simulation with a horizontal displacement of 6.25, 12.5 and 25% D are shown in Figure B.7.

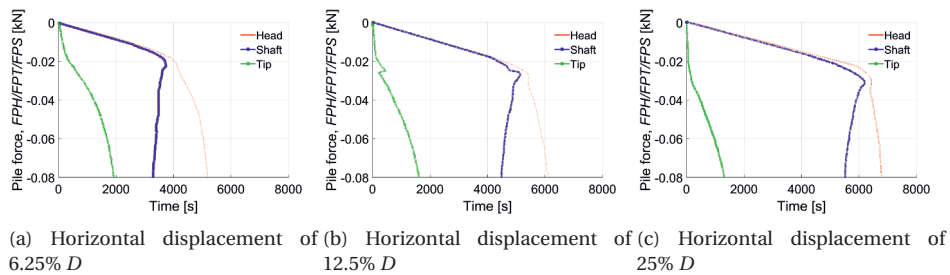


Figure B.7: Pile loads as a function of pile displacement

It can be seen from Figure B.7 that the shaft friction is very sensitive with the horizontal prescribed displacement, increase of more than 1200 kN per 6.25% D , while the influence of Δu_x on the tip capacity is small and in a negative direction. The tip capacity decreases with the increase of Δu_x due to the stress relaxing under the pile tip. The shaft friction hence is far higher than the tip capacity. Besides, the shaft friction is fully mobilized at much higher displacement level (5% D) in comparison with the simulation of prescribed Δu_x (less than 2% D).

C

CALCULATION PHASES IN FOUR SIMULATION SCHEMES

The calculation process in PLAXIS is composed of several construction phases. The full list of all construction phases is defined as follows:

1. Initially the material of the whole calculation domain is soil. The vertical soil stress is calculated from the self-weight with the phreatic level is assumed to be at the ground surface. The horizontal soil stress is generated by K_0 -procedure which is based on the Jaky's formula $K_0 = 1 - \sin \phi$. The hydrostatic pore pressure is generated in the whole geometry according to the phreatic line.
2. (This is an optional phase) The interface between the soil cluster and the soil cluster at the pile location is applied prescribed displacement. After the equilibrium at the end of this phase, the stress state in the soil is tended to take into account the influence of the pre-loading processes.
3. The pile is located by changing the material properties of the soil cluster at the pile location from soil to pile which will change the state of stress around the pile. During this phase, the stress state of the soil cluster is recalculated to reach new equilibrium state.
4. (This is an optional phase) The material properties of the soil cluster inside a slice of R along the shaft is changed from normal soil to looser soil. The material properties of the soil cluster inside a square of $3D \times 3D$ right under the pile tip is changed from normal soil to denser soil.
5. All displacements are set to zero while keeping the stress state as obtained from the previous steps. If the prescribed displacements are used to pre-stressing the soil, a relaxation of the stress around the pile occurs.
6. (This is an optional phase) The interface elements along the pile shaft are activated. By activating the interface elements after all the pre-stressing steps, numerical difficulties are avoided [38, 39].
7. (This phase is used only as the final phase of the static test simulation) A downward prescribed displacement is applied at the pile head.

8. (This phase is used only as the final phase of the dynamic test simulation) A downward force is applied at the pile head.

Each simulation scheme then consists of several construction phases:

- Scheme 1 : construction phases number 1, 3, 5 and 7 or 8.
- Scheme 2 : construction phases number 1, 3, 5, 6 and 7 or 8.
- Scheme 3 : construction phases number 1, 3, 4, 5, 6 and 7 or 8.
- Scheme 4 : construction phases number 1, 2, 3, 4, 5, 6 and 7 or 8.

LIST OF NOTATIONS

The following list briefly describes acronyms and symbols that are used within the body of the thesis. All of the acronyms and symbols in this list are already defined in the text.

Acronyms

- Acce The derived acceleration of the pile head. (Chapter 4)
- C, CEP The close-ended pile. (Chapter 4)
- CFA Continuous Flight Auger pile. (Chapter 2)
- CPT The cone penetration or cone penetrometer test. (Chapter 2)
- Displ The measured displacement of the pile head. (Chapter 4)
- E The pre-embedded installation method. (Chapter 4)
- FPH The pile head applied-force. (Chapter 4)
- FPS The derived pile shaft force. (Chapter 4)
- FPT The measured pile tip reaction-force. (Chapter 4)
- HP The H-section bearing piles. (Chapter 2)
- J The jacked-in installation method. (Chapter 4)
- LVDT The linear variable displacement transducer used for measuring position. (Chapter 2)
- O, OEP The open-ended pile. (Chapter 4)
- PIV The particle image velocimetry method. (Chapter 2)
- PLT The pile load test series. (Chapter 4)
- PPT The pore pressure transducer. (Chapter 3)
- PPT-1 The pore pressure transducer 1 at the depth of $0.5 D$. (Chapter 4)
- PPT-2 The pore pressure transducer 2 at the depth of $0.5 D$. (Chapter 4)
- PPT-3 The pore pressure transducer 3 at the depth of $0.5 D$. (Chapter 4)
- PPT-4 The pore pressure transducer 4 at the depth of $1.5 D$. (Chapter 4)
- PPT-5 The pore pressure transducer 5 at the depth of $1.5 D$. (Chapter 4)

- PPT-6 The pore pressure transducer 6 at the depth of $1.5 D$. (Chapter 4)
- PPT-BC The pore pressure transducer at the bed container. (Chapter 4)
- PPT-PT The pore pressure transducer at the pile tip. (Chapter 4)
- PTU The partition of time unity method for time-integration. (Chapter 6)
- RLT, R The rapid load test. (Chapter 4)
- Sa Sand - the pile load test with sandy soil. (Chapter 4)
- Si Silt - the pile load test with silty soil. (Chapter 4)
- SLT, S The static load test. (Chapter 4)
- SPT The standard penetration test. (Chapter 2)
- Velo The derived velocity of the pile head. (Chapter 4)
- Vi Viscous fluid - the pile load test with viscous fluid. (Chapter 4)
- Wa Water - the pile load test with still water. (Chapter 4)

Greek letters

- α The compressibility parameter, Equation 6.1. (Chapter 6)
- α The damping coefficient determined from the model pile tests, Equation 2.5. (Chapter 2)
- β The damping coefficient determined from the model pile tests, Equation 2.5. (Chapter 2)
- σ_s The partial solid stress vector. (Chapter 6)
- δ The friction angle between the soil and pile wall. (Chapter 5)
- η The drainage factor. (Chapter 1)
- Γ The time-like parameter controlling the numerical dissipation in the PTU scheme. (Chapter 6)
- γ The volumetric weight of the pore fluid. (Chapter 3)
- γ_{sat} The saturated unit weight. (Chapter 7)
- γ_{unsat} The unsaturated unit weight. (Chapter 7)
- ν The Poisson ratio. (Chapter 7)
- ν The kinematic viscosity of the fluid. (Chapter 3)
- ϕ The soil friction angle (Chapter 2). In this thesis ϕ is, generally, the peak friction angle.

ϕ_M	The resistance factor to obtain the static bearing capacity from the rapid bearing capacity. (Chapter 1)
ϕ_{inter}	The friction angle between the soil and the pile surface. (Chapter 7)
ψ	The dilation angle of soil. (Chapter 7)
ρ	The densities of the mixture. (Chapter 6)
ρ	The mass density of the pore fluid. (Chapter 3)
ρ_s	The densities of the solid phase. (Chapter 6)
ρ_w	The densities of the fluid phase. (Chapter 6)
$\rho..$	The mass densities, Equation 6.2. (Chapter 6)
σ'_v	The effective vertical stress. (Chapter 4)
σ_v	The overburden pressure at the point of interest. (Chapter 5)
σ_w	The fluid stress scalar. (Chapter 6)
τ	The soil shear strength. (Chapter 2)
τ_d	The limiting values of the rapid pile shaft friction, Equation 2.5. (Chapter 2)
τ_s	The limiting values of the static pile shaft friction, Equation 2.5. (Chapter 2)
$\tilde{\beta}$	The Biot coefficient for the fluid flow. (Chapter 6)
ζ	The soil compressibility factor, Equation 4.6. (Chapter 4)

Latin letters

D	The diameter of the pile. (Chapter 3)
$\bar{\mathbf{u}}$	The nodal displacement. (Chapter 6)
$\bar{\mathbf{v}}$	The nodal velocity. (Chapter 6)
Δt	The time increment between two consecutive recorded data. Chapter 4.
$\hat{a}, \hat{b}, \hat{c}, \hat{d}$	The constants for the relationship between R and η , Equation 5.1. (Chapter 5)
$\bar{\mathbf{u}}_s$	The nodal displacements of the solid skeleton. (Chapter 6)
$\bar{\mathbf{u}}_w$	The nodal displacements of the pore fluid. (Chapter 6)
\mathbf{D}	The fourth order tensor defining a constitutive law for the solid skeleton. (Chapter 6)
\mathbf{I}	The identity vector, Equation 6.1. (Chapter 6)
\mathbf{N}_p	The shape functions for the fluid. (Chapter 6)

\mathbf{N}_u	The shape functions for the solid. (Chapter 6)
\mathbf{u}_s	The displacement of the solid skeleton. (Chapter 6)
\mathbf{u}_w	The displacement of the fluid phase. (Chapter 6)
$\tilde{\alpha}$	The Biot tortuosity parameter. (Chapter 6)
\tilde{M}	The Biot coefficient of compressibility of the two-phase material. (Chapter 6)
A	The parameter takes into account the strength of the soil and the excess pore pressure at the pile tip, Equation 4.5. (Chapter 4)
a, a_t	The acceleration of the pile. (Chapter 2)
A_f	The side surface area of a pile. (Chapter 5)
a_i	The pile acceleration at the time step i . Chapter 4.
A_p	The gross end area of a pile. (Chapter 5)
b	The viscous coefficient, Equation 6.2. (Chapter 6)
C	The damping coefficient. (Chapter 2)
c	The cohesion of soil. (Chapter 7)
c	The velocity of stress wave propagation in a pile. (Chapter 2)
C_0, C_2	The soil constants, Equation 4.8. (Chapter 4)
D_C	The container diameter. (Chapter 3)
D_i	The inner diameter of a pipe pile. (Chapter 3)
D_r	The relative density of a soil sample. (Chapter 4)
d_{10}	The diameter at which 10% of the sample's mass is comprised of particles with a diameter less than this value. (Chapter 2)
d_{50}	The diameter at which 50% of the sample's mass is comprised of particles with a diameter less than this value. (Chapter 2)
d_{90}	The diameter at which 90% of the sample's mass is comprised of particles with a diameter less than this value. (Chapter 3)
E_c	The soil compressive strength. (Chapter 2)
E_e	The soil elastic modulus. (Chapter 2)
E_{50}	The soil secant modulus corresponding to 50% of the ultimate shear stress. (Chapter 2)
E_{oed}	The oedometer modulus. (Chapter 7)

E_{ref}	The Young modulus. (Chapter 7)
E_{ur}	The unloading/Reloading modulus. (Chapter 7)
f	The unit skin friction capacity of a pile. (Chapter 5)
F_{const}	The pile force related to the constitutive rate effect. Chapter 4.
F_{damp}	The pile force related to the damping effect. Chapter 4.
$F_{inertia}$	The inertial force of the pile mass. (Chapter 2)
F_{max}	The maximum rapid pile force. Chapter 4.
F_{pwp}	The pile force related to the pore pressure effect. Chapter 4.
F_{rap}	The applied rapid load. (Chapter 2)
F_{rap}^{ult}	The ultimate rapid load, Equation 2.6 and 2.7. (Chapter 2)
F_{rate}	The pile force related to the penetration rate effect. Chapter 4.
F_{soil}	The soil resistance of the pile. (Chapter 2)
F_{static}	The static pile force. Chapter 3.
F_{up}	The rapid pile force at the value of the maximum displacement or the so-called unloading point. Chapter 4.
F_u	The static resistance. (Chapter 2)
F_v	The damping resistance. (Chapter 2)
G	The soil shear modulus. (Chapter 3)
g	The gravitational acceleration. (Chapter 3)
G_{50}	The secant shear modulus at 50% the ultimate shear stress. (Chapter 4)
G_{max}	The maximum shear modulus. (Chapter 2)
H	The Heaviside function. (Chapter 6)
h_m, h_p	The depth in the model and the corresponding depth in the prototype. (Chapter 3)
I_r	The rigidity index of the soil. (Chapter 4)
K	The spring stiffness represented the full static behaviour of the pile reaction. (Chapter 2). The intrinsic permeability of the soil. (Chapter 3)
k	The hydraulic conductivity of the soil. (Chapter 3)

K_0	The coefficient of lateral earth pressure (the ratio of horizontal to vertical normal effective stress). (Chapter 2)
K_w	The stiffness of the fluid phase. (Chapter 6)
L	The length of the tested pile. (Chapter 2)
M	The pile mass. (Chapter 2)
m	The power parameter in the Hardening-Soil model. (Chapter 7)
N	The ratio of the centrifugal acceleration level over the gravitational acceleration. (Chapter 3)
n	The porosity of the soil. (Chapter 3)
N_q	The dimensionless bearing capacity factor. (Chapter 5)
N_w	The wave number of a pile load test. (Chapter 2)
p	The hydrostatic pore pressure. (Chapter 5)
p	The pore pressure in Biot's equation $u - p$. (Chapter 6)
p'	The mean effective stress. (Chapter 2)
$p(r^*)$	The excess pore pressure at the distance r^* from the pile center. (Chapter 4)
p_a	The atmospheric pressure. (Chapter 4)
p_{ref}	The reference stress. (Chapter 7)
Q	The factor considering the compressibility and the over-consolidation of the soil, Equation 4.9. (Chapter 4)
q	The unit end bearing capacity of a pile. (Chapter 5)
q_c	The cone penetration resistance, Equation 4.8. (Chapter 4)
Q_f	The skin friction resistance of a pile. (Chapter 5)
Q_p	The total end bearing of a pile. (Chapter 5)
R	The empirical reduction factor. (Chapter 1)
R	The normalised pile force which is the ratio of the rapid force over the static force. (Chapter 5)
r	The pile radius. (Chapter 3)
r^*	The distance from the pile center. (Chapter 4)
R_{max}	The normalisation of the maximum pile force. Chapter 4.

R_{up}	The normalisation of the unloading point pile force. Chapter 4.
T	The duration of the applied load. (Chapter 2). The loading duration of a pulse. (Chapter 3)
t	The wall thickness of a pipe pile. (Chapter 3)
U	The fluid displacement in Biot's equation $u - U$. (Chapter 6)
u	The solid displacement in Biot's equation $u - p$. (Chapter 6)
u_i	The pile displacement at the time step i . Chapter 4.
v, v_t	The velocity of the pile head. (Chapter 2)
v_i	The pile velocity at the time step i . Chapter 4.
v_s	The lowest pile velocity used to determine the ultimate static shaft friction, Equation 2.5. (Chapter 2)
v_{ave}	The average load rate of a rapid loading test. (Chapter 3)
w	The relative fluid displacement in Biot's equation $u - w - p$. (Chapter 6)

REFERENCES

- [1] ABRANTES, A. E., AND YAMAMURO, J. A. Experimental and data analysis techniques used for high strain rate tests on cohesionless soil. *Geotechnical testing journal* 25, 2 (2002), 128–151.
- [2] ADEJUMO, T. W., AND BOIKO, I. L. Effect of Installation Techniques on the Allowable Bearing Capacity of Modeled Circular Piles in Layered Soil. *International Journal of Science, Engineering and Technology Research* 2 (2013), 1536–1542.
- [3] AGUIAR, S. D., RAZAVI, A. M. F., CABALLERO, F. L., AND SANTOS, J. A. Soil-Structure interface modeling: Application to pile axial loading. In *The 12th International Conference of International Association for Computer Methods and Advances in Geomechanics* (2008), Goa, India.
- [4] AKERS, S. A. *Uniaxial strain response of Enewetak Beach sand*. Technical report - U.S. Army Engineer Waterways Experiment Station, Corps of Engineers, 1986.
- [5] AL-KHOURY, R., WEERHEIJM, J., DINGERDIS, K., AND SLUYS, L. J. An adaptive time integration scheme for blast loading on a saturated soil mass. *Computers and Geotechnics* 38 (2011), 448–464.
- [6] AL-MHAIDIB, A. I. Bearing capacity of a model pile in sand under different loading rates. In *Proceedings of the 9th international offshore and polar engineering conference* (1999), Brest, France, pp. 724–730.
- [7] AL-MHAIDIB, A. I. *Shearing rate effect on interfacial friction between sand and steel*. Technical report - Department of Civil Engineering, King Saud University, 2005.
- [8] ALLARD, M. A., AND SCHENKEVELD, F. M. The Delft geotechnics model pore fluid for centrifuge tests. In *Centrifuge 94* (1994), Balkema, Rotterdam.
- [9] ALLERSMA, H. G. B. *Optical analysis of stress and strain in photoelastic particle assemblies*. PhD thesis, Delft University of Technology, 1987.
- [10] ALTAEE, A., AND FELLENIUS, B. H. Physical modeling in sand. *Canadian Geotechnical Journal* 31, 3 (1994), 420–431.
- [11] ANDERSEN, K. H., AND SCHJETNE, K. Database of friction angles of sand and consolidation characteristics of sand, silt, and clay. *Journal of Geotechnical and Geoenvironmental Engineering* 139, 7 (2013), 1140–1155.
- [12] ANDERSON, W. F., HANH, N. D., AND HYDE, A. F. L. A new analysis of data from a statnamic tests on piles in clay. In *Proc. of 10th Int. Conf. on piling and deep foundation* (2006), Balkema, pp. a–b.
- [13] ARCHEEWA, E. *The effect of loading rate on bearing capacity of saturated sand*. MSc thesis, UNESCO-IHE, Delft, The Netherlands, 2005.
- [14] ARGYRIS, J. H., AND MLEJNEK, H. P. *Dynamics of Structures*. Elsevier, 1991.
- [15] ASTM D1143-81. Standard method of testing piles under static axial compressive load. *American Society for Testing and Materials* 04.08 (1989), 179–189.
- [16] AUBRAM, D. Development and experimental validation of an arbitrary Lagrangian-Eulerian (ALE) method for soil mechanics. *geotechnik* 38, 3 (Sept. 2015), 193–204.
- [17] BAKKER, K. J., HOEFSLOOT, F. J. M., AND JONG, E. D. Dynamic analysis of large diameter piles Statnamic load test. In *Numerical Methods in Geotechnical Engineering NUMGE 2010* (2010), CRC Press, pp. 613–618.

- [18] BALDI, G., BELLOTTI, R., GHIONNA, V. N., JAMIOLKOWSKI, M., AND PASQUALINI, E. Interpretation of CPT's and CPTU's, Second part: drained penetration of sands. In *Proc. 4th Int. Geotechnical Seminar on Field Instrumentation and In Situ Measurements* (Singapore, 1986), vol. Vol. 2, pp. 195–203.
- [19] BØDKER, L. G_{max} for sand by bender elements at anisotropic stress states. In *12th Nordic Geotechnical Conference* (1996), Icelandic Geotechnical Society.
- [20] BEER, E. E. D. Different behaviour of bored and driven piles. In *Proceedings of the 1st International Geotechnical Seminar on Deep Foundation on Bored and Auger Piles* (1988), Balkema, pp. 47–78.
- [21] BEER, E. E. D., AND WALLAYS, M. *Franki Piles with Overexpanded Bases*. La Technique des Travaux, No. 333, 1972.
- [22] BELLOTTI, R., GHIONNA, V., JAMIOLKOWSKI, M., ROBERTSON, P. K., AND PETERSON, R. W. Interpretation of moduli from self-boring pressuremeter tests in sand. *Géotechnique* 39, 2 (1989), 269–292.
- [23] BELLOTTI, R., GHIONNA, V. N., JAMIOLKOWSKI, M., MANASSERO, M., AND PASQUALINI, E. Evaluation of sand strength from CPT. In *Titolo volume non avalorato* (Paris (France), 1983), vol. Vol. 2, pp. 195–203.
- [24] BEREZANTZEV, V. C., KRISTOFOROV, V., AND GOLUBKOV, V. Load-bearing capacity and deformation of piled foundations. In *Proc. 5th Int. Conf. Soil Mechanics and Foundation Engineering* (1961), Paris.
- [25] BERMINGHAM, P., AND JANES, M. C. An innovative approach to load testing of high capacity piles. In *Proc. of Int. Conf. on piling and deep foundation* (1989), Balkema, pp. 409–413.
- [26] BFER, G. An isoparametric joint/interface element for finite element analysis. *International Journal for Numerical Methods in Engineering* 21, 4 (1985), 585–600.
- [27] BIELEFELD, M. W., AND MIDDENDORP, P. Statnamic simulation. In *Proc. 1st Int. Statnamic Loading Test Seminar* (1995), Balkema, pp. 13–22.
- [28] BIOT, M. A. General theory of three-dimensional consolidation. *J. Appl. Phys.* 12 (1941), 155–164.
- [29] BIOT, M. A. Theory of Elasticity and Consolidation for a Porous Anisotropic Solid. *Journal of Applied Physics* 26, 2 (Feb. 1955), 182–185.
- [30] BIOT, M. A. Theory of propagation of elastic waves in a fluid-saturated porous solid. ii. high-frequency range. *J. Acous. Soc. Am.* 28 (1956), 168–178.
- [31] BIOT, M. A. Theory of propagation of elastic waves in a fluidsaturated porous solid. ii. higher frequency range. *The Journal of the Acoustical Society of America* 28, 2 (Mar. 1956), 179–191.
- [32] BIOT, M. A. Mechanics of deformation and acoustic propagation in porous media. *J. Appl. Phys.* 33 (1962), 1482–1498.
- [33] BIOT, M. A., AND WILLIS, D. G. The elastic coefficients of the theory of consolidation. *Journal of Applied Mechanics* 24 (1957), 594–601.
- [34] BOLTON, M. D. The strength and dilatancy of sands. *Géotechnique* 36, 1 (1986), 65–78.
- [35] BOLTON, M. D., AND GUI, M. W. *The study of relative density and boundary effects for cone penetration tests in centrifuge*. Technical report - Cambridge University, 1993.
- [36] BOLTON, M. D., GUI, M. W., GARNIER, J., CORTE, J. F., BAGGE, G., LAUE, J., AND RENZI, R. Centrifuge cone penetration tests in sand. *Géotechnique* 49, 4 (1999), 543–552.
- [37] BONITA, J. A. *The Effects of Vibration on the Penetration Resistance and Pore Water Pressure in Sands*. PhD thesis, Virginia Tech University, 2000.
- [38] BRINGGREVE, R. B. J., VERMEER, P. A., AND BAKKER, K. J. *Plaxis: Finite Element Code for Soil and Rock Analyses:[user's Guide]*. AA Balkema, 1998.

- [39] BROERE, W., AND TOL, A. F. V. Modelling the bearing capacity of displacement piles in sand. In *Proceedings of the Institution of Civil Engineers, Geotechnical Engineering* 159 (2006), ICE, GE3.
- [40] BROWN, D. A. Evaluation of Static Capacity of Deep Foundations from Statnamic Testing. 403–414.
- [41] BROWN, M. J. *The rapid load testing of piles in fine grained soils*. PhD thesis, University of Sheffield, United Kingdom, 2004.
- [42] BROWN, M. J. Design methods based upon rapid pile load tests. In *International Symposium on Design of Piles in Europe* (Leuven, Belgium, Apr. 2016).
- [43] BROWN, M. J., AND HYDE, A. F. L. Some observations on Statnamic pile testing. *Proceedings of the Institution of Civil Engineers - Geotechnical Engineering* 159, 4 (Oct. 2006), 269–273.
- [44] BROWN, M. J., AND POWELL, J. M. Comparison of Rapid Load Test Analysis Techniques in Clay Soils. *Journal of Geotechnical and Geoenvironmental Engineering* 139, 1 (Mar. 2012), 152–164.
- [45] BURLAND, J. B., AND BURBBIDGE, M. C. Settlement of foundations on sand and gravel. *ICE Proceedings* 78, 6 (1985), 1325–1381.
- [46] BUTLER, H. D., AND HOY, H. E. *Users Manual for the Texas Quick-Load Method for Foundation Load Testing*. Federal Highway Administration, Office of Development, Washington, DC, 1977.
- [47] BYRNE, P. M., PARK, S.-S., BEATY, M., SHARP, M., GONZALES, L., AND ABDOUN, T. Numerical modeling of dynamic centrifuge tests. In *13th World Conference in Earthquake Engineering* (2004).
- [48] CARTER, J. P., BOOKER, J. R., AND YEUNG, S. K. Cavity expansion in cohesive frictional soils. *Geotechnique* 36, 3 (1986), 349–358.
- [49] CASAGRANDE, A., AND SHANNON, W. L. Strength of soils under dynamic loads. *Proceedings of the American Society of Civil Engineers* 74, 4 (1948), 591–608.
- [50] CHAI, J. C., CARTER, J. P., MIURA, N., AND HINO, K. Coefficient of consolidation from piezocone dissipation test result. In *Proc. of Inter. Symp. on Lowland Technology, ISLT2004* (2004).
- [51] CHAN, A. H.-C. *A Unified Finite Element Solution to Static and Dynamic Problems in Geomechanics*. PhD thesis, Department of Civil Engineering, University College of Swansea, 1988.
- [52] CHAN, A. H.-C., FAMIYESIN, O. O., AND WOOD, D. M. A Fully Explicit u-w Scheme for Dynamic Soil and Pore Fluid Interaction. In *APCOM Hong Kong* (1991).
- [53] CHARUE, N. *Loading rate effects on pile load-displacement behaviour derived from back-analysis of two load testing procedures*. PhD thesis, Université catholique de Louvain, Belgium, 2004.
- [54] CHIN, F. K. Estimation of the Ultimate Load of Piles not Carried to Failure. In *Proceedings of the 2nd Southeast Asian Conference on Soil Engineering* (1970), Singapore, pp. 81–90.
- [55] CHONG, M. K. Density changes of sand on cone penetration resistance. In *Proceedings of the first international symposium on penetration testing* (1988).
- [56] CHUNG, J., AND HULBERT, G. M. A time integration algorithm for structural dynamics with improved numerical dissipation: the generalized- method. *Journal of Applied Mechanics* 60 (1993), 371–375.
- [57] CHUNG, S., RANDOLPH, M., AND SCHNEIDER, J. Effect of Penetration Rate on Penetrometer Resistance in Clay. *Journal of Geotechnical and Geoenvironmental Engineering* 132, 9 (2006), 1188–1196.
- [58] CLARK, J. I. The Settlement and Bearing Capacity of Very Large Foundations on Strong Soils: 1996 R.M Hardy Keynote Address. *Canadian Geotechnical Journal* 35, 1 (1998), 131–145.
- [59] CLAYTON, C. R. I., AND DIKRAN, S. S. Pore water pressure generated during dynamic penetration testing. In *Proc. 2nd Eur. Sym. on Penetration Testing* (1982), Amsterdam.

- [60] CLAYTON, C. R. I., SIMONS, N. E., AND INSTONE, S. J. Research on dynamic penetration testing of sands. In *Penetration Testing 1988* (1988), Rotterdam.
- [61] COMMISSION, S. P. *Recommendations for pile driving test and routine test loading of piles*. Royal Swedish Academy of Engineering Sciences Commission on Pile Research, 1970.
- [62] DARCY, H. *Les fontaines publiques de la ville de Dijon*. 1856.
- [63] DAVISSON, M. T. *High Capacity Piles - Lecture Series of Innovations in Foundation Construction*. American Society of Civil Engineers, 1972.
- [64] DAYAL, U., AND ALLEN, J. H. The effect of penetration rate on the strength of remoulded clay and sand sample. *Canadian Geotechnical Journal* 12 (1975), 336–348.
- [65] DEWOOLKAR, M. M., KO, H. Y., STADLER, A. T., AND ASTANEH, S. M. F. A substitute pore fluid for seismic centrifuge modeling. *Geotechnical Testing Journal* 22, 3 (1999), 196–210.
- [66] DIJKSTRA, J. *Influence of loading rate on pile capacity in sand*. MSc thesis, Delft University of Technology, 2004.
- [67] DIJKSTRA, J. *On the modelling of pile installation*. PhD thesis, Delft University of Technology, 2009.
- [68] DIJKSTRA, J., BROERE, W., AND HEERES, O. M. Numerical simulation of pile installation. *Computers and Geotechnics* 38, 5 (2011), 612–622.
- [69] DUNCAN, J. M., AND CHANG, C.-Y. Nonlinear Analysis of Stress and Strain in Soils. *Journal of the Soil Mechanics and Foundations Division* 96, 5 (1970), 1629–1653.
- [70] DURGUNOGLU, H. T., AND MITCHELL, J. K. *Static penetration resistance of soils*. University of California, Berkeley, 1973.
- [71] EIKSUND, G., AND NORDAL, S. Dynamic model pile testing with pore pressure measurements. In *Proc. 5th Int. Conf. Application of Stress Wave Theory to Piles* (1996), Orlando, Florida.
- [72] ENGIN, H. K., BRINKGREVE, R. B. J., AND VAN TOL, A. F. Approximation of pile installation effects: a practical tool. *Proceedings of the Institution of Civil Engineers - Geotechnical Engineering* 168, 4 (Aug. 2015), 319–334.
- [73] FARR, J. V. One dimensional loading-rate effects. *Journal of Geotechnical Engineering* 116, 1 (1990), 119–135.
- [74] FELLENIUS, B. H. Test loading of piles and new proof testing procedure. *Journal of the Geotechnical Engineering Division* 101 (1975), 855–869.
- [75] FELLENIUS, B. H. *What capacity value to choose from the results of a static loading test*. The newsletter of the Deep Foundation Institute, 2001.
- [76] FILLUNGER, P. Neuere Grundlagen für die statische Berechnung von Talsperren. *Zeitschrift des Österreichischen Ingenieur - und Architektenvereins* 23 (1914), 441–447.
- [77] FILLUNGER, P. Versuche über die Zugfestigkeit bei allseitigem Wasserdruck. *Österreichische Wochenschrift für den öffentlichen Baudienst* 29 (1915), 443–448.
- [78] FILLUNGER, P. *Erdbaumechanik*. Tech. rep., 1936.
- [79] FINNIE, I. M., AND RANDOLPH, M. F. Bearing response of shallow foundations on uncemented calcareous soil. In *Centrifuge 94* (1994), Balkema, Rotterdam.
- [80] FIORAVANTE, V. On the shaft friction modelling of non-displacement piles in sand. *Soils and Foundations* 42, 2 (2002), 23–33.

- [81] FISCHER, K. A., SHENG, D., AND ABBO, A. J. Modeling of pile installation using contact mechanics and quadratic elements. *Computers and Geotechnics* 34, 6 (Nov. 2007), 449–461.
- [82] FLEMING, K., WELTMAN, A., RANDOLPH, M., AND ELSON, K. *Piling engineering, 3rd Ed.* Taylor & Francis Group, 2009.
- [83] FLEMMING, W. G. K. *The bearing capacity of pile groups.* PhD thesis, Queen's University of Belfast, 1958.
- [84] FOEKEN, R. J. V., MIDDENDORP, P., AND COURAGE, W. M. G. Application of stress wave method for automatic signal matching and Statnamic predictions. In *Proc. 2nd Int. Statnamic Loading Test Seminar* (1998), Balkema, pp. 345–354.
- [85] FONSECA, A. V. D., AND SANTOS, J. *International Prediction Event on the Behaviour of Bored, CFA and Driven Piles in CEFEUP/ISC2 experimental site - 2003.* University of Porto, 2003.
- [86] FORAY, P., BALACHOWSKI, L., AND RAULT, G. Scale effect in shaft friction due to the localisation of deformations. In *Proceedings International Conference Centrifuge 98* (1998), Balkema, Rotterdam.
- [87] FRANK, R., GUENOT, A., AND HUMBERT, P. Numerical analysis of contacts in geomechanics. In *4th International conference on numerical methods in geomechanics* (1982), Balkema, Rotterdam.
- [88] FUKUOKA, H. Variation of the friction angle of granular materials in the high-speed high-stress ring shear apparatus. *Bulletin of the Disaster Prevention Research Institute* 41, 4 (1991), 243–279.
- [89] GAN, J. K. M., FREDLUND, D. G., AND RAHARDJO, H. Determination of the shear strength parameters of an unsaturated soil using the direct shear test. *Canadian Geotechnical Journal* 25, 3 (Aug. 1988), 500–510.
- [90] GARNIER, J., GAUDIN, C., SPRINGMAN, S. M., CULLIGAN, P. J., GOODINGS, D., KONIG, D., KUTTER, B., PHILLIPS, R., RANDOLPH, M. F., AND THOREL, L. Catalogue of scaling laws and similitude questions in geotechnical centrifuge modelling. *International Journal of Physical Modelling in Geotechnics* 1, 3 (2007).
- [91] GARNIER, J., AND KÖNIG, D. Scale effects in piles and nail loading tests in sand. In *Proceedings International Conference Centrifuge 98* (1998), Balkema, Rotterdam.
- [92] GENNARO, V. D., FRANK, R., BOSCO, G., AND CANOU, J. Effet de la vitesse de chargement sur le comportement mécanique de pieux modèle en chambre d'étalonnage - The effect of loading rate on the mechanical behaviour of model piles in calibration chamber. In *Proceedings of the 15th International Conference on Soil Mechanics and Geotechnical Engineering* (2001), Balkema, Rotterdam, pp. 885–888.
- [93] GEONAMICS. Statnamic theory and analysis, 2015.
- [94] GHABOUSSI, J., AND DIKMAN, S. U. Liquefaction analysis of horizontally layered sands. *Journal of Geotechnical Division* 3 (1978), 341–356.
- [95] GHABOUSSI, J., WILSON, E. L., AND ISENBURG, J. Finite element for rock joint interfaces. *Journal of the Soil Mechanics and Foundations Division* 99 (1973), 833–848.
- [96] GIBSON, G. C., AND COYLE, H. M. *Soil damping constants related to common soil properties in sands and clays.* Technical report - Texas Transportation Institute, 1968.
- [97] GLADWELL, I., AND THOMAS, R. Stability properties of the Newmark, Houbolt and Wilson- β methods. *International Journal for Numerical and Analytical Methods in Geomechanics* 4 (1980), 143–158.
- [98] GONIN, H., COELUS, G., AND LEONARD, M. Theory and performance of a new dynamic method of pile testing. In *Proc. 2nd Int. Conf. Application of stress-wave theory to piles* (1984), Balkema, pp. 403–410.
- [99] GRIFFITHS, D. V. Numerical modelling of interfaces using conventional finite elements. In *5th International conference on numerical methods in geomechanics* (1985), Balkema, Rotterdam.

- [100] GRINTEN, J. G. M. v. D. *An experimental study of shock-induced wave propagation in dry, water-saturated, and partially saturated porous media*. PhD thesis, Eindhoven University of Technology, 1987.
- [101] GRINTEN, J. G. M. v. D., DONGEN, M. E. H. v., AND KOGEL, H. v. D. Strain and pore pressure propagation in a water-saturated porous medium. *Journal of Applied Physics* 62, 12 (1987), 4682–4687.
- [102] GRINTEN, J. G. M. v. D., DONGEN, M. E. H. v., MARINUS, E. H., AND KOGEL, H. v. D. A shock-tube technique for studying pore-pressure propagation in a dry and water-saturated porous medium. *Journal of Applied Physics* 58, 8 (1985), 2937–2942.
- [103] GUI, M. W., AND BOLTON, M. D. Geometry and scale effects in CPT and pile design. In *Geotechnical Site Characterization* (1998), Balkema, Rotterdam.
- [104] GUI, M. W., AND JENG, D. S. Application of Cavity Expansion Theory in Predicting Centrifuge Cone Penetration Resistance. *Open Civil Engineering Journal* 3 (2009), 1–6.
- [105] H. S. YU, AND J. K. MITCHELL. Analysis of Cone Resistance: Review of Methods. *Journal of Geotechnical and Geoenvironmental Engineering* 124, 2 (Feb. 1998), 140–149.
- [106] HA, T.-G., JANG, I.-S., CHOO, Y.-S., AND CHUNG, C.-K. Evaluation of coefficient of consolidation for dilatancy dissipation in piezocone test in overconsolidated cohesive soils. *KSCE Journal of Civil Engineering* 18, 2 (Mar. 2014), 475–487.
- [107] HAMANN, T., QIU, G., AND GRABE, J. Application of a Coupled Eulerian–Lagrangian approach on pile installation problems under partially drained conditions. *Computers and Geotechnics* 63 (Jan. 2015), 279–290.
- [108] HANH, N. D. *Rapid load testing of piles in clay*. PhD thesis, University of Sheffield, United Kingdom, 2006.
- [109] HANSEN, J. B. Hyperbolic Stress-Strain Response. Cohesive Soils. *Journal of the Geotechnical Engineering Division* 89 (1963), 241–242.
- [110] HARDIN, B. O., AND BLACK, W. L. Sand Stiffness Under Various Triaxial Stresses. *Journal of Soil Mechanics & Foundations Division* 92 (1966), 27–42.
- [111] HARDY, S. *The implementation and application of dynamic finite element analysis in geotechnical problems*. PhD thesis, Imperial College of Science, Technology and Medicine, 2003.
- [112] HEALY, K. A. *Triaxial tests upon saturated fine silty sand - Report No. 11*. Contract report - U.S. Army Engineer Waterways Experiment Station, Corps of Engineers, 1962.
- [113] HEALY, K. A. *The dependence of dilatation in sand on rate of shear strain - Report No. 13*. Contract report - U.S. Army Engineer Waterways Experiment Station, Corps of Engineers, 1963.
- [114] HEEREMA, E. P. Relationships between wall friction, displacement, velocity and horizontal stress in clay and in sand for pile driveability analysis. *Ground Engineering* 12, 1 (1979), 55–61.
- [115] HENKE, S., AND GRABE, J. Simulation of pile driving by 3-dimensional Finite-Element analysis. In *17th European young geotechnical engineers conference* (2006).
- [116] HILBERT, H. M., HUGHES, T. J. R., AND TAYLOR, R. L. Improved numerical dissipation for time integration algorithms in structural mechanics. *International Journal of Earthquake Engineering and Structural Dynamics* 5 (1977), 283–292.
- [117] HÖLSCHER, P. *Dynamical response of saturated and dry soils*. PhD thesis, Delft University of Technology, 1995.
- [118] HÖLSCHER, P., AND BARENDIS, F. B. J. The relation between soil-parameters and one-dimensional toe-model. In *Proc. 4th Int. Conf. Application of Stress Wave Theory to Piles* (1992), Balkema, Rotterdam.

- [119] HÖLSCHER, P., AND BARENDIS, F. B. J. Dynamic model pile testing with pore pressure measurements. In *Proc. 5th Int. Conf. Application of Stress Wave Theory to Piles* (1996), Orlando, Florida.
- [120] HÖLSCHER, P., BRASSINGA, H. E., TOL, A. F. V., MIDDENDORP, P., AND REVOORT, E. Rapid load field tests interpreted with the new guideline. In *Proceedings of the 17th International Conference on Soil Mechanics and Foundation Engineering* (2009), Alexandria, Egypt.
- [121] HÖLSCHER, P., AND TOL, A. F. V. Database of field measurements of SLT and RLT for calibration. In *Rapid Load Testing on Piles* (2009), Taylor & Francis Group, London, UK.
- [122] HÖLSCHER, P., TOL, A. F. V., AND HUTTEMAN, M. *Field test Rapid load Testing Waddinxveen*. Factual report - Deltares, 2009.
- [123] HÖLSCHER, P., VAN TOL, A. E., AND HUY, N. Q. Rapid pile load tests in the geotechnical centrifuge. *Soils and Foundations* 52, 6 (Dec. 2012), 1102–1117.
- [124] HOLEYMAN, A., COUVREUR, J.-M., AND CHARUE, N. Results of dynamic and kinetic pile load tests and outcome of an international prediction event.
- [125] HOLEYMAN, A. E. Keynote lecture: Technology of pile dynamic testing. In *Proc. 4th Int. Conf. Application of stress-wave theory to piles* (1992), Balkema, pp. 195–216.
- [126] HOLEYMAN, A. E., AND CHARUE, N. International pile capacity prediction event at Limelette. In *Belgian Screw Pile Technology: Proceedings of the Symposium* (Brussels, Belgium, May 2003), CRC Press, pp. 215–234.
- [127] HORIKOSHI, K., KATO, K., AND MATSUMOTO, T. Finite element analyses of Statnamic loading test of pile. In *Proc. 2nd Int. Statnamic Loading Test Seminar* (1998), Balkema, pp. 295–302.
- [128] HOUBOLT, J. C. A recurrence matrix solution for the dynamic response of elastic aircraft. *Journal of the Aeronautical Sciences* 17 (1950), 540–550.
- [129] HOULSBY, G. T. How the dilatancy of soils affects their behaviour. In *Proceedings of the tenth European conference on soil mechanics and foundation engineering* (1991), Florence, Italy.
- [130] HOULSBY, G. T., AND SCHNAID, F. Interpretation of Shear Moduli from Cone-Pressuremeter Tests in Sand. *Géotechnique* 44, 1 (1994), 147–164.
- [131] HOUSE, A. R., OLIVEIRA, J. R. M., AND RANDOLPH, M. F. Evaluating the Coefficient of Consolidation Using Penetration Tests. *International Journal of Physical Modelling in Geotechnics 1*, International Journal of Physical Modelling in Geotechnics (2001), 17–26(9).
- [132] HSU, Y. S., COLLISON, C. H., DEAN, E. T. R., AND JAMES, R. G. Techniques for saturating sand with oil. In *Centrifuge 94* (1994), Balkema, Rotterdam.
- [133] HU, G. C. Y. Bearing capacity of foundations with overburden shear. *Sols Soils* 13 (1965), 11–18.
- [134] HUANG, M., AND ZIENKIEWICZ, O. C. New unconditionally stable staggered solution procedures for coupled soil-pore fluid dynamic problems. *International Journal for Numerical Methods in Engineering* 43 (1998), 1029 – 1052.
- [135] HUAT, B. B., AND PAVADAI, M. *Foundation Engineering: Design and Construction in Tropical Soils*. Taylor & Francis Group, London, UK, 2006.
- [136] HUGHES, T. J. R. *The finite element method, linear static and dynamic finite element analysis*. Dover, 2000.
- [137] HUNGR, O., AND MORGENSTERN, N. R. High velocity ring shear tests on sand. *Géotechnique* 34 (1984), 415–421.

- [138] HYDE, A. F. L., ANDERSON, W. F., AND ROBINSON, S. A. Rate effects in clay soils and their relevance to Statnamic pile testing. In *Proc. 2nd Int. Statnamic Loading Test Seminar* (1998), Balkema, pp. 303–309.
- [139] INSTITUTE, A. P. *Recommended Practice for Planning, Designing and Constructing Fixed Offshore Platforms – Working Stress Design*. American Petroleum Institute, API RP 2A-WSD, 21st edition, 2000.
- [140] JACKSON, J. G., ROHANI, B., AND EHRGOTT, J. Q. Loading rate effects on compressibility of sand. *Journal of Geotechnical Engineering Division* 106, 8 (1980), 839–852.
- [141] JAMIOLKOWSKI, M., LO PRESTI, D. C. F., AND MANASSERO, M. Evaluation of relative density and shear strength of sands from CPT and DMT. In *Titolo volume non avvalorato* (2001), pp. 201–238.
- [142] JANBU, N. Soil compressibility as determined by oedometer and triaxial tests. In *European Conference on Soil Mechanics and Foundation Engineering* (1965), Neisbaden, Germany.
- [143] JEZEQUEL, J. F. Les pénétromètre statiques. Influence du mode d’emploi sur la résistance de pointe. *Laboratoire Central des Ponts et Chaussées, Bulletin de Liaison* 36 (1969), 151–160.
- [144] JOSHI, R. C., AND SHARMA, H. D. Prediction of ultimate pile capacity from load tests on bored and belled, expanded base compacted and driven piles. In *Proceedings International Symposium on Prediction and Performance in Geotechnical Engineering* (1987), Algebra, Canada, pp. 135–144.
- [145] JUSTASON, M. D., MULLINS, G., ROBERTSON, D. T., AND KNIGHT, W. F. A comparison of static and STATNAMIC load tests in sand: A case study of the Bayou Chico bridge in Pensacola, Florida. In *Proc. 2nd Int. Statnamic Loading Test Seminar* (1998), Balkema, pp. 43–53.
- [146] JUSTIN, C. J. *Ultimate Pile Capacity of Bored Pile and Driven Pile at Ara Damansara*. MSc thesis, Universiti Teknologi Petronas, Malaysia, 2010.
- [147] KAMP, W. G. B. T. The influence of the rate of penetration on the cone resistance $q_{c,s}$ in sand. In *Proc. 2nd Eur. Sym. on Penetration Testing* (1982), Amsterdam.
- [148] KARA, O., AND GUNDUZ, Z. Correlation between CPT and SPT in Adapazari, Turkey. In *2nd International Symposium on Cone Penetration Testing* (2010), untington Beach, CA, USA.
- [149] KATONA, M. G. A simple contact-friction interface element with application to buried culverts. *International Journal for Numerical and Analytical Methods in Geomechanics* 7 (1983), 371–384.
- [150] KATONA, M. G., AND ZIENKIEWICZ, O. C. A unified set of single step algorithms, Part 3: the beta-m method, a generalization of the Newmark scheme. *International Journal for Numerical Methods in Engineering* 21 (1985), 1345–1359.
- [151] KO, H.-Y. Modeling seismic problems in centrifuges. In *Centrifuge 94* (1994), Balkema, Rotterdam.
- [152] KOBAYASHI, T., AND FUKAGAWA, R. Characterization of deformation process of CPT using X-ray TV imaging technique. In *Third international conference on deformation characteristics of geomaterials* (2003).
- [153] KONTAE, S. *Development of time integration schemes and advanced boundary conditions for dynamic geotechnical analysis*. PhD thesis, Imperial College of Science, Technology and Medicine, 2006.
- [154] KRAFT, L. M. Performance of axially loaded pipe piles in sand. *Journal of Geotechnical Engineering* 117, 2 (1991), 272–296.
- [155] KULHAWY, F. H. Limiting tip and side resistances, fact or fallacy. In *Symposium on Analysis and Design of Pile Foundations* (1984), American Society of Civil Engineers, pp. 80–98.
- [156] KULHAWY, F. H., AND MAYNE, P. W. *Manual on estimating soil properties for foundation design*. Technical report - Electric Power Research Institute, 1990.

- [157] KUSAKABE, O., KUWABARA, F., AND MATSUMOTO, T. Research activities toward standardization of rapid pile load test methods in Japan. In *Proc. 2nd Int. Statnamic Loading Test Seminar* (1998), Balkema, pp. 219–238.
- [158] KUTTER, B. L. Recent advances in centrifuge modeling of seismic shaking. In *Proceedings of the 3rd International Conference on Recent Advances in Geotechnical Earthquake Engineering and Soil Dynamics* (1995).
- [159] KUTTER, B. L. Phenomena associated with undrained and partly drained dilatant soil. In *Proceedings of the 6th International Conference on Physical Modelling in Geotechnics* (2006), Hong Kong.
- [160] LADANYI, B., AND JOHNSTON, G. H. Behavior of circular footings and plate anchors embedded in permafrost. *Canadian Geotechnical Journal* 11 (1974), 531–533.
- [161] LANGEN, H. V., AND VERMEER, P. A. Interface elements for singular plasticity points. *International Journal for Numerical and Analytical Methods in Geomechanics* 15, 5 (1991), 301–315.
- [162] LEE, J., SALGADO, R., AND CARRARO, J. A. H. Stiffness degradation and shear strength of silty sands. *Canadian Geotechnical Journal* 41, 5 (2004), 831–843.
- [163] LEE, J., SALGADO, R., AND PAIK, K. Estimation of load capacity of pipe piles in sand based on cone penetration test results. *Journal of Geotechnical and Geoenvironmental Engineering* 129, 6 (2003), 391–403.
- [164] LEE, K. L., SEED, H. B., AND DUNLOP, P. Effect of Transient Loading on the Strength of Sand. In *Proceedings of the 7th International Conference on Soil Mechanics and Foundation Engineering* (1969), Mexico City, Mexico.
- [165] LEHANE, B. M., AND WHITE, D. J. Lateral stress changes and shaft friction for model displacement piles in sand. *Canadian Geotechnical Journal* 42 (2005), 1015–1029.
- [166] LEWIS, C. L. *Analysis of Axial Statnamic Testing by the Segmental Unloading Point Method*. MSc thesis, University of South Florida, Tampa, 1999.
- [167] LEWIS, R. W., AND SCHREFLER, B. A. *The Finite Element Method in the Deformation and Consolidation of Porous Media*. Wiley, 1987.
- [168] LONG, M. Comparing dynamic and static test results of bored piles. *Proceedings of Institution of Civil Engineers* 160 (2007), 43–49.
- [169] LOTTUM, H. V., AND HÖLSCHER, P. *Project 1200419: Centrifuge tests on Rapid Pile Loading on closed- and opened-end Piles*. Factual report - Deltares, 2010.
- [170] LUNNE, T., AND CHRISTOFFERSEN, H. Interpretation of cone penetrometer data for offshore sands. In *Proc. Offshore Technology Conference OTC4464* (Houston, 1982), Holland, pp. 181–192.
- [171] M. JAMIOLKOWSKI, D. C. F. LO PRESTI, AND M. MANASSERO. Evaluation of Relative Density and Shear Strength of Sands from CPT and DMT. *Soil Behavior and Soft Ground Construction*.
- [172] MADABHUSHI, S. P. G. Effect of pore fluid in dynamic centrifuge modeling. In *Centrifuge 94* (1994), Balkema, Rotterdam.
- [173] MAHUTKA, K., KÖNIG, F., AND GRABE, J. Numerical modeling of pile jacking, driving and vibro driving. In *Proceedings of International Conference on Numerical Simulation of Construction Processes in Geotechnical Engineering for Urban Enviroment* (2006), Balkema, Rotterdam.
- [174] MANSUR, C. I., AND KAUFMAN, J. M. Pile Tests, Low-Sill Structure, Old River, Louisiana. *Journal of Soil Mechanics & Foundations Division* 82 (1956), 1–33.

- [175] MATSUMOTO, T. Development of a rapid pile load test method using a falling mass attached with spring and damper. In *Proc. 7th Int. Conf. Application of stress-wave theory to piles* (2004), Balkema, pp. 351–358.
- [176] MATSUMOTO, T., AND NISHIMURA, S. Wave propagation phenomena in statnamic test of a steel pipe pile. In *Proc. 5th Int. Conf. Application of Stress Wave Theory to Piles* (1996).
- [177] MAZURKIEWICZ, B. K. *Test Loading of Piles According to Polish Regulations*. Royal Swedish Academy of Engineering Sciences Commission on Pile Research, 1972.
- [178] MCVAY, M. C., KUO, C. L., AND GUISSINGER, A. L. *Calibrating Resistance Factors in the Load and Resistance Factor Design of Stanamic Loading Testing*. Florida Department of Transportation, 2003.
- [179] MEIJERS, P. *Soil response during an explosion in a tunnel*. Deltares, DC-COB project, 2009.
- [180] MEIJERS, P. *Validation implementation Biot in PLAXIS*. Deltares, DC-COB project, 2009.
- [181] MES, J. M., AND McDERMOTT, R. J. s. Pile driveability is unpredictable in sand or silt. *Petroleum Engineer* 2, 2 (1976), 76–92.
- [182] MEYERHOF, G. G. *The bearing capacity of sand*. PhD thesis, University of London, London, England, 1950.
- [183] MEYERHOF, G. G. The ultimate bearing capacity of foundations. *Geotechnique* 2, 4 (1951), 301–331.
- [184] MEYERHOF, G. G. Some recent research on the bearing capacity foundations. *Canadian Geotechnical Journal* 1, 1 (1953), 16–26.
- [185] MÜHLHAUS, H. B., AND VARDOLAKIS, I. The thickness of shear bands in granular materials. *Géotechnique* 37, 3 (Sept. 1987), 271–283.
- [186] MICHAEL FITZGERALD, AND DEREK ELSWORTH. Evolution of the Pore-Pressure Field around a Moving Conical Penetrometer of Finite Size. *Journal of Engineering Mechanics* 136, 3 (Mar. 2010), 263–272.
- [187] MIDDENDORP, P. Statnamic, eine Alternative für statische Probelastungen. In *Fachseminar "Pfahl-Symposium 95"* (Braunschweig, 1995), Balkema, pp. 1–15.
- [188] MIDDENDORP, P. Statnamic the engineering of art. In *Proc. 6th Int. Conf. Application of stress-wave theory to piles* (2000), Balkema, pp. 551–562.
- [189] MIDDENDORP, P. *Report Rapid Load Testing Waddinxveen, Profound*. Factual report - Profound, 2008.
- [190] MIDDENDORP, P., BERMINGHAM, P., AND KUIPER, B. Stanamic Load Testing of Foundation Piles. In *Proc. 4th Int. Conf. Application of stress-wave theory to piles* (1992), Balkema, pp. 581–588.
- [191] MIDDENDORP, P., BERMINGHAM, P., AND KUIPER, B. Statnamic load testing of foundation piles. In *Application of Stress-Wave Theory to Piles* (1992), Balkema, Rotterdam.
- [192] MIDDENDORP, P., AND BIELEFELD, M. W. Stanamic load testing and the influence of stress wave phenomena. In *Proc. 1st Int. Statnamic Loading Test Seminar* (1995), Balkema, pp. 207–220.
- [193] MIDDENDORP, P., AND WEELE, P. J. v. Application of characteristic stress wave method to offshore practice. In *Proceedings of 3rd International Conference on Numerical Methods in Offshore Piling* (1986), Balkema, pp. a–b.
- [194] MIKASA, M., AND TAKADA, N. Significance of centrifugal model tests in soil mechanics. In *Proc. 8th Int. Conf. Soil Mechanics and Foundation Engineering* (1973), Moscow.
- [195] MITCHELL, J. K., GUZIKOWSKI, F., AND VILLET, W. C. B. *The Measurement of Soil Properties in-situ*. Report - University of California, Berkeley, 1978.

- [196] MITCHELL, J. K., AND LUNNE, T. A. Cone Resistance as Measure of Sand Strength. *Journal of the Geotechnical Engineering Division* 104, 7 (1978), 995–1012.
- [197] MOHAN, D., JAIN, G. S., AND JAIN, M. P. A new approach to load tests. *Géotechnique* 17 (1967), 274–283.
- [198] MOLENKAMP, F. Application of non-linear elastic model. *International Journal for Numerical and Analytical Methods in Geomechanics* 16 (1992), 131–150.
- [199] MORGANO, C. M. *Effects of Pore Water Pressure Variation Under Dynamic Loads*. Report - PDA Users Day 1990: Cleveland, OH, 1990.
- [200] NAGGAR, M. H. E., AND BALDINELLI, M. J. V. Stress Wave Analysis of Statnamic Load Test for Pile Capacity Prediction. In *Proc. 2nd Int. Statnamic Loading Test Seminar* (1998), Balkema, pp. a–b.
- [201] NAGGAR, M. H. E., AND BALDINELLI, M. J. V. Interpretation of axial Statnamic load test using an automatic signal matching technique. *Canadian Geotechnical Journal* 37 (2000), 927–942.
- [202] NAGGAR, M. H. E., AND NOVAK, M. Analytical model for an innovative pile test. *Canadian Geotechnical Journal* 29 (1992), 569–579.
- [203] NAVFAC. *Foundation and Earth Structures*. U.S. Department of the Navy, 1984.
- [204] NEWMARK, N. M. A method of computation for structural dynamics. *Journal of Engineering Mechanics Division* 85 (1959), 67–94.
- [205] NGUYEN, C. T., AND HÖLSCHER, P. *Project 1200419: Centrifuge tests on Rapid Pile Loading 2011*. Factual report - Deltares, 2012.
- [206] NGUYEN, Q. H. *Rapid load testing of pile in sand*. PhD thesis, Delft University of Technology, 2008.
- [207] NGUYEN, T. C. *Investigation into soil displacement near a jacked-in pile in sand*. MsC thesis, Delft University of Technology, 2008.
- [208] NICOLA, A. D., AND RANDOLPH, M. F. The plugging behavior of driven and jacked piles in sand. *Géotechnique* 47, 4 (1997), 841–856.
- [209] OLIVEIRA, J. R. M. S., ALMEIDA, M. S. S., MOTTA, H. P. G., AND ALMEIDA, M. C. F. Influence of penetration rate on penetrometer resistance. *Journal of Geotechnical and Geoenvironmental Engineering* 137, 7 (2011), 695–703.
- [210] OMIDVAR, M., ISKANDER, M., AND BLESS, S. Stress-strain behavior of sand at high strain rates. *International Journal of Impact Engineering* 49 (Nov. 2012), 192–213.
- [211] OPSTAL, A. T. P. J., AND DALEN, J. H. v. Proefbelasting op de Maasvlakte (in Dutch). *Cement* 2 (1996), 53–62.
- [212] PAIKOWSKY, S. G. *Innovative Load Testing Systems*. National Cooperative Highway Research Program, 2006.
- [213] PANDE, G. N., AND SHARMA, K. G. On joint/interface elements and associated problems of numerical ill-conditioning. *International Journal for Numerical and Analytical Methods in Geomechanics* 3, 3 (1979), 293–300.
- [214] PARK, K. C. An improved stiffly stable method for direct integration of nonlinear structural dynamic equations. *Journal of Applied Mechanics ASME* 42 (1975), 464–470.
- [215] PARK, S.-S., AND BYRNE, P. M. Stress densification and its evaluation. *Canadian Geotechnical Journal* 41, 1 (Feb. 2004), 181–186.
- [216] PHILLIPS, R., AND VALSANGKAR, A. J. *An experimental investigation of factors affecting penetration resistance in granular soils in centrifuge modeling*. Technical report - Cambridge University, 1987.

- [217] PHUONG, N. T. V., VAN TOL, A. F., ELKADI, A. S. K., AND ROHE, A. Numerical investigation of pile installation effects in sand using material point method. *Computers and Geotechnics* 73 (Mar. 2016), 58–71.
- [218] POTYONDY, J. G. Skin friction between various soils and construction materials. *Géotechnique* 11, 4 (1961), 831–853.
- [219] POULOS, H. G. Keynote lecture: Pile testing-From the designer's viewpoint. In *Proc. 2nd Int. Statnamic Loading Test Seminar* (1998), Balkema, pp. 3–21.
- [220] PRANDTL, L. *Über die Härte plastischer Körper - On the hardness of plastic bodies*. Nachr. Ges. Wiss. Göttingen, Math.-Phys. Kl., 1920.
- [221] PRESTI, D. C. F. L. *Mechanical behavior of Ticino sand from resonant column tests*. PhD thesis, Politecnico di Torino, 1987.
- [222] PRESTI, D. C. F. L., JAMIOLKOWSKI, M., PALLARA, O., CAVALLARO, A., AND PEDRONI, S. Shear modulus and damping of soils. *Géotechnique* 47, 3 (1997), 603–617.
- [223] PREVOST, J. H. Nonlinear transient phenomena in saturated porous media. *Computer Methods in Applied Mechanics and Engineering* 30 (1982), 3–18.
- [224] PREVOST, J. H. Wave propagation in fluid-saturated porous media: An efficient finite element procedure. *Soil Dynamics and Earthquake Engineering* 4, 4 (1985), 183–202.
- [225] PUCKER, T., AND GRABE, J. Numerical simulation of the installation process of full displacement piles. *Computers and Geotechnics* 45 (Sept. 2012), 93–106.
- [226] QIU, G., HENKE, S., AND GRABE, J. Application of a Coupled Eulerian-Lagrangian approach on geomechanical problems involving large deformations. *Computers and Geotechnics* 38, 1 (2011), 30–39.
- [227] QIU, G., HENKE, S., AND GRABE, J. Application of a Coupled Eulerian-Lagrangian approach on geomechanical problems involving large deformations. *Computers and Geotechnics* 38, 1 (Jan. 2011), 30–39.
- [228] RAHMAN, M. S., GABR, M. A., SARCIA, R. Z., AND HOSSAIN, M. S. *Load and Resistance Factor Design (LRFD) for Analysis/Design of Piles Axial Capacity*. North Carolina Department of Transportation, 2005.
- [229] RANDOLPH, M. F. Science and empiricism in pile foundation design. *Géotechnique* 53, 10 (2003), 847–875.
- [230] REIDING, F. J., MIDDENDORP, P., AND BREDERODE, P. J. v. A digital approach to sonic pile testing. In *Proc. 2nd Int. Conf. Application of stress-wave theory to piles* (1984), Balkema, pp. 47–a.
- [231] RENDULIC, L. Porenziffer und Porenwasserdruck in Tonen. *Der Bauingenieur* 17 (1936), 559–564.
- [232] RICE, J. R., AND CLEARY, M. P. Some basic stress-diffusion solutions for fluid saturated elastic porous media with compressible constituents. *Rev. Geophys. Space Phys.* 14 (1976), 227–241.
- [233] RIETDIJK, J., SCHENKEVELD, F. M., SCHAMINEE, P. E. L., AND BEZUIJEN, A. The drizzle method for sand sample preparation. *Proceedings of the International Conference on Physical Modelling in Geotechnics* (2010).
- [234] ROBINSKY, E., AND MORRISON, C. Sand displacement and compaction around model friction piles. *Canadian Geotechnical Journal* 1, 2 (1964), 81–93.
- [235] ROBINSKY, E., SAGAR, W. L., AND MORRISON, C. Effect of shape and volume on the capacity of model piles in sand. *Canadian Geotechnical Journal* 1, 4 (1964), 189–204.
- [236] RUSSO, G. Full-scale load tests on instrumented piles. In *Proceedings of the Institution of Civil Engineers, Geotechnical Engineering* 157 (2004), ICE, GE3.

- [237] SACHDEVA, T. D., AND RAMAKRISHNAN, C. V. A finite element solution for the two-dimensional elastic contact problems with friction. *International Journal for Numerical Methods in Engineering* 17, 8 (1981), 1257–1271.
- [238] SAITO, R., FUKUOKA, H., AND SASSA, K. Experimental study on the rate effect on the shear strength. In *Disaster Mitigation of Debris Flows, Slope Failures and Landslides: Proceedings of the INTERPRAEVENT International Symposium* (2006), Universal Academy Press, Tokyo, Japan, pp. 421–427.
- [239] SALGADO, R., BANDINI, P., AND KARIM, A. Shear strength and stiffness of silty sand. *Journal of Geotechnical and Geoenvironmental Engineering* 126, 5 (2000), 451–462.
- [240] SATIBI, S. *Numerical analysis and design criteria of embankments on floating piles*. PhD thesis, Institute for Geotechnic, Stuttgart University, 2009.
- [241] SCHELLINGERHOUT, A. J. G., AND REVOORT, E. Pseudo static pile load tester. In *Proc. 5th Int. Conf. Application of stress-wave theory to piles* (1996), Balkema, pp. 251–260.
- [242] SCHIMMING, B. B., HAAS, A. M., AND SAXE, H. C. Study of dynamic and static failure envelopes. *Journal of Soil Mechanics & Foundations Division* 92 (1966), 105–124.
- [243] SCHMERTMANN, J. H. GUIDELINES FOR CONE PENETRATION TEST. (PERFORMANCE AND DESIGN).
- [244] SCHOFIELD, A. N. Cambridge geotechnical centrifuge operations. *Géotechnique* 30, 3 (1980), 227–268.
- [245] SEARLE, I. W., AND BARTHOLOMEW, R. F. The behaviour of driven cast in situ and bored piles in weathered chalk. *Géotechnique* 26 (1976), 21–32.
- [246] SEDRAN, G., STOLLE, D. F. E., AND HORVATH, R. G. An investigation of scaling and dimensional analysis of axially loaded piles. *Canadian Geotechnical Journal* 38 (2000), 530–541.
- [247] SEED, H. B., AND LUNDGREN, R. Investigation of the effect of transient loading on the strength and deformation characteristics of saturated sands. In *Proceedings of 57th Annual Meeting of the Society, ASTM* (1954), ASTM.
- [248] SEIDEL, J. P. The use of the signal matching approach to the analysis of Statnamic tests. In *Proc. 5th Int. Conf. Application of stress-wave theory to piles* (1996), Balkema, pp. 1051–1061.
- [249] SHENG, D., EIGENBROD, K. D., AND WRIGGERS, P. Finite element analysis of pile installation using large-slip frictional contact. *Computers and Geotechnics* 32, 1 (Jan. 2005), 17–26.
- [250] SHUBLAQ, J. Soil disturbance due to installation of model piles and pile groups. *Soils and Foundations* 32, 4 (1992), 17–26.
- [251] SMEULDERS, D. M. J. *On wave propagation in saturated and partially saturated porous media*. PhD thesis, Eindhoven University of Technology, 1992.
- [252] STEWART, D. P., CHEN, Y. R., AND KUTTER, B. L. Experience with the use of methylcellulose as a viscous pore fluid in centrifuge models. *Geotechnical Testing Journal* 21, 4 (1998), 365–369.
- [253] STUIT, H. G. *Sand in the Geotechnical Centrifuge*. PhD thesis, Delft University of Technology, 1995.
- [254] TAKEMURA, J., AND KOUDA, M. Tests results and discussions: Cone Penetration Tests. In *Centrifuge 98: Proceedings of the International Conference, IS-Tokyo, Vol. 2* (1999), Balkema, pp. 1109–1116.
- [255] TAYLOR, R. N. *Geotechnical Centrifuge Technology*. Blackie Academic & Professional, 2005.
- [256] TERZAGHI, K. Discussion of pile driving formulas. *Proceedings of American Society of Civil Engineers* 68, 2 (1942), 311–323.
- [257] TERZAGHI, K. *Theoretical soil mechanics*. Wiley, New York, 1943.

- [258] TOL, A. F. V., HUYN, N. Q., AND HÖLSCHER, P. Rapid model pile load tests in the geotechnical centrifuge: Pore pressure distribution and effects. In *Rapid Load Testing on Piles* (2009), Taylor & Francis Group, London, UK.
- [259] TOLOOYAN, A., AND GAVIN, K. Modelling the Cone Penetration Test in sand using Cavity Expansion and Arbitrary Lagrangian Eulerian Finite Element Methods. *Computers and Geotechnics* 38, 4 (June 2011), 482–490.
- [260] TSUBAKIHARA, Y., AND KISHIDA, H. Frictional behavior between normally consolidated clay and steel by two direct shear type apparatus. *Soils and Foundations* 33, 2 (1993), 1–13.
- [261] UESUGI, M., AND KISHIDA, H. Frictional resistance at yield between dry sand and mild steel. *Soils and Foundations* 26, 4 (1986), 139–149.
- [262] VEEN, C. V. The Bearing Capacity of a Pile. In *Proceedings of the 3rd International Conference on Soil Mechanics and Foundation Engineering* (1953), Zurich, Switzerland, pp. 84–90.
- [263] VERRUIJT, A. Elastic storage of aquifers. In *Flow Through Porous Media*, (1969), Academic Press, New York.
- [264] VESIC, A. S. Bearing capacity of deep foundations in sand. *Highway Research Record* 39 (1963), 112–153.
- [265] VESIC, A. S. Expansion of Cavities in Infinite Soil Mass. *Journal of the Soil Mechanics and Foundations Division* 98, 3 (1972), 265–290.
- [266] VESIC, A. S. *Design of Pile Foundation, National Cooperative Highway Research Program*. Transportation Research Board, Washington, D.C, 1977.
- [267] VESIC, A. S., BANKS, D. C., AND WOODARD, J. M. An experimental study of dynamic bearing capacity of footings on sand. In *Proceedings of the 6th International Conference on Soil Mechanics and Foundation Engineering* (1965), University of Toronto Press, Toronto.
- [268] VON TERZAGHI, K. Die Berechnung der Durchlässigkeitsziffer des Tones aus dem Verlauf der Hydrodynamischen Spannungserscheinungen. *Akademie der Wissenschaften in Wien, Sitzungsberichte, Mathematisch-naturwissenschaftliche Klasse IIa* (1923), 125–128.
- [269] VON TERZAGHI, K. Auftrieb und Kapillardruck an betonierten Talsperren. *Die Wasserwirtschaft* 26 (1933), 397–399.
- [270] VON TERZAGHI, K. The shearing resistance of saturated soils and the angle between the planes of shear. In *First Int. Conf. Soil Mech.* (1936), vol. 1, Harvard University, pp. 54–56.
- [271] WATANABE, K., AND KUSAKABE, O. The effect of loading rate on bearing capacity of pile foundations. In *Proceedings of Eighth International Conference on Urban Earthquake Engineering* (2011), Universal Academy Press, Tokyo, Japan, pp. 501–508.
- [272] WATANABE, K., AND KUSAKABE, O. Reappraisal of loading rate effects on sand behavior in view of seismic design for pile foundation. *Soils and Foundations* 53, 2 (2013), 215–231.
- [273] WEHNERT, M., AND VERMEER, P. A. Numerical analyses of load tests on bored piles. In *Numerical Methods in Geomechanics NUMOG IX* (2004), Ottawa, Canada.
- [274] WELTMAN, A. J. *Pile Load Testing Procedure*. Construction Industry Research and Information Association (CIRIA), London, 1980.
- [275] WHITAKER, T. The Constant Rate of Penetration test for the determination of the ultimate bearing capacity of a pile. *Proceedings of Institution of Civil Engineers* 26 (1963), 119–123.
- [276] WHITAKER, T., AND COOKE, R. W. A new approach to pile testing. In *Proceedings of the 5th International Conference on Soil Mechanics and Foundation Engineering* (1961), Paris, France, pp. 171–176.

- [277] WHITE, D. J. *An investigation into the behavior of pressed-in piles*. PhD thesis, Churchill College, University of Cambridge, 2002.
- [278] WHITE, D. J., AND BOLTON, M. D. Observing friction fatigue on a jacked pile. In *Centrifuge and constitutive modelling: Two extremes* (2002).
- [279] WHITE, D. J., AND BOLTON, M. D. Displacement and strain paths during plane-strain model pile installation in sand. *Géotechnique* 54, 6 (2004), 375–397.
- [280] WHITE, D. J., AND LEHANE, B. M. Friction fatigue on displacement piles in sand. *Géotechnique* 54, 10 (2004), 645–658.
- [281] WHITMAN, R. V. The behaviour of soils under transient loadings. In *Proceedings of the 4th International Conference on Soil Mechanics and Foundation Engineering* (1957).
- [282] WHITMAN, R. V. *The response of soils to dynamic loadings*. Contract report - U.S. Army Engineer Waterways Experiment Station, Corps of Engineers, 1970.
- [283] WHITMAN, R. V., AND HEALY, K. A. Shear strength of sands during rapid loading. *Journal of Soil Mechanics & Foundations Division* 88 (1962), 99–132.
- [284] WHITMAN, R. V., AND LASCHER, U. Footings for protective structures. In *Proceedings of the Symposium on Protective Structures for Civilian Populations* (1965), National Research Council, Washington D.C., pp. 151–158.
- [285] WILSON, E. L., FARHOOMAND, I., AND BATHE, K. J. Nonlinear dynamic analysis of complex structures. *Earthquake Engineering and Structural Dynamics* 1 (1973), 241–252.
- [286] WOLF, H., KÖNIG, D., AND TRIANTAFYLIDIS, T. Experimental investigation of shear band patterns in granular material. *Journal of Structural Geology* 25, 8 (2003), 1229–1240.
- [287] WOLTMAN, R. Beiträge zur Hydraulischen Architectur. *Dritter Band. Johann Christian Dietrich. Göttingen* (1794).
- [288] WOOD, W. L., BOSSAK, M., AND ZIENKIEWICZ, O. C. An alpha modification of Newmark's method. *International Journal for Numerical Methods in Engineering* 15 (1981), 1562–1566.
- [289] WROTH, C. P., RANDOLPH, M. F., HOULSBY, G. T., AND FAHEY, M. *A Review of the Engineering Properties of Soils, with Particular Reference to the Shear Modulus*. CUED/D-Soils TR75, Cambridge University, 1979.
- [290] YAGI, N., ENOKI, M., AND YATABE, R. Influence of pore water pressure on dynamic and static penetration testings. In *Proc. 2nd Eur. Sym. on Penetration Testing* (1982), Amsterdam.
- [291] YAGI, N., ENOKI, M., AND YATABE, R. Development of a penetrometer capable of applying pore pressure. In *Penetration Testing 1988* (1988), Rotterdam.
- [292] YAMAMURO, J. A., AND ABRANTES, A. E. Behavior of medium sand under very high strain rates. In *Proceedings of 1st Japan-U. S. Workshop on Testing, Modeling, and Simulation* (2003), Boston, Massachusetts, USA.
- [293] YAMAMURO, J. A., ABRANTES, A. E., AND LADE, P. V. Effect of strain rate on the stress-strain behavior of sand. *Journal of Geotechnical and Geoenvironmental Engineering* 137, 12 (2011), 1169–1178.
- [294] YAMAMURO, J. A., AND LADE, P. V. Effects of strain rate on instability of granular soils. *Geotechnical testing journal* 16, 3 (1993), 304–313.
- [295] YAMASHITA, S., JAMIOLKOWSKI, M., AND PRESTI, D. C. F. L. Stiffness nonlinearity of three sands. *Journal of Geotechnical and Geoenvironmental Engineering* 126, 10 (2000), 929–938.

- [296] YANG, J., THAM, L. G., LEE, P. K. K., CHAN, S. T., AND YU, F. Behaviour of jacked and driven piles in sandy soil. *Géotechnique* 56 (2006), 245–259.
- [297] YASUFUKU, N., AND HYDE, A. F. L. Pile end-bearing capacity in crushable sands. *Géotechnique* 45, 4 (1995), 663–676.
- [298] YASUFUKU, N., OCHIAI, H., AND OHNO, S. Pile End-Bearing Capacity of Sand Related to Soil Compressibility. *Soils and Foundations* 41, 4 (2001), 59–71.
- [299] YE, F. J., GOH, S. H., AND LEE, F. H. A method to solve Biot u-U formulation for soil dynamics applications using the ABAQUS/explicit platform. In *Numerical Methods in Geotechnical Engineering* (2010), Taylor and Francis Group.
- [300] YU, H. S. *Cavity expansion theory and its application to the analysis of pressuremeters*. PhD thesis, University of Oxford, England, 1990.
- [301] YU, H. S., AND MICHELL, J. K. Analysis of cone resistance: Review of methods. *Journal of Geotechnical and Geoenvironmental Engineering* 124, 2 (1998), 140–149.
- [302] ZENG, X., WU, J., AND YOUNG, B. A. Influence of viscous fluids on properties of sand. *Geotechnical Testing Journal* 21, 1 (1998), 45–51.
- [303] ZIENKIEWICZ, O. C. Basic formulation of static and dynamic behaviour of soil and other porous media. In *Numerical Methods in Geomechanics* (1982), Holland.
- [304] ZIENKIEWICZ, O. C., CHAN, A. H.-C., PASTOR, M., SCHREFLER, B., AND SHIOMI, T. *Computational Geomechanics with Special Reference to Earthquake Engineering*. John Wiley and Sons Ltd., 1999.
- [305] ZIENKIEWICZ, O. C., AND SHIOMI, T. Dynamic behavior of saturated porous media: the generalized Biot formulation and its numerical solution. *Int. J. Numer. Anal. Methods Geomech.* 8 (1984), 71–96.
- [306] ZIENKIEWICZ, O. C., AND SHIOMI, T. Dynamic behaviour of saturated porous media; The generalized Biot formulation and its numerical solution. *International Journal for Numerical and Analytical Methods in Geomechanics* 8, 1 (Jan. 1984), 71–96.
- [307] ZIENKIEWICZ, O. C., AND TAYLOR, R. L. *The Finite Element Method for Solid and Structural Mechanics, Sixth Edition*, 6 ed. Butterworth-Heinemann, Sept. 2005.
- [308] ZIENKIEWICZ, O. C., WOOD, W. L., AND TAYLOR, R. L. An alternative single step algorithm for dynamic problems. *Earthquake Engineering and Structural Dynamics* 8 (1980), 31–40.

ACKNOWLEDGEMENTS

My PhD study has been a long and fascinating journey. I want to express my gratitude to professors, friends and my parents who made it possible for me to accomplish this study and who are with me during my journey.

First and foremost, I would like to express my gratitude to my promotor, Prof. A. Frits van Tol, and co-promotor, Dr. Paul Hölscher, whose expertise, understanding and sympathy contribute greatly to my PhD study. Prof. van Tol, it has been a great honour to study with you, thanks for bringing me into the geotechnic field and offering me this captivating topic. Thank you also for being so patient with me, for numerous sharp but open ideas and discussions, and for countless time to revise my thesis. Paul, it has been a great pleasure to work with you. Thanks for plenty of fruitful discussions, dedications for every meeting and countless comments on my thesis. In this PhD study, I definitely can not come to this stage of writing the acknowledgments without the support and encouragement of Prof. van Tol and Paul, I appreciate you two.

I would like to thank my committee members: Prof. Andrei Metrikine, Prof. Kenneth Gavin, Prof. Adam Bezuijen, Dr. Michael Brown and Dr. Piet Meijers, for their insightful feedbacks, constructive comments and encouragements. Your deliberate comments and suggestion throughout my thesis greatly improves the clarity and completeness. I appreciate your support.

This research is financially supported by CICAT Management Center for International Cooperation (Valorisation Center) and Deltares. Their contributions are gratefully acknowledged. The hospitality of the Geotechnical Laboratory of the Civil Engineering department of Delft University of Technology and the support from the Geotechnical department of Thuy Loi University, especially Prof. Trinh Minh Thu, is greatly appreciated. Special thanks to Ms. Veronique van der Vast for her fully support and encouragement from the very beginning of my study in TU Delft.

I would like to appreciate the assistance and support from the geotechnical team in Deltares who contributed greatly to my thesis: Ferry for the model preparation; Rob, Frans and Thijs for the mechanical and electrical setup and the execution of the experimental modelling; Frits, Paul and Adam for the on-flight discussion and adaption of the experimental program; Piet for the detail report and fruitful discussion on Plaxis-PTU; Jelke for many interesting discussions; Haike and Annemieke for the data extraction and the factual report; Son for the illustration and cover.

During many years away from home, I met great people who shared special times with me. Special thanks are given for Phu-Hang-Tin-Ben, Son-Linh-Sumo, Phuong, Tam, Trung, Yen, Trang-litte Tiger, Becky, Khoa who are always with me in the good or bad moments. Phu, Son and Trung, although we are apart a lot of times and durations, you are more than a friend to me, thank you.

Besides special people, I also have a great fortune to meet many friends that make my life colourful, I want to give my thanks for them: Ngoc Ha, Dang-Tam, Minh-Vinh, Hung,

Dung, Thanh, Nghi, Vinh, Elazbietta, Binh, Duong-Quynh Anh, Vinh-Diem, Anam, Steve, Ashley, Nhat Anh, Tung, David, Tin, Phan Anh, Cher, Romano, Chin, Thien, Samantha, Hieu, Kazunari-Chizuru-Mizuki, Nhu, Thang-Mai Anh, Aaron-YingNan , Cuong-bowl, Sanh-Hoang Anh, Kambiz, John-the Motor, Freddie, Duoc, Tung, Simone, Anders, Ya-Jun, Jiao, Quyen, Ngan, Takeshi, Khanh, Cuong-Anh, Liem, Victor, Quang, Tuan-Yen, Wei, Viet, Bach Duong, Hung and many others.

Lastly but never enough, I am deeply indebted to my parents for their continuous support, encouragement and sacrifice. I would like to express my utmost appreciation for them; this thesis is dedicated to my parents.

CURRICULUM VITÆ

Chi Thanh NGUYEN

29-07-1983 [Gmail](#)
Born in Sofia, Bulgaria [ORCID](#)
Vietnamese nationality [ResearchGate](#)

EDUCATION

- 2001–2006 BSc in Hydraulic Engineering
Thuy Loi University, Viet Nam
- 2006–2008 MSc in Geotechnical Engineering
Delft University of Technology, The Netherlands
Thesis: Investigation into soil displacement near a jacked-in
pile in sand
Supervisors: prof. ir. A.F. van Tol & dr. ir. J. Dijkstra
- 2009–2017 PhD in Geotechnical Engineering
Delft University of Technology, The Netherlands
Thesis: Modelling of pile load tests in granular soils
Promotor: prof. ir. A.F. van Tol & dr. ir. P. Hölscher

RESEARCH EXPERIENCE

- 2014–2015
(15 months) Researcher in Computational Geomechanics
The University of Adelaide, Australia
Topic: Constitutive modelling for localised failure of geo-
materials
Computational modelling of crack propagation
- 2015–2016
(15 months) Researcher in Computational Geomechanics
Monash University, Australia
Topic: SPH modelling of granular materials and soil-water
interaction
MPM programming for solid mechanics

Propositions

accompanying the dissertation

MODELLING OF PILE LOAD TESTS IN GRANULAR SOILS

by

Chi THANH NGUYEN

1. The asymmetric response of pore pressures transducers that are symmetrically installed around a pile, demonstrates that the failure in the soil during a rapid load test is asymmetric.
2. The influence of the excess pore pressure on the increase of the rapid resistance over the static resistance is stronger for a pile in a loosely packed granular soil bed than for a densely packed bed.
3. The influence of the excess pore pressure on the increase of the rapid resistance over the static resistance is stronger for the embedded pile than for the jacked pile.
4. In research of granular soils, continuum is a convenient definition but not a good one because it can scarcely give an insight into the real behaviour of granular soils.
5. For the analysis of pile-soil interaction, numerical modelling must be supported with intensive calibrations.
6. Before doing an experiment, one should know the general outcomes; surprising results, which are assumed to be correct, are an extra gift.
7. Silence is only a relative definition for a living being.
8. It seems that conflicts and warfare are generated by the discussion about borders and countries, but religion and, in a broader view, behavioural standards of people are more important.
9. In football, a good team is based on responsibility, but the best team is based on blind faith and a bit of luck.
10. A doctoral title is a certificate to start a research career; however, only by continuously doing research a person can keep on holding that title.

These propositions are regarded as opposable and defensible, and have been approved as such by the promotor prof. ir. A.F. van Tol and the copromotor Dr. P. Hölscher.

Stellingen

behorende bij het proefschrift

MODELLEREN VAN PROEFBELASTINGEN OP PALEN IN GRANULAIR MATERIAAL

door

Chi THANH NGUYEN

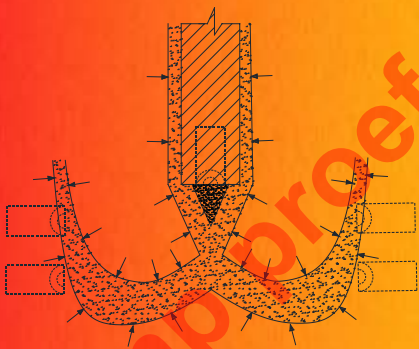
1. De asymmetrische respons van waterspanningsopnemers die symmetrisch rondom een paal zijn geïnstalleerd, toont aan dat het bezwijken in de bodem tijdens een snelle proefbelasting asymmetrisch is.
2. De invloed van de wateroverspanningen op de toename van de weerstand tijdens een snelle proefbelasting ten opzichte van de weerstand tijdens een statische proefbelasting is groter voor een paal in een losgepakt granulaire materiaal dan voor een dichtgepakte materiaal.
3. De invloed van de wateroverspanningen op de toename van de weerstand tijdens een snelle proefbelasting ten opzichte van de weerstand tijdens een statische proefbelasting is groter voor een in de grond gevormde paal dan voor een geprefabriceerde paal.
4. Bij het onderzoek van granulaire grond is continuüm een handige beschrijving, maar niet een goede, omdat het nauwelijks inzicht kan geven in het echte gedrag van granulaire grond.
5. Numerieke analyse van paal-grond interactie moet worden ondersteund met intensieve kalibraties.
6. Voorafgaand aan de uitvoering van een experiment, moet men de algemene uitkomsten kennen ; verrassende resultaten, die verondersteld worden juist te zijn, zijn een extra cadeau.
7. Stilte is slechts een relatieve definitie voor een levend wezen.
8. Het lijkt dat conflicten en oorlogsvoering ontstaan ten gevolge van discussie over grenzen en landen, maar religies en, in een bredere opvatting, gedragsstandaarden van mensen zijn veel belangrijker.
9. Bij voetbal is een goed team gebaseerd op verantwoordelijkheid, maar het beste team is gebaseerd op blind vertrouwen en een beetje geluk.
10. Een doctors titel is een certificaat om een onderzoeksloopbaan te starten; Alleen door voortdurend onderzoek te doen kan een persoon die titel blijven behouden.

Deze stellingen worden beschouwd als opponeerbaar en verdedigbaar geacht en zijn als zodanig goedgekeurd door de promotor prof. ir. A.F. van Tol en de co-promotor Dr. P. Hölscher.

Invitation

You are cordially invited to the public defense of my PhD dissertation entitled

MODELLING OF PILE LOAD TESTS IN GRANULAR SOILS LOADING RATE EFFECTS



The defense will take place on
Tuesday 17 October 2017
at 12:30 hours
in the Senaatszaal of
the Aula Congress Centre at
Delft University of Technology
(Mekelweg 5 in Delft).



Prior to the defense,
at 12:00 hours,
I will give a brief presentation
about my research.

You are kindly invited to a
reception right after the
ceremony.